Università degli Studi di Genova

SCUOLA DI SCIENZE MATEMATICHE, FISICHE E NATURALI

Electron quantum optics at fractional filling factor: minimal excitation states and interferometry

Thesis for the Doctoral degree in Physics

March 2018

PhD candidate	Luca Vannucci
Supervisor	Prof. Maura Sassetti
External supervisor	Dr. Dario Ferraro (IIT)
Referee	Prof. Fabrizio Dolcini (Politecnico di Torino)
Referee	Prof. Thomas Schmidt (Uni. Luxembourg)

Contents

Introduction

Quantum optics is the branch of physics dealing with light and light-matter interaction at the microscopic quantum level. The striking ability in creating, manipulating and measuring quantum states of the electromagnetic field achieved in the last thirty years has provided some simple yet fundamental tests for the quantum mechanical behavior of single-photon states [1].

In a similar fashion, the on-demand generation of single-electron states in mesoscopic systems has recently opened the way to the fascinating field of Electron Quantum Optics (EQO), where individual fermionic quantum states are manipulated one by one in ballistic, coherent conductors [2]. In this way it is possible to reproduce quantum-optical experiments and setups in solid state devices, using fermionic degrees of freedom (electrons in mesoscopic systems) instead of bosonic ones (photons in waveguides and optical cavities). The full correspondence between photonic quantum optics and EQO is built on the following three ingredients (see Fig. I.1):

- ✓ *Fermionic waveguides.* They are provided by one-dimensional topological edge states emerging in the Quantum Hall (QH) regime [3]. By applying a strong perpendicular magnetic field to a Two-Dimensional Electron Gas (2DEG), bulk conduction is suppressed by a finite bulk gap between valence and conduction bands, but metallic states appear at the edge of the system due to the topologically non-trivial structure of the bulk [4]. Chirality of the edge states forbids electron backscattering, thus providing efficient waveguides for fermionic degrees of freedom.

- ✓ *Beam splitters.* In a typical quantum-optical experiment, photon beams are manipulated with the help of beam splitters. In QH systems, a negative gate voltage can partially deplete the underlying 2DEG and distort the path of the edge states. This constriction is called Quantum Point Contact (QPC) and represents an effective beam splitter for electrons, allowing for tunable transmission and reflection of the fermionic beam impinging on the barrier.

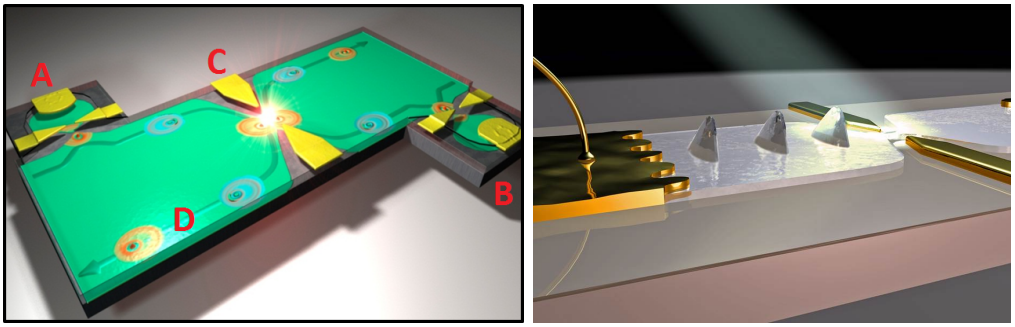

Figure I.1: Left: the essence of electron quantum optics. Photon guns are replaced by single electron sources (A and B), a QPC (C) serves as an electronic beam splitter and one-dimensional edge states (D) are the solid state analogue of photon waveguides. Right: artistic view of the voltage pulse source theoretically described by L. Levitov. Credits: B. Plaçais's group at LPA-ENS (http://www.phys.ens.fr/~placais/), D.C. Glattli's group at CEA Saclay (http://nanoelectronics.wikidot.com/).

✓ *Single-electron sources.* Two recipes have been proposed to extract a single electron out of the filled Fermi sea in fermionic systems. First, the so-called driven mesoscopic capacitor [5] consists of a quantum dot connected to the 2DEG through an additional QPC. A periodic drive of the energy levels of the dot leads to the separate injection of an electron and a hole into the system for each period of the drive [6]. Alternatively, one can excite a single electron above the Fermi sea by applying well defined voltage pulses to a quantum conductor, as suggested by L. Levitov and coworkers [7–9]. Remarkably, they found that Lorentzian pulses with quantized area $\int dt\, V(t) = n\frac{h}{e}$ $(n \in \mathbb{N})$ injects particle-like excitations only.

Single-electron sources based on mesoscopic capacitors and levitons (as Levitov's single-electron excitations have been dubbed [10]) were both experimentally reported, using a fermionic analogue of the Hanbury Brown-Twiss (HBT) experiment to explore single-electron excitations in the energy domain and a collisional Hong-Ou-Mandel (HOM) interferometry to shed light on their wavefunction in the time domain [10–12].

Despite evident analogies and similarities with traditional photonic quantum optics, EQO brings into play two new features that are inherently characteristic of electronic systems. Firstly, single-photon states are usually created on a real quantum mechanical vacuum (i.e. zero-particle state), while single-electron states are always generated on top of a completely different ground state with its own dynamics, namely the filled Fermi sea. The contribution of the Fermi sea have to be carefully taken into account in the framework of EQO. Nevertheless, a fermionic analogue of Roy J. Glauber's theory of optical coherence [13] can be developed circumventing this complication [14], and theoretical predictions are in excellent agreement with experiments [10–12, 15–

18].

Even more importantly, solid state systems can be heavily affected by interactions, and the ground state of a fermionic system can show *correlations*. For instance, the Fractional Quantum Hall (FQH) effect [19] is a paradigmatic example of the dramatic consequences of electron-electron interactions. Here, a new strongly correlated phase emerge in the quantum liquid, with quasiparticle excitations carrying a fraction of the electron charge [20] and whose statistical properties are neither bosonic nor fermionic, but belongs to the more general class of anyons [21]. The fact that FQH systems host topologically protected chiral modes at the edge [22] let us envisage an exciting generalization of EQO, including correlated ground states and properly taking into account all the striking phenomena that come along with electron-electron interactions in one dimensional systems [23]. This is precisely the aim of the present thesis, in which I present the theory of EQO in the FQH regime.

I begin from the physics of noise in mesoscopic systems, which is reviewed in the introductory **Chapter 1**. Here I summarize the so-called Floquet scattering approach to deal with photoassisted transport in coherent mesoscopic conductors. This is a crucial first step, as experimental activity in EQO rely on the measurement of the current-current correlation spectrum, i.e. noise, in the presence of high-frequency periodic sources.

In **Chapter 2** I review the discovery of the QH effect and its topological interpretation, and show how to take advantage of the ballistic edge states arising in the QH regime. Two types of single-electron sources are then discussed, both from the theoretical and experimental point of view. A particular attention is devoted to minimal excitation states of quantum conductors, also called *levitons*.

Chapter 3 is basically the core of this thesis. The field-theoretical approach to the edge states of the FQH regime and their capacitive coupling with a voltage source are discussed. It is then shown how minimal excitations in the FQH regime arise in response to appropriately designed voltage pulses, and how to detect such states in a HBT interferometer.

A similar analysis is carried out in **Chapter 4**, where I focus on minimal excitations for heat transport instead of the ordinary charge transport. Here I consider the heat current flowing in response to periodic voltage pulses and discuss the auto-correlation spectrum of heat-heat and mixed charge-heat fluctuations. The robustness of minimal excitation states with respect to an arbitrary overlap is also examined.

Finally, **Chapter 5** is devoted to HOM interferometry, namely the physics of colliding identical excitations. I show that FQH single-leviton collisions bear a universal HOM signature identical to their Fermi liquid analog, while multiple-leviton interferometry generates surprising dips and bumps in the zero-frequency charge noise.

Several **Appendices** are used to illustrate technical parts of the calculations (such as the evaluation of photoassisted coefficients, Green's functions,

and useful commutation relations), and to discuss in more detail the theoretical formalism used in the main text (for instance, the Keldysh nonequilibrium Green's function approach).

This thesis is based on the following papers co-authored by myself:

- ✓ Ref. [24]: J. Rech, et al., "Minimal Excitations in the Fractional Quantum Hall Regime", Phys. Rev. Lett. **118**, 076801 (2017) (Chapters 3 and 5);
- ✓ Ref. [25]: L. Vannucci, et al., "Minimal excitation states for heat transport in driven quantum Hall systems", Phys. Rev. B **95**, 245415 (2017) (Chapter 4);
- ✓ Ref. [26]: L. Vannucci, et al., "Photoassisted shot noise spectroscopy at fractional filling factor", arXiv:1709.05112, [J. Phys. Conf. Ser., in press] (Chapter 3);
- ✓ Ref. [27]: F. Ronetti, et al., "Crystallization of Levitons in the fractional quantum Hall regime", arXiv:1712.07094 (Chapter 5).

Other publications not included in this thesis are:

- ✓ Ref. [28]: G. Dolcetto, et al., "Current enhancement through a time-dependent constriction in fractional topological insulators", Phys. Rev. B **90**, 165401 (2014);
- ✓ Ref. [29]: L. Vannucci, et al., "Interference-induced thermoelectric switching and heat rectification in quantum Hall junctions", Phys. Rev. B **92**, 075446 (2015);
- ✓ Ref. [30]: F. Ronetti, et al., "Spin-thermoelectric transport induced by interactions and spin-flip processes in two-dimensional topological insulators", Phys. Rev. B **93**, 165414 (2016).

Chapter 1

Noise in mesoscopic physics

In this Chapter we present an overview of the physics of noise in mesoscopic systems. These are systems whose size is sufficiently small to be affected by quantum mechanics but still contain a macroscopic number of particles. We point out the importance of noise measurements by showing that quantum fluctuations contains information that is usually invisible in more traditional quantities, such as the average electrical current. After a general description of different sources of noise, we introduce the scattering matrix formalism that will allow us to deal with some notable examples. We conclude with an introduction to the photoassisted shot noise, which will be the central quantity of interest in the rest of this thesis.

1.1 "The noise is the signal"

In our daily experience, the word *noise* is in general intended as a synonym of *disturbance*. When we think on noise we imagine an unpleasant (and usually unwanted) sound that interferes with the one we are paying attention to, or just bothers us someway.

This meaning is translated almost literally in the field of electronics. For any experiment one can imagine to carry out in the lab, the signal one would like to measure is generally hidden behind a certain amount of disturbance, which is once again called noise. Experimentalists usually fight against any possible source of stochastic fluctuations that may affect the precision of a measurement, in such a way to extract the quantity of interest out of the background noise.

But what if the noise itself were the signal of interest? This statement, which may at first sound extremely counterintuitive, was first expressed by

Rolf Landauer, one of the fathers of mesoscopic physics, and turns out to be profoundly true [31]. In the course of the past 30 years, condensed matter physicists gradually realized that noise in mesoscopic physics contains a huge amount of information that is usually hidden in quantities we often look at, such as the electrical current. Connections between noise and electronic temperature, conductance, elementary charge, quantum statistics and emission/absorption spectrum were highlighted and deeply scrutinized.

From a quantitative point of view, we will describe the noise in terms of the current-current correlation function throughout this thesis. Assuming that an electrical current $J(t)$ flows from the source to the drain electrode of a generic conductor (classical or quantum), current fluctuations around the expectation value $\langle J(t)\rangle$ are described by the quantity

$$\Delta J(t) = J(t) - \langle J(t)\rangle \,. \tag{1.1}$$

Here the symbol $\langle X\rangle$ stands for the quantum average value of the operator X over an equilibrium configuration described by the density matrix ρ, i.e. $\langle X\rangle = \mathrm{Tr}(\rho X)$. The autocorrelation function of current fluctuations is

$$C(t,\tau) = \langle \Delta J(t)\Delta J(t+\tau)\rangle = \langle J(t)J(t+\tau)\rangle - \langle J(t)\rangle \langle J(t+\tau)\rangle \,. \tag{1.2}$$

In time-translation invariant systems, $C(t,\tau)$ does not depend on the variable t and we can write

$$C(\tau) = \langle \Delta J(t)\Delta J(t+\tau)\rangle = \langle \Delta J(0)\Delta J(\tau)\rangle \,. \tag{1.3}$$

The noise power (or spectral density) is the Fourier transform of $C(\tau)$, namely[1]

$$S(\omega) = 2\int_{-\infty}^{+\infty} d\tau\, e^{i\omega\tau} \langle \Delta J(t)\Delta J(t+\tau)\rangle \,. \tag{1.4}$$

1.2 Thermal noise

Thermal agitation is the first fundamental source of noise we consider. At finite temperature, thermal agitation of the carriers causes fluctuations of the electrical current flowing through a conductor. Surprisingly, equilibrium fluctuations of the current are directly related to the conductance of the system, as we show here below.

Let us consider a generic classical conductor at equilibrium, described e.g. by Drude theory [33]. In this framework, electron are assumed to be independent free particles and are substantially treated by methods ot the kinetic theory. They relax to the thermal equilibrium state only through collisions, which happen with a probability per unit time γ known as *relaxation rate*.

[1] We put an additional factor 2 in front of the Fourier transform for normalization purposes, as usually done in the literature [32].

Suppose now that the system has cross-sectional area A and length L, and is in thermodynamic equilibrium with the environment at temperature θ. Current J in the x direction (which is oriented along the length L of the sample) is related to the momentum of the carriers and the charge density. For the single electron contribution we can write [34]

$$J_1(t) = -\frac{e}{mL}p(t), \tag{1.5}$$

where p is the x component of the particle momentum. Since momenta are randomly distributed, the expectation value for the current vanishes, namely $\langle J_1(t)\rangle = 0$. Let us now compute the current-current correlation function:

$$C_1(\tau) = \langle \Delta J_1(t)\Delta J_1(t+\tau)\rangle = \frac{e^2}{m^2L^2}\langle p(t)p(t+\tau)\rangle\,. \tag{1.6}$$

Correlation of momenta at different times decays exponentially as the difference in time increases, thus the momentum correlation function can be written as $\langle p(t)p(t+\tau)\rangle = \alpha e^{-\gamma|\tau|}$.[2] For a system in equilibrium at temperature θ, we get the value of the constant α observing that the average value of $p^2(t)$ in the steady state must satisfy the well known equipartition theorem. This readily gives $\alpha = mk_{\mathrm{B}}\theta$.

Consider that the volume $A\cdot L$ contains N independent particles. The total current-current correlation function is just

$$C(\tau) = NC_1(\tau) = \frac{Ne^2}{mL^2}k_{\mathrm{B}}\theta e^{-\gamma|\tau|} = G\gamma k_{\mathrm{B}}\theta e^{-\gamma|\tau|}, \tag{1.8}$$

where we have recognized the conductance $G = 1/R$. The latter is given by

$$G = \sigma\frac{A}{L} = \frac{Ne^2}{mL^2\gamma}, \tag{1.9}$$

with $\sigma = \frac{N}{AL}\frac{e^2}{m\gamma}$ the Drude conductance. The noise spectral power as defined in the previous section is thus

$$S(\omega) = 2G\gamma k_{\mathrm{B}}\theta\int_{-\infty}^{+\infty} d\tau\, e^{i\omega\tau}e^{-\gamma|\tau|} = 4Gk_{\mathrm{B}}\theta\frac{1}{1+\frac{\omega^2}{\gamma^2}}. \tag{1.10}$$

[2] This follows from the fact that $p(t) \sim e^{-\gamma t}$ in the Drude model, and from the assumption that the correlation function cannot diverge exponentially for negative values of τ, hence the absolute value on τ. This rather intuitive physical assumption can be proved more rigorously by solving the Langevin equation for a particle subjected to both a dissipative force with damping rate γ and a stochastic force $F(t)$ [35, 36]

$$\dot{p}(t) = -\gamma p(t) + F(t). \tag{1.7}$$

Solving for $p(t)$ and evaluating the momentum correlation function we get the exponential decay $e^{-\gamma|\tau|}$.

In typical metallic systems, where γ is of the order of $10^{13} \sim 10^{14}$ s^{-1} [33], this signal is approximately constant over a very large frequency range up to $\omega \approx \gamma$ and is given by

$$S(0) = 4Gk_B\theta. \tag{1.11}$$

This is the famous Johnson-Nyquist formula for the thermal noise [37, 38]. It states that the equilibrium noise $S(0)$ is proportional to the electrical conductance G, with the proportionality substantially given by the temperature θ. This phenomenon was first noted at Bell labs by J.B. Johnson in 1926 working on a vacuum tube amplifier, and subsequently explained by H. Nyquist on the basis of energy balance considerations in a transmission line.

It is worth emphasizing a very important aspect of Eq. (1.11). Thermal noise is an equilibrium statistical property of the system, while the conductance tells us how the conductor reacts and dissipates energy when it is driven out of equilibrium by applying a non-zero voltage bias. The Johnson-Nyquist result shows a remarkably profound link between equilibrium fluctuations and dissipative properties of a system (in linear response). It was indeed demonstrated that the Johnson-Nyquist formula is nothing but a particular manifestation of a far more general relation known as *fluctuation-dissipation theorem* [39].

Equation (1.11) is thus a first example of information encoded in the noise. For instance, we can measure the temperature by looking at the ratio $S(0)/G$, which is more or less the essence of the *noise thermometry* technique [40–42]. However, we can fully appreciate the power behind Landauer's quote by moving on to non-equilibrium noise in quantum conductors.

1.3 Shot noise

As we all know, an electric current is nothing but the flow of discrete particles with quantized charge. The charge of the carrier can be different, depending on the system we consider. In metal and semiconductors the current is carried either by electrons, with negative charge $-e$, or by holes, with positive charge $+e$. In superconductors two electrons can bound together to form the so-called Cooper pair, and the fundamental carrier has charge $-2e$. A more exotic situation is represented by the FQH effect, where quasiparticles and quasiholes with a fraction of the electron charge can carry the current. The most prominent example is the FQH effect at filling factor $\nu = 1/3$, which shows excitations with charge $\pm e^* = \pm e/3$. In all these cases the granularity of the electric current gives rise to a new type of noise, which is called *shot noise*. Walter Schottky first predicted the occurrence of this kind of fluctuations in an almost ideal vacuum tube where every other source of disturbance was eliminated [43]. He used the German word *Schroteffekt* (literally, shot effect) to distinguish this second source of noise from thermal effects (*Wärmeeffekt*).

Let us give an intuitive derivation of the origin of shot noise by considering an ideal experiment in which two electronic reservoirs are separated by a

barrier. A certain amount of particles is emitted from, say, the left reservoir and moves towards the barrier. Let us assume that particles can be randomly transmitted to the right reservoir or reflected back to the left side, with all transmission or reflection events independent from each other. This is a very good approximation, for instance, for the case of two metals separated by a thin insulating layer, where transmission events are uncorrelated. If N particles are transmitted on average in the interval Δt (i.e. the transmission rate $\lambda = N/\Delta t$ is constant and known), the probability distribution for having k particles transmitted in the same interval through the conductor is given by the Poisson distribution

$$P(k) = e^{-N}\frac{N^k}{k!}. \tag{1.12}$$

Now, imagine that we can measure the current by looking at how many particles are transmitted in the interval Δt. If each particle carries a charge q, the current is given by $I = qk/\Delta t$, and its average value is $\langle I\rangle = \sum_{k=0}^{\infty}(qk/\Delta t)P(k)$. To calculate the average current and its fluctuation we use the characteristic function of the distribution, given by $\chi(\beta) = \left\langle e^{i\beta k}\right\rangle$. This is a very useful tool to calculate all the momenta, which can be inferred from $\chi(\beta)$ through derivation with respect to β:

$$\langle k^n\rangle = (-i)^n\frac{\partial\chi}{\partial\beta}\bigg|_{\beta=0}. \tag{1.13}$$

For the Poisson distribution, the characteristic function reads

$$\chi(\beta) = \sum_{k=0}^{+\infty} e^{i\beta k}e^{-N}\frac{N^k}{k!} = \exp\left[N(e^{i\beta}-1)\right], \tag{1.14}$$

and the first and second momenta are easily found to be $\langle k\rangle = N$ and $\langle k^2\rangle = N^2 + N$. Thus, the current and its fluctuations are given by

$$\langle I\rangle = \frac{qN}{\Delta t}, \tag{1.15}$$

$$\left\langle \Delta I^2\right\rangle = \left\langle I^2\right\rangle - \langle I\rangle^2 = \frac{q^2N}{(\Delta t)^2}. \tag{1.16}$$

Let us now look for the spectral density of the noise. We emphasize that averaging over the time Δt corresponds to filtering the signal in the frequency domain. The effective bandwith is $\Delta\omega = 2\pi\Delta f = \pi/\Delta t$ [44]. Recalling the definition Eqs. (1.3) and (1.4) we have

$$\left\langle \Delta I^2\right\rangle = C(0) = \frac{1}{2}\int_{-\infty}^{+\infty}\frac{d\omega}{2\pi}S(\omega) = \frac{\Delta\omega}{2\pi}S, \tag{1.17}$$

where we have considered $S(\omega)$ as constant in the bandwith $\Delta\omega$ (i.e. we have assumed a *white noise* spectrum). We finally obtain the very important result

$$S = 2\Delta t\left\langle \Delta I^2\right\rangle = 2q\left\langle I\right\rangle, \tag{1.18}$$

known as Schottky relation[3]. As we see from Eq. (1.18), the noise is proportional to the charge of the carriers and the average value of the current. This is rooted in the fact that, for a Poissonian distribution, the average number $\langle k \rangle$ of events occurring in the time interval Δt equals the variance $\langle k^2 \rangle - \langle k \rangle^2$. The astonishing consequence of Eq. (1.18) is that we are able to measure the charge q just by looking at the noise-to-current ratio.

Two unconventional manifestation of this statement deserve to be mentioned. When considering a junction between a normal metal (N) and a superconductor (S), transport at energies below the gap of the superconductor is determined by the so called Andreev reflection [46]. An electron traveling from the normal metal to the superconductor is transmitted as a Cooper pair, and a hole is reflected back to fulfill charge conservation. The total transferred charge is thus $2e$, and several experiments have reported the doubling of shot noise in a N-S junction with respect to N-N contacts. [47–49]. Such an idea was also used to demonstrate that quasiparticles in the FQH regime carry a fraction of the electron charge, as we will discuss later on [50–52].

Let us remark that the origin of shot noise is much different from thermal noise. The latter is a property of an equilibrium system caused by fluctuations in the occupation number. The former is instead an intrinsically nonequilibrium characteristic which only emerges when we drive a current through the system. It should also be noticed that a random reflection or transmission of particles is necessary: in a perfectly transmitting or completely insulating system there is no shot noise. We'll come back to this important point when dealing with shot noise in the scattering formalism.

1.4 Partition noise

We have already seen that thermal and shot noises provide information about the dissipative properties of a system, the temperature, and the charge of the carriers. Here we discuss how statistical properties of particles can be extrapolated from a special kind of shot noise, called *partition noise*.

We consider idealized one-particle or two-particle experiments conducted in some sort of optical table, as shown in Fig. 1.1. Here particles (either bosons or fermions) coming from input channels 1 and 2 collide on a semi-transparent mirror (also called *beam splitter*) and exit in output arms 3 and 4. The mirror allows transmission with probability T and reflection with probability $R = 1 - T$. We describe incoming particles in second quantization with creation and annihilation operators $a_i^\dagger$, a_i $(i = 1, 2)$, while operators $b_j^\dagger$ and b_j $(j = 3, 4)$ take care of outgoing particles. For the sake of simplicity we consider one single mode in each channel (i.e. operators $a^\dagger$, a, $b^\dagger$ and b create and annihilate

[3] One should note that there is no barrier between cathode and anode in Schottky's vacuum tube, and the transmission is almost perfect. However, the source of randomness is rooted in the emission probability from the cathode and gives rise to the same physics we discussed above [45].

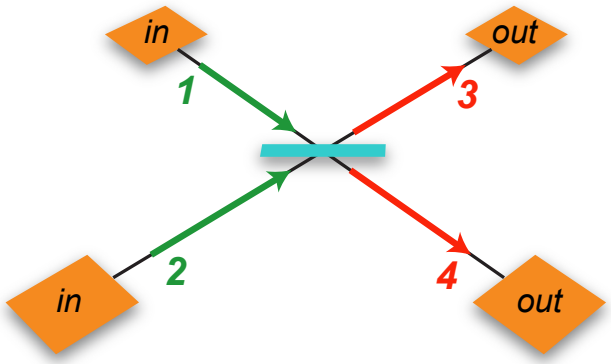

Figure 1.1: Optical setup for two-particle interferometry. Incoming particles, traveling in input channels 1 and 2, impinge on the beam splitter in the middle (thin blue layer). They are either reflected (with probability R) or transmitted (with probability $T = 1 - R$) into output channels 3 and 4. Two detectors are placed at the end of output arms 3 and 4.

particles with a single, well defined value of momentum and energy; spin plays no role in this discussion). The relation between input and output operators writes $b_j = \sum_i s_{ji} a_i$ or, in matrix form,

$$\begin{pmatrix} b_3 \\ b_4 \end{pmatrix} = \begin{pmatrix} s_{31} & s_{32} \\ s_{41} & s_{42} \end{pmatrix} \begin{pmatrix} a_1 \\ a_2 \end{pmatrix}. \tag{1.19}$$

The 2×2 matrix in Eq. (1.19) is called *scattering matrix* of the beam splitter. We highlight that, in order to conserve commutation and anticommutation relations of incoming operators, the scattering matrix has to be unitary. For instance, for bosonic particles obeying $[a_i, a_j^\dagger] = \delta_{ij}$ we impose $[b_i, b_j^\dagger] = \delta_{ij}$. This is satisfied only if

$$\sum_l s_{il} s_{jl}^* = \delta_{ij}, \tag{1.20}$$

which is indeed the condition for a unitary matrix. For fermionic anticommutation relations $\{a_i, a_j^\dagger\} = \delta_{ij}$ we similarly require $\{b_i, b_j^\dagger\} = \delta_{ij}$, and obtain Eq. (1.20) once again. A convenient parametrization in terms of reflection and transmission probabilities satisfying Eq. (1.20) is

$$\begin{pmatrix} s_{31} & s_{32} \\ s_{41} & s_{42} \end{pmatrix} = \begin{pmatrix} \sqrt{R} & i\sqrt{T} \\ i\sqrt{T} & \sqrt{R} \end{pmatrix}. \tag{1.21}$$

Occupation numbers in input and output arms are given, respectively, by $n_i = a_i^\dagger a_i$ $(i = 1, 2)$ and $n_j = b_j^\dagger b_j$ $(j = 3, 4)$. Relations between input and output number operators read

$$n_3 = R n_1 + T n_2 + i\sqrt{RT}(a_1^\dagger a_2 - a_2^\dagger a_1), \tag{1.22}$$

$$n_4 = T n_1 + R n_2 - i\sqrt{RT}(a_1^\dagger a_2 - a_2^\dagger a_1). \tag{1.23}$$

We notice that the above equations fulfill the expected conservation of the total number operator, since $n_1 + n_2 = n_3 + n_4$.

Consider first the situation with only one particle incident on the beam splitter. Suppose, for instance, that input 2 is in the vacuum state and a single boson (or fermion) impinges on the mirror from channel 1. We have thus $\langle n_1 \rangle = 1$, $\langle n_2 \rangle = 0$ and $\langle (\Delta n_1)^2 \rangle = \langle (\Delta n_2)^2 \rangle = 0$ (with $\Delta n_i = n_i - \langle n_i \rangle$). Let us consider the expected values for n_3 and n_4 in output arms and their fluctuations. One immediately finds the reasonable results $\langle n_3 \rangle = R$ and $\langle n_4 \rangle = T$ for the occupation numbers, which only reveal reflection and transmission properties of the mirror in a simple fashion. Similarly, one obtains the following auto-correlation and cross-correlation signals between outputs

$$\left\langle \Delta n_3^2 \right\rangle = \left\langle \Delta n_4^2 \right\rangle = - \left\langle \Delta n_3 \Delta n_4 \right\rangle = RT. \tag{1.24}$$

Fluctuation in the detected number of particles described by Eq. (1.24) are called *partition noise*, since they are due only to random partition occurring at the beam splitter. In particular, partition noise for the simple case of a one-particle state in input arm 1 is proportional to the product RT and vanishes both for a completely transparent and a completely reflecting barrier. This is due to the fact that in both cases there is no random partition of the incoming "beam", as only one output arm is accessible. As a result, occupation number of the output states cannot fluctuate. We note that no difference between fermions and bosons arises in the above result. This is not a great surprise, since the different character of bosonic and fermionic statistics becomes manifest only in multi-particle states. We thus move to the more interesting case of two-particle interference.

1.4.1 Two particle interferometry

Imagine now that both input channels of the setup in Fig. 1.1 host a particle, either a boson or a fermion. We must assume that the two particles arrive *simultaneously* at the beam splitter in order to observe the effect of multi-particle physics. In this case, the average number of particles detected at both outputs reads

$$\langle n_3 \rangle = R \langle n_1 \rangle + T \langle n_2 \rangle = R + T = 1, \tag{1.25}$$

$$\langle n_4 \rangle = T \langle n_1 \rangle + R \langle n_2 \rangle = T + R = 1. \tag{1.26}$$

Therefore, each detector measures exactly one particle on average, regardless of the statistics and the transmission coefficient of the mirror. Let us now consider the average value $\langle n_3^2 \rangle$. We have

$$\begin{aligned} \left\langle n_3^2 \right\rangle &= R^2 \left\langle n_1^2 \right\rangle + T^2 \left\langle n_2^2 \right\rangle + 2RT \left\langle n_1 n_2 \right\rangle + RT \left\langle a_1^\dagger a_2 a_2^\dagger a_1 + a_2^\dagger a_1 a_1^\dagger a_2 \right\rangle = \\ &= 1 + RT(2 \pm 2), \end{aligned} \tag{1.27}$$

where the upper sign accounts for the bosonic case, while the lower accounts for fermions. Here the different sign in the last contribution is due to the fact $a_i a_i^\dagger = 1 \pm a_i^\dagger a_i$, depending on the statistics. Equation (1.27) is manifestly symmetric with respect to the mutual exchange of R with T, thus $\langle n_4^2 \rangle = \langle n_3^2 \rangle$. From the conservation relation $n_1 + n_2 = n_3 + n_4$ we easily obtain the average value $\langle n_3 n_4 \rangle$, which reads

$$\begin{aligned} \langle n_3 n_4 \rangle &= RT \left[\langle n_1^2 \rangle + \langle n_2^2 \rangle - \langle n_1 \rangle - \langle n_2 \rangle - (2 \pm 2) \langle n_1 n_2 \rangle \right] + \langle n_1 n_2 \rangle \\ &= 1 - RT(2 \pm 2). \end{aligned} \tag{1.28}$$

We finally obtain the following relation for the average fluctuations of the occupation numbers

$$\langle \Delta n_3^2 \rangle = \langle \Delta n_4^2 \rangle = - \langle \Delta n_3 \Delta n_4 \rangle = RT(2 \pm 2). \tag{1.29}$$

A very different behavior for bosons and fermions emerges. If we compare the above result with twice the partition noise of a single source [Eq. (1.24), so to speak], we see that fluctuations for the bosonic case are doubled, while fluctuations for the fermionic case are completely suppressed, namely

$$\mathcal{R} = \frac{\langle \Delta n_3^2 \rangle_{2 \text{ particles}}}{2 \langle \Delta n_3^2 \rangle_{1 \text{ particle}}} = \begin{cases} 2 & \text{for bosons,} \\ 0 & \text{for fermions.} \end{cases} \tag{1.30}$$

What is the physical origin of this result? The answer can be traced back to Eq. (1.28), which basically measures of the probability of detecting one particle in both output arms. Indeed, operator $n_3 n_4$ gives a nonzero contribution to the average only in such cases where the two input particles are scattered into two different outputs (otherwise, either n_3 or n_4 is zero). This happens when they are both reflected or both transmitted at the beam splitter. In the case of fermionic particles, Eq. (1.28) just reads $\langle n_3 n_4 \rangle = 1$, independently of the transmission coefficient of the barrier. The interpretation is simple: two indistinguishable fermions must avoid each other because of the Pauli exclusion principle. As a result, exactly one particle is always recorded in each detector, with no fluctuations. Bosons, instead, behave in a much different way. Equation (1.28) tells us that the probability that two bosons exit on opposite sides is $P(1,1) = 1 - 4T(1-T)$. Probabilities of finding 2 particles in output 3 and no particle in 4 or viceversa are equal (for symmetry reasons) and given by $P(2,0) = P(0,2) = 2T(1-T)$. $P(1,1)$ is obviously 1 for $T = 0$ and $T = 1$. Conversely, in the region where $T \approx R$ the probability $P(1,1)$ is strongly suppressed, and vanishes exactly for $T = R = 0.5$. Interestingly enough, this means that two indistinguishable bosons are forced to exit on the same channel in a symmetric beam splitter with equal transmission and reflection probability.

We now comment on the possible outcome of a more realistic experiment, in which wavepackets with a finite spatial extension are sent to the interferometer

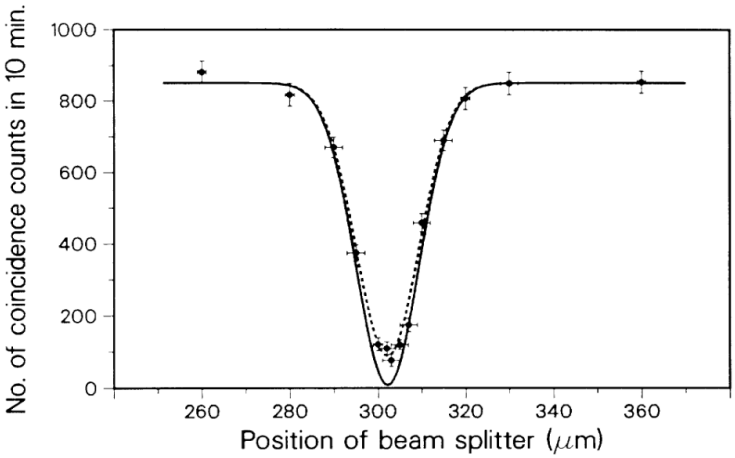

Figure 1.2: From Ref. [53]. The number of photon coincidences in the output arms of the interferometer is reported against the position of the beam splitter, which controls the delay between arrivals. An almost complete dip around 302 μm is evident. The interferometer is in this case nearly perfectly symmetric, as a direct measurement of the transmission coefficient yields $R/T \approx 0.95$.

and do not reach the beam splitter simultaneously, but with a certain time delay t_D. We assume that the measurement is carried out for a sufficiently long time in order to record both particles in the detectors, independently of the delay (in other words, the measurement lasts for a time $\tau \gg t_D$). We start the discussion by considering the bosonic case. When the delay is long enough to avoid any significant overlap between the wavepackets at the beam splitter, the measurement is well described by the single particle picture given in Eq. (1.24) times a factor 2. On the other hand, for $t_D = 0$ we expect to see the suppression of coincidence counts described above in Eq. (1.28). An intermediate regime with partial overlap between packets gives rise to partial suppression of the signal. Thus, the number of coincidence counts plotted as a function of t_D has the shape of a dip, whose width is linked to the temporal extension of wavepackets. This is basically the effect observed by C.K. Hong, Z.Y. Ou and L. Mandel (HOM) in an optical two-photons interferometer. We report the HOM result in Fig. 1.2. The figure shows the number of coincidence counts recorded in 10 minutes against the position of the beam splitter. Indeed, the delay between two incoming photons is here controlled by displacing the beam splitter from its symmetry position, giving rise to different time of flights along input channels. The signal clearly drops from approximately 850 photon coincidences every 10 minutes to a minimum of less than 100 counts. The lack of perfect destructive interference is reasonably explained within the experimental apparatus. The estimated length of photon wave packets is approximately 100 fs. This effect, which states that photons in a symmetric beam splitter exits on the same side, is called *photon bunching*.

Is it possible to realize a similar experiment with fermions? The answer is

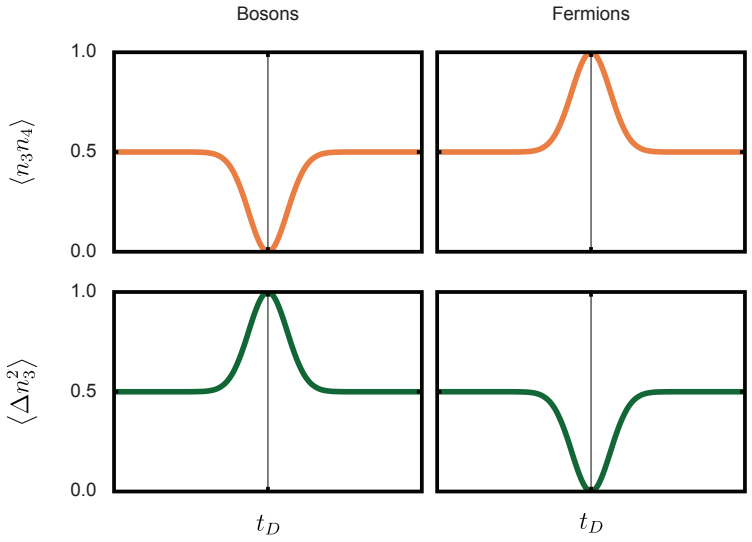

Figure 1.3: Comparison between boson bunching and fermion anti-bunching in a symmetric interferometer with $T = R = 1/2$. When two wavepackets with finite temporal extension collide at the beam splitter, different scenarios may emerge depending on the statistics and the time delay t_D between arrivals. At $t_D = 0$ the number of coincidence counts for bosons gets suppressed, while the one for fermions is enhanced [see Eq. (1.28)]. Fluctuations in the particle number measured by a single detector behave the opposite way: bosonic fluctuations are enhanced near $t_D = 0$, while fermionic ones are suppressed [see Eq. (1.29)].

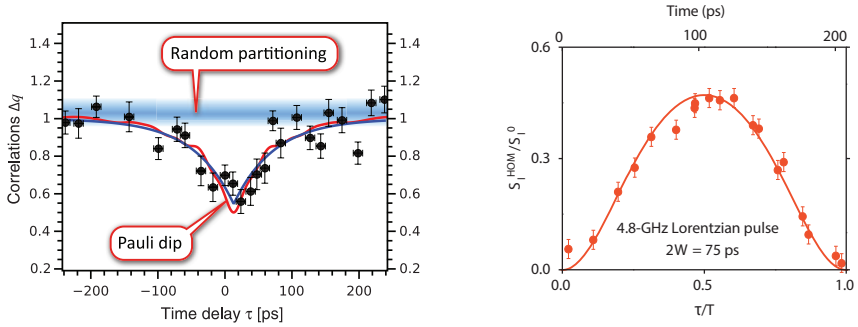

Figure 1.4: Fermionic HOM effect realized using two different single-electron sources in EQO (more details will follow in Chapter 2). A driven-quantum-dot setup known as *mesoscopic capacitor* is used on the left (figure taken from Ref. [12]), while a train of Lorentzian pulses is exploited on the right (figure adapted from Ref. [10]). In both cases the Pauli dip, namely the suppression of shot noise as a function of the delay τ, is evident. Note that both sources periodically emit single-electron excitations, and the corresponding HOM trace is periodic in τ with period T. However, the left panel is centered around $\tau = 0$, while the right panel shows a full period from $\tau = 0$ to $\tau = T$.

yes, and the framework within which this can be made is now called Electron Quantum Optics (EQO), in analogy with the traditional photonic quantum optics. We will introduce this field in the next Chapter and we'll deal with EQO throughout the rest of this thesis. Anticipating some results from the next Chapter, we briefly comment on the fermionc HOM experiments realized in Refs. [12] and [10]. Here, for practical purposes, fluctuations in one of the output arms are recorded instead of coincidence counts. One should notice that fluctuations in the particle number experience exactly the opposite effect compared to coincidence counts. Indeed, as expressed in Eq. (1.30) and summarized in Fig. 1.3, $\langle \Delta n_3^2 \rangle$ gets suppressed in the fermionic case and enhanced in the bosonic case. Hence the HOM effect for electrons is viewed as a dip in the noise known as *Pauli dip*, since it originates from the Pauli exclusion principle which prevents two electrons from exiting on the same arm. This statistical effect is called *fermion anti-bunching*, as opposed to the bunching effect displayed by bosons. Figure 1.4 shows two experimental detection of the Pauli dip in EQO experiments. We will give further details on the realization of the fermionic HOM experiment in the next Chapter, explaining how time-coherent single-electron sources are implemented, as well as electronic waveguides and beam splitters. For the moment, it is sufficient to notice that the noise measured in one of the output channels and normalized to twice the single particle partition noise drops significantly as the time delay between arrivals vanishes.

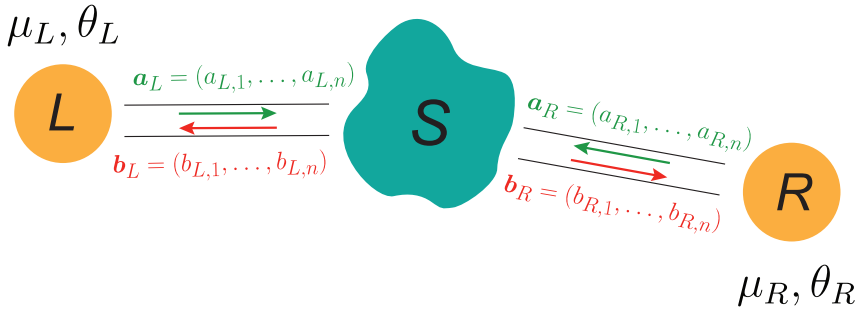

Figure 1.5: The essence of the scattering picture of quantum transport. The system is viewed as two reservoirs at equilibrium connected to the central scattering region through ballistic waveguides. The equilibrium distribution in each reservoir is described by the chemical potential $\mu_{L/R}$ and the temperature $\theta_{L/R}$. Amplitudes entering the central region from the reservoirs (green) are mixed by the scattering matrix of the systems and emerges as new outgoing amplitudes (red).

1.5 An introduction to the scattering matrix formalism

In this section we present the scattering matrix formalism, which is a very powerful method allowing to tackle a variety of problems regarding shot noise in mesoscopic physics. We actually sowed the seed of the scattering matrix formalism in the previous section, when we described the physics of two-particle interferometers in terms of a 2×2 matrix relating input and output states. In this Section we generalize this approach to a full quantum mechanical treatment of phase coherent, non-interacting quantum conductors. However, this Section is intended as a short introduction to the topic and is not complete. We'll mainly rely on Ref. [32] and the original paper on the scattering matrix method in the operator formalism by M. Büttiker [54], although other excellent reviews and books are available in the literature (see, e.g., Refs.[55–58]).

The statement of the problem is well summarized in Fig. 1.5. We consider a two-terminal quantum conductor, which consists of two electronic reservoirs, each one connected to the central scattering region by a coherent waveguide (or *lead*). Electronic reservoirs contain a very large number of particles and are assumed to be described by an equilibrium state with well defined chemical potential $\mu_{L/R}$ and temperature $\theta_{L/R}$. Electrons in the reservoirs thus follow the Fermi distribution

$$f_\alpha(E) = \frac{1}{e^{(E-\mu_\alpha)/(k_B\theta_\alpha)} + 1}, \quad \alpha = \{L, R\}. \tag{1.31}$$

Driving the system out of equilibrium corresponds to setting different chemical potentials and/or temperatures in different terminals. The dynamics in the conductor is entirely phase-coherent, which means that only elastic scattering events take place in the conductor, and energy is overall conserved (note,

however, that there must be some inelastic mechanism inside the reservoirs in order to achieve an equilibrium distribution).

Let us start the discussion with the simple case of a two-terminal quantum conductor. For each lead, we consider that the longitudinal direction coincides with the z axis. Due to strong confinement, motion in the transverse directions x, y is quantized and described by the set of orthonormal functions $\chi_{L/R,n}(x,y)$, labeled by the discrete index n. Let us introduce operators $a_{\alpha,n}(E)$ that annihilate an electron with total energy E in the n-th channel going from terminal α to the central scattering region.[4] They obey anticommutation relations

$$\left\{a_{\alpha,n}(E), a^{\dagger}_{\beta,m}(E')\right\} = \delta_{\alpha,\beta}\delta_{n,m}\delta(E-E'). \tag{1.32}$$

Note that the total energy E is determined by the sum of energies in the longitudinal and transverse channels, with the transverse energy in the n-th channel given by $E_{L,n}$. Similarly, operators $b_{\alpha,n}(E)$ annihilate an electron with energy E in the n-th channel going in the opposite direction. If N transverse channels are accessible, the field operator in the left waveguide reads

$$\psi_L(\boldsymbol{r},t) = \int_0^{+\infty} dE\, e^{-iEt/\hbar} \sum_{n=1}^{N} \frac{\chi_{L,n}(x,y)}{\sqrt{2\pi\hbar v_{L,n}(E)}} \left[a_{L,n}(E)e^{ik_{L,n}z} + b_{L,n}(E)e^{-ik_{L,n}z}\right], \tag{1.33}$$

with $v_{L,n}(E) = (\hbar/m)k_{L,n}(E)$ and $k_{L,n}(E) = \sqrt{2m(E-E_{L,n})}/\hbar$ for a quadratic dispertion.[5] Note that an analogous relation holds for the right waveguide. However, current conservation allows us to focus solely on the left side of the conductor. Relation between input and output operators is given, as in the previous section, by the scattering matrix of the system. Due to the presence of two terminals and N conduction channels per side, the full system is described by a $2N \times 2N$ matrix s. It reads

$$b_{\alpha,i} = \sum_{\beta=L,R} \sum_{j=1}^{N} s_{\alpha\beta,ij}\, a_{\beta,j}. \tag{1.34}$$

However, collecting operators in vectors $\boldsymbol{a}_\alpha = (a_{\alpha,1}, \ldots, a_{\alpha,N})$ and $\boldsymbol{b}_\alpha = (b_{\alpha,1}, \ldots, b_{\alpha,N})$ with $i = L, R$ allows for a compact expression of the scattering matrix in terms of four blocks:

$$\begin{pmatrix} \boldsymbol{b}_L \\ \boldsymbol{b}_R \end{pmatrix} = \begin{pmatrix} r & t' \\ t & r' \end{pmatrix} \begin{pmatrix} \boldsymbol{a}_L \\ \boldsymbol{a}_R \end{pmatrix} = s \begin{pmatrix} \boldsymbol{a}_L \\ \boldsymbol{a}_R \end{pmatrix}. \tag{1.35}$$

Here, each block r, t, t' and r' is a $N \times N$ matrix. Coefficients for r are given by $r_{ij} = s_{LL,ij}$, and similar relations hold for the remaining three blocks. Blocks

[4] To avoid confusion, we label terminals with Greek indices $\{\alpha, \beta, \ldots\}$ and use Roman indices $\{n, m \ldots\}$ for transverse channels.

[5] The integral in Eq. (1.33) runs from 0 to $+\infty$, as we are dealing with electrons with parabolic dispertion $E = \hbar^2k^2/(2m)$. Different dispertion relations may lead to different limits of integration.

on the diagonal account for reflection back to the left and right reservoirs respectively, while off-diagonal blocks describe transport, respectively, from left to right and from right to left. The scattering matrix is in general unitary, $ss^\dagger = \mathbb{1}$, and additional symmetries (such as time reversal, if present) further constrain the block components of s.

We now give the general results for current and noise in the scattering matrix formalism. For the sake of brevity, we focus on the main passages and refer the reader interested in a more detailed discussion to the literature [32, 56]. The one-dimensional current operator in the left lead is obtained by integrating the quantum-mechanical three-dimensional current density [59, 60] in the transverse directions x and y:

$$I_L(z,t) = \frac{\hbar e}{2im}\int dx\,dy\,\left[\psi_L^\dagger(\boldsymbol{r},t)\partial_z\psi_L(\boldsymbol{r},t) - \partial_z\psi_L^\dagger(\boldsymbol{r},t)\psi_L(\boldsymbol{r},t)\right]. \tag{1.36}$$

Let us insert the field operator Eq. (1.33) into Eq. (1.36). After some algebra, and neglecting the energy dependence of $v_{L,n}(E)$,[6] one gets the following position-independent result for the current operator:

$$I_L(t) = \frac{e}{h}\sum_{n=1}^{N}\int dE_1 dE_2 e^{i(E_1-E_2)t/\hbar}\left[a_{L,n}^\dagger(E_1)a_{L,n}(E_2) - b_{L,n}^\dagger(E_1)b_{L,n}(E_2)\right]. \tag{1.37}$$

In a very reasonable fashion, the current is given by a balance between incoming and outgoing particles, integrated over all the energy states.

The expectation value for I_L is found by recalling that particles going from the reservoirs to the scattering region are in an equilibrium state described by Eq. (1.31). Then operators $a_{\alpha,n}$ obey

$$\left\langle a_{\alpha,n}^\dagger(E_1)a_{\beta,n'}(E_2)\right\rangle = \delta_{\alpha,\beta}\delta_{n,n'}\delta(E_1-E_2)f_\alpha(E_1). \tag{1.38}$$

We now write Eq. (1.37) solely in terms of the operators $a_{\alpha,n}$, $a_{\alpha,n}^\dagger$ thanks to Eq. (1.34), and use the above relation to find the current in terms of the Fermi distribution in the reservoirs. We find

$$\begin{aligned}\langle I_L\rangle &= \frac{e}{h}\sum_{n=1}^{N}\int dE\left[f_L(E) - \sum_{\beta=L,R}\sum_{m=1}^{N} s_{L\beta,nm}^* s_{L\beta,nm} f_\beta(E)\right] = \\ &= \frac{e}{h}\sum_{n=1}^{N}\int dE\left\{\left[1-\sum_{m=1}^{N}|r_{nm}|^2\right]f_L(E) - \sum_{m=1}^{N}|t_{nm}|^2 f_\beta(E)\right\} = \\ &= \frac{e}{h}\int dE\,\mathrm{Tr}\left(t^\dagger t\right)\left[f_L(E) - f_R(E)\right].\end{aligned} \tag{1.39}$$

[6] This is a reasonable assumption in most cases, since only energies in a narrow window around the Fermi level play a relevant role, while $v_{L,n}(E)$ typically varies significantly on a much bigger scale. Therefore, we can safely assume the velocity $v_{L,n}(E)$ as constant.

The last passage follows from the unitarity of the scattering matrix. Indeed from $s^\dagger s = \mathbb{1}$ one finds $r^\dagger r + t^\dagger t = \mathbb{1}$ which leads to $\sum_m (|r_{nm}|^2 + |t_{nm}|^2) = 1$. We note that Eq. (1.39) is manifestly basis-independent, for it involves the trace of the matrix $t^\dagger t$. It can be expressed in terms of the eigenvalues $T_n(E)$ of $t^\dagger t$ in the following way:

$$\langle I_L \rangle = \frac{e}{h} \sum_{n=1}^{N} \int dE\, T_n(E) \left[f_L(E) - f_R(E) \right]. \tag{1.40}$$

Equation (1.40) gives the current in a mesoscopic two-terminal system in terms of the transmission eigenvalues in a very general way, as long as electron-electron interactions do not play a prominent role. It should be noticed that, in an equilibrium configuration with $\mu_L = \mu_R$ and $\theta_L = \theta_R$, Fermi distributions in the reservoirs are exactly the same and no current flows though the sample.

Consider now the situation in which the two-terminal system is driven out of equilibrium by a voltage bias V. For instance, imagine that the electrochemical potential in the left reservoir is brought below the Fermi level, namely $\mu_L = E_\mathrm{F} - eV$ while $\mu_R = E_\mathrm{F}$, with equal temperature θ on both sides. As the energy scale set by eV is usually much smaller than E_F, the integral in Eq. (1.40) is dominated by a small energy window of width $\sim eV$ around the Fermi level. Thus, we can neglect the energy dependence of $T_n(E)$ in this short interval and perform the integration over the Fermi distributions, getting

$$\langle I_L \rangle \approx \frac{e}{h} \sum_{n=1}^{N} T_n(E_\mathrm{F}) \int dE \left[f_L(E) - f_R(E) \right] = \frac{e^2}{h} V \sum_{n=1}^{N} T_n(E_\mathrm{F}), \tag{1.41}$$

where the last passage holds for $E_\mathrm{F} \gg \{eV, k_\mathrm{B}\theta\}$. Thus, the conductance $G = \langle I_L \rangle / V$ for a two-terminal mesoscopic system in presence of N conduction channels is generally given by[7]

$$G = \frac{e^2}{h} \sum_{n=1}^{N} T_n. \tag{1.42}$$

This famous and very important result is known as *Landauer-Büttiker formula* [61–64]. It relates the conductance of a phase coherent quantum conductor to the transmission eigenvalues of the available conduction channels.

We now apply the scattering matrix formalism to the calculation of the noise spectrum. We focus on the autocorrelation spectrum of $\Delta I_L = I_L - \langle I_L \rangle$, which is given by

$$S(\omega) = 2 \int_{-\infty}^{+\infty} d\tau\, e^{i\omega\tau} \left\langle \Delta I_L(t) \Delta I_L(t+\tau) \right\rangle. \tag{1.43}$$

[7] In the following, the notation T_n without the energy argument stands for the n-th transmission eigenvalue evaluated at the Fermi level, i.e. $T_n \equiv T_n(E_\mathrm{F})$.

The calculation relies on the same passages used for $\langle I_L \rangle$ (one only resorts to Wick's theorem to evaluate the four-operator average $\langle a^\dagger_{\alpha_1,n_1} a_{\alpha_2,n_2} a^\dagger_{\alpha_3,n_3} a_{\alpha_4,n_4} \rangle$ as a product of two operator averages). At the end of the day, one is left with

$$S(\omega) = 2\frac{e^2}{h}\int dE\ \mathrm{Tr}\big(tt^\dagger tt^\dagger\big)\{f_L(E)[1-f_L(E-\hbar\omega)]+ \tag{1.44}$$

$$+ f_R(E)[1-f_R(E-\hbar\omega)]\}+ \tag{1.45}$$

$$+ 2\frac{e^2}{h}\int dE\ \mathrm{Tr}\big(rr^\dagger tt^\dagger\big)\{f_L(E)[1-f_R(E-\hbar\omega)]+ \tag{1.46}$$

$$+ f_R(E)[1-f_L(E-\hbar\omega)]\}. \tag{1.47}$$

This is once again a basis-independent formula, which can be rewritten in terms of the eigenvalues using the relations $\mathrm{Tr}\big(tt^\dagger tt^\dagger\big) = \sum_n T_n^2(E)$ and $\mathrm{Tr}\big(rr^\dagger rr^\dagger\big) = \sum_n R_n^2(E) = \sum_n [1-T_n(E)]^2$. The final result is

$$S(\omega) = 2\frac{e^2}{h}\sum_{n=1}^{N}\int dE\, T_n^2(E)\{f_L(E)[1-f_L(E-\hbar\omega)]+ \tag{1.48}$$

$$+ f_R(E)[1-f_R(E-\hbar\omega)]\}+ \tag{1.49}$$

$$+ 2\frac{e^2}{h}\sum_{n=1}^{N}\int dE\, R_n(E)T_n(E)\{f_L(E)[1-f_R(E-\hbar\omega)]+ \tag{1.50}$$

$$+ f_R(E)[1-f_L(E-\hbar\omega)]\}. \tag{1.51}$$

We will be interested in the zero frequency noise $S(0)$, and drop the argument (0) to make the notation simpler. As for the calculation of the current, we assume a dc voltage drop of the form $\mu_R = E_\mathrm{F} = \mu_L + eV$ and no temperature gradient. One then finds that the products of Fermi distributions give nonvanishing contributions only in very thin energy windows around the Fermi level, and the zero-frequency shot noise is governed by transmission and reflection eigenvalues at the Fermi level. Finally, one gets

$$S = 4\frac{e^2}{h}k_\mathrm{B}\theta\sum_{n=1}^{N}T_n^2 + 2\frac{e^2}{h}eV\coth\left(\frac{eV}{2k_\mathrm{B}\theta}\right)\sum_{n=1}^{N}T_n(1-T_n). \tag{1.52}$$

This is a rather general result, provided that E_F is still the largest energy scale in the problem. However, it is instructive to focus on particular cases to fully appreciate the physic contained in Eq. (1.52).

Equilibrium (thermal) noise

We use the fact that $\coth(x) = 1/x + O(x)$ around $x = 0$ to find the limit $V \to 0$ in Eq. (1.52) (i.e. the noise at equilibrium). We find

$$S = 4\frac{e^2}{h}k_\mathrm{B}\theta\sum_{n=1}^{N}T_n = 4Gk_\mathrm{B}\theta, \tag{1.53}$$

thus recovering the Johnson-Nyquist relation between thermal noise and conductance already discussed in Section 1.2, Eq. (1.11).

Shot noise at zero temperature

Using $\lim_{x\to\pm\infty}\coth(x) = \pm 1$ we immediately find the behavior of S at temperature $\theta = 0$:

$$S = 2\frac{e^2}{h}e|V|\sum_{n=1}^{N} T_n(1-T_n). \tag{1.54}$$

Equation (1.54) was first derived by G. Lesovik in 1989 [65]. We notice that the shot noise vanishes both for completely open ($T_n = 1$) or completely closed ($T_n = 0$) channels. As in the case of the two particle interferometer discussed in Section 1.4.1, the motivation is straightforward: in both cases particles have no choice, for they can only be reflected back to the original reservoir ($T_n = 0$) or fully transmitted to the opposite one ($T_n = 1$). As a result, the current across the system cannot fluctuate.

Interestingly enough, the zero-frequency shot noise does not follow the Schottky relation Eq. (1.18). The latter is only recovered in the low transmission limit, where all contributions T_n^2 can be safely neglected and the shot noise reads

$$S = 2\frac{e^2}{h}e|V|\sum_{n=1}^{N} T_n = 2e\left\langle I_L\right\rangle. \tag{1.55}$$

In practice, when at least one of the transmission eigenvalues is large enough to deviate significantly from the linear approximation, Eq. (1.54) shows us that the shot noise is suppressed below the Poissonian value predicted by Schottky. In such cases, the noise is said to be *sub-Poissonian*. Let us remember that Schottky description assumes uncorrelated transmission events. We have thus discovered that the shot noise in a mesoscopic conductor with generic transmission eigenvalues T_n bears signatures of statistical correlation between particles. Effect of quantum statistics are only washed out in the low transmission regime, where transmission events are rare enough to be substantially uncorrelated. An efficient way to measure the degree of deviation from the Schottky value relies on the so called Fano factor, which is given by the ratio

$$F = \frac{S}{2e\left\langle I_L\right\rangle}, \tag{1.56}$$

which was introduced by U. Fano in a completely different context [66]. The Fano factor is $F = 1$ for a Schottky-like process, while it drops below one for sub-Poissonian noise. In the framework of the scattering matrix formalism it reads

$$F = \frac{\sum_{n=1}^{N} T_n(1-T_n)}{\sum_{n=1}^{N} T_n}. \tag{1.57}$$

The scattering matrix formalism is extremely powerful, as it is able to predict the current and noise measured in a generic mesoscopic system on the basis of simple input/output relations. Experimental evidence for the validity of this approach is reviewed in the following section.

1.6 Experiments on shot noise

1.6.1 Tunnel junctions

A tunnel junction is made of a thin insulating layer separating two conducting electrodes. As electrons have to move through the insulator, transmission probability is very low and we can safely neglect all terms $\sim T_n^2$ in Eq. (1.52). As a result, the two-terminal shot noise at finite temperature reads

$$S = 2\frac{e^2}{h} eV \coth\left(\frac{eV}{2k_B\theta}\right) \sum_{n=1}^{N} T_n = 2e \coth\left(\frac{eV}{2k_B\theta}\right) \langle I_L \rangle . \tag{1.58}$$

An experiment by H. Birk *et al.* measured fluctuations in the tunneling current flowing from a scanning tunneling microscope tip to an Au film [67]. Such a setup can be safely considered as a tunnel junction and should test the validity of Eq. (1.58). The experiment found excellent agreement with the theory, as shown in Fig. 1.6. In particular, two very different regimes emerge from Eq. (1.58), corresponding to the opposite limits $x = eV/k_B\theta \gg 1$ and $x \ll 1$. At high voltage (or very low temperature) we have $\coth(x) = \pm 1$ and the Schottky noise $S = 2e\langle I \rangle$ is recovered. In the opposite limit, thermal fluctuations dominate and we get the Johnson-Nyquist result $S = 4Gk_B\theta$. The result of Ref. [67] provides a nice experimental evidence for the crossover between these two regimes: the shot noise as reported in Fig. 1.6 grows linearly with $|\langle I \rangle|$ at low temperature, but deviates from the linear behavior at sufficiently high temperature. In the latter case it is approximately constant around the point $\langle I \rangle = 0$. It's worth noticing that the ratio $S/\langle I \rangle$ is in this case a universal function of $eV/k_B\theta$. As such, it can be used to extract the temperature with a great degree of precision, since the voltage drop is usually a known quantity. The technique relying on such a scheme is known as shot noise thermometry [42].

1.6.2 Conductance and noise of a quantum point contact

We have seen that the scattering matrix description of quantum transport relies on transmission/reflection properties of the electronic channel involved. However, under ordinary conditions, electronic motion in metals is usually affected by a huge number of random events (electron-electron collisions, scattering with phonons, scattering against impurities and so on) which makes the dynamics unpredictable. Thus, in order for the scattering approach to become

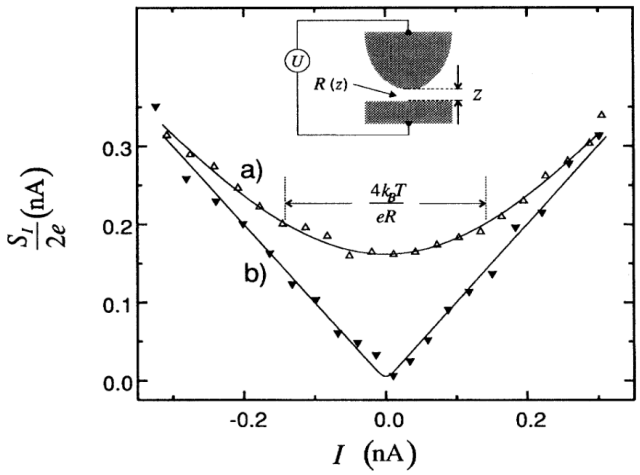

Figure 1.6: Shot noise versus current in a tunnel junction as reported by Ref. [67]. The junction is realized with a scanning tunneling microscope tip positioned above a layer of Au, as suggested by the inset. The two set of points correspond to temperature $\theta = 300\,\mathrm{K}$ and tunneling resistance $R_T = 0.32\,\mathrm{G\Omega}$ for empty triangles, $\theta = 77\,\mathrm{K}$ and $R_T = 2.7\,\mathrm{G\Omega}$ for filled triangles. The agreement with solid lines, calculated from Eq. (1.58), is excellent.

effective, one must deal with a quantum system where the motion is quantized into a finite number of sub-bands and the sources of reflectivity are known and, in principle, controllable.

For this reason, experiments are usually conducted in a 2DEG obtained at the interface between two carefully chosen semiconductors. Here, electronics levels are quantized to due confinement and the mobility can be made high enough to attain a ballistic transport regime. With this scheme, one almost completely eliminates unwanted reflection events and reaches a quantum regime where electronic sub-bands are quantized. Now, in order to alter the transmission properties of each sub-band, a metallic gate is usually deposited on top of the sample in such a way to deplete electrostatically the underlying portion of the 2DEG. This structure is called QPC and creates a controllable constriction in the electron gas: indeed, a change in the gate voltage reflects into a change in the width of the constriction, and thus in the transmission probability across the sample.

According to Eq. (1.42), such a system will show a step-like two-terminal conductance as a function of the gate voltage when driven out of equilibrium. This is exactly what Bart van Wees and collaborators reported in 1988 in a seminal experiment, which showed the conductance quantization of a QPC for the first time [68]. Their result is reported in Fig. 1.7 together with a scheme of the QPC. While sweeping the gate voltage, the conductance in unit of $2e^2/h$ displays a series of plateaus corresponding to integer values, with the factor 2 due to spin degeneracy. Jumps between adjacent plateaus are interpreted as

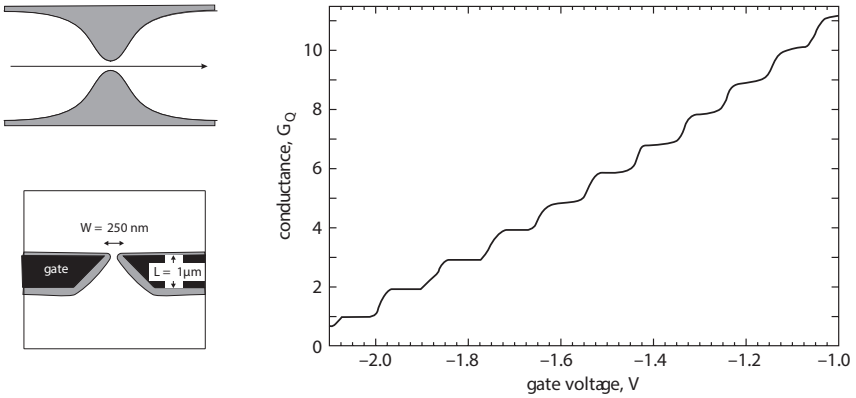

Figure 1.7: Top left: a QPC consists of a narrow constriction in a 2DEG. This geometry allows to control the number of open channels available for transport. Bottom left: scheme of the QPC used in Ref. [68]. Right: experimental evidence of quantized conductance in a QPC as measured by B.J. van Wees *et al.* [68]. Figure adapted from [56].

the closing or opening of a new transmission channel. In this regard, it is worth noticing that transmission eigenvalues in such a system are not expected to be exactly step-like. Rather, they are a smooth function of the gate voltage, and so is the transition between successive plateaus. A similar result was subsequently reported in Ref. [69].

Since conductance of a QPC is extremely well described by the Laudauer-Büttiker formalism, it is natural to expect that the scattering approach will be equally valid for the shot noise. Equation (1.54) states that the shot noise should vanish when all channels are either completely open or completely closed, that is, in correspondence of conductance plateaus. On the contrary, peaks should be observed when the conductance jumps from one plateau to the next one, cause this happens when one of the channels is only partially open (so that both T_n and $1-T_n$ are nonzero). This oscillation between suppression and peaks was experimentally demonstrated at the Weizmann institute [70] and Saclay [71], as shown in Fig. 1.8.

Since the mid '90s, shot noise suppression below the Poissonian level has been reported in a number of situations [32]. Beenakker and Büttiker argued that the scattering approach is still somewhat valid also for non-ballistic conductors in the diffusive regime, provided that phase coherence is preserved (i.e. the conductor is much longer that the mean free path of electrons, but still shorter than the typical inelastic scattering length) [72]. In this case, transmission eigenvalues are not fixed, but randomly distributed according to a bimodal function. Current and noise are then obtained as an ensemble average in the framework of the random matrix theory [73]. It turns out that the Fano factor is $F = 1/3$ and it is universal for every diffusive metal. The 1/3 suppression of shot noise was subsequently demonstrated in the experiment by M. Henny *et al.* [74].

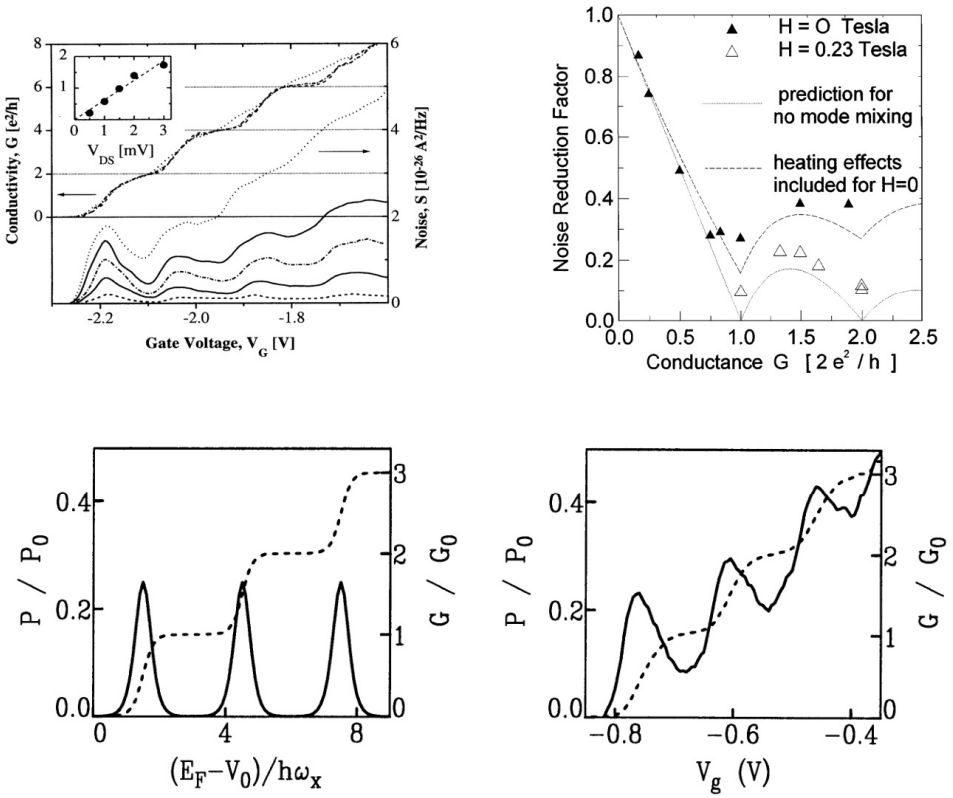

Figure 1.8: Suppression of shot noise in a QPC. Top left: data by Reznikov *et al.* [70] show that the noise drops whenever the conductance is quantized in unit of e^2/h, as suggested by Eq. (1.54). Different curves are generated by different values of the source-drain voltage V_{DS}. Top right: a similar experiment by Kumar *et al.* [71] reports minima of the Fano factor introduced in Eq. (1.57) for $G = n \cdot 2e^2/h$, $n \in \mathbb{N}$. The factor 2 is due to spin degeneracy. Bottom: theory (left) and unpublished data (right) from Reznikov *et al.* at lower temperature $T = 0.4$ K (from Ref. [58]). Suppression of the shot noise, although not complete, is clearly visible.

Surprisingly, an atomically thin junction displays the same physics of the QPC. This result was pointed out in the experiment H. Van den Brom and J. van Ruitenbeek, who basically used Eqs. (1.54) to infer the number of electronic channels contributing to transport in Au and Al contacts and their transmission properties [75].

After a countless stream of glaring examples of the usefulness of noise in mesoscopic physics, we are now convinced that Rolf Landauer was indeed right: quite often, the noise *is* the signal.

1.7 Photoassisted shot noise

We now come to a crucial point for the development of this thesis: the connection between shot noise and ac driven quantum systems, which will bring us to the physics of Photoassisted Shot Noise (PASN).

1.7.1 Tien-Gordon model

This tale starts in the early '60s, that is, well before the development of mesoscopic physics. Relying on the tunneling Hamiltonian approach, works by J. Bardeen and M. Cohen and collaborators showed that the tunneling current in a superconductor-insulator-superconductor junction can be expressed in terms of the Fermi distributions $f_{A/B}(E)$ and the density of states $\rho_{A/B}(E)$ of the two superconducting layers A and B [76, 77]. In the presence of a dc voltage bias $V_{\rm dc}$, their result reads

$$I_{AB} = C \int dE\, \rho_A(E)\rho_B(E)[f_A(E) - f_B(E)] \tag{1.59}$$

to lowest order in the tunneling, where $f_A(E)$ is the equilibrium Fermi distribution for layer A and $f_B(E) = f_A(E + eV_{\rm dc})$. Here, C is an unimportant constant related to the tunneling amplitude. In 1962 Dayem and Martin put a superconducting tunnel junction in a microwave cavity and observed that, while sweeping the dc bias across the junction, the tunneling current developed multiple steps instead of the expected single jump. Interestingly, steps were separated by an increase of $\hbar\omega/e$ in the dc bias, where ω is the angular frequency of the microwave field [78]. An example of such features is shown in Fig. 1.9.

Tien and Gordon were able to explain the experimental observation in a remarkably simple way [79]. Assume that, in the absence of any voltage bias, the two superconducting layers A and B are described by time-independent Hamiltonians $H_{A/B,0}$, and electronic wavefunctions are given by $\psi_{A/B,0}(\boldsymbol{r}, t) = \psi_{A/B,0}(\boldsymbol{r})e^{-iEt/\hbar}$. Then, switching on the microwave field and neglecting its interaction with the insulating layer, a potential difference between layers A and B is set up. Taking the former as a reference, the Hamiltonian for B reads

$$H_B = H_{B,0} + V_{\rm ac}\cos(\omega t). \tag{1.60}$$

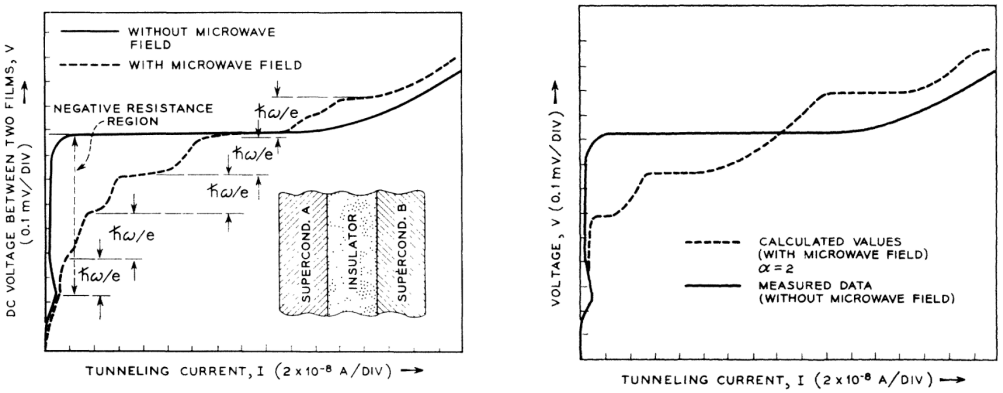

Figure 1.9: Left: experimental results by Dayem and Martin, showing recurring structures separated by steps of $\hbar\omega/e$ in the voltage bias [78]. Right: theoretical curve obtained by Tien and Gordon for $\alpha = eV_{\rm ac}/(\hbar\omega) = 2$ juxtaposed with the measured signal without microwave radiation. From Ref. [79].

Here a crucial assumption has been made, namely that the potential oscillates in time but is spatially uniform. By solving the full Schrödinger equation for this new Hamiltonian, it turns out that a purely time-dependent voltage cannot modify the spatial distribution of the wavefunction, which is indeed given by

$$\psi_B(\boldsymbol{r},t) = \psi_{B,0}(\boldsymbol{r})e^{-iEt/\hbar}e^{-i\alpha\sin(\omega t)}, \quad \alpha = \frac{eV_{\rm ac}}{\hbar\omega}. \tag{1.61}$$

The only effect of the oscillating bias is to add a new phase factor to the wavefunction. We get a very meaningful physical insight by realizing that the time periodic phase factor $e^{-i\alpha\sin(\omega t)}$ can be easily written as a Fourier series, thanks to the integral representation of the Bessel function $J_n(x)$ [80]. The wavefunction then reads

$$\psi_B(\boldsymbol{r},t) = \sum_{n=-\infty}^{\infty} J_n(\alpha)\psi_{B,0}(\boldsymbol{r})e^{-i(E+n\hbar\omega)t/\hbar}. \tag{1.62}$$

Now the physics becomes clear. Assuming a position-independent voltage bias, electronic states at energy E are modified into an infinite superposition of states at energies $E+n\hbar\omega$, each one weighted by the amplitude $J_n(\alpha)$. In other words, the ac potential induces inelastic scattering events where electrons can absorb ($n>0$) or emit ($n<0$) an integer number of energy quanta $\hbar\omega$ from the oscillating field (i.e. photons). The problem is now fully equivalent to an infinite set of dc junctions with an effective voltage $\widetilde{V}_n = V_{\rm dc} + n\hbar\omega$. The natural consequence of this fact is that the dc component of the tunneling currents now reads

$$I_{AB} = C\int dE \sum_{n=-\infty}^{\infty} |J_n(\alpha)|^2 \rho_A(E)\rho_B(E+n\hbar\omega)[f_A(E)-f_B(E+n\hbar\omega)]. \tag{1.63}$$

We see an interesting effect in Eq. (1.63). In a dc junction, an electron in A with energy E can only tunnel in a corresponding empty energy state E in B. Now, by absorbing or emitting photons, it gains access to all energy states $E + n\hbar\omega$, with n an integer. The term *photoassisted transport* is ultimately due to this simple and rather intuitive idea.

Applying Eq. (1.63) to the experimental setup of Ref. [78], one obtains the theoretical curve shown in the right panel of Fig. 1.9. It can be seen that, due to the photoassisted effect, features of the dc current are replicated at every integer multiple of $\hbar\omega$. Any isolated peculiarity of the dc curve occurring at a given value V_0 of the voltage, such as peak, step, cusp, etc., is replicated at $V_0 + \hbar\omega n/e$. The magnitude of the original peculiarity is spread between the new ones with the weights $J_n(\alpha)$ [56]. This is, in short, the essence of the photoassisted transport formalism.

Although specifically derived for the case of a superconducting tunnel junction, ideas by Tien and Gordon turned out to be extremely general and far reaching. With the birth of mesoscopic physics, the photoassisted formalism has been first applied to tunneling currents in quantum dots [81, 82], and then to the study of shot noise in phase coherent conductors. An experiment by R. Schoelkopf and collaborators [83], inspired by earlier theoretical work by G. Lesovik and L. Levitov [84], has shown the validity of Tien-Gordon approach in describing the shot noise in diffusive metallic systems whose length is shorter than the inelastic mean free path. The very same research group demonstrated, in a subsequent work, that photoassisted features occurring at $V_{\rm ac} = n\hbar\omega/e$ in a normal conductor are shifted to $V'_{\rm ac} = n\hbar\omega/(2e)$ when a normal metal-superconductor junction is investigated [48]. This happens due to Andreev reflection mechanism, which leads to the transfer of a charge $2e$ across the interface instead of e [46].

1.7.2 Floquet scattering matrix

The connection between the Tien-Gordon model and the scattering approach has been developed in a number of works covering the late '90s and early 2000s, and finally formalized in the so called Floquet scattering matrix approach [85–87]. In what follows, we summarize the main points of this useful formalism. Consider the same two-terminal configuration of Sec. 1.5 in the presence of a time dependent bias $V(t) = V_{\rm dc} + V_{\rm ac}(t)$ applied to the left reservoir. Assume also that $V_{\rm ac}(t)$ is a time-periodic function with period $T = 2\pi/\omega$ which averages to zero over one period. Recalling Eq. (1.37), the current operator in the scattering approach is expressed as a balance between particles going from the lead to the scattering region (represented by $a_{\alpha,n}$, $a^\dagger_{\alpha_n}$) and from the scattering region to the leads ($b_{\alpha,n}$, $b^\dagger_{\alpha,n}$). As in the Tien-Gordon model, we now assume that the energy distribution of particles incoming from left is modified by the ac field. We write them as a superposition of particles at energy $E + l\hbar\omega$,

namely

$$a_{L,n}(E) = \sum_{l=-\infty}^{+\infty} p_l \, a'_{L,n}(E - l\hbar\omega), \tag{1.64}$$

where operators $a'_{L,n}(E)$ are distributed according to the equilibrium distribution of reservoir L (which still contains a finite dc offset due to the dc component $V_{\rm dc}$ of the bias). Here, coefficients p_l are the absorption or emission amplitudes given by

$$p_l = \int \frac{dt}{T} e^{il\hbar\omega t} e^{-i(e/\hbar)\int_0^t dt' \, V_{\rm ac}(t')}. \tag{1.65}$$

They are nothing but the generalization of the Bessel function of Tien-Gordon model for an arbitrary time-periodic ac voltage. The calculation of current and noise now follows the one presented in Sec. 1.5, with the only difference given by the new nonequilibrium distribution of incoming particles given by Eq. (1.64). We only quote the final result for the dc component of the current, which (not so surprisingly) reads

$$\overline{\langle I_L \rangle} = \frac{e}{h} \sum_{n=1}^{N} \int dE \, T_n(E) \sum_{l=-\infty}^{+\infty} |p_l|^2 \left[f_L(E - l\hbar\omega) - f_R(E) \right]. \tag{1.66}$$

Here (and in the rest of the thesis) we use the notation $\overline{X} = T^{-1} \int_0^T dt \, X(t)$ for the temporal average of the quantity X over one period T. If transmission eigenvalues vary slowly enough with respect to the energy scale $eV_{\rm dc}$, we take T_n out of the integral, as in Sec. 1.5. Since $\sum_l |p_l|^2 = 1$ and $\sum_l l|p_l|^2 = 0$ (see Appendix A), we are left with the same result of the dc case, namely

$$\overline{\langle I_L \rangle} = \frac{e}{h} \sum_{n=1}^{N} T_n \sum_{l=-\infty}^{+\infty} |p_l|^2 (eV_{\rm dc} + l\hbar\omega) = \frac{e^2}{h} V_{\rm dc} \sum_{n=1}^{N} T_n. \tag{1.67}$$

Thus, in the case of almost constant transmission and linear IV response, the effect of photoassisted transport is completely washed out and the current is just proportional to the dc component of the voltage drive. This is a reasonable result for an ordinary metal. Let us notice that this cancellation does not arise in the original theory by Tien and Gordon since they take into account a superconducting tunnel junction (whose IV response is as much nonlinear as possible!).

We now turn the attention on the zero-frequency PASN, defined as

$$\mathcal{S} = 2 \int_0^T \frac{dt}{T} \int_{-\infty}^{+\infty} d\tau \, \langle \Delta I_L(t) I_L(t+\tau) \rangle \, . \tag{1.68}$$

As for the photossisted current, the calculation is lengthy but straightforward, and follows step by step the one shown in Sec. 1.5 for the dc case. However,

in this case we get a far less trivial result:

$$\begin{aligned}\mathcal{S} = 2\frac{e^2}{h}\sum_{n=1}^{N}\int dE\, T_n^2(E)\times \\ \times\left\{\sum_l |p_l|^2 f_L(E-l\hbar\omega)[1-f_L(E-l\hbar\omega)] + f_R(E)[1-f_R(E)]\right\} + \\ + 2\frac{e^2}{h}\sum_{n=1}^{N}\int dE\, R_n(E)T_n(E)\times \\ \times\sum_l |p_l|^2\left\{f_L(E-l\hbar\omega)[1-f_R(E)] + f_R(E)[1-f_L(E-l\hbar\omega)]\right\}.\end{aligned} \tag{1.69}$$

Interestingly enough, the equilibrium term (first two lines) stays unaffected by the ac drive, thanks to the property $f_{L/R}(E)[1-f_{L/R}(E)] = -k_B\theta\partial_E f_{L/R}(E)$. This is not the case, however, for the nonequilibrium part of the noise. Neglecting the variation of transmission eigenvalues with energy we get

$$\begin{aligned}\mathcal{S} = 4\frac{e^2}{h}k_B\theta\sum_{n=1}^{N}T_n^2 + \\ + 2\frac{e^2}{h}\sum_{n=1}^{N}T_n(1-T_n)\sum_l |p_l|^2(eV_{dc}+l\hbar\omega)\coth\left(\frac{eV_{dc}+l\hbar\omega}{2k_B\theta}\right).\end{aligned} \tag{1.70}$$

Differently from the averaged current, the PASN is drastically modified by the ac drive even in the case of a simple metallic system with linear IV characteristic. The reason is pretty simple. For a dc voltage bias, the shot noise is proportional to $eV\coth(eV/k_B\theta)$ and is thus nonlinear in V. In Eq. (1.70) we see an infinite superposition of dc signals driven by an effective bias $V_{dc}+l\hbar\omega/e$. In this case the series in l is not trivial and bears signature of the photoassisted transport mechanism. At zero temperature the equilibrium term vanishes and the PASN is

$$\mathcal{S} = 2\frac{e^2}{h}\sum_{n=1}^{N}T_n(1-T_n)\sum_l |p_l|^2|eV_{dc}+l\hbar\omega|. \tag{1.71}$$

We briefly comment on the interesting case of $V_{dc}=0$, for which we know from Eq. (1.67) that the dc component of the current vanishes. In this genuinely ac case, the PASN is proportional to $\sum_{n=1}^{N}T_n(1-T_n)$ times a factor which depends on the distribution of coefficients p_l, but is certainly nonzero. This is a paradigmatic example of PASN: we have recovered the physics of dc shot noise [see Eq. (1.54)] even in the absence of dc transport! We report in Fig. 1.10 some experimental results by L. Reydellet *et al.* investigating this very case [88]. The measured noise is in excellent agreement with the theory, Eq. (1.70).

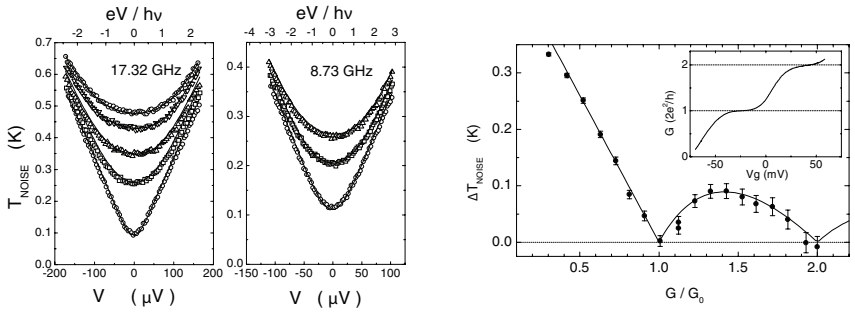

Figure 1.10: PASN observed in the absence of dc transport by L. Reydellet *et al.* [88]. Left: the so-called noise temperature (namely, the ratio $T_N = \mathcal{S}/(4Gk_B)$) agrees very well with theoretical expectation even with no adjustable parameters. Right: after subtracting the equilibrium contribution, the noise temperature displays the typical pattern $\sim \sum_n T_n(1-T_n)$ already shown in Fig. 1.8.

In particular, the behavior $\mathcal{S} \sim \sum_{n=1}^{N} T_n(1-T_n)$ is clearly visible in the right panel of Fig. 1.10, as the PASN vanishes totally whenever the conductance takes values that are integer multiples of $2e^2/h$, with the factor 2 once again due to spin degeneracy.

The photoassisted transport formalism has found several applications in the description of quantum pumps, resonant double-barrier structures and driven quantum dots [89]. More recently, it has been used to characterize the physics of coherent single-electron sources in EQO, which will constitute the bulk of the next Chapter.

Chapter 2

Electron quantum optics

This second Chapter presents the field of electron quantum optics and all the ingredients that make EQO possible. We will focus on the revolutionary discovery of the QH effect and its one-dimensional edge states. Then we will discuss the physics of single-electron sources, which represent fundamental building blocks for EQO recently implemented in experiments. Finally we introduce the FQH effect, and propose an extension of EQO to this unconventional and fascinating regime.

2.1 The quantum Hall effect

The discovery of the QH effect is one of the most revolutionary events in physics during the last 40 years. Lots of the modern achievements of condensed matter theory have been triggered by the experimental observation reported by Klaus von Klitzing and collaborators in 1980 [3].

In a simple picture, the physics of the QH effect is the following: a gas of electrons is forced to move in a two-dimensional plane and is immersed in a strong, perpendicular magnetic field. As we briefly mentioned in the previous Chapter, a 2DEG can form, for instance, at the interface between two semiconductors due to the bending of the bands (although the original measurement by von Klitzing was performed with a field-effect transistor). When such a system is prepared, the classical Drude model would predict a simple linear behavior for the transverse resistance (also called Hall resistance) as a function of the magnetic field B [90]. Yet, at sufficiently low temperature and high magnetic field a very peculiar phenomenon takes place: the Hall resistance can only take values which are integer fractions of a universal resistance quantum, as shown in Fig. 2.1. Such values do not depend on the presence of

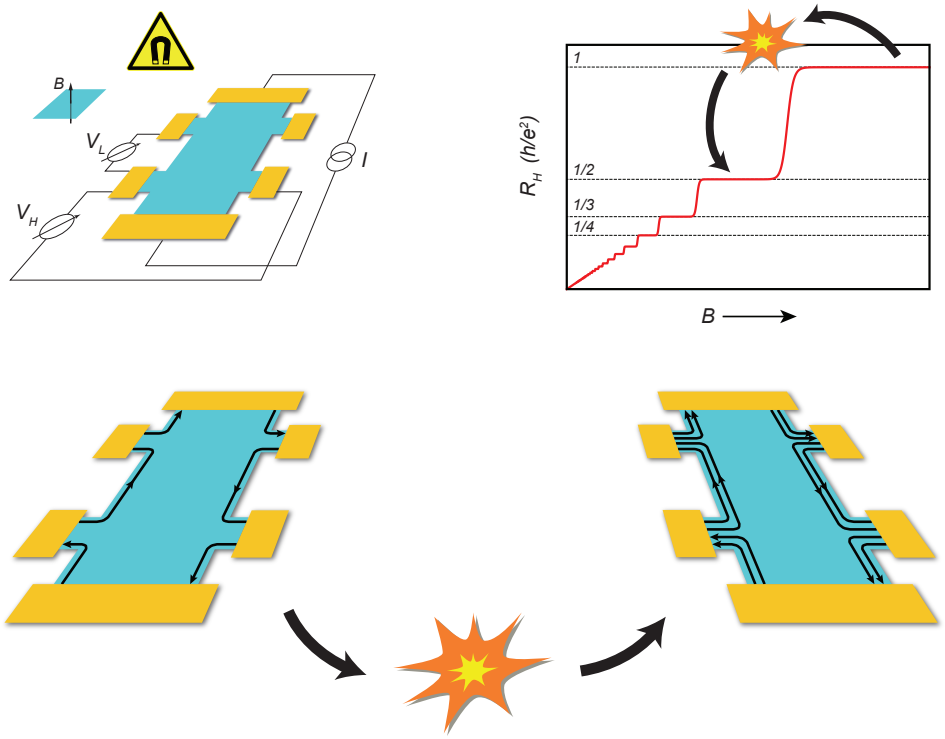

Figure 2.1: The QH effect in a nutshell. Top left: Electrons confined in a planar two-dimensional geometry are immersed in a strong magnetic field perpendicular to the plane. A current I is driven longitudinally along the system and the Hall resistance $R_H = V_H/I$ is measured. Top right: Qualitative behavior of the Hall resistance as a function of the magnetic field B. At low field the resistance is almost proportional to B, but well defined plateaus develop for sufficiently high B. They correspond to integer fractions of h/e^2 with a precision up to 1 part in 10^{10}. Bottom: The current is carried by chiral edge states topologically protected from backscattering while the bulk is insulating, hence the striking precision in the quantization. Jumps between neighboring plateaus lead to topological phase transitions were a new metallic state is created or removed at the edge.

impurities, on the dimensions of the sample and on its shape, but only on two fundamental constants, namely the electron charge e and Planck's constant h:

$$R_{\mathrm{H}} = \frac{h}{Ne^2}, \quad N \in \mathbb{N}. \tag{2.1}$$

Jumps among the different plateaus identified by the above equation happen abruptly as the strength of the magnetic field is varied, but when the resistance is flat, it is really very flat. So flat that it has been used in metrology [91, 92]. Important questions hence emerge: why is the resistance so stable? Which is the nature of the phase transition that takes place when the system jumps from one plateau to another?

The answer to these two questions has been given by D.J. Thouless and coworkers by means of one of the more elegant and remarkable formulas of condensed matter physics: the one defining the TKNN invariant (from the initials of the four authors) [93]. In their original work, they have considered a two-dimensional system of electrons in the presence of the periodic crystalline potential and a strong perpendicular magnetic field, and they have computed the conductance of such a system by using the Kubo formula [94]. The presence of a periodic potential is crucial: we can use the Bloch theorem and say that eigenstates of the Hamiltonian $H(\boldsymbol{r}) = \boldsymbol{p}^2/(2m) + U(\boldsymbol{r})$, with $\boldsymbol{p} = -i\hbar\boldsymbol{\nabla}$ and $U(\boldsymbol{r} + \boldsymbol{R}) = U(\boldsymbol{r})$, are of the form [33]

$$\psi^{(n)}_{\boldsymbol{k}}(\boldsymbol{r}) = e^{i\boldsymbol{k}\cdot\boldsymbol{r}} u^{(n)}_{\boldsymbol{k}}(\boldsymbol{r}), \tag{2.2}$$

where $u_{\boldsymbol{k}}(\boldsymbol{r})$ has the same periodicity of the crystalline potential [i.e. $u(\boldsymbol{r} + \boldsymbol{R}) = u(\boldsymbol{r})$]. Here, $\boldsymbol{R}$ is a generic vector of the Bravais lattice. For a rectangular lattice with primitive vectors $\boldsymbol{a} = (a, 0)$ and $\boldsymbol{b} = (0, b)$, we have $\boldsymbol{R} = m\boldsymbol{a} + n\boldsymbol{b}$, for any integers m, n. The function $u^{(n)}_{\boldsymbol{k}}$ is given by the eigenvalue problem

$$H_{\boldsymbol{k}} u^{(n)}_{\boldsymbol{k}} = E^{(n)}_{\boldsymbol{k}} u^{(n)}_{\boldsymbol{k}}, \tag{2.3}$$

where $H_{\boldsymbol{k}} = e^{-i\boldsymbol{k}\cdot\boldsymbol{r}} H(\boldsymbol{r}) e^{i\boldsymbol{k}\cdot\boldsymbol{r}}$ is the momentum-space Bloch Hamiltonian.

Still, an important remark is worth being underlined. In the presence of an external magnetic field, we have to replace the momentum operator with $\boldsymbol{p} - e\boldsymbol{A}$ where $\boldsymbol{A}$ is the vector potential. Correspondingly, the Hamiltonian reads

$$H(\boldsymbol{r}) = \frac{(\boldsymbol{p} - e\boldsymbol{A})^2}{2m} + U(\boldsymbol{r}). \tag{2.4}$$

In order for the eigenstates of the Hamiltonian (2.4) to still have the form of Bloch states (2.2), the crystalline momentum has to be a good quantum number. In other words, discrete translation operators in the x and y directions (which we call T_x and T_y) have to commute with H and with each other. Due to the presence of the vector potential they read

$$T_x = e^{ia'(p_x - eA_x)/\hbar}, \quad T_y = e^{ib'(p_y - eA_y)/\hbar}. \tag{2.5}$$

Note that two new lengths a', b' appear in the above equation. The reason for choosing two new constants instead of the periods a, b of the lattice will become evident in a moment. The magnetic field is assumed to be perpendicular to the xy plane, $\boldsymbol{B} = (0, 0, B)$. It is easy to show that the symmetric gauge $\boldsymbol{A} = \frac{1}{2}\boldsymbol{B} \times \boldsymbol{r}$ guarantees that $[T_x, H] = [T_y, H] = 0$. However, translation operators do not commute with each other,

$$T_x T_y = T_y T_x e^{-ia'b'Be/\hbar}. \tag{2.6}$$

It seems that the Bloch theorem is applicable only under the special condition $a'b'Be/\hbar = 2\pi p$, with p an integer. However, we can get out of trouble thanks to a simple and extremely clever trick [93, 95]. Suppose that the magnetic flux per unit cell $\phi = abB$ corresponds to a rational number of flux quanta $\phi_0 = h/e$, namely $\phi/\phi_0 = p/q$ with p, q integers. Then, let us choose $b' = b$ and write

$$\frac{a'bBe}{\hbar} = \frac{a'}{a} 2\pi \frac{abBe}{h} = \frac{a'}{a} 2\pi \frac{p}{q}. \tag{2.7}$$

It is clear that, if we focus on a bigger unit cell with $a' = qa$, the additional phase in Eq. (2.6) vanishes and the Bloch theorem is fully applicable! The reciprocal lattice is then described by the unit momenta $k_a = 2\pi/(qa)$ and $k_b = 2\pi/b$, and the corresponding Brillouin zone is called *Magnetic Brillouin zone* [95].

We can now get back to the TKNN work. For the present case of a rectangular lattice with periodic boundary conditions, the magnetic Brillouin zone is, geometrically speaking, a torus. Thouless and collaborators were able to show that the Hall conductance can be expressed as an integral, over the Brillouin zone, of a quantity that does not depend on the energy levels of the system, but on all the occupied eigenstates. The TKNN result is

$$G_{\mathrm{H}} = \sum_n G_{\mathrm{H}}^{(n)}, \tag{2.8}$$

where each contribution $G_{\mathrm{H}}^{(n)}$ is given by an integral in the momentum space involving Bloch states of the n-th band,

$$G_{\mathrm{H}}^{(n)} = \frac{e^2}{h} \frac{1}{2\pi} \iint_{\mathrm{BZ}} dk_x dk_y \, i \left[\left\langle \frac{\partial u_{k_x,k_y}^{(n)}}{\partial k_x} \middle| \frac{\partial u_{k_x,k_y}^{(n)}}{\partial k_y} \right\rangle - \left\langle \frac{\partial u_{k_x,k_y}^{(n)}}{\partial k_y} \middle| \frac{\partial u_{k_x,k_y}^{(n)}}{\partial k_x} \right\rangle \right], \tag{2.9}$$

and the sum in Eq. (2.8) is extended over all filled bands [93]. This behavior immediately sounds odd: we usually learn that the current, in linear response, is mainly a property of the states close to the Fermi energy, something very different from the TKNN result. Moreover, and most importantly, the value of $G_{\mathrm{H}}^{(n)}$ can only be an integer multiple of the conductance quantum e^2/h. There is a profound reason for this precise quantization which is rooted in the mathematical field of topology. But to fully appreciate the link with topology, we have to resort to a powerful tool called *Berry phase*.

2.1.1 Berry phase and topology

Suppose that the Hamiltonian H of a quantum system depends on a set of N parameters, collected in the vector $\boldsymbol{\xi}$. At each instant, there is a set of eigenstates $\{|n(\boldsymbol{\xi})\rangle\}$ satisfying the Schrödinger equation

$$H(\boldsymbol{\xi})\,|n(\boldsymbol{\xi})\rangle = E^{(n)}(\boldsymbol{\xi})\,|n(\boldsymbol{\xi})\rangle\,, \tag{2.10}$$

which constitute the natural basis. Let us now suppose that the system is initially prepared in the n-th eigenstate, and then follows an adiabatic evolution in time represented by a path C in the parameter space. According to the adiabatic theorem, a slow evolution in the parameter space leaves the system in the n-th eigenstate, provided that there is a gap between the eigenvalue $E^{(n)}$ and the rest of the spectrum [96]. Namely, if the quantum state at the initial instant t_0 is $|\psi(t_0)\rangle = |n[\boldsymbol{\xi}(t_0)]\rangle$, the final state must be proportional to $|n[\boldsymbol{\xi}(t)]\rangle$ times, at most, an additional phase factor: $|\psi(t)\rangle = e^{i\phi^{(n)}(t)}\,|n[\boldsymbol{\xi}(t)]\rangle$. To calculate the phase we consider the full Schrödinger equation for $|\psi(t)\rangle$,

$$i\hbar\partial_t\left[e^{i\phi^{(n)}}\,|n(\boldsymbol{\xi})\rangle\right] = H(\boldsymbol{\xi})e^{i\phi^{(n)}}\,|n(\boldsymbol{\xi})\rangle = E^{(n)}e^{i\phi^{(n)}}\,|n(\boldsymbol{\xi})\rangle\,, \tag{2.11}$$

and take the inner product with $\langle n(\boldsymbol{\xi})|$. After an integration in time we readily obtain

$$\phi^{(n)} = -\frac{1}{\hbar}\int_{t_0}^{t} E^{(n)}(\boldsymbol{\xi})dt' + \int_{t_0}^{t} i\,\langle n(\boldsymbol{\xi})|\,\partial_{t'}\,|n(\boldsymbol{\xi})\rangle\,dt'. \tag{2.12}$$

Thus, the additional phase factor is due both to the usual time evolution of the eigenstate and the path in the parameter space. This second contribution, which we'll denote with $\gamma^{(n)}$, is of purely geometrical origin, since we can rewrite it as

$$\gamma^{(n)} = \int_C \boldsymbol{A}^{(n)}(\boldsymbol{\xi})\cdot d\boldsymbol{\xi}, \quad \boldsymbol{A}^{(n)}(\boldsymbol{\xi}) = i\,\langle n(\boldsymbol{\xi})|\boldsymbol{\nabla} n(\boldsymbol{\xi})\rangle\,, \tag{2.13}$$

with $\boldsymbol{\nabla} = (\frac{\partial}{\partial\xi_1},\ldots,\frac{\partial}{\partial\xi_N})$. The quantity $\boldsymbol{A}^{(n)}(\boldsymbol{\xi})$ is called *Berry connection*.

The emergence of this phase factor isn't quite a surprise and does not seem to be so interesting at first. Indeed, it has been known from the very beginning of the quantum theory that a suitable gauge transformation washes out the effect of the geometrical phase. But this is not always possible. In 1983 Michael Berry pointed out what all physicists had missed for almost 60 years: when a quantum system undergoes a time evolution which is a cycle (i.e. it describes a closed loop in the parameter space), the geometrical phase cannot be gauged away and must have a physical meaning [97]. Indeed, a gauge transformation acts on the eigenstates as

$$|n[\boldsymbol{\xi}(t)]\rangle \to |n'[\boldsymbol{\xi}(t)]\rangle = e^{i\Lambda[\boldsymbol{\xi}(t)]}\,|n[\boldsymbol{\xi}(t)]\rangle\,, \tag{2.14}$$

where $\Lambda(\boldsymbol{\xi})$ is any differentiable function. From Eq. (2.13) it is evident that the properties of $\boldsymbol{A}$ under gauge transformation are formally comparable to a

vector potential, as $\boldsymbol{A}' = \boldsymbol{A} - \boldsymbol{\nabla}\Lambda(\boldsymbol{\xi})$. We thus get the following transformation for $\gamma^{(n)}$

$$\gamma^{(n)} \to \gamma^{(n)\prime} = \gamma^{(n)} - \Lambda[\xi(t)] + \Lambda[\xi(t_0)]. \tag{2.15}$$

But a full cyclic evolution implies that $\Lambda[\xi(t)] = \Lambda[\xi(t_0)] + 2\pi N$, with N an integer, to ensure that we get back to the initial state $|n[\boldsymbol{\xi}(t_0)]\rangle$. We thus find that $\gamma^{(n)}$, which is now called *Berry phase*, is gauge invariant modulo 2π and the full phase factor $e^{i\gamma^{(n)}}$ is *absolutely* gauge invariant.

It was Barry Simon from Caltech to immediately elucidate the link between this "remarkable and rather mysterious result" (in Berry's own words) and the TKNN formula [98]. In particular, the Berry phase as written in the Eq. (2.13) defines a curvature, which is given by

$$\Omega^{(n)}_{\alpha\beta} = \partial_\alpha A^{(n)}_\beta - \partial_\beta A^{(n)}_\alpha \tag{2.16}$$

(here we use $\partial_\alpha = \partial/\partial\xi_\alpha$). Simon then realized that there the physics of the Berry curvature is nothing but the physics of vector bundles and their integral invariants, and the integral of the Berry curvature over a closed surface must be an integer multiple of 2π.[1] Thus the quantity

$$C^{(n)} = \frac{1}{2\pi}\iint_S dx_\alpha \times dx_\beta\, \Omega^{(n)}_{\alpha\beta} \tag{2.17}$$

is an integer, which is called Chern number.

Berry phase in Bloch bands

The link with the TKNN invariant comes in the following way. Changing the quasi-momentum across the magnetic Brillouin zone can be viewed as an adiabatic, cyclic evolution of the momentum-space Hamiltonian $H_{\boldsymbol{k}}$, since we have periodic boundary conditions. Then, for each band we can define the Berry phase and curvature in terms of the two-dimensional momentum $\boldsymbol{k} = (k_x, k_y)$, which plays the role of the set of parameters $\boldsymbol{\xi}$. Reinterpreting the TKNN result in this way, one finds that the Hall conductance in unit of e^2/h is nothing but the integral of the Berry curvature over the (closed) magnetic Brillouin zone summed over the filled bands, and is thus an integer number:

$$\frac{\sigma_{\mathrm{H}}}{e^2/h} = \sum_n \iint_{\mathrm{BZ}} dk_x dk_y\, \Omega^{(n)}_{k_x k_y} = N. \tag{2.18}$$

A nice analogy with mathematics in thus recovered. A theorem due to Gauss and Bonnet states that, for a closed surface with Gaussian curvature K the quantity [100]

$$\chi = \frac{1}{2\pi}\int_S K\, dA, \tag{2.19}$$

[1] For a demonstration of this fact on a simple surface, like a sphere in $\mathbb{R}^3$, see e.g. Ref. [99].

which is called Euler characteristic, is an integer number linked to *number of holes* g in geometric structures (in particular one has $\chi = 2 - 2g$). The Euler characteristic is left invariant by a smooth deformation of the manifold which doesn't close or open new holes, and is thus called *topological invariant*. The Hall conductance for the n-th band behaves exactly the same way when considering smooth deformations of the Hamiltonian, since $\sigma_{\mathrm{H}}^{(n)}$ is the integral of a curvature over the Brillouin zone. In mathematics, all manifold with identical χ are said to be topologically equivalent, while different χ correspond to topologically distinct surfaces. Similarly, we can refer to the different quantum Hall plateau as *topologically different* quantum phases.

The phase transition among separate states (i.e. separate Hall plateaus) is not associated with a symmetry breaking and the behavior of a local order parameter, but it is related to an integral, hence a global property of the system, changing value as soon as the conductance jumps from one plateau to the next one. This is the deep revolution that the QH effect brought in condensed matter physics. A new phase of matter was discovered, which doesn't fit the usual classification in terms of symmetry breaking and order parameters of the Landau-Ginzburg theory [101]. Instead, it is understood in terms of a global property (an integral over the Brillouin zone) with all the characteristics of a topological invariant.

2.1.2 Edge states

Still, who carries the current in this topological system? Bertrand Halperin, inspired by a beautiful Gedanken experiment by Nobel laureate Robert Laughlin [102], demonstrated that the current is carried by metallic states at the edges of the sample [4].

To understand why, consider an intuitive semi-classical picture of electrons constrained in a finite region of the plane by hard-wall boundary conditions. In the presence of a strong perpendicular magnetic field the trajectory is circular, with a radius that decreases with increasing magnetic field as $1/B$. For sufficiently high magnetic fields, particles describe very small circular orbits whose radius is much smaller than the linear dimensions of the sample, and no conduction can take place through the bulk. But what happens at the edges? Here, electrons hit the wall before completing a full cycle and, as a result of multiple collisions with the boundary, they move along the edge describing the so-called skipping orbits shown in Fig. 2.2.

On a more quantitative point of view the physics is the following: energy levels of a two-dimensional system of non-interacting charged particles in a perpendicular magnetic field are given by the highly degenerate Landau levels [59]

$$E_n = \hbar\omega_B \left(n + \frac{1}{2}\right), \tag{2.20}$$

where $\omega_B = eB/m$ is the cyclotron frequency. Each level can accommodate a

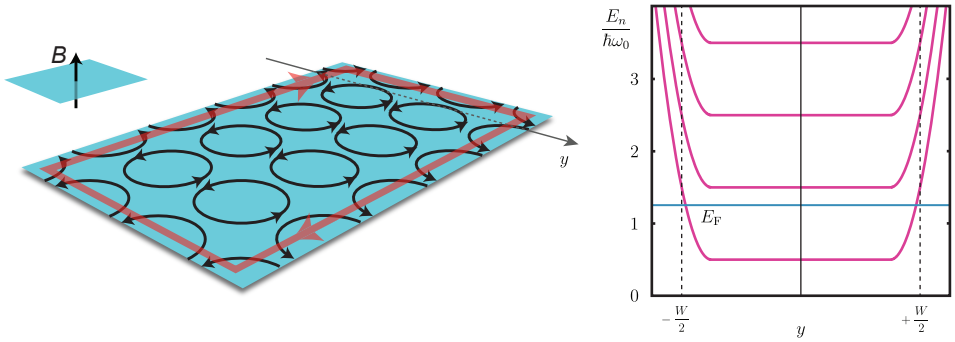

Figure 2.2: Left: in a semi-classical approximation, electrons in a plane with a perpendicular magnetic field describe circular orbits. For very high magnetic fields their radius is much smaller than the linear dimensions of the sample, and the system behaves mainly as an insulator, as no electron can be transported through the bulk. Still, electrons at edges collide against the wall and their circular motion is interrupted, giving rise to chiral edge states. Right: sketch of the energy levels of the 2DEG.

number $N_{\text{deg}} = \phi/\phi_0$ of electrons, where ϕ is the total magnetic flux through the plane and $\phi_0 = h/e$ is the flux quantum. If the 2DEG hosts a total number N of electrons, the fraction of occupied Landau levels is thus

$$\nu = \frac{N}{N_{\text{deg}}} = \frac{hn_e}{eB}, \tag{2.21}$$

with n_e the electron density in the system. Such a quantity is usually named *filling factor*.

Due to translational invariance (here we can safely neglect the periodicity of the crystalline potential) energy levels in the bulk are spatially homogeneous. Inside the sample we have the typical spectrum of an insulator, shown schematically in Fig. 2.2. Indeed, as long as we stay away from the edges, for each possible value of the Fermi level E_F the highest occupied band is always separated from the lowest unoccupied one by an energy gap $\hbar\omega_B$. However, the situation is very different close to the edge of the sample. Here the spectrum is shifted with respect to the Landau levels, due to the fact that the wavefunction has to vanish at the edge. As a result, the Fermi level always crosses the energy spectrum both on the right side ($y = W/2$) and on the left side ($y = -W/2$), giving rise to metallic edge states.

However, a key role in the physics of the QH effect is played by disorder, which has often a dramatic effect on transport properties, as demonstrated by the paradigmatic Anderson localization [103]. The important result shown by Halperin is that this intuitive picture of edge states is not significantly altered by disorder. On the contrary, disorder is even useful in this case, as it helps localizing the bulk states in correspondence of plateaus of G_H, while edge states remain extended and carry a current even in the presence of disorder in the sample [4].

The fact that the current flows at the edge brings several very important implications, all consistent with experimental observations. First, the motion is chiral and electrons on the same edge move along the same direction, dictated by the external magnetic field. They would reverse their direction of motion only by reaching the opposite edge, where they can find a backward-propagating channel. But this is impossible (or, at least, exponentially suppressed) since the system is insulating in the bulk! The chiral edge states of the QH effect are thus topologically protected from backscattering and realize a perfect, dissipationless conductor. A vanishing longitudinal resistance is indeed always measured in correspondence of transverse resistance plateaus. Second, it's now clear that all details about the host sample (shape, presence of impurities, material) are irrelevant. What really matters is the boundary between the electron gas and the vacuum, were current-carrying edge states develop. Finally, plateaus of G_{H} are in one to one correspondence with the number of edge states. Indeed, if the Hall conductance in the presence of a single edge state is $G_0 = e^2/h$, n boundary states generate a conductance $G_{\mathrm{H}} = nG_0$, accounting for the step-like behavior $R_{\mathrm{H}} = 1/G_{\mathrm{H}}$. Jumping from one resistance plateau to the next one corresponds to closing or opening a new channel at the edge. Thus, in this context, the integer n is nothing but the filling factor ν.

With the QH effect and its topological interpretation, the era of topological states of matter was born. A plethora of states which are defined by their topology rather than by their symmetries have been discovered and understood since the '80s. Moreover, when forced to have an interface with something topologically different (most often, the vacuum), those states necessarily show robust metallic edges. This is a particular manifestation of a rather general phenomenon called *bulk-boundary correspondence*: what happens at the edge is nothing but a manifestation of topological properties of the bulk.

2.2 Electron quantum optics

The discovery of topological states of matter and their protected edge states has triggered a huge number of theoretical proposals and cutting-edge experiments. Very recently, it has been realized that such one-dimensional, dissipationless conductors are the best possible candidate to realize electronic waveguides. Indeed, if one were able to generate coherent few-electron excitations along the edge stated of a QH system, the topological protection would allow for ballistic transport over distances of the order of several μm (which is a rather remarkable distance) and, as a consequence, for they coherent manipulation in interferometric setups. To this end, a 2DEG in the QH regime can be equipped with a QPC in order to deviate, reflect or manipulate in any possible way the flow of QH edge states.

Going back to the simple two-particle interferometer we described in Sec. 1.4.1, it seems that we have found a possible physical implementation in

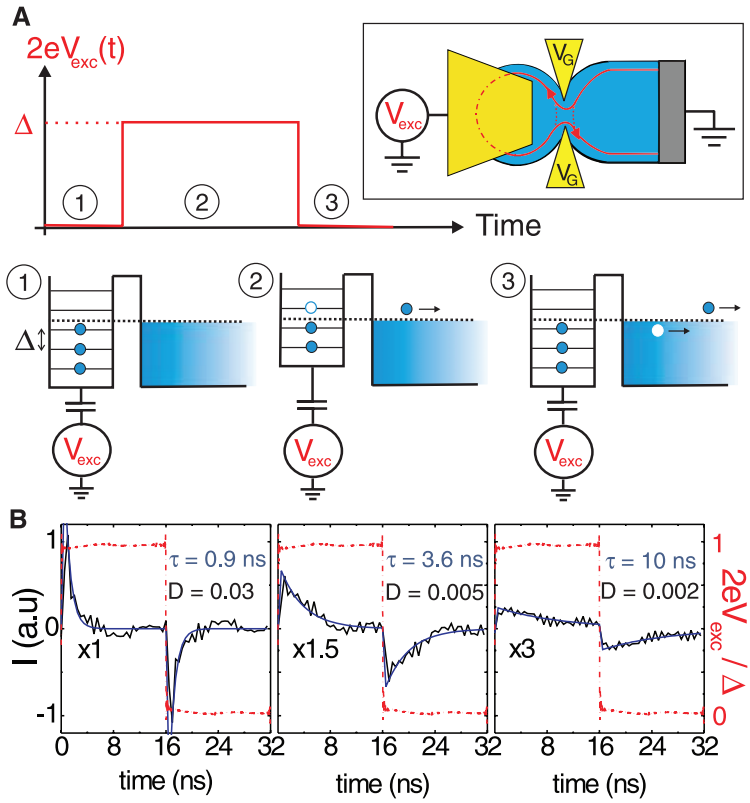

Figure 2.3: The driven mesoscopic capacitor. A: a narrow loop is defined along the edge states of a QH system thanks to a QPC (yellow gates with dc voltage V_G). This creates a strongly confined region with discrete energy levels separated by an energy Δ. A second gate driven with a square voltage V_{exc} is able to raise and lower the energy levels periodically. This results in a periodic emission of an electron and a hole from the confined region to the rest of the 2DEG. B: time resolved current measurements show the typical exponential relaxation of an RC circuit. From [6].

fermionic systems. Quantum Hall edge states can provide input and output channels for electrons, and a QPC is able to reflect or transmit particles at a tunable rate. But the only missing piece to perform individual fermionic interferometry is possibly also the hardest one to achieve: a device which is able to inject an on-demand and controlled train of electronic excitations in QH edge states.

2.2.1 Single-electron sources

A breakthrough in this direction was achieved in 2007, when the paper by G. Fève and collaborators reported the first experimental realization of a coherent single-electron emitter [6].

The physics of this remarkable device relies on earlier work by M. Büttiker, who investigated a quantum analogue of the RC circuit which he called *meso-*

scopic capacitor [5, 104]. We show in Fig. 2.3 the principle behind its operation. In a 2DEG, a small island is isolated from the rest of the system thanks to a QPC. The island is small enough to be assimilated to a quantum dot with discrete energy levels. A dc gate voltage (indicated with V_G in the figure) controls the transmission D from the island to the rest of the 2DEG, which is driven in the QH regime thanks to a sufficiently high magnetic field. A second gate V_{exc} is capacitively coupled to the dot in order to control the Fermi energy of electrons in the dot.

Now, let us consider the cartoon schematically depicted in the second row of Fig. 2.3. At the initial step (1), the Fermi level of the 2DEG lies between two energy levels of the dot. Next, acting on V_{exc} the energy levels of the dot are suddenly risen by a fixed amount Δ, which corresponds to the spacing between levels (2). The electron that previously occupied the highest filled level is now above E_F in energy. It can now escape the dot at a tunneling rate $\Gamma = \tau^{-1} \approx D\Delta/h$, where τ is the relaxation time of the dot [6]. As a final step, the gate voltage is brought back to the initial value so that energy levels of the dot are realigned with their starting configuration (3). Now the opposite scenario is realized: an empty level has moved below the Fermi level, and an electron from the free 2DEG can tunnel into the dot at the same rate Γ to occupy this empty level. The net result is the emission of a *hole* from the dot to the rest of the 2DEG. By driving V_{exc} with a square wave this up/down cycle is repeated periodically, leading to the alternate emission of an electron and a hole for each period of the drive. It's worth noticing that the ac amplitude of the square voltage has to be of the order of Δ/e, in such a way to raise a single level above the Fermi level.

In view of the analogy with the classical capacitor, current driven by the mesoscopic capacitor is expected to show the typical charging/discharging behavior of an RC circuit. Indeed, the time dependent current reported in the bottom row of Fig. 2.3 shows a good agreement with an exponential relaxation. As expected, the emission time τ extracted with an exponential fit increases as the transmission D of the QPC is lowered.

As said, the 2DEG within which the mesoscopic capacitor is realized is subjected to a strong magnetic field. Electrons and holes outgoing from the dot are thus directly emitted into the edge states of the QH regime, which take care of the coherent propagation of the injected wavepacket. In this framework, a partitioning experiment for a stream of single-electron and single-hole excitations was realized in Ref. [11] by the ENS Paris team, in the same spirit of the optical HBT experiment [105–107]. The optical beam splitter was effectively replaced by an additional QPC with tunable transmission, that was placed downstream of the emitter.

Even more intriguingly, an HOM experiment with identical fermions was subsequently performed by the same group and reported in Ref. [12]. In a two-arm interferometer, such as the one schematically described in Sec. 1.4.1 of the previous chapter, a pair of mesoscopic capacitors were tuned in such a

way to have identical energy levels and emission times. Simultaneous collisions of identical electrons and holes at the QPC showed the expected anti-bunching effect predicted for fermionic particles and already described in Chapter 1 [see Fig. 1.4]. These experiments show that, combining QH edge states as ballistic waveguides for electrons, a mesoscopic capacitor as an on-demand single-electron gun and a QPC in the role of a beam splitter, the time for coherent manipulation of single-electrons in optical-like setup has come. This new field, which promises to be extremely fruitful for the realization of quantum technologies, has been named Electron Quantum Optics (EQO) [2].

2.2.2 The leviton

An equally effective yet conceptually simpler idea to conceive single-electron excitations was discussed in a series of theoretical paper by L. Levitov and coworkers, who showed how to excite a single electron above the Fermi sea applying well defined voltage pulses to a quantum conductor [7–9]. In particular, the pulse *must have a Lorentzian shape with quantized area* in order to generate an electron-like excitation with no additional hole-like contribution. The formalism used by Levitov and collaborators is quite general. Without going into the details of their work, we summarize the main points and demonstrate how they are related to the PASN when considering periodic voltage pulses.

Exciting a single electron above the filled Fermi sea might look at first a pretty challenging task. Applying time-dependent voltage pulses to a conductor is, in some sense, similar to shaking a water tank: we generate a huge number of ripples with peaks and valleys, which we call, for the case of fermions in a metallic system, particle and hole excitations. Extracting a single water droplet without affecting the rest of the equilibrium surface seems to be extremely difficult, if not impossible.

Levitov *et al.* developed a theory of electron counting statistics to study what happens when a non-interacting quantum conductor is shaken with a voltage pulse $V(t)$. They found that the new quantum state generated after the pulse depends strongly on the Faraday flux

$$\Phi = \int_{-\infty}^{+\infty} dt\, V(t). \tag{2.22}$$

The key result is the following. In general, the presence of a nonzero Faraday flux generates a new ground state which is orthogonal to the initial one. This fact bears an interesting resemblance with the orthogonality catastrophe, where the insertion of a single impurity in a crystal lattice leads to a new orthogonal many-particle ground state in the thermodynamic limit [108]. From the point of view of transport properties, the orthogonality catastrophe leads to a logarithmic divergence in the current noise due to the fact that the voltage pulse excites infinitely many particle-hole pairs. However, a very special configuration is obtained when the Faraday flux is an integer multiple of the

flux quantum $\phi_0 = h/e$. For $\Phi = n\phi_0$ the logarithmic divergence vanishes, for the two ground states are no more orthogonal. Thus, if we want to cause a minimal disturbance to the Fermi sea we must choose a voltage pulse whose integral is quantized in terms of the flux quantum ϕ_0, namely

$$\frac{e}{h}\int_{-\infty}^{+\infty} dt\, V(t) = n, \quad n \in \mathbb{N}. \tag{2.23}$$

This is a constraint on the average value (i.e. dc component) of the pulse. It remains to establish which pulse shape does the job in the best way.

Let us consider Levitov quantization condition (2.23) in terms of the PASN. We assume that the conductor is driven with a periodic stream of voltage pulses, instead of a single one. In the presence of any sort of barrier with finite transmission/reflection we can use Eq. (1.71) to write the zero temperature shot noise,

$$\mathcal{S} = \frac{e^2\omega}{\pi}\sum_{n=1}^{N} T_n(1-T_n)\sum_{l=-\infty}^{+\infty} |p_l|^2|q+l|, \tag{2.24}$$

with $\omega = 2\pi/T$ the angular frequency of the drive. Here we have introduced the parameter $q = eV_{\rm dc}/(\hbar\omega)$ which is linked to the dc component of the voltage drive. We note that, in order to minimize the noise, we must follow the quantization condition Eq. (2.23) which fixes the value of $V_{\rm dc}$. Thus, for a given q we have to find the optimal shape minimizing the noise. Let us assume that $q > 0$ and rewrite $\mathcal{S}$ in the following way

$$\begin{aligned}\mathcal{S} &\propto \sum_{l>-q} |p_l|^2(q+l) + \sum_{l<-q} |p_l|^2|q+l| = \sum_{l=-\infty}^{+\infty} |p_l|^2(q+l) + 2\sum_{l<-q} |p_l|^2|q+l| = \\ &= q + 2\sum_{l<-q} |p_l|^2|q+l|,\end{aligned} \tag{2.25}$$

where we have used the properties $\sum_l |p_l|^2 = 1$ and $\sum_l l|p_l|^2 = 0$ demonstrated in the Appendix A. It's clear that the noise attains the minimal value when $\sum_{l<-q} |p_l|^2|q+l| = 0$. But this is a sum involving only positively defined terms! As such, it vanishes only when all coefficients p_l vanishes for $l < -q$.

Now, we recall that p_l are the Fourier coefficients of the time dependent signal $e^{-i\varphi(t)}$, with $\varphi(t) = (e/\hbar)\int_0^t dt'\, V_{ac}(t')$. The condition for minimal noise reads thus

$$p_l = \int_{-T/2}^{+T/2} \frac{dt}{T} e^{il\hbar\omega t} e^{-i\frac{e}{\hbar}\int_0^t dt'\, V_{ac}(t')} = \int_{-T/2}^{+T/2} \frac{dt}{T} e^{i(l+q)\hbar\omega t} e^{-i\frac{e}{\hbar}\int_0^t dt'\, V(t')} = 0 \tag{2.26}$$

for $l < -q$. Taking the limit of infinite period, which brings us back to the single-pulse situation discussed by Levitov, we get the condition

$$p(\varepsilon) = \int_{-\infty}^{+\infty} dt\, e^{-i\varepsilon t} f(t) = 0, \quad f(t) = e^{-i\frac{e}{\hbar}\int_0^t dt'\, V(t')}, \tag{2.27}$$

for positive ε. From complex analysis, we now see that this condition is fulfilled if the function $f(t)$ has no pole in the lower half of the complex plane [109–111]. However, we also know that $f(t)$ must have at least one pole in the upper-half plane [otherwise $p(\varepsilon)$ vanishes everywhere!], and also that $|f(t)| = 1$. The simplest function satisfying this condition is

$$f(t) = \frac{t - t_0 + iW}{t - t_0 - iW}, \tag{2.28}$$

where W and t_0 are real quantities and $W > 0$. We immediately get the shape of the voltage, which is indeed a Lorentzian pulse of width W centered around t_0:

$$V(t) = i\frac{\hbar}{e}\frac{d}{dt}\ln f(t) = \frac{\hbar}{e}\frac{2W}{(t-t_0)^2 + W^2}. \tag{2.29}$$

This pulse satisfies Eq. (2.23), as $(e/h)\int dt\, V(t) = 1$. We get to a very important conclusion: a Lorentzian pulse with area $\int dt\, V(t) = h/e$ is the *smallest possible pulse that minimizes the shot noise in a quantum conductor*. As such, the quantum state generated by applying the pulse (2.29) to a conductor at equilibrium is also called *minimal excitation state*. The result obtained by Levitov and collaborators is very general. They demonstrated that an arbitrary superposition of optimal pulses with the same sign but with different values of t_0 and W is still a minimal excitation state. As already noticed in the original paper, optimal pulses behave like solitons in integrable non-linear systems [7]. Thus, a periodic train of quantized Lorentzian pulses minimizes the shot noise even without considering the limit $T \to \infty$ as we did in Eq. (2.27). Indeed, one can evaluate the explicit expression for the discrete coefficient p_l in the periodic case and check that they all vanish for $l < -q$ (see Appendix A).

It's worth emphasizing an aspect, which is extremely useful when looking for experimental evidence of the minimal excitation state. From Eqs. (2.24) and (2.25), we see that the PASN can be rewritten as

$$\mathcal{S} = \frac{e^2 q\omega}{\pi}\sum_{n=1}^{N} T_n(1 - T_n) + \Delta\mathcal{S}, \tag{2.30}$$

where the first term is just the shot noise in the presence of a dc bias equal to the average value of the pulse. The additional term $\Delta\mathcal{S}$, which we'll name *excess noise*, vanishes in the case of optimal Lorentzian pulses. Indeed, it can be shown that $\Delta\mathcal{S}$ is proportional to the number of holes excited by the voltage drive [9, 112]. The experimental search for minimal excitation states is thus focused heavily on the measurement of a vanishing excess noise.

2.2.3 Experimental evidence

Experiments performed at CEA Saclay in 2013 demonstrated for the first time the validity of Levitov's approach [10]. We report below the results of Ref. [10] together with their theoretical interpretation.

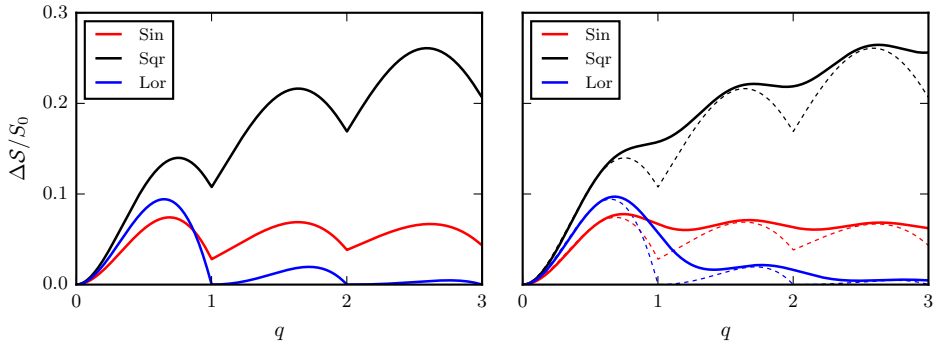

Figure 2.4: Theoretical expectation for the PASN as a function of q associated to periodic signals in Eqs. (2.33), in units of S_0. Left panel: zero temperature case. Right panel: finite temperature case with $k_B\theta = 0.1\,\hbar\omega$. For comparison, curves at $\theta = 0$ are reported as dashed lines from the left panel. In both cases the dimensionless width of Lorentzian pulses is $\eta = 0.1$.

A 2DEG in a two-terminal geometry was fabricated in a GaAs/Ga(Al)As heterojunction. The two ohmic contacts were connected to an arbitrary pulse generator with a broadband 40 GHz transmission line. The 2DEG was equipped with a QPC with tunable transmission in such a way to realize a controllable partition of the periodic stream of pulses. Measurements were performed with a single transmitted transversal mode (this can be checked with a simple dc conductance measurement).

We first comment on the behavior of the PASN as a function of the parameter $q = eV_{\rm dc}/(\hbar\omega)$ expected from the theory. Firstly, it should be noticed that the current emitted from the contact to the single-mode conductor is $I_0(t) = G_0 V(t)$ for each of the two spin polarizations, with $G_0 = e^2/h$ [the total current emitted is of course $2I_0(t) = (2e^2/h)V(t)$]. It follows that the charge associated with one period of the pulse for each spin polarization is

$$Q = \frac{e^2}{h}\int_0^T dt\, V(t) = \frac{e^2}{\hbar\omega}\int_0^T \frac{dt}{T} V(t) = eq. \tag{2.31}$$

Thus, q also measures the number of electrons associated with each pulse. We also note that the condition (2.23) to achieve an optimal flux quantization is equivalent to the request of integer charge per pulse, $q = n$. The excess noise ΔS at zero temperature reads

$$\Delta\mathcal{S} = \mathcal{S} - S_{\rm dc} = S_0\left(\sum_{-\infty}^{+\infty} |p_l|^2 |l+q| - q\right) = 2S_0 \sum_{l<-q}^{+\infty} |p_l|^2 |l+q|, \tag{2.32}$$

where we have collected all constants in $S_0 = T_1(1-T_1)e^2\omega/\pi$, and T_1 is the transmission of the single mode. Once we have chosen a waveform, this expression depends on the values of photoassisted coefficients p_l for that particular

drive. To make contact with experiments, we consider a sinusoidal drive, a square voltage and a periodic train of Lorentzian pulses given respectively by

$$V_{\mathrm{sin}}(t) = V_{\mathrm{dc}}[1 - \cos(\omega t)], \tag{2.33a}$$

$$V_{\mathrm{sqr}}(t) = 2V_{\mathrm{dc}} \sum_{k=-\infty}^{+\infty} \Theta\left(t - kT\right) \Theta\left(\frac{T}{2} - t + kT\right), \tag{2.33b}$$

$$V_{\mathrm{Lor}}(t) = \frac{V_{\mathrm{dc}}}{\pi} \sum_{k=-\infty}^{+\infty} \frac{\eta}{\eta^2 + (t/T - k)^2}, \tag{2.33c}$$

where the periodic Lorentzian drive has been written in terms of the width-to-period ratio $\eta = W/T$. We have calculated the corresponding coefficients in Appendix A. The excess noise predicted by PASN theory for this three cases is reported in the left panel of Fig. 2.4. All curves show a non-monotonic behavior with minima in correspondence of integer values of q, showing the validity of the condition (2.23) derived by Levitov *et al.* for avoiding the orthogonality catastrophe. However, only the Lorentzian voltage pulse can reach the sought-after value $\Delta\mathcal{S} = 0$: both the sinusoidal and the square drive stay well above zero even in such cases where the charge per pulse q is an integer number.

Experiments, however, cannot reach a temperature $\theta = 0$. It is thus instructive to have a look at the finite temperature case. In such case, we know from Eq. (1.70) that a coth factor is needed to account for finite temperature corrections. The excess noise is now

$$\Delta\mathcal{S} = S_0 \left\{ \sum_{-\infty}^{+\infty} |p_l|^2 (l+q) \coth\left[\frac{(l+q)\omega}{2k_{\mathrm{B}}\theta}\right] - q \coth\left(\frac{q\omega}{2k_{\mathrm{B}}\theta}\right) \right\}, \tag{2.34}$$

and is reported in the right panel of Fig. 2.4 for the same three voltage pulses. We see that $\Delta\mathcal{S}$ does not vanish anymore, even for integer q. This is to be expected, as thermal fluctuations can generate particle-hole pairs (and thus additional contribution to the noise) even if the waveform meets the criteria for optimal injection. The subtraction of the partition noise due to thermal excitations emitted by the reservoirs, which for integer q is of the order of $\sim 2k_{\mathrm{B}}\theta/(\hbar\omega)|p_{-q}|^2$, should give an indication of the "cleanliness" of the injected pulse (see the online supplementary information to Ref. [10]).

We now show the outcome of the experiment reported in Ref. [10]. Points shown in Fig. 2.5, left panel, confirm the hierarchy established by theory, see Fig. 2.4 for comparison. The dashed threshold corresponds to the thermal contribution due to the reservoirs, which for this particular case is substantially equal for the cosine and Lorentzian drive. The Lorentzian curve matches almost exactly the dashed level, indicating that no additional noise is generated by the train of voltage pulses. The right panel of Fig. 2.5 shows another set of data for sharper Lorentzian pulses and higher-frequency sinusoidal drive. This time the reservoir contributions are different, but we still observe that

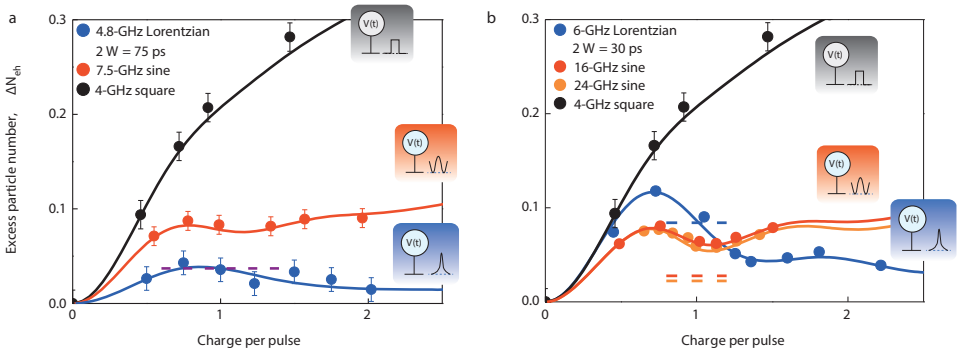

Figure 2.5: Experimental evidence of the leviton (from Ref. [10]). The excess particle number, given by $\Delta\mathcal{S}/S_0$, is measured as a function of the dimensionless dc voltage q. Square, sinusoidal and Lorentzian waveforms with different frequency are considered. Contributions due to thermal excitations emitted by the reservoirs for the sinusoidal and Lorentzian drive are reported in both panel as dashed lines (for the left panels they are almost coincident). Lorentzian pulses in left and right panels have dimensionless width $\eta = 0.18$ and $\eta = 0.09$ respectively. The temperature is $\theta = 39$ mK.

the sinusoidal voltage generates some extra noise which is due to the excitation of particle-hole pairs, while the Lorentzian one does not.

All these features point toward the observation of the minimal excitation state predicted by Levitov. The authors of Ref. [10] have proposed the name *leviton* (i.e. Levitov soliton) for this new type of quasiparticle excitation.

It is worth observing that the leviton seems to be easier to implement with respect to the driven mesoscopic capacitor protocol. Indeed, it's sufficient to apply carefully chosen voltage pulses to a two terminal quantum conductor, thus drastically simplifying the fabrication process of the single-electron gun. For instance, an HOM experiment with levitons can be implemented by feeding two ohmic contacts with the very same pulse generator, with the only care of introducing a tunable time delay in the transmission line. The outcome of such an experiment, which was indeed realized still in Ref. [10] and demonstrates the predicted anti-bunching effect for fermions, has been already shown in the previous Chapter, fig. 1.4.

2.3 Towards electron quantum optics at fractional filling factor

2.3.1 The fractional quantum Hall effect

We have seen that the QH effect, with conductance plateaus at integer values of the filling factor, is well understood in terms of a topological invariant that can only take integer values. However, even before this picture was completed, a notable exception was already reported. In 1982, while Thouless and

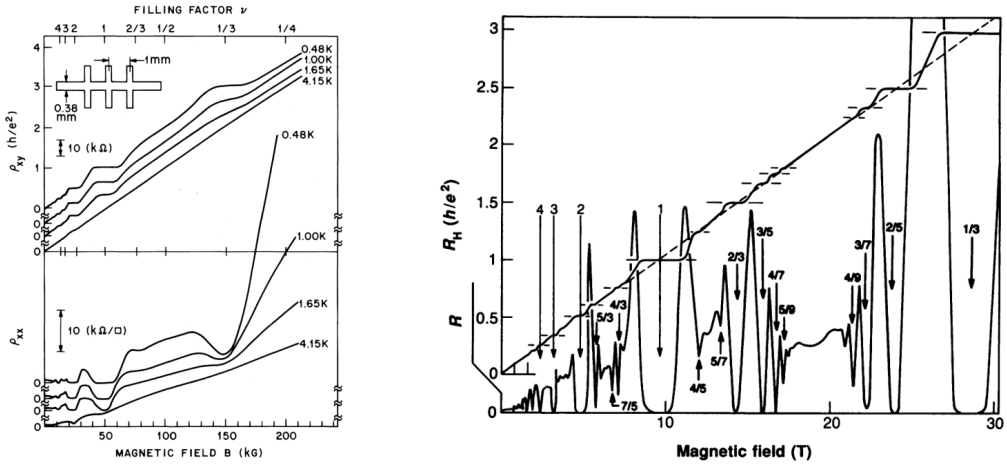

Figure 2.6: Left: first observation of the FQH effect (from Ref. [19]). A plateau in the Hall resistivity (ρ_{xy}) develops at $\nu = 1/3$, in correspondence of a suppression of the longitudinal resistivity (ρ_{xx}). Right: the rich phenomenology of the FQH effect (from Ref. [113]).

co-workers were finalizing their interpretation of the TKNN integral, Tsui, Stormer and Gossard published their results on the observation of a quantum Hall plateau at $\nu = 1/3$ [19]. The left panel (top and bottom) of Fig. 2.6 shows the first observation of the FQH effect, with the emergence of a Hall plateau at $\nu = 1/3$. This fact sounds definitely puzzling, and has inspired a huge number of theoretical and experimental work in the following years. It has opened the fascinating field of the FQH effect, which, as of today, is still extensively studied.

A first theoretical interpretation of the data shown in Fig. 2.6 was subsequently published by Laughlin in 1983 [20]. He realized that the missing ingredient in the theoretical interpretation of QH effects were electron-electron interactions, and that the FQH effect must originate from a strongly correlated quantum state. Relying on the analytical properties of the wavefunction of an electron in the lowest Landau level, and most of all on a brilliant physical intuition, he worked out a variational wavefunction to describe the formation of new type of quantum liquid. It turned out that the overlap between Laughlin variational wavefunction and the real wavefunction, calculated numerically for few-particle states, is of the order of 99%. Although being simple (or, probably, precisely for this reason) it catches the physics: the FQH effect originates from the formation of an uncompressible fluid of quasiparticle excitations, each one carrying a *fraction of the electron charge*. This phenomenon occurs at very precise values of the filling factor given by the so called Laughlin sequence [20]

$$\nu = \frac{1}{2n+1}, \quad n \in \mathbb{N}. \tag{2.35}$$

In the following years, a number of fractional plateaus of the Hall conductance have been reported, as the right panel of Fig. 2.6 shows. A great majority of

them correspond to the values [114]

$$\nu = \frac{p}{2pn+1}, \quad p \in \mathbb{Z},\, n \in \mathbb{N}. \tag{2.36}$$

This second series is known as Jain sequence, and gives back the Laughlin values for the case $p = 1$. However, some notable exceptions with integer denominator have been spotted, like the exotic $\nu = 5/2$ FQH state [115, 116]. These are extremely interesting due to their quasiparticles with non-Abelian statistics that may be useful for quantum computation [117].

Similarly to the integer QH already described, the FQH effect is characterized by the emergence of conducting states at the edge of the system, where the quantum fluid meets the vacuum. As we will see in the next chapter, the basic idea is that the ground state of the FQH forms an incompressible fluid, whose low-energy excitations are deformations that change its shape, but not its area. They move chirally as one-dimensional charge density waves along the edge of the fluid [22].

We won't give a detailed discussion of Laughlin variational approach, for which we refer to the literature [90]. It would require a thorough illustration of the physics of Landau levels and the analytical properties of wavefunctions in the lowest Landau level, together with the analogy with a plasma of charged particles that demonstrates the fractional charge of quasiparticles. This would take an impressive amount of pages (and time!) in this thesis. We will, however, describe the experimental observation of the fractional charges predicted by Laughlin. Two observations were published independently in 1997 by the CEA Saclay group and the Weizmann Institute of Science and helped the cause of Laughlin, Tsui and Stormer, who were awarded the Nobel prize one year later [50, 51].

2.3.2 Measuring a fractional charge

The demonstration that Laughlin quasiparticles carry fractional charge is one of the best exemplification of the power of noise measurements. Back in Section 1.3 we argued that the shot noise can reveal the charge of the carriers, an information that is usually invisible in the current alone. Experiments carried out in 1997 in the FQH regime rely exactly on this principle, which we describe here below.

Consider a 2DEG in the FQH regime with filling factor $\nu = 1/3$. When the system is driven out of equilibrium thanks to a source-drain voltage V_{sd}, an electrical current $I_0 = G_{\mathrm{H}} V_{\mathrm{sd}}$ circulates, with $G_{\mathrm{H}} = \nu e^2/h$. It is carried along the chiral edge states, as the bulk is insulating.

Now, imagine that a QPC is created in the middle of the sample thanks to a pair of metallic gates. By applying a negative voltage V_{G} to the gates, part of the current I_0 is reflected into the opposite edge state as shown in Fig. 2.7a. The physical mechanism responsible for reflection of the current is the *tunneling of fractional quasiparticles* with charge $e^* = \nu e$ from top to bottom edges,

and the corresponding backscattering current I_B is subjected to fluctuations due the random nature of reflection. If the tunneling between opposite edges is sufficiently weak, we can assume that each tunneling event is independent from the others. This regime is commonly named *weak backscattering* configuration. Then, in view of the rather general description of Poissonian shot noise we formulated in Sec. 1.3, the noise will be proportional to the charge of the carriers and the backscattering current:

$$S = 2e^* I_B. \tag{2.37}$$

This is valid in the low temperature regime (i.e. $k_B\theta \ll e^* V_{sd}$). Although a complete understanding of current and fluctuations in Laughlin edge states requires a field-theoretical approach and the notion of chiral Luttinger liquid, Eq. (2.37) should be valid as long as the backscattering can be described as an uncorrelated tunneling of fractional quasiparticles.[2] In the next chapter we will carry out a detailed calculation of shot noise and backscattering current for the FQH edge states in the framework of the chiral Luttinger liquid theory. We will see that the final result totally agrees with Eq. (2.37) in the weak backscattering regime.

In this context, Saminadayar *et al.* measured the shot noise due to a weak backscattering current and reported the noise-vs-current curve shown in Fig. 2.7b [50]. Experimental points approximately follow a straight line in the Poissonian noise regime (i.e. when the energy scale set by the voltage bias is much higher than thermal energy). The slope is $e^* = e/3$, and clearly departs from the dotted line representing the slope e. In contrast, the inset shows that the curve has slope e in the integer QH regime, where the current is carried by integer electrons. The bottom left panel of Fig. 2.7c reports similar results by De-Picciotto *et al.* [51]. The measured fluctuations follow again the predicted behavior for $e^* = e/3$, which is sharply different from the curve obtained for integer electrons.

Finally, Fig. 2.7d adds further evidence for the fact that what is measured is not simply the filling factor, but the actual charge of quasiparticles. Indeed, excitations of Laughlin FQH states carry a fraction of the electron charge that is exactly equal to the filling factor (and thus to the conductance in unit of e^2/h). This may lead to a rather annoying ambiguity in the interpretation of the results. For instance, earlier works had already claimed to have measured the fractional charge in different systems through Aharonov-Bohm oscillations [118], but it was demonstrated that they were only accessing the filling factor of the QH liquid [119]. However, the measurement carried out by Reznikov *et al.* found the predicted charge $e^* = e/5$ for the state $\nu = 2/5$ of the Jain sequence (2.36). Their data are reported in Fig. 2.7d, and erase any doubt about a possible misunderstanding [52].

[2] The word *uncorrelated* used here is to be intended as a synonym of *independent tunneling events*. It should not be confused with electron-electron correlations that give rise to the FQH state, for which we also use the word *correlated*.

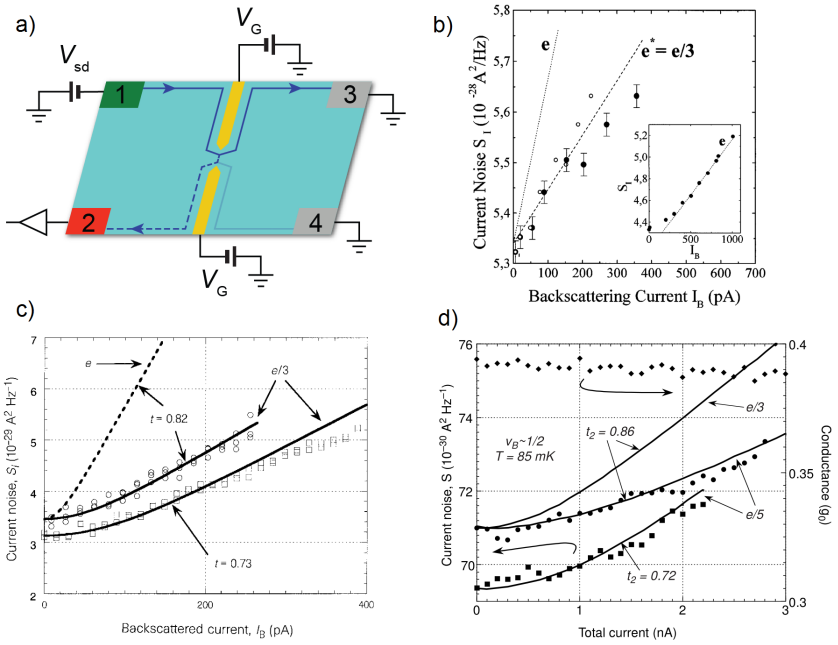

Figure 2.7: Measurement of the fractional charge of Laughlin quasiparticles. A current is driven along the edge states of a 2DEG in the FQH regime, schematically shown in panel a. A QPC in the middle reflects part of the current, generating fluctuations in the backscattering current I_B. The shot noise then follows the linear behavior $S = 2e^* I_B$, with $e^* = e/3$ or $e^* = e/5$ in the present case. From Refs. [50] (panel b), [51] (c) and [52] (d).

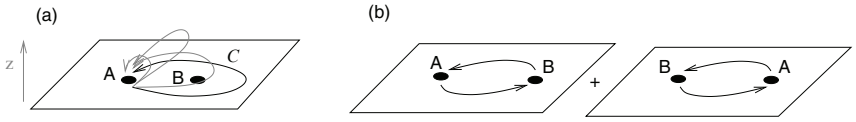

Figure 2.8: Two exchanges of identical particles (b) are equivalent to a full cycle of one particle around the other (a). From [122]

These observations prove that the variational theory by Laughlin, predicting fractionally charged quasiparticle as low-energy excitations of the FQH fluid, was indeed extremely convincing.

2.3.3 Anyons and fractional statistics

Peculiarities of FQH quasiparticles do not end with the their fractional charge. They also possess a fractional statistical angle, in the sense that the exchange of two quasiparticle does not lead to a simple factor ± 1 in the many-body wavefunction. In fact, they are neither bosons nor fermions: since the statistical angle can be in principle any, they are called *anyons* [21].

The reason for this oddity is not due to the physics of the QH effect, but is instead a general property of quantum mechanics in two dimensions [120, 121]. Let us briefly revisit the problem of indistinguishable particles in three dimensions. Consider two identical particles A and B described by the wavefunction $\psi(\boldsymbol{r}_1, \boldsymbol{r}_2)$, where the three dimensional vectors $\boldsymbol{r}_1$ and $\boldsymbol{r}_2$ describe the spatial coordinates of the particles. Now, let us exchange particle A with particle B. Due to indistinguishability, the probability density must be conserved in the process: $|\psi(\boldsymbol{r}_1, \boldsymbol{r}_2)|^2 = |\psi(\boldsymbol{r}_2, \boldsymbol{r}_1)|^2$. It follows that the wavefunction can, at most, pick up a phase factor $e^{i\theta}$. Then, let us perform a second exchange. It is clear that the wavefunction has now accumulated the total phase $e^{i2\theta}$. At the same time, we also know that we got back to the initial state $\psi(\boldsymbol{r}_1, \boldsymbol{r}_2)$. The only solution is that $e^{i2\theta} = 1$. This defines two possibility for the statistical angle θ, corresponding to the usual classification of identical particles in the two classes of bosons ($\theta = 0$) and fermions ($\theta = \pi$).

This fact has a simple interpretation in terms of topology of the space where particles live. As suggested by Fig. 2.8, two successive exchanges are equivalent to the situation where particle B is fixed and particle A describe a full cycle around B. But in three dimension, this is also equivalent to the situation in which particle A never moved. In fact, the path described around particle B can be deformed in such a way that it collapses to a single point without being cut.

Now, let us imagine a similar procedure in two dimensions. We see from Fig. 2.8 that we immediately run into a problem: the path cannot be deformed without passing through particle B! It seems that two successive exchanges of identical particles may not map into the very same quantum state, but into a new quantum state that retains some information about the braiding of

particles. This means that we have to relax the constraint on θ into a more general description in terms of *arbitrary statistical angles*. In a few words, this has to do with the fact that $\mathbb{R}_3$ without a point is a simply connected space, while $\mathbb{R}_2$ without a point is not.

We define the statistical angle through the phase accumulated after an *anti-clockwise* exchange of the two particle:

$$\psi(\boldsymbol{r}_2, \boldsymbol{r}_1) = e^{i\theta}\psi(\boldsymbol{r}_1, \boldsymbol{r}_2). \tag{2.38}$$

For $\theta = \{0, \pi\}$ we get back to the known case of bosons and fermions, but exotic possibilities with *any* value of θ are in principle admissible. Such particles are thus called *anyons*. Laughlin quasiparticles belong exactly to this class, with a statistical angle $\theta = \nu\pi$ linked to the filling factor [123, 124].

At this stage we cannot give a convincing demonstration of the fractional statistics of Laughlin quasiparticles. We will see how it emerges naturally from the commutation of two quasiparticles in the field theoretical approach discussed in the next Chapter.

2.3.4 Electron quantum optics with fractional states

To summarize, we have seen that a 2DEG in a strong perpendicular magnetic field behaves in a quite unexpected way. Its transverse conductance is precisely quantized in units of e^2/h, and the reason for that is rooted in the topological structure of Bloch bands.

The most glaring manifestation of topological protection is the emergence of chiral metallic edge states propagating in a well defined direction dictated by the magnetic field. They realize one-dimensional, dissipationless electronic channels that can be exploited to control and manipulate single-electron excitations generated by on-demand mesoscopic sources. This is, in a few words, the essence of EQO.

However, we have also seen that QH physics emerges at fractional values of the transverse conductance. In this case it is due to the formation of a new strongly correlated phase, where quasiparticles with fractional charge and statistics exist.

Since also FQH systems host topologically protected chiral modes at their edge, we can envisage an exciting generalization of EQO to the fractional regime. Challenging fundamental questions immediately arise: do minimal excitations states exist on a strongly correlated ground state? If yes, what charge do they carry? Is it possible to realize time-resolved interferometry of anyons?

In the next Chapters we will explore these fascinating possibilities.

Chapter 3

Minimal excitations at fractional filling factor

In the third Chapter we develop the theory of minimal excitation states in the FQH regime. We first introduce the field theoretical approach to the FQH effect and its edge states, and show how to construct a field operator for Laughlin quasiparticles in the framework of the bosonization approach. Then, we describe the coupling of the edge states with a pair of voltage contacts and turn to the main problem of identifying clean voltage pulses in the FQH regime. We show that Lorentzian pulses carrying integer charge, i.e. levitons, are the only minimal excitation states at fractional filling factor. The present Chapter is based on the results published in Refs. [24, 26].

3.1 Edge state theory of the FQHE

As a first step towards a theoretical analysis of EQO at fractional filling factor, we need a suitable theory to deal with FQH edge states. Following the original work by X.G. Wen [22], in this Section we will construct an effective field theory for the bulk that reflects the phenomenology of the FQH effect without any assumption about the microscopic model. Then, the corresponding edge theory will arise from the restriction of the bulk theory to the boundary. As we will show, the interesting result is that edge excitations of the FQH effect are described by *one-dimensional chiral bosonic modes*.

Let us start from the Lagrangian density for a system of charged particles in an electromagnetic field. We consider the usual coupling $A_\mu J^\mu$ between the conserved current J^μ and the external electromagnetic field A_μ:

$$\mathcal{L}_A = A_\mu J^\mu. \tag{3.1}$$

Since the QH system lies on the plane, all vectors consist of two spatial coordinates x and y and the temporal coordinate t. Using the typical convention of field theories, we will denote the latter with the index 0, and the spatial coordinates with indexes 1 and 2. We will adopt the convention of summation over repeated indexes, resorting to Greek letters when dealing with all values $(0, 1, 2)$ and Roman indexes for the case of purely spatial values $(1, 2)$. From now on, we will work with natural units $\hbar = c = 1$.

Consider a two-dimensional system of N electrons with charge $-e$ ($e > 0$), whose charge and current densities are denoted with J^0 and $\boldsymbol{J} = (J^1, J^2)$ respectively. We are looking for a theory that describes the response of a Laughlin FQH system with filling factor $\nu = 1/(2n+1)$ to a small variation of the electromagnetic fields. First of all, a variation of charge density $\delta J^0 = -e\delta n_e$ is linked to the filling factor and the variation of the magnetic field δB by the relation $\delta n_e = \frac{\nu e}{2\pi}\delta B$, obtained from Eq. (2.21) (note that $h = 2\pi$ in natural units). On the other hand, the current δJ^i due to the application of an electric field δE_j in the transverse direction is governed by the Hall resistance $\rho_{xy} = \frac{2\pi}{\nu e^2}$ (the longitudinal resistance ρ_{xx} vanishes on a quantum Hall plateau). In terms of the three-vector δJ these constraints correspond to

$$\frac{\delta J^0}{(-e)} = \delta n_e = \frac{\nu e}{2\pi}\delta B, \qquad \delta J^i = \frac{\nu e}{2\pi}\varepsilon^{ij}\delta E_j. \tag{3.2}$$

Here, ε^{ij} is the anti-symmetric symbol with two indexes. The above relations can be compactly recast as

$$\delta J^\mu = -\frac{\nu e^2}{2\pi}\varepsilon^{\mu\rho\sigma}\partial_\rho \delta A_\sigma, \tag{3.3}$$

where we have similarly used the anti-symmetric symbol $\varepsilon^{\mu\rho\sigma}$ with three indexes. It's worth underlining that the field A_μ describes perturbations of the electromagnetic fields around a given Hall state with a fixed filling factor, and does not include the uniform background magnetic field that gives rise to the QH effect. The latter is taken for granted and is, in some sense, implicitly included in Eq. (3.3) through the filling factor [125, 126].

We now focus on the Lagrangian (3.1) and try to rewrite it in such a way to recover Eq. (3.3) from the equations of motion. To this end, it is useful to introduce a new $U(1)$ gauge field a_μ and write the current in terms of the latter. The only possibility for a conserved, gauge invariant current in 2+1 dimension is [126]

$$J^\mu = -\frac{e}{2\pi}\varepsilon^{\mu\rho\sigma}\partial_\rho a_\sigma. \tag{3.4}$$

We thus add a new term $\mathcal{L}_{\text{CS}} = a_\mu J^\mu$ to the total Lagrangian density, which therefore reads

$$\mathcal{L} = \mathcal{L}_{\text{CS}} + \mathcal{L}_A = \frac{m}{4\pi}\varepsilon^{\mu\rho\sigma}a_\mu\partial_\rho a_\sigma - \frac{e}{2\pi}\varepsilon^{\mu\rho\sigma}A_\mu\partial_\rho a_\sigma. \tag{3.5}$$

It's worth noticing that the new term $\mathcal{L}_{\text{CS}}$, which is called *Chern-Simons Lagrangian*, originates from very general considerations about symmetries and conserved currents in 2+1 dimensions, and is the only relevant term when focusing on the long-distance and large-time physics (i.e. low-energy physics) [125, 126]. In this field-theoretical approach, a_μ can be viewed as an emergent field that lives only inside the material, arising from the collective behavior of many underlying electrons [90, 127].

It's important to point out a significant *caveat* at this stage. The fact that we choose to work with a single emergent gauge field a_μ is already extremely restrictive on the physics: as we will show in a moment, this gives rise to an effective field theory with a single chiral mode at each boundary. Such a description is thus only appropriate for Laughlin FQH states. Indeed, for filling factor of the Jain sequence, edge modes are much more complicated and consist of several channels with, in some cases, different propagation directions [22]. Coupling among these channels can lead to a physical description with only one charged mode responsible for charge transport, and additional neutral modes carrying no charge but finite energy [128, 129]. Assuming a filling factor in the Laughlin sequence $\nu = 1/(2n+1)$ simplifies drastically the structure at the edge, since it guarantees that a single edge mode develops at the boundary. Thus, a Laughlin fractional system seems to be the most natural framework to implement EQO protocols in the FQH regime.

It's immediate to verify that the Euler-Lagrange equations,

$$\partial_\rho \frac{\delta \mathcal{L}}{\delta \partial_\rho a_\mu} - \frac{\delta \mathcal{L}}{\delta a_\mu} = 0, \tag{3.6}$$

lead exactly to Eq. (3.3) when $m = 1/\nu$. Interestingly enough, the Chern-Simons term in Eq. (3.5) seems to work well for a QH system if we choose the arbitrary constant m to be the reciprocal of the filling factor ($m = 1/\nu$). We will see in the next Section that creation and annihilation electronic operators can be defined in a proper way only if m is an odd integer, thus recovering the Laughlin sequence $\nu = 1/(2n+1)$, with $n \in \mathbb{N}$.

Let us notice an important fact: Eq. (3.5) is not gauge invariant. Indeed under gauge transformations

$$\begin{cases} a'_\mu = a_\mu + \partial_\mu \Lambda, \\ A'_\mu = A_\mu + \partial_\mu f, \end{cases} \tag{3.7}$$

the Lagrangian $\mathcal{L}$ transforms as

$$\mathcal{L}' = \mathcal{L} + \frac{1}{4\pi\nu} \varepsilon^{\mu\rho\sigma} \partial_\mu \Lambda \partial_\rho a_\sigma - \frac{e}{2\pi} \varepsilon^{\mu\rho\sigma} \partial_\mu f \partial_\rho a_\sigma. \tag{3.8}$$

We note however that the additional terms involve only derivatives of the fields a_μ. If we assume that the latter vanish at infinity (both in space and time coordinates), we thus recover the gauge invariance of the action S

$$S = \int d^3x\, \mathcal{L} = \int d^3x \left(\frac{1}{4\pi\nu} \varepsilon^{\mu\rho\sigma} a_\mu \partial_\rho a_\sigma - \frac{e}{2\pi} \varepsilon^{\mu\rho\sigma} A_\mu \partial_\rho a_\sigma \right). \tag{3.9}$$

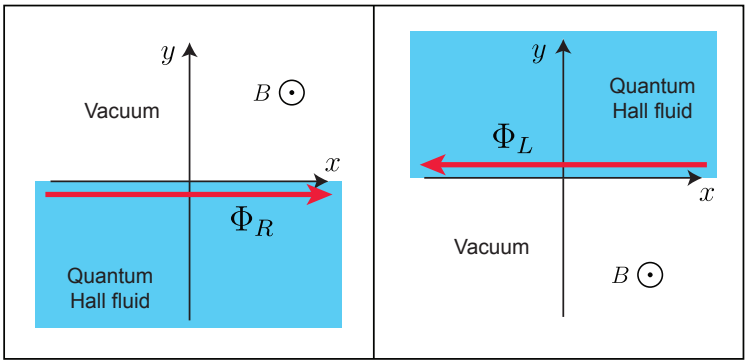

Figure 3.1: When a Laughlin QH system is confined to a limited region of space, a topologically protected edge state appears at the boundary between the QH fluid and the vacuum. Left: when confining to the lower half plane, the edge state has right-moving character (the magnetic field points towards the positive semi-axis z). Right: with the same magnetic field, confinement in the upper half plane generates a left-moving mode.

The Lagrangian (3.5) has another peculiar property: the Hamiltonian density obtained from Eq. (3.5) vanishes identically, namely

$$\mathcal{H} = \frac{\delta \mathcal{L}}{\delta \partial_t a_\mu} \partial_t a_\mu - \mathcal{L} = 0. \tag{3.10}$$

As a consequence, there's no dynamics for the field a_μ. This fact is a common feature of topological field theories [90, 127].

We have seen that topological edge states emerge as soon as we create a boundary between two topologically different regions, the simplest example being an interface between the QH fluid and the vacuum. What happens to $\mathcal{L}$ if we introduce a boundary? Let us consider the quadratic part in the field a_μ (i.e. the Chern-Simons term $\mathcal{L}_{\text{CS}} = \frac{1}{4\pi\nu}\varepsilon^{\mu\rho\sigma} a_\mu \partial_\rho a_\sigma$), and imagine that the system is confined in the lower half of the xy plane, as shown in the left panel of Fig. 3.1. The dramatic consequence of this assumption is the breaking of gauge invariance also for the action integral S. Indeed, we recall that the action (3.9) is gauge invariant only thanks to the vanishing of fields at infinity. However, the integral on y runs now from $-\infty$ to 0, and the argument of throwing away a total derivative because of the vanishing of a_μ at the boundary does not hold anymore. Under transformations (3.7), the action integral generated by $\mathcal{L}_{\text{CS}}$ transforms as $S \to S + \Delta S$ with

$$\begin{aligned} \Delta S &= \int_{-\infty}^{+\infty} dt \int_{-\infty}^{+\infty} dx \int_{-\infty}^{0} dy \frac{1}{4\pi\nu} \varepsilon^{\mu\rho\sigma} \partial_\mu \Lambda \partial_\rho a_\sigma = \\ &= \int_{-\infty}^{+\infty} dt \int_{-\infty}^{+\infty} dx \frac{1}{4\pi\nu} \Big[\Lambda(\partial_t a_x - \partial_x a_t) \Big]_{y=0}. \end{aligned} \tag{3.11}$$

To recover gauge invariance, we must impose either that gauge transformations (3.7) vanish at the edge, i.e. $\Lambda(x, y = 0, t) = 0$, or that fields satisfy $\partial_t a_x(x, y =$

$0,t) - \partial_x a_t(x, y = 0, t) = 0$, so that $\Delta S = 0$. We choose the first alternative, in such a way to avoid a restriction on the fields. This gives us the freedom of choosing a gauge fixing condition.

As a first try for the gauge fixing, we impose $a_t = 0$ and treat the equation of motion for a_t as a constraint:

$$\partial_\rho \frac{\delta \mathcal{L}_{\text{CS}}}{\delta \partial_\rho a_t} - \frac{\delta \mathcal{L}_{\text{CS}}}{\delta a_t} = 0 \quad \Longrightarrow \quad \partial_x a_y - \partial_y a_x = 0. \tag{3.12}$$

This last equation can be solved by introducing a new scalar field $\Phi_R(x, y, t)$, where reason for the label R will become clear in a moment. We write

$$\begin{cases} a_x(x, y, t) = -\sqrt{\nu}\partial_x \Phi_R(x, y, t), \\ a_y(x, y, t) = -\sqrt{\nu}\partial_y \Phi_R(x, y, t), \end{cases} \tag{3.13}$$

and insert the new field in the action integral. From the result we will try to infer a Lagrangian for the FQH edge. Since $a_t = 0$ we have

$$\begin{aligned} S &= \int dt \int dx \int_{-\infty}^{0} dy \frac{1}{4\pi\nu}(a_y \partial_t a_x - a_x \partial_t a_y) = \\ &= \int dt \int dx \int_{-\infty}^{0} dy \frac{1}{4\pi}(\partial_y \Phi_R \partial_t \partial_x \Phi_R - \partial_x \Phi_R \partial_t \partial_y \Phi_R). \end{aligned} \tag{3.14}$$

We integrate by parts the first term with respect to x. This does not introduce any additional boundary term, as the fields $a_i = -\sqrt{\nu}\partial_i \Phi_R$ still vanish at infinity. Equation (3.14) now becomes

$$S = -\int dt \int dx \int_{-\infty}^{0} dy \frac{1}{4\pi} \partial_y (\partial_x \Phi_R \partial_t \Phi_R) = -\int dt \int dx \frac{1}{4\pi} \partial_x \Phi_R \partial_t \Phi_R \Big|_{y=0}. \tag{3.15}$$

This last equation can be interpreted in terms of an action integral defined on the edge,

$$S_R = \iint dt\, dx \mathcal{L}_R, \tag{3.16}$$

from which we recover the Lagrangian

$$\mathcal{L}_R = -\frac{1}{4\pi} \partial_x \Phi_R \partial_t \Phi_R. \tag{3.17}$$

Note that fields $\partial_x \Phi_R$ and $\partial_t \Phi_R$ in the above equation are now defined for $y = 0$, that is, they live on the edge! They only depend on the variables x and t. For the sake of simplicity, in the following we will use the notation

$$\Phi_R(x, t) \equiv \Phi_R(x, 0, t). \tag{3.18}$$

Unfortunately, the edge Lagrangian in Eq. (3.17) still does not work well for our purposes. Indeed it is easy to verify that it still generates a trivial, vanishing

Hamiltonian, and hence no dynamics for the fields. We have to find a way to introduce a propagation velocity in the theory. The solution is to work with the more general gauge fixing condition

$$a_t + v a_x = 0, \tag{3.19}$$

which allows us to introduce a new parameter v in the theory. As we will see in the following, v is exactly the propagation velocity for density waves along the FQH edge states. In a hydrodynamical picture of the edge excitations, v can be related to the electric field responsible for confinement and to the uniform background magnetic field generating Landau quantization, namely $v = |\boldsymbol{E}|/|\boldsymbol{B}|$ [22]. It is worth noticing that, thanks to the change of variables

$$\begin{cases} x' &= x - vt \\ y' &= y \\ t' &= t \end{cases}, \qquad \begin{cases} a_{x'} &= a_x \\ a_{y'} &= a_y \\ a_{t'} &= a_t + v a_x \end{cases}, \tag{3.20}$$

Eq. (3.19) maps into the gauge fixing condition $a_t = 0$ already discussed. In the new coordinates the Lagrangian reads

$$\mathcal{L}_R = -\frac{1}{4\pi}\partial_x \Phi_R (\partial_t + v\partial_x)\Phi_R. \tag{3.21}$$

Finally, by evaluating the Hamiltonian density $\mathcal{H}_R$ from $\mathcal{L}_R$ we obtain the non-vanishing edge Hamiltonian

$$H_R = \int_{-\infty}^{+\infty} dx\, \mathcal{H}_R = \int_{-\infty}^{+\infty} dx \frac{v}{4\pi}(\partial_x \Phi_R)^2. \tag{3.22}$$

This is the typical Hamiltonian for a system of free bosons moving with velocity v, in the direction dictated by the sign of v. At this stage, it is extremely useful to underline a relation between the bosonic field Φ_R and the one-dimensional electron density ρ_R at the edge. We thus integrate the two-dimensional particle density

$$\frac{J^0}{(-e)} = \frac{1}{2\pi}(\partial_x a_y - \partial_y a_x) \tag{3.23}$$

along the thickness of the edge, which we assume to have a very small width λ along the y direction [130]. We have

$$\rho_R(x) = \frac{1}{2\pi}\int_{-\lambda}^{0} dy (\partial_x a_y - \partial_y a_x). \tag{3.24}$$

As the width λ is extremely small, the first term can be evaluated in the limit $\lambda \to 0$ considering $\partial_x a_y$ as constant in that range:

$$\int_{-\lambda}^{0} dy \partial_x a_y \approx \lambda \partial_x a_y \Big|_{y=0} \to 0. \tag{3.25}$$

Conversely, the second term is found by considering that the fields a_μ vanish outside the QH fluid, i.e. for $y \geq 0$. We get

$$\int_{-\lambda}^{0} dy \partial_y a_x = -a_x\Big|_{y=-\lambda} = \sqrt{\nu}\partial_x \Phi_R(x,0,t). \tag{3.26}$$

Thus, the particle density along the edge is proportional to the derivative of the bosonic field Φ_R:

$$\rho_R = -\frac{\sqrt{\nu}}{2\pi}\partial_x \Phi_R. \tag{3.27}$$

Now, let us consider the equation of motion for Φ_R. From the edge Lagrangian (3.21) we get

$$(\partial_t + v\partial_x)\partial_x \Phi_R = 0. \tag{3.28}$$

Since $\partial_x \Phi_R$ is proportional to the density ρ_R, one obtains a propagation equation for the electron density, which reads

$$\partial_t \rho_R + v\partial_x \rho_R = 0. \tag{3.29}$$

We clearly see that edge excitations are chiral as expected. Indeed, Eq. (3.29) is solved by any function of the form

$$\rho_R(x,t) = f(x - vt). \tag{3.30}$$

This is the typical functional form of a wave propagating rigidly at speed v towards right, hence the reason for the label R.

It is now time to quantize the Hamiltonian (3.22) in terms of the Fourier components $\rho_{R,k}$ of the density, which read

$$\rho_{R,k} = \int_{-\frac{L}{2}}^{+\frac{L}{2}} dx\, e^{-ikx}\rho_R(x). \tag{3.31}$$

Correspondingly, the density is given by

$$\rho_R(x) = \frac{1}{L}\sum_{k=-\infty}^{+\infty} e^{ikx}\rho_{R,k}. \tag{3.32}$$

Here we have assumed that the system is a one-dimensional channel with finite length L extending from $-L/2$ to $L/2$. The allowed values for the momentum are $k = 2\pi n/L$, with $n \in \mathbb{N}$, due to periodic boundary conditions. The Hamiltonian (3.22) becomes

$$H_R = \frac{2\pi v}{\nu L}\sum_{k>0} \rho_{R,k}\rho_{R,-k} + \frac{\pi v}{\nu L}N_R^2, \tag{3.33}$$

where we have separated all the contributions for $k \neq 0$ from the term $k = 0$, which we identify with the total number of particles $N_R = \int dx\, \rho_R = \rho_{R,0}$ with

respect to the equilibrium value $N_R^{(0)}$. We now impose canonical commutation relations between $\rho_{R,k}$ and its conjugate variable $\pi_{R,k}$:

$$[\rho_{R,k}, \pi_{R,q}] = i\delta_{k,q}. \tag{3.34}$$

From Hamilton's equation it's immediate to verify that $\pi_{R,q}$ satisfies

$$\dot{\pi}_{R,q} = -\frac{\partial H_R}{\partial \rho_{R,q}} = -\frac{2\pi v}{\nu L}\rho_{R,-q}. \tag{3.35}$$

Since the Fourier transform of Eq. (3.29) reads $\dot{\rho}_{R,q} = -ivq\rho_{R,q}$, we also get

$$\pi_{R,q} = i\frac{2\pi}{q\nu L}\rho_{R,-q}. \tag{3.36}$$

for $q \neq 0$. The canonical commutation relations are thus

$$\begin{cases} [\rho_{R,k}, \rho_{R,q}] = \dfrac{k\nu L}{2\pi}\delta_{k,-q}, & \text{if } k, q \neq 0, \\ [\rho_{R,0}, \pi_{R,0}] = i. \end{cases} \tag{3.37}$$

This is known as Kac-Moody algebra [131]. The fact that commutation relations for the density operator of FQH edge states follow the Kac-Moody algebra should not come as a surprise. Indeed, this is the typical structure of all one-dimensional theories of interacting fermions, which follow the paradigm of the Tomonaga-Luttinger liquid [132–135].

As a final step, we introduce bosonic creation and annihilation operators $b_{R,k}^\dagger$ and $b_{R,k}$. For $k > 0$ they are defined as

$$b_{R,k} = \sqrt{\frac{2\pi}{k\nu L}}\rho_{R,k}, \quad b_{R,k}^\dagger = \sqrt{\frac{2\pi}{k\nu L}}\rho_{R,-k}. \tag{3.38}$$

Using the above mentioned operators, the Hamiltonian is now made of a zero-mode term which depends on the total number of electron in the system, plus a bosonic term which describes a linear excitation spectrum with energy $\varepsilon_k = vk$, namely

$$H_R = \sum_{k>0} vk\, b_{R,k}^\dagger b_{R,k} + \frac{\pi v}{\nu L}N_R^2. \tag{3.39}$$

Quite remarkably, we have obtained a diagonal Hamiltonian in the bosonic operators $b_{R,k}^\dagger$, $b_{R,k}$ and the number operator N_R.

Let us now consider the opposite case in which the QH system lies in the upper half-plane (see Fig. 3.1, right panel). By applying a similar formalism, we expect to find an edge mode at $y = 0$ propagating in the opposite direction. As we did before, we choose $a_t - va_x = 0$ as our gauge fixing condition. We now introduce the new field Φ_L, whose spatial derivatives are linked to the fields a_x and a_y:

$$\begin{cases} a_x = -\sqrt{\nu}\partial_x\Phi_L, \\ a_y = -\sqrt{\nu}\partial_y\Phi_L. \end{cases} \tag{3.40}$$

We obtain the following edge Lagrangian,

$$\mathcal{L}_L = \frac{1}{4\pi}\partial_x\Phi_L(\partial_t - v\partial_x)\Phi_L, \tag{3.41}$$

which indeed describes regressive modes propagating in the negative x direction (and that's why we used the label L). Integrating over a small width λ at the edge we find the left-moving density, which is given by

$$\rho_L = \frac{\sqrt{\nu}}{2\pi}\partial_x\Phi_L. \tag{3.42}$$

The density ρ_L satisfies the equation of motion $\partial_t\rho_L - v\partial_x\rho_L = 0$, and its Fourier components obey the Kac-Moody algebra

$$[\rho_{L,k}, \rho_{L,q}] = -\frac{k\nu L}{2\pi}\delta_{k,-q}. \tag{3.43}$$

The Hamiltonian for the left movers can be written as in Eq. (3.39), provided that we define the new creation and annihilation operators for left-moving excitations as

$$b_{L,k} = \sqrt{\frac{2\pi}{k\nu L}}\rho_{L,-k}, \quad b^\dagger_{L,k} = \sqrt{\frac{2\pi}{k\nu L}}\rho_{L,k}. \tag{3.44}$$

We finally obtain

$$H_L = \frac{v}{4\pi}\int_{-\infty}^{+\infty} dx(\partial_x\Phi_L)^2 = \sum_{k>0} vk\, b^\dagger_{L,k}b_{L,k} + \frac{\pi v}{\nu L}N_L^2. \tag{3.45}$$

with N_L the number of left moving particles with respect the value $N_L^{(0)}$ at equilibrium. In the following we will assume that the edge is sufficiently long to discard safely the terms $\sim 1/L$ in H_R and H_L. This is a good approximation in most of the experimental setups investigating edge state transport in the QH regime, whose typical dimensions are of the order of several μm. Finite size effects, which require a careful treatment of the terms $\sim 1/L$, become important in strongly confined structures such as, for instance, quantum dots [136].

3.2 Bosonization

We have obtained an effective one-dimensional theory for the FQH edge states by restricting the bulk action to the boundary. The result is pretty interesting: excitations of a one-dimensional liquid of interacting fermions behave as *collective bosonic modes*, which propagate chirally along the edge. However, we still miss an ingredient to complete the picture: since the fields $\Phi_{R/L}$ describe neutral ripples of the incompressible liquid, how do we add or remove charge at the edge? The answer was first pointed out by X.G. Wen and relies on the *bosonization approach*.

The key observation is the following. An electronic annihilation operator $\Psi^{(\mathrm{el})}_{R/L}$ must remove one integer charge from the edge. Thus, it is mandatory that its commutation relation with the total electron density reads

$$\left[\rho_{R/L}(x), \Psi^{(\mathrm{el})}_{R/L}(y)\right] = -\delta(x-y)\Psi^{(\mathrm{el})}_{R/L}(y). \tag{3.46}$$

Wen noted that the Kac-Moody algebra (3.37) implies that $\rho_{R/L}$ and $\Phi_{R/L}$ satisfy the following commutation relations

$$\left[\Phi_{R/L}(x), \Phi_{R/L}(y)\right] = \pm i\pi\,\mathrm{sign}(x-y), \tag{3.47}$$
$$\left[\rho_{R/L}(x), \Phi_{R/L}(y)\right] = -i\sqrt{\nu}\delta(x-y). \tag{3.48}$$

These last two equations are demonstrated in Appendix B. He then postulated that the electronic operator must be proportional to the exponential of the bosonic field: $\Psi^{(\mathrm{el})}_{R/L} \propto \exp\left(-i\frac{1}{\sqrt{\nu}}\Phi_{R/L}\right)$ [137]. To see that this is indeed the right intuition, let us check that this choice is consistent with Eq. (3.46). Here we resort to the Baker-Campbell-Hausdorff theorem [138]

$$e^{-B}Ae^{B} = A + [A,B] + \frac{1}{2!}[[A,B],B] + \frac{1}{3!}[[[A,B],B],B] + \ldots \tag{3.49}$$

which implies the very useful formula $[A, e^B] = Ce^B$, with $C = [A,B]$, valid as long as $[A,C] = [B,C] = 0$ [see Eq. (C.6) in Appendix C]. Using this result, together with Eq. (3.48), we immediately get the desired result:

$$\begin{aligned}\left[\rho_{R/L}(x), e^{-i\frac{1}{\sqrt{\nu}}\Phi_{R/L}(y)}\right] &= -i\frac{1}{\sqrt{\nu}}\left[\rho_{R/L}(x), \Phi_{R/L}(y)\right] e^{-i\frac{1}{\sqrt{\nu}}\Phi_{R/L}(y)} = \\ &= -\delta(x-y)e^{-i\frac{1}{\sqrt{\nu}}\Phi_{R/L}(y)}.\end{aligned} \tag{3.50}$$

Moreover, the operator $\exp\left(-i\frac{1}{\sqrt{\nu}}\Phi_{R/L}\right)$ has another very interesting property: it obeys fermionic anti-commutation relation when ν belongs to the Laughlin sequence. This can be verified by using formula (C.8) from Appendix C, namely $e^Ae^B = e^Be^Ae^C$, which is valid again for the case $[A,C] = [B,C] = 0$. Exchanging two exponential operators (or *vertex operators*, as they are frequently named in conformal field theory [139]) one gets

$$\begin{aligned}e^{-i\frac{1}{\sqrt{\nu}}\Phi_{R/L}(x)}e^{-i\frac{1}{\sqrt{\nu}}\Phi_{R/L}(y)} &= \\ &= e^{-i\frac{1}{\sqrt{\nu}}\Phi_{R/L}(y)}e^{-i\frac{1}{\sqrt{\nu}}\Phi_{R/L}(x)}\exp\left\{-\frac{1}{\nu}\left[\Phi_{R/L}(x), \Phi_{R/L}(y)\right]\right\} = \\ &= e^{-i\frac{1}{\sqrt{\nu}}\Phi_{R/L}(y)}e^{-i\frac{1}{\sqrt{\nu}}\Phi_{R/L}(x)}\exp\left\{\mp\frac{i\pi}{\nu}\,\mathrm{sign}(x-y)\right\},\end{aligned} \tag{3.51}$$

thanks to the commutation relations (3.47). Surprisingly, the last result tells us that the vertex operator $\exp\left(-i\frac{1}{\sqrt{\nu}}\Phi_{R/L}\right)$ behaves as a boson if $1/\nu$ is an

even integer, but is instead a fermion when $1/\nu$ is an odd integer. The latter is exactly the case of the Laughlin sequence (2.35). In this context, the function $\mathrm{sign}(x-y)$ in the phase factor has a simple physical interpretation: in two dimensions, clockwise or anti-clockwise rotations give rise to statistical phases with opposite sign.

At this point we notice that the addition or removal of an electron at the edge is not the simplest excitation of the FQH fluid. We can also add or remove a Laughlin quasiparticle with fractional charge $e^* = \nu e$. Annihilation of a quasiparticle is implemented by the operator $\Psi^{(\mathrm{qp})}_{R/L} \propto \exp\left(-i\sqrt{\nu}\Phi_{R/L}\right)$. Indeed, following the demonstration given for the electronic field, it's rather easy to show that the commutator of $\Psi^{(\mathrm{qp})}_{R/L}$ with the total density gives

$$\begin{aligned}\left[\rho_{R/L}(x), e^{-i\sqrt{\nu}\Phi_{R/L}(y)}\right] &= -i\sqrt{\nu}\left[\rho_{R/L}(x), \Phi_{R/L}(y)\right] e^{-i\sqrt{\nu}\Phi_{R/L}(y)} = \\ &= -\nu\delta(x-y)e^{-i\sqrt{\nu}\Phi_{R/L}(y)}. \end{aligned} \tag{3.52}$$

This means that $\exp\left(-i\sqrt{\nu}\Phi_{R/L}\right)$ changes the total density by a fraction ν of an electron! Thus, the vertex operator $\Psi^{(\mathrm{qp})}_{R/L}$ effectively represents the annihilation of a Laughlin quasiparticle at the edge. Moreover, it also implements the fractional statistical properties we anticipated in Sec. 2.3.3. Exchanging two quasiparticles leads to

$$\begin{aligned} & e^{-i\sqrt{\nu}\Phi_{R/L}(x)} e^{-i\sqrt{\nu}\Phi_{R/L}(y)} = \\ & \quad = e^{-i\sqrt{\nu}\Phi_{R/L}(y)} e^{-i\sqrt{\nu}\Phi_{R/L}(x)} \exp\left\{-\nu\left[\Phi_{R/L}(x), \Phi_{R/L}(y)\right]\right\} = \\ & \quad = e^{-i\sqrt{\nu}\Phi_{R/L}(y)} e^{-i\sqrt{\nu}\Phi_{R/L}(x)} \exp\left\{\mp i\nu\pi\,\mathrm{sign}(x-y)\right\} \end{aligned} \tag{3.53}$$

and, thus, to the accumulation of a nontrivial fractional statistical angle $\nu\pi$. As for the electronic case, the sign of the statistical angle depends on the direction of rotation.

The picture described above can be formalized in the framework of the Tomonaga-Luttinger theory, which is a powerful and rather general method to deal with interacting fermions in one dimension [23, 138, 140]. Indeed, the fact that low-energy excitations of fermionic systems are collective bosonic waves is a recurring feature of one-dimensional quantum physics. It allows for an exact solution of the interacting problem, a miracle that never occurs in higher dimensions. The complete expression for electronic and quasiparticle field are

$$\Psi^{(\mathrm{el})}_{R/L}(x) = \frac{F^{(\mathrm{el})}_{R/L}}{\sqrt{2\pi a}} e^{\pm i k_{\mathrm{F}} x} e^{-i\frac{1}{\sqrt{\nu}}\Phi_{R/L}(x)}, \tag{3.54}$$

$$\Psi^{(\mathrm{qp})}_{R/L}(x) = \frac{F^{(\mathrm{qp})}_{R/L}}{\sqrt{2\pi a}} e^{\pm i k_{\mathrm{F}} x} e^{-i\sqrt{\nu}\Phi_{R/L}(x)}. \tag{3.55}$$

The operators $F^{(\mathrm{el/qp})}_{R/L}$ are called Klein factors [23, 138, 140]. They effectively raise or lower the particle number by one unit. Moreover, they have a crucial

role in determining the correct anti-commutation relations between operators on different edges. The new parameter a plays the role of a short distance cut-off, which is used to regularize some notable quantities such as electronic and quasiparticles Green's functions that would otherwise lead to diverging contributions. It gives rise to the corresponding high-energy cutoff $\omega_c = v/a$. Finally, note also that we have introduced the exponential $e^{\pm ik_F x}$ to take into account that bosonic excitations are constructed on top of a filled many-electron system with Fermi momentum k_F [135].

We point out an interesting duality between electron and quasiparticle fields emerging from Eqs. (3.54) and (3.55). Apart from the different Klein factors, which by the way do not play a prominent role in the problems considered in this thesis, the bosonized parts of the fields are related by the transformation $\nu \to 1/\nu$. This duality will be extremely useful when calculating the transport properties of the edge states in presence of tunneling: once we get the result for, say, tunneling of quasiparticles, we can easily infer the corresponding electronic contribution by performing the substitution $\nu \to 1/\nu$ in the scaling exponents [141].

Finally, we also quote the full expression for the bosonic fields $\Phi_{R/L}$ in terms of the operators $b_{R/L}$ and $b^\dagger_{R/L}$. They are given by

$$\Phi_{R/L}(x) = i\sqrt{\frac{2\pi}{L}} \sum_{k>0} \frac{e^{-ak/2}}{\sqrt{k}} \left(e^{\pm ikx} b_{R/L,k} - e^{\mp ikx} b^\dagger_{R/L,k} \right). \tag{3.56}$$

With the help of the bosonized expression for electronic and quasiparticle field, and the Kac Moody algebra of bosonic degrees of freedom, we are now in a position to tackle the problem of edge states transport in the FQH regime with a suitable theoretical apparatus. Since we are dealing with chiral edge states, this theory is known as *chiral Luttinger liquid theory*.

We conclude this section with a pair of important remarks. Firstly, filling factors belonging to the Laughlin sequence are given by $\nu = 1/(2n+1)$, with n a positive integer. As such, they also include the integer filling factor $\nu = 1$ for the case $n = 0$. But we know from the last Chapter that the integer QH effect is fully understood in the non-interacting, single-particle picture of the scattering matrix formalism. Thus, results obtained with bosonization at $\nu = 1$ must coincide with the Fermi liquid result obtained in the scattering approach. In Appendix B we show, indeed, that the chiral Luttinger liquid theory at $\nu = 1$ is formally identical to a one-dimensional theory of free chiral fermions with a linear spectrum.

3.3 Voltage pulse sources and equations of motion

With the field-theoretical description of the edge excitations developed in the previous Section, we are now ready to tackle the theoretical analysis of EQO

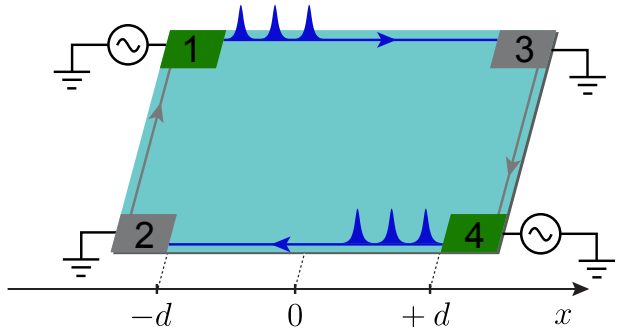

Figure 3.2: A QH system in a four-terminal setup. Edge modes circulate clockwise along the boundary. Two voltage sources are connected to terminals 1 and 4 and can send voltage pulses through the conductor, while terminals 2 and 3 are used as drain contacts for the current.

at fractional filling factor. As a first step, we will show how to couple a pair of voltage pulse sources to the edge states of the FQH system.

Let us consider the four-terminal setup shown in Fig. 3.2. Imagine that two pulse generators are connected to terminals 1 and 4, while contact 2 and 3 are grounded. A voltage pulse applied in contact 1 generates a finite electrical current flowing towards right along the top edge, as shown in the Figure. The current equilibrates in the ohmic contact 3, that serves as the drain contact for the current. Similarly, pulses generated in terminal 4 flow towards left along the bottom edge mode, and are absorbed in terminal 2. We will describe both the top and bottom edges in terms of a chiral Luttinger liquid with filling factor belonging to the Laughlin sequence.

Let us notice that the edge modes circulate also between terminals 2-1 and 3-4. However, they do not contribute to the non-equilibrium transport properties of this system, as they originate from an equilibrium reservoir. We will thus neglect these "vertical" modes and consider a system with two infinitely long edge states lying on the top and bottom edges, shown with blue lines in Fig. 3.2.

Before going on, it is worth recapping the key points of the model by recalling the most useful quantities. The Hamiltonian for the counter-propagating conducting states on the opposite edges is

$$H_0 = \frac{v}{4\pi} \int dx \left[(\partial_x \Phi_R)^2 + (\partial_x \Phi_L)^2 \right], \tag{3.57}$$

where $\Phi_{R/L}$ are given by Eq. (3.56) and satisfy bosonic commutation relations

$$[\Phi_{R/L}(x), \Phi_{R/L}(y)] = \pm i\pi \, \mathrm{sign}(x-y). \tag{3.58}$$

Electron densities on opposite edges are described by the operators

$$\rho_{R/L}(x) = \mp \frac{\sqrt{\nu}}{2\pi} \partial_x \Phi_{R/L}(x). \tag{3.59}$$

Finally, the bosonic picture is related to creation and annihilation of quasiparticles and electrons through bosonization identities

$$\Psi^{(\mathrm{el})}_{R/L}(x) = \frac{F^{(\mathrm{el})}_{R/L}}{\sqrt{2\pi a}} e^{\pm i k_{\mathrm{F}} x} e^{-i\frac{1}{\sqrt{\nu}}\Phi_{R/L}(x)}, \tag{3.60a}$$

$$\Psi^{(\mathrm{qp})}_{R/L}(x) = \frac{F^{(\mathrm{qp})}_{R/L}}{\sqrt{2\pi a}} e^{\pm i k_{\mathrm{F}} x} e^{-i\sqrt{\nu}\Phi_{R/L}(x)}, \tag{3.60b}$$

where the fields $\Psi^{(\mathrm{el})}_r(x)$ and $\Psi^{(\mathrm{qp})}_r(x)$ annihilate respectively an electron and a Laughlin quasiparticle at the coordinate x along the r-moving edge ($r = \{R, L\}$).

We now introduce the coupling with the external voltage sources. Two functions $\mathcal{V}_R(x,t)$ and $\mathcal{V}_L(x,t)$ describe the application of a space- and time-dependent voltage to the right and left moving edges respectively. We assume a simple capacitive coupling $e\rho \cdot V$, which leads to the new following term in the Hamiltonian:

$$H_V = -\frac{e\sqrt{\nu}}{2\pi}\int dx \mathcal{V}_R(x,t)\partial_x\Phi_R(x) + \frac{e\sqrt{\nu}}{2\pi}\int dx \mathcal{V}_L(x,t)\partial_x\Phi_L(x). \tag{3.61}$$

Let us look for the time evolution of bosonic fields $\Phi_{R/L}$ in the presence of such a coupling. We will denote the space- and time-dependent fields with $\Phi_{R/L}(x,t)$. Assuming that the system is initially at equilibrium at the initial time $t = 0$, one must have $\Phi_{R/L}(x,0) \equiv \Phi_{R/L}(x)$, with the latter given by Eq. (3.56). Equations of motion for bosonic fields in the presence of $\mathcal{V}_R$ and $\mathcal{V}_L$ are readily obtained, and reads

$$(\partial_t \pm v\partial_x)\Phi_{R/L}(x,t) = e\sqrt{\nu}\mathcal{V}_{R/L}(x,t). \tag{3.62}$$

This equation is known as *inhomogeneous transport equation* and can be solved in the following way [142]. We first focus on the right moving edge and consider the homogeneous equation in the presence of the boundary condition at the initial instant $t = 0$:

$$\begin{cases} (\partial_t + v\partial_x)\phi_R(x,t) = 0, \\ \phi_R(x, t=0) = \Phi_R(x). \end{cases} \tag{3.63}$$

Here (and in the rest of the thesis) we have denoted solution of the homogeneous equation with the lowercase letter ϕ. The solution to the above equation is trivial, but we prefer to solve it with a general method which allows for a solution of the non-homogeneous problem as well. For each value of (x,t), let us introduce the new function $z(s) := \phi_R(x+vs, t+s)$. It's easy to verify that $z(s)$ is constant, since for the derivative $\dot{z} = \frac{d}{ds}z$ one has

$$\dot{z}(s) = v\partial_x\phi_R(x+vs, t+s) + \partial_t\phi_R(x+vs, t+s) = 0. \tag{3.64}$$

This means that the function ϕ_R is itself constant along the straight line passing through (x,t) with direction given by the 2D vector $(v,1)$. In particular the

function at $s = -t$, which is given by $z(-t) = \phi_R(x - vt, 0) = \Phi_R(x - vt)$ because of the boundary condition, must be equal to $z(0) = \phi_R(x, t)$. The solution to the homogeneous equation is thus

$$\phi_R(x, t) = \Phi_R(x - vt). \tag{3.65}$$

Let us now consider what happens when we add the source term $\mathcal{V}_R(x, t)$. In this case the function $Z(s) = \Phi_R(x+vs, t+s)$ is not constant, and its derivative yields

$$\dot{Z}(s) = v\partial_x\Phi_R(x+vs, t+s)+\partial_t\Phi_R(x+vs, t+s) = e\sqrt{\nu}\mathcal{V}_R(x+vs, t+s). \tag{3.66}$$

Integrating this last equation between $s = -t$ and $s = 0$ we get

$$\int_{-t}^{0} ds\, \dot{Z}(s) = \int_{-t}^{0} ds\, e\sqrt{\nu}\mathcal{V}_R(x + vs, t + s) = \int_{0}^{t} dt'\, e\sqrt{\nu}\mathcal{V}_R\left[x - v(t - t'), t'\right]. \tag{3.67}$$

However, this must also be equal to $Z(0) - Z(-t) = \Phi_R(x, t) - \Phi_R(x - vt, 0)$. Since the initial condition is still $\Phi_R(x - vt, 0) = \Phi_R(x - vt)$, we obtain the following solution for the time evolution of Φ_R in the presence of a generic space and time-dependent voltage:

$$\begin{aligned}\Phi_R(x, t) &= \Phi_R(x - vt) + \int_0^t dt'\, e\sqrt{\nu}\mathcal{V}_R\left[x - v(t - t'), t'\right] = \\ &= \phi_R(x, t) + \int_0^t dt'\, e\sqrt{\nu}\mathcal{V}_R\left[x - v(t - t'), t'\right].\end{aligned} \tag{3.68}$$

To solve the equation for Φ_L, it is sufficient to follow a similar method while inverting the sign of v. We finally get the full solution for both right and left moving fields, which reads

$$\begin{aligned}\Phi_{R/L}(x, t) &= \Phi_{R/L}(x \mp vt) + e\sqrt{\nu}\int_0^t dt'\, \mathcal{V}_{R/L}\left[x \mp v(t - t'), t'\right] = \\ &= \phi_{R/L}(x, t) + e\sqrt{\nu}\int_0^t dt'\, \mathcal{V}_{R/L}\left[x \mp v(t - t'), t'\right].\end{aligned} \tag{3.69}$$

The full solution in the presence of $\mathcal{V}_R$ and $\mathcal{V}_L$ is thus given by the free chiral bosonic modes $\phi_{R/L}(x, t) = \Phi_{R/L}(x \mp vt)$ in the equilibrium configuration ($\mathcal{V}_L = \mathcal{V}_R = 0$) plus an additional term which depends on the integral of $\mathcal{V}_{R/L}$. In passing, we notice that we have solved the equations of motion by switching from a partial differential equation to an ordinary differential equation thanks to the parametrization $Z(s) = \Phi_{R/L}(x \pm vs, t + s)$. This is a special case of a more general method known as *method of characteristics* [142].

Invoking the bosonization identities Eqs. (3.60) we also get the full time evolution of electron and quasiparticle field operators:

$$\Psi^{(\mathrm{el})}_{R/L}(x, t) = \psi^{(\mathrm{el})}_{R/L}(x, t) \exp\left\{-ie\int_0^t dt'\, \mathcal{V}_{R/L}\left[x \mp v(t - t'), t'\right]\right\}, \tag{3.70a}$$

$$\Psi^{(\mathrm{qp})}_{R/L}(x, t) = \psi^{(\mathrm{qp})}_{R/L}(x, t) \exp\left\{-ie^*\int_0^t dt'\, \mathcal{V}_{R/L}\left[x \mp v(t - t'), t'\right]\right\}, \tag{3.70b}$$

Once again, the quantities

$$\psi^{(\mathrm{el})}_{R/L}(x,t) = \frac{F^{(\mathrm{el})}_{R/L}}{\sqrt{2\pi a}} e^{\pm i k_{\mathrm{F}} x} e^{-i\frac{1}{\sqrt{\nu}}\phi_{R/L}(x,t)}, \tag{3.71}$$

$$\psi^{(\mathrm{qp})}_{R/L}(x,t) = \frac{F^{(\mathrm{qp})}_{R/L}}{\sqrt{2\pi a}} e^{\pm i k_{\mathrm{F}} x} e^{-i\sqrt{\nu}\phi_{R/L}(x,t)}. \tag{3.72}$$

play the role of electronic and quasiparticle fields at equilibrium ($\mathcal{V}_R = \mathcal{V}_L = 0$). We conclude that, when capacitively coupled with the voltage gates, both electrons and Laughlin quasiparticles experience a phase shift which is proportional to their charge (e for electrons, $e^* = \nu e$ for quasiparticles) and to the integral of $\mathcal{V}_{R/L}$.

3.3.1 Infinitely long voltage contacts

In order to model the experimentally relevant situation of infinite, homogeneous contacts, we will consider factorizations of the form

$$\mathcal{V}_R(x,t) = \Theta(-x-d)\Theta(t)V_R(t), \tag{3.73a}$$

$$\mathcal{V}_L(x,t) = \Theta(x-d)\Theta(t)V_L(t), \tag{3.73b}$$

where d is a positive length (see Fig. 3.3, top panel). We will focus on the regions downstream of the voltage contacts (that is, $x \geq -d$ for the right-moving top edge and $x \leq d$ for the left-moving mode at the bottom boundary). Here the fields $\Phi_{R/L}$ at $t > 0$ read

$$\begin{aligned}\Phi_{R/L}(x,t) &= \phi_{R/L}(x,t) + e\sqrt{\nu}\int_0^t dt' \Theta\left[\left(t \mp \frac{x}{v} - \frac{d}{v}\right) - t'\right] V_{R/L}(t') = \\ &= \phi_{R/L}(x,t) + \Theta\left(t \mp \frac{x}{v} - \frac{d}{v}\right) e\sqrt{\nu}\int_0^{t\mp\frac{x}{v}-\frac{d}{v}} dt' V_{R/L}(t').\end{aligned} \tag{3.74}$$

Since the signal propagates at finite velocity v, the causality principle imposes that regions whose distance from the contacts exceeds the value vt cannot feel the influence of the voltage drive at a given instant $t > 0$, hence the presence of the Heaviside step function $\Theta\left(t \mp \frac{x}{v} - \frac{d}{v}\right)$ in the above equation. Interestingly, a voltage pulse $V_{R/L}(t)$ generates a deformation in the electronic density with identical shape. One indeed has

$$\rho_{R/L}(x,t) = \mp\frac{\sqrt{\nu}}{2\pi}\partial_x\phi_{R/L}(x,t) + \Theta\left(t \mp \frac{x}{v} - \frac{d}{v}\right)\frac{e^*}{2\pi}V_{R/L}\left(t \mp \frac{x}{v} - \frac{d}{v}\right). \tag{3.75}$$

We will always assume that the causality condition $\pm x + d < vt$ imposed by the step function in Eq. (3.74) is satisfied. As a consequence, annihilation

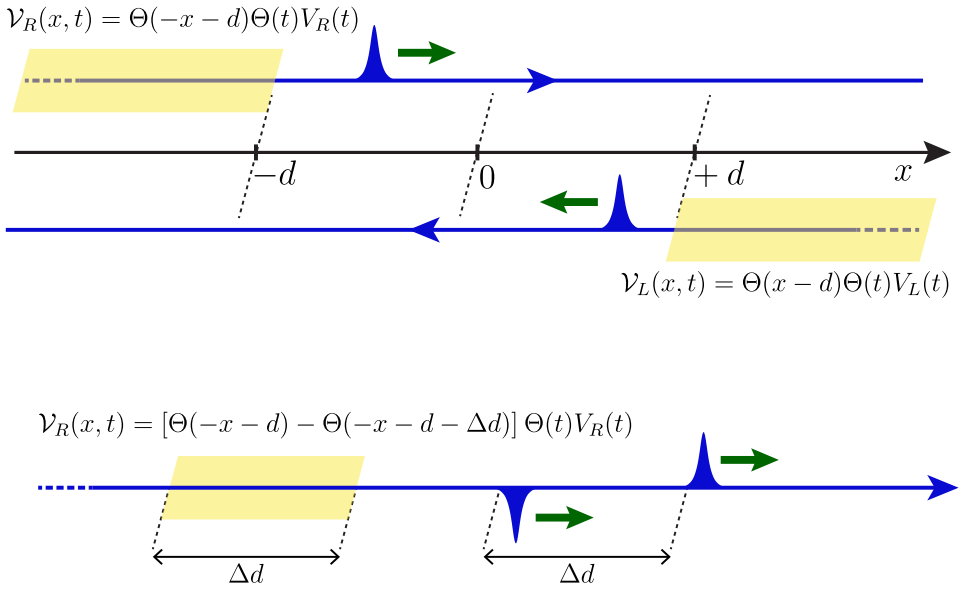

Figure 3.3: Top: capacitive coupling between a pair of infinite, homogeneous voltage contacts and the chiral edge modes. Bottom: finite voltage contact with length Δd coupled with the right-moving edge.

operators for electrons and Laughlin quasiparticle are given by

$$\Psi^{(\mathrm{el})}_{R/L}(x,t) = \psi^{(\mathrm{el})}_{R/L}(x,t)\exp\left\{-ie\int_0^{t\mp\frac{x}{v}-\frac{d}{v}} dt' V_{R/L}(t')\right\}, \tag{3.76a}$$

$$\Psi^{(\mathrm{qp})}_{R/L}(x,t) = \psi^{(\mathrm{qp})}_{R/L}(x,t)\exp\left\{-ie^*\int_0^{t\mp\frac{x}{v}-\frac{d}{v}} dt' V_{R/L}(t')\right\}. \tag{3.76b}$$

The unimportant constant time shift $\frac{d}{v}$ will be omitted throughout this thesis.

3.3.2 Finite-length contacts

Before going on it's important to emphasize that a capacitive coupling does not account, strictly speaking, for charge injection into the edge modes, since the coupling Hamiltonian Eq. (3.61) *cannot add or remove electrons on the edge*. It can only rearrange the electronic density in neutral density waves, with $\int_{-\infty}^{+\infty} dt\,\rho_{R/L}(x,t)$ unaffected by the presence of the voltage drive.

To see how this may be in accordance with Eq. (3.75), consider for the moment the model with a finite-length voltage contact shown in the bottom panel of Fig. 3.3. Let us focus on the right-moving edge and write

$$\mathcal{V}_R(x,t) = [\Theta(-x-d) - \Theta(-x-d-\Delta d)]\,\Theta(t)V_R(t), \tag{3.77}$$

with $\Delta d > 0$. Inserting this new factorization into Eq. (3.69) and calculating

$\rho_R = -\frac{\sqrt{\nu}}{2\pi}\partial_x \Phi_R$ leads to

$$\rho_R(x,t) = \mp\frac{\sqrt{\nu}}{2\pi}\partial_x\phi_R(x,t) + \Theta\left(t - \frac{x}{v} - \frac{d}{v}\right)\frac{e^*}{2\pi}V_R\left(t - \frac{x}{v} - \frac{d}{v}\right) + \\ - \Theta\left(t - \frac{x}{v} - \frac{d+\Delta d}{v}\right)\frac{e^*}{2\pi}V_R\left(t - \frac{x}{v} - \frac{d+\Delta d}{v}\right). \tag{3.78}$$

The electronic density is now deformed in two bumps with opposite sign which, due to chirality, propagate rigidly at a fixed distance Δd. An integration over space (or, equivalently, time) immediately shows that the total particle number is unaffected by the voltage drive, since the two pulses compensate each other perfectly.

The model with an infinite contact is recovered for the case $\Delta d \to +\infty$, where there's no region of space that can satisfy the causality condition $vt > x + d + \Delta d$ imposed by the step function linked to the negative pulse in Eq. (3.78). Here, the second negative pulse is subjected to an infinite delay, and never participates in the dynamics. However, we are not injecting a finite charge into the edge modes. We are simply pushing negative pulses infinitely distant in space (and, correspondingly, in time).

With this *caveat* in mind, we will use from now on the infinite contact model, which gives rise to the phase-shift of quasiparticle and electronic operators shown in Eqs. (3.76).

3.4 Tunneling at the QPC

We have seen in Section 2.2 of the previous Chapter that EQO is basically built upon three ingredients: electronic waveguides, coherent single electron sources and beam splitters. We can now describe all the ingredients on the basis of the theoretical model introduced in the present Chapter. Waveguides are implemented by QH edge states, whose Hamiltonian has been introduced in Eq. (3.57) for fractional filling factor belonging to the Laughlin sequence. To model the source we use Eq. (3.61), which accounts for the separate coupling of left and right moving modes with two voltage gates. We now introduce the missing piece, namely an effective description for the beam splitter.

We imagine that two additional gates create a QPC at the position $x = 0$, as shown in Fig. 3.4, allowing for tunneling of electrons and quasiparticles between opposite edges. The corresponding tunneling operators are

$$H_T^{(\mathrm{qp})} = \Lambda \Psi_R^{(\mathrm{qp})\dagger}(0)\Psi_L^{(\mathrm{qp})}(0) + \mathrm{h.c.} = \sum_{\varepsilon=+,-}\left[\Lambda \Psi_R^{(\mathrm{qp})\dagger}(0)\Psi_L^{(\mathrm{qp})}(0)\right]^{\varepsilon}, \tag{3.79}$$

$$H_T^{(\mathrm{el})} = \Lambda \Psi_R^{(\mathrm{el})\dagger}(0)\Psi_L^{(\mathrm{el})}(0) + \mathrm{h.c.} = \sum_{\varepsilon=+,-}\left[\Lambda \Psi_R^{(\mathrm{el})\dagger}(0)\Psi_L^{(\mathrm{el})}(0)\right]^{\varepsilon}, \tag{3.80}$$

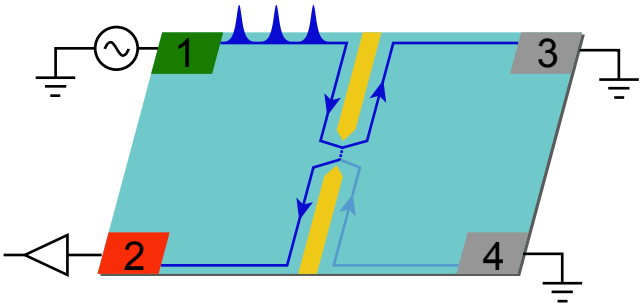

Figure 3.4: Four terminal geometry as in Fig. 3.2, but in the presence of a QPC at the coordinate $x = 0$. Here the voltage source connected to terminal 4 is switched off. Backscattering current is collected in contact 2 (red).

with Λ the constant tunneling amplitude. Note that we have introduced the very useful notation [55]

$$[X]^{\varepsilon} = \begin{cases} X, & \text{if } \varepsilon = +, \\ X^{\dagger}, & \text{if } \varepsilon = -. \end{cases} \tag{3.81}$$

The time evolution of both $H_T^{(\mathrm{qp})}$ and $H_T^{(\mathrm{el})}$ is immediately found by using the time-dependent fields in Eqs. (3.76). We will assume that the QPC operates in the weak backscattering regime, which means that the barrier is almost transparent and only a small amount of particles are reflected back into the opposite chiral mode. We therefore treat backscattering at the QPC as a small perturbation with respect to the Hamiltonian $H_0 + H_V$, and evaluate the tunneling current and its fluctuation spectrum to lowest nonvanishing order in the parameter Λ. We will perform calculations in an interaction picture where operators evolve in time according to $H_0 + H_V$, while quantum states evolve with $H_T^{(\mathrm{qp/el})}$ (see Appendix D for details about the interaction picture).

In this regime, both electrons and fractional quasiparticles are allowed to tunnel from one edge mode to the opposite. We will first consider the case of Laughlin quasiparticles and obtain the backscattering current due to the tunneling operator $H_T^{(\mathrm{qp})}$. Then, the result for electrons can be readily obtained with the substitution $\nu \to 1/\nu$, as already discussed in Section 3.2. We will see in the following that tunneling of quasiparticles dominates over electrons in the weak backscattering regime, and is the only relevant process in the renormalization group sense [143, 144].

3.4.1 Current

Let us now focus on the backscattering current induced by the quasiparticle tunneling term, Eq. (3.79). We assume that the voltage source coupled to the left-moving mode is switched off, while the one coupled to right-moving excitations sends a finite current along the top edge (see Fig. 3.4). We will

call this configuration *HBT setup*, due to the similarity with the optical HBT experiment [105, 106]. Due to the presence of the QPC, part of the current is deviated into the bottom edge. We infer the tunneling current from the temporal variation of the left-moving electron density ρ_L (which is, by the way, compensated by an identical variation with opposite sign in the right-moving density, because of current conservation). It can be measured, for instance, by looking at the total current flowing into terminal 2 (see Fig. 3.4). The latter is zero in the absence of tunneling.

We will use the notation J_C for the charge current operator, in order to distinguish from the heat current J_Q that will be the main subject of the next Chapter. The backscattered current operator reads

$$J_C = e\dot{N}_L = -ie\left[N_L, H_T^{(\mathrm{qp})}\right], \tag{3.82}$$

where $N_L = \int dx\, \rho_L$ is the total number of left-moving particles. We now bosonize the tunneling Hamiltonian with the help of Eqs. (3.60) and make use of the formula $[A, e^B] = Ce^B$, with $C = [A, B]$ [Appendix C, Eq. (C.6)], to get

$$\begin{aligned} J_C &= -ie\frac{\sqrt{\nu}}{2\pi}\int dx\left[\partial_x\Phi_L(x), \frac{\Lambda}{2\pi a}e^{i\sqrt{\nu}\Phi_R(0)}e^{-i\sqrt{\nu}\Phi_L(0)} + \mathrm{h.c.}\right] = \\ &= -ie\frac{\sqrt{\nu}}{2\pi}\frac{\Lambda}{2\pi a}e^{i\sqrt{\nu}\Phi_R(0)}e^{-i\sqrt{\nu}\Phi_L(0)}\int dx\left[\partial_x\Phi_L(x), (-i\sqrt{\nu})\Phi_L(0)\right] + \mathrm{h.c.} = \\ &= ie^*\frac{\Lambda}{2\pi a}e^{i\sqrt{\nu}\Phi_R(0)}e^{-i\sqrt{\nu}\Phi_L(0)} + \mathrm{h.c.} = \\ &= ie^*\sum_{\varepsilon=+,-}\varepsilon\left[\Lambda{\Psi_R^{(\mathrm{qp})}}^\dagger(0)\Psi_L^{(\mathrm{qp})}(0)\right]^\varepsilon. \end{aligned} \tag{3.83}$$

Note that we have neglected the Klein factors in the intermediate steps of the above calculation, as they can be safely omitted in a system with only two edges [145]. Since we are focusing on quasiparticle operators, we will drop the label $^{(\mathrm{qp})}$ from quasiparticle fields $\Psi_{R/L}^{(\mathrm{qp})}$ for brevity. Using Eqs. (3.76) we find the time dependent operator $J_C(t)$, which is given by

$$J_C(t) = ie^*\sum_{\varepsilon=+,-}\varepsilon e^{i\varepsilon e^*\int_0^t V(t')dt'}\left[\Lambda\psi_R^\dagger(0,t)\psi_L(0,t)\right]^\varepsilon. \tag{3.84}$$

We now evaluate the expectation value of the backscattered current $J_C(t)$ using the Keldysh contour formalism [55, 146]. This is a powerful tool to tackle nonequilibrium problems in terms of quasiparticle Green's functions, and basically works in the following way (a more detailed introduction to the Keldysh formalism is developed in Appendix D). We imagine that the unperturbed system (in this case, the free edge states in the presence of voltage pulses) was initially at equilibrium in the far past ($t = -\infty$), and that the perturbation (here, the tunneling) was then adiabatically switched on. We introduce a closed contour c_K for the temporal variable t which runs from

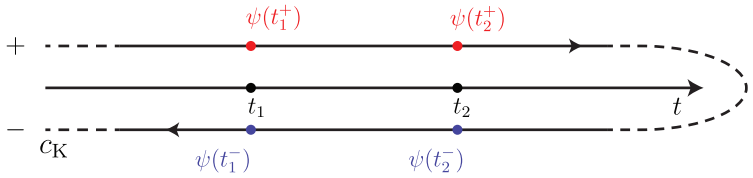

Figure 3.5: Keldysh contour for the calculation of non-equilibrium Green's functions. Operators are ordered along a path that evolves first from $t = -\infty$ to $+\infty$ (upper branch, label $+$) and then back from $+\infty$ to $-\infty$ (lower branch, label$-$).

$t = -\infty$ to $t = +\infty$ and then back again to $t = -\infty$, as shown in Fig. 3.5. Each field operator can now lie either on the upper branch of the contour (from $-\infty$ to $+\infty$) or on the lower one (from positive to negative times). We use the notation t^η, with $\eta = \{+, -\}$, to label times in the two branches of the Keldysh contour. We finally introduce a new time-ordering operator $T_{\rm K}$ which arranges field operators according to their position along the twofold contour. With this trick, one can relate any expectation value to a quantum average over the initial equilibrium state at $t = -\infty$, as we explain in more detail in Appendix D. Any reference to the final non-equilibrium state is thus avoided. The price to pay it that Green's function have now a 2×2 matrix structure in the space of Keldysh labels η. However, each entry of the matrix is in relation with an appropriate real-time Green's function, as we will show in a moment.

To calculate the average value of the current $J_C(t)$, we must place the time coordinate t somewhere along the Keldysh contour. A common choice is a symmetric combination of the upper and lower contour, $J_C(t) = \frac{1}{2}\sum_\eta J_C(t^\eta)$. The expectation value of the current then reads

$$\begin{aligned}\langle J_C(t)\rangle &= \frac{1}{2}\sum_{\eta=+,-}\left\langle T_{\rm K} J_C(t^\eta) e^{-i\int_{c_{\rm K}} H_T(t')dt'}\right\rangle = \\ &= \frac{1}{2}\sum_{\eta,\eta'}\left\langle T_{\rm K} J_C(t^\eta) e^{-i\eta'\int_{-\infty}^{+\infty} H_T(t'^{\eta'})dt'}\right\rangle, \end{aligned} \tag{3.85}$$

where η and η' label the two branches of $c_{\rm K}$. A perturbative expression for $\langle J_C(t)\rangle$ is then readily obtained by expanding the exponential as a power series, and retaining the lowest nonvanishing order in Λ. At first order in the

perturbation we obtain

$$\begin{aligned}\langle J_C(t)\rangle &= -\frac{i}{2}\sum_{\eta,\eta'}\eta'\int_{-\infty}^{+\infty}dt'\left\langle T_{\rm K}J_C(t^\eta)H_T(t'^{\eta'})\right\rangle = \\ &= \frac{e^*}{2}\sum_{\eta,\eta'}\eta'\int_{-\infty}^{+\infty}dt'\sum_{\varepsilon,\varepsilon'}\varepsilon e^{i\varepsilon e^*\int_0^t V(t'')dt''}e^{i\varepsilon' e^*\int_0^{t'}V(t'')dt''}\times \\ &\quad\times\left\langle T_{\rm K}\left[\Lambda\psi_R^\dagger(0,t^\eta)\psi_L(0,t^\eta)\right]^\varepsilon\left[\Lambda\psi_R^\dagger(0,t'^{\eta'})\psi_L(0,t'^{\eta'})\right]^{\varepsilon'}\right\rangle = \\ &= \frac{e^*}{2}|\Lambda|^2\sum_{\eta,\eta'}\eta'\int_{-\infty}^{+\infty}dt'\times \\ &\quad\times\left\{e^{ie^*\int_{t'}^t V(t'')dt''}\left\langle T_{\rm K}\psi_R^\dagger(0,t^\eta)\psi_R(0,t'^{\eta'})\right\rangle\left\langle T_{\rm K}\psi_L(0,t^\eta)\psi_L^\dagger(0,t'^{\eta'})\right\rangle\right. \\ &\quad\left.-e^{-ie^*\int_{t'}^t V(t'')dt''}\left\langle T_{\rm K}\psi_R(0,t^\eta)\psi_R^\dagger(0,t'^{\eta'})\right\rangle\left\langle T_{\rm K}\psi_L^\dagger(0,t^\eta)\psi_L(0,t'^{\eta'})\right\rangle\right\}.\end{aligned} \tag{3.86}$$

We must now find the quasiparticle Green's function. Using the formula $e^Ae^B = e^{A+B}e^{C/2}$ valid for $C=[A,B]$ and $[A,C]=[B,C]=0$ [Appendix C, Eq. (C.14)] we find

$$\begin{aligned}&\left\langle T_{\rm K}\psi_{R/L}^\dagger(0,t^\eta)\psi_{R/L}(0,t'^{\eta'})\right\rangle = \\ &\qquad = \frac{1}{2\pi a}\left\langle T_{\rm K}e^{i\sqrt{\nu}\left[\phi_{R/L}(0,t^\eta)-\phi_{R/L}(0,t'^{\eta'})\right]}\right\rangle e^{\frac{\nu}{2}\left[\phi_{R/L}(0,t),\phi_{R/L}(0,t')\right]}.\end{aligned} \tag{3.87}$$

We now use the following important result. If an operator X is a linear combination of bosonic operators b_k and $b_k^\dagger$, then the thermal average $\langle e^X\rangle$ performed over an equilibrium state described by the free bosonic Hamiltonian $H=\sum_k\varepsilon_k b_k^\dagger b_k$ is

$$\left\langle e^X\right\rangle = e^{\frac{1}{2}\langle X^2\rangle}, \tag{3.88}$$

as demonstrated, for instance, in Ref. [138]. This is exactly the case of the fields $\phi_{R/L}$, which are linear in the operators $b_{R/L,k}$ and $b_{R/L,k}^\dagger$ [see Eq. (3.56)]. The quasiparticle Green's function then becomes

$$\begin{aligned}&\left\langle T_{\rm K}\psi_{R/L}^\dagger(0,t^\eta)\psi_{R/L}(0,t'^{\eta'})\right\rangle = \\ &\quad = \frac{1}{2\pi a}e^{-\frac{\nu}{2}\left\langle\phi_{R/L}^2(0,t^\eta)+\phi_{R/L}^2(0,t'^{\eta'})-\phi_{R/L}(0,t^\eta)\phi_{R/L}(0,t'^{\eta'})-\phi_{R/L}(0,t'^{\eta'})\phi_{R/L}(0,t^\eta)\right\rangle}\times \\ &\qquad\times e^{\frac{\nu}{2}\left[\phi_{R/L}(0,t),\phi_{R/L}(0,t')\right]} = \\ &\quad = \frac{1}{2\pi a}e^{\nu\left\langle\phi_{R/L}(0,t^\eta)\phi_{R/L}(0,t'^{\eta'})-\phi_{R/L}^2(0,0)\right\rangle}.\end{aligned} \tag{3.89}$$

In the last equality we have used the fact that $\left\langle\phi_{R/L}^2(0,t^\eta)\right\rangle = \left\langle\phi_{R/L}^2(0,t'^{\eta'})\right\rangle = \left\langle\phi_{R/L}^2(0,0)\right\rangle$, since thermal averages are invariant under time translations

due to symmetry considerations. We also used again Eq. (C.14) to commute $\phi_{R/L}(0,t'^{\eta'})$ past $\phi_{R/L}(0,t^{\eta})$. The problem of evaluating the quasiparticle Green's functions is thus reduced to the calculation of the bosonic correlator

$$\mathcal{G}^{\eta\eta'}(t,t') = \left\langle \phi_{R/L}(0,t^{\eta})\phi_{R/L}(0,t'^{\eta'}) - \phi^2_{R/L}(0,0) \right\rangle , \tag{3.90}$$

which is a 2×2 matrix in the space of Keldysh contour indexes. However, each entry of the 2×2 matrix is related to the standard one-dimensional Green's function through

$$\begin{pmatrix} \mathcal{G}^{++}(t,t') & \mathcal{G}^{+-}(t,t') \\ \mathcal{G}^{-+}(t,t') & \mathcal{G}^{--}(t,t') \end{pmatrix} = \begin{pmatrix} \mathcal{G}(|t-t'|) & \mathcal{G}(-t+t') \\ \mathcal{G}(t-t') & \mathcal{G}(-|t-t'|) \end{pmatrix} , \tag{3.91}$$

where the real-time bosonic correation function $\mathcal{G}(\tau)$ has been calculated in Appendix E. It reads

$$\begin{aligned} \mathcal{G}(\tau) &= \left\langle \phi_{R/L}(0,\tau)\phi_{R/L}(0,0) \right\rangle - \left\langle \phi^2_{R/L}(0,0) \right\rangle = \\ &= \ln \left[\frac{\left| \Gamma\left(1+\frac{1}{\beta\omega_c}+i\frac{\tau}{\beta}\right)\right|^2}{\Gamma^2\left(1+\frac{1}{\beta\omega_c}\right)(1+i\omega_c\tau)} \right] \approx \ln \left[\frac{\pi\frac{t}{\beta}}{\sinh\left(\pi\frac{t}{\beta}\right)(1+i\omega_c t)} \right] . \end{aligned} \tag{3.92}$$

Here $\beta = \theta^{-1}$ is the inverse temperature (we have set $k_B = 1$), ω_c is the high energy cutoff and the last equality was obtained in the limit $\beta\omega_c \gg 1$. Note that there is no label R/L as the Green's function $\mathcal{G}(\tau)$ is equal for both right-moving and left-moving modes.

The calculation of $\left\langle T_K \psi_{R/L}(0,t^{\eta})\psi^{\dagger}_{R/L}(0,t'^{\eta'}) \right\rangle$ is very similar and yields an identical result. We find

$$\begin{aligned} &\left\langle T_K \psi_{R/L}(0,t^{\eta})\psi^{\dagger}_{R/L}(0,t'^{\eta'}) \right\rangle = \\ &\qquad = \left\langle T_K \psi^{\dagger}_{R/L}(0,t^{\eta})\psi_{R/L}(0,t'^{\eta'}) \right\rangle = \frac{1}{2\pi a}\exp\left[\nu\mathcal{G}^{\eta\eta'}(t,t')\right] , \end{aligned} \tag{3.93}$$

with $\mathcal{G}^{\eta\eta'}(t,t')$ given by the matrix representation Eq. (3.91). We now use the latest result in Eq. (3.86) to find

$$\begin{aligned} \langle J_C(t)\rangle &= ie^*|\lambda|^2 \sum_{\eta,\eta'} \eta' \int_{-\infty}^{+\infty} d\tau \sin\left[e^* \int_{t-\tau}^{t} V(t'')dt'' \right] e^{2\nu\mathcal{G}^{\eta\eta'}(\tau)} = \\ &= 2ie^*|\lambda|^2 \int_0^{+\infty} d\tau \sin\left[e^* \int_{t-\tau}^{t} V(t'')dt'' \right] \left[e^{2\nu\mathcal{G}(\tau)} - e^{2\nu\mathcal{G}(-\tau)} \right] , \end{aligned} \tag{3.94}$$

where we have introduced the rescaled tunneling coupling $\lambda = \Lambda/(2\pi a)$.

To make contact with the photoassisted transport formalism, we now imagine that the voltage source sends time-periodic pulses to the conductor with

period T.[1] Then, as one should expect, the current arising in response to a periodic drive is itself periodic. The signal in Eq. (3.94) satisfies indeed $\langle J_C(t+T)\rangle = \langle J_C(t)\rangle$, since

$$\sin\left[e^*\int_{t+T-\tau}^{t+T} V(t'')dt''\right] = \sin\left[e^*\int_{t-\tau}^{t} V(t''+T)dt''\right] = \sin\left[e^*\int_{t-\tau}^{t} V(t'')dt''\right]. \tag{3.95}$$

We can thus compute the tunneling current averaged over one period, which reads

$$\begin{aligned}\overline{\langle J_C(t)\rangle} &= \int_0^T \frac{dt}{T}\langle J_C(t)\rangle = \\ &= 2ie^*|\lambda|^2\left\{\int_0^{+\infty} d\tau\int_0^T \frac{dt}{T}\sin\left[e^*\int_{t-\tau}^{t} V(t'')dt''\right]e^{2\nu\mathcal{G}(\tau)}\right. \\ &\quad \left.+\int_{-\infty}^{0} d\tau\int_{-\tau}^{T-\tau}\frac{dt}{T}\sin\left[e^*\int_{t}^{t+\tau} V(t'')dt''\right]e^{2\nu\mathcal{G}(\tau)}\right\}. \end{aligned} \tag{3.96}$$

In the second term we have used the fact that $\int_0^T dt\, f(t)$ is equivalent to $\int_\alpha^{T+\alpha} dt\, f(t)$ for a periodic function f with period T. Performing the change of variable $t' = t+\tau$ we now get

$$\begin{aligned}\overline{\langle J_C(t)\rangle} &= 2ie^*|\lambda|^2\left\{\int_0^{+\infty} d\tau\int_0^T \frac{dt}{T}\sin\left[e^*\int_{t-\tau}^{t} V(t'')dt''\right]e^{2\nu\mathcal{G}(\tau)}\right. \\ &\quad \left.+\int_{-\infty}^{0} d\tau\int_{0}^{T}\frac{dt'}{T}\sin\left[e^*\int_{t'-\tau}^{t'} V(t'')dt''\right]e^{2\nu\mathcal{G}(\tau)}\right\} = \\ &= 2ie^*|\lambda|^2\int_0^T\frac{dt}{T}\int_{-\infty}^{+\infty} d\tau\sin\left[e^*\int_{t-\tau}^{t} V(t'')dt''\right]e^{2\nu\mathcal{G}(\tau)}. \end{aligned} \tag{3.97}$$

The factor $\sin\left[e^*\int_{t-\tau}^{t} V(t'')dt''\right]$ can be written in terms of the photoassisted coefficients $p_l(\alpha)$ introduced in Chapter 1, Eq. (1.65). One has

$$\sin\left[e^*\int_{t-\tau}^{t} V(t'')dt''\right] = \frac{1}{2i}\sum_{l,m}\left[p_l^*(\alpha)p_m(\alpha)e^{i(l-m)\omega t}e^{i(q+m)\omega\tau} - \text{c.c.}\right]. \tag{3.98}$$

Here the parameters q and α are related to the dc and ac amplitudes of the voltage drive, namely $q = e^*V_{\rm dc}/\omega$ and $\alpha = e^*V_{\rm ac}/\omega$. As such, q can be interpreted as the number of electrons carried in a single period of the drive,

[1] Strictly speaking, voltage drives in Eqs. (3.73) cannot be completely periodic in time due to the presence of the step function $\Theta(t)$. However, one can imagine to move the switching-on from $t=0$ to an infinitely distant time $t_0 = -\infty$. Equation of motions remain substantially identical, except for a different extreme of integration in the phase accumulated by Laughlin quasiparticle operators, which now reads $\exp\left\{-ie^*\int_{t_0}^{t\mp\frac{x}{v}-\frac{d}{v}} dt' V_{R/L}(t')\right\}$. Quasiparticle fields thus differ from the ones in Eqs. (3.76) by a constant phase factor $\exp\left\{-ie^*\int_{t_0}^{0} dt' V_{R/L}(t')\right\}$, which is completely negligible for our purposes.

since the integral over one period of the injected current $I_0(t) = \nu\frac{e^2}{2\pi}V(t)$ yields $Q = \int_0^T dt\,\nu\frac{e^2}{2\pi}V(t) = eq$. We stress that this is only a mathematical correspondence between the dc amplitude q and the integral of $I_0(t)$, and the parameter q can safely take non-integer value without violating any fundamental principle. We now insert Eq. (3.98) into Eq. (3.97). Integration over t gives a Kroenecker delta $\delta_{l,m}$ and one is finally left with

$$\overline{\langle J_C(t)\rangle} = 2ie^*\,|\lambda|^2 \sum_{l=-\infty}^{+\infty} |p_l(\alpha)|^2 \int_{-\infty}^{+\infty} d\tau \sin\left[(q+l)\,\omega\tau\right] e^{2\nu\mathcal{G}(\tau)}. \tag{3.99}$$

It's extremely useful to switch from integration in the time domain to the energy domain. We thus introduce the function $P_g(\tau) = e^{g\mathcal{G}(\tau)}$ and its Fourier transform $\hat{P}_g(E) = \int dt\, e^{iE\tau} P_g(\tau)$, the anti-Fourier transform being $P_g(\tau) = \frac{1}{2\pi}\int dE\, e^{-iE\tau}\hat{P}_g(E)$. The function $\hat{P}_g(E)$ at finite temperature $\theta > 0$ has been calculated in Appendix F and is given by [23, 147–149]

$$\begin{aligned}\hat{P}_g(E) &= \left(\frac{2\pi\theta}{\omega_c}\right)^{g-1} \frac{e^{E/(2\theta)}}{\omega_c}\mathcal{B}\left(\frac{g}{2} - i\frac{E}{2\pi\theta}, \frac{g}{2} + i\frac{E}{2\pi\theta}\right) = \\ &= \left(\frac{2\pi\theta}{\omega_c}\right)^{g-1} \frac{e^{E/(2\theta)}}{\Gamma(g)\omega_c}\left|\Gamma\left(\frac{g}{2} - i\frac{E}{2\pi\theta}\right)\right|^2.\end{aligned} \tag{3.100}$$

It's useful to note that $\hat{P}_g(E)$ is nothing but a Fermi distribution (with energy E counted with respect to the chemical potential, i.e. $\mu = 0$) multiplied by an effective tunneling Density Of States (DOS) [29, 150]. We have indeed $\hat{P}_g(E) = \mathcal{D}_g(E)n_F(-E)$, with

$$\mathcal{D}_g(E) = \frac{(2\pi)^g}{\Gamma(g)\omega_c}\left(\frac{\theta}{\omega_c}\right)^{g-1} \frac{\left|\Gamma\left(\frac{g}{2} - i\frac{E}{2\pi\theta}\right)\right|^2}{\left|\Gamma\left(\frac{1}{2} - i\frac{E}{2\pi\theta}\right)\right|^2}. \tag{3.101}$$

With the help of these new definitions Eq. (3.99) can be finally recast as a simple sum over l

$$\overline{\langle J_C(t)\rangle} = e^*\,|\lambda|^2 \sum_{l=-\infty}^{+\infty} |p_l(\alpha)|^2 \left\{\hat{P}_{2\nu}\left[(q+l)\,\omega\right] - \hat{P}_{2\nu}\left[-(q+l)\,\omega\right]\right\}, \tag{3.102}$$

as for the case of the Tien-Gordon model and the Floquet scattering matrix formalism (see Chapter 1, Section 1.7). It's worth noticing that a connection with the tunneling rate formalism and the detailed balance relation can be made manifest in Eq. (3.102). We can interpret the function $\Gamma_{RL}(E) = e^*\,|\lambda|^2\,\hat{P}_{2\nu}(E)$ as the tunneling rate from the right-moving to the left-moving edge at energy E. Then, the l-th contribution to the current is just the difference between the right-to-left rate at bias $(q+l)\omega$, namely $\Gamma_{RL}[(q+l)\omega]$, and the opposite left-to-right contribution, $\Gamma_{LR}[(q+l)\omega] = \Gamma_{RL}[-(q+l)\omega]$. As we

show in Appendix F, the tunneling rate satisfies the detailed balance relation $\Gamma_{RL}(-E) = e^{-\beta E}\Gamma_{RL}(E)$. The total averaged current is then

$$\overline{\langle J_C(t)\rangle} = e^* |\lambda|^2 \sum_{l=-\infty}^{+\infty} |p_l(\alpha)|^2 \left[1 - e^{-(q+l)\beta\omega}\right] \hat{P}_{2\nu}\left[(q+l)\,\omega\right]. \tag{3.103}$$

3.4.2 Noise

The zero-frequency shot noise is related to the autocorrelation function of current fluctuations, which reads

$$C_C(t,t') = \langle \Delta J_C(t) \Delta J_C(t')\rangle = \langle J_C(t) J_C(t')\rangle - \langle J_C(t)\rangle \langle J_C(t')\rangle, \tag{3.104}$$

with $\Delta J_C(t) = J_C(t) - \langle J_C(t)\rangle$ the operator representing backscattered current fluctuations. We adopt again the Keldysh formalism to set up a perturbative expansion for the noise. The autocorrelation function is thus

$$C_C(t,t') = \left\langle T_{\rm K} \Delta J_C(t^+) \Delta J_C(t'^-) e^{-i\int_{c_{\rm K}} H_T(t'')dt''}\right\rangle, \tag{3.105}$$

where we have chosen to place the operator $\Delta J_C(t)$ in the forward branch of the Keldysh contour and $\Delta J_C(t')$ in the opposite backward branch. Since the operator $J_C(t^+)J_C(t'^-)$ is itself $O(|\Lambda|^2)$ [see Eq. (3.84)] and $\langle J_C(t^+)\rangle \langle J_C(t'^-)\rangle$ is $O(|\Lambda|^4)$ [see Eq. (3.102)], the first non-vanishing term in the perturbation expansion is just

$$\begin{aligned}
&\left\langle T_{\rm K} J_C(t^+) J_C(t'^-)\right\rangle = \\
&= -(e^*)^2 \sum_{\varepsilon,\varepsilon'} \varepsilon\varepsilon' e^{i\varepsilon e^* \int_0^t V(t'')dt''} e^{i\varepsilon' e^* \int_0^{t'} V(t'')dt''} \times \\
&\quad \times \left\langle T_{\rm K} \left[\Lambda \psi_R^\dagger(0,t^+)\psi_L(0,t^+)\right]^\varepsilon \left[\Lambda \psi_R^\dagger(0,t'^-)\psi_L(0,t'^-)\right]^{\varepsilon'}\right\rangle = \\
&= (e^*)^2 |\Lambda|^2 \left\{ e^{ie^*\int_{t'}^t V(t'')dt''} \left\langle T_{\rm K}\psi_R^\dagger(0,t^+)\psi_R(0,t'^-)\right\rangle \left\langle T_{\rm K}\psi_L(0,t^+)\psi_L^\dagger(0,t'^-)\right\rangle \right. \\
&\quad \left. + e^{-ie^*\int_{t'}^t V(t'')dt''} \left\langle T_{\rm K}\psi_R(0,t^+)\psi_R^\dagger(0,t'^-)\right\rangle \left\langle T_{\rm K}\psi_L^\dagger(0,t^+)\psi_L(0,t'^-)\right\rangle \right\}.
\end{aligned} \tag{3.106}$$

We now use the bosonic representation of quasiparticle Green's functions in Eq. (3.93). In particular, we are only interested in the function $\mathcal{G}^{+-}(t,t') = \mathcal{G}(t'-t)$. We thus obtain

$$C_C(t,t') = 2(e^*)^2 |\lambda|^2 \cos\left[e^* \int_{t'}^t V(t'')dt''\right] e^{2\nu\mathcal{G}(t'-t)}. \tag{3.107}$$

To get the time-averaged zero-frequency shot noise we integrate over both the variables t' and t. Recalling that we are dealing with time dependent pulses

with period T, the integral on t' will run over the entire real axis, while the integral over t runs over a single period, $0 < t < T$. The noise is

$$\begin{aligned}\mathcal{S}_C &= 2\int_0^T \frac{dt}{T}\int_{-\infty}^{+\infty} d\tau\, C_C(t,t+\tau) = \\ &= 4(e^*)^2\,|\lambda|^2 \int_0^T \frac{dt}{T}\int_{-\infty}^{+\infty} d\tau\, \cos\left[e^*\int_{t+\tau}^{t} V(t'')dt''\right] e^{2\nu\mathcal{G}(\tau)}. \end{aligned} \tag{3.108}$$

Once again, due to the fact that we consider a periodic voltage signal $V(t)$, we use the photoassisted coefficients p_l to expand $\cos\left[e^*\int_{t+\tau}^{t} V(t'')dt''\right]$ into a Fourier series:

$$\cos\left[e^*\int_{t+\tau}^{t} V(t'')dt''\right] = \frac{1}{2}\sum_{l,m}\left[p_l^*(\alpha)p_m(\alpha)e^{i(l-m)\omega t}e^{-i(q+m)\omega\tau} + \text{c.c}\right]. \tag{3.109}$$

Inserting this sum in the last equation and integrating over t leads to

$$\mathcal{S}_C = 4(e^*)^2\,|\lambda|^2 \sum_{l=-\infty}^{+\infty} |p_l(\alpha)|^2 \int_{-\infty}^{+\infty} d\tau \cos\left[(q+l)\,\omega\tau\right] e^{2\nu\mathcal{G}(\tau)}. \tag{3.110}$$

As for the backscattering current, we recognize that the above equation contains the Fourier transform $\hat{P}_g(E)$ of the quasiparticle Green's function $e^{g\mathcal{G}(\tau)}$. We can thus rewrite the noise as

$$\mathcal{S}_C = 2(e^*)^2\,|\lambda|^2 \sum_{l=-\infty}^{+\infty} |p_l(\alpha)|^2 \left\{\hat{P}_{2\nu}\left[(q+l)\,\omega\right] + \hat{P}_{2\nu}\left[-(q+l)\,\omega\right]\right\}. \tag{3.111}$$

The noise has a different structure with respect to the current $\overline{\langle J_C\rangle}$ in terms of the tunneling rate Γ_{RL}. It involves the sum $\Gamma_{RL}(E) + \Gamma_{RL}(-E)$, rather than the difference. Using the detailed balance relation $\Gamma_{RL}(-E) = e^{-\beta E}\Gamma_{RL}(E)$ we get

$$\mathcal{S}_C = 2(e^*)^2\,|\lambda|^2 \sum_{l=-\infty}^{+\infty} |p_l(\alpha)|^2 \left[1 + e^{-(q+l)\beta\omega}\right] \hat{P}_{2\nu}\left[(q+l)\,\omega\right]. \tag{3.112}$$

Equations (3.102) and (3.111) are very general. They describe the photoassisted averaged current $\overline{\langle J_C(t)\rangle}$ and noise $\mathcal{S}_C$ for generic temperature and periodic voltage drive in a Laughlin FQH state. As such, they represent the starting point in the quest for minimal excitation states at fractional filling factor. Before discussing the behavior of current and noise as a function of different voltage signals $V(t)$, we focus on the interesting limits of (i) zero-temperature photoassisted transport and (ii) dc transport at generic temperature θ.

3.4.3 Zero temperature expression

Let us start with the zero temperature limit of Eqs. (3.102) and (3.111) At $\theta = 0$, the tunneling rate reads

$$\hat{P}_g(E) = \frac{2\pi}{\Gamma(g)\omega_c^g} E^{g-1}\Theta(E). \tag{3.113}$$

Here we resorted to the asymptotic form $|\Gamma(x+iy)| \sim \sqrt{2\pi}|y|^{x-1/2}e^{-\pi|y|/2}$ for $y \to \pm\infty$ known from textbooks, see e.g. Ref. [80]. The last equation shows the well known power-law behavior of the DOS typical of the Luttinger liquid theory. Sum and difference of tunneling rates are thus

$$\hat{P}_{2\nu}\left[(q+l)\,\omega\right] - \hat{P}_{2\nu}\left[-(q+l)\,\omega\right] = \frac{2\pi\omega^{2\nu-1}}{\Gamma(2\nu)\omega_c^{2\nu}}|q+l|^{2\nu-1}\,\mathrm{sign}\,(q+l)\,, \tag{3.114}$$

$$\hat{P}_{2\nu}\left[(q+l)\,\omega\right] + \hat{P}_{2\nu}\left[-(q+l)\,\omega\right] = \frac{2\pi\omega^{2\nu-1}}{\Gamma(2\nu)\omega_c^{2\nu}}|q+l|^{2\nu-1}. \tag{3.115}$$

We now insert these results in Eqs. (3.102) and (3.111) and get

$$\overline{\langle J_C(t)\rangle}\big|_{\theta=0} = \frac{e^*}{\omega}|\lambda|^2\frac{2\pi}{\Gamma(2\nu)}\left(\frac{\omega}{\omega_c}\right)^{2\nu}\sum_{l=-\infty}^{+\infty}|p_l(\alpha)|^2\,|q+l|^{2\nu-1}\,\mathrm{sign}[(q+l)], \tag{3.116}$$

$$\mathcal{S}_C\big|_{\theta=0} = \frac{(e^*)^2}{\omega}|\lambda|^2\frac{4\pi}{\Gamma(2\nu)}\left(\frac{\omega}{\omega_c}\right)^{2\nu}\sum_{l=-\infty}^{+\infty}|p_l(\alpha)|^2\,|q+l|^{2\nu-1}. \tag{3.117}$$

We have recovered something very similar to Eq. (1.71), which describes the PASN at zero temperature in the noninteracting scattering approach. However, here the l-th contributions to the current and noise are not linear as in the noninteracting case, but follow a power law behavior with exponent $2\nu - 1$. We notice that, for filling factor in the Laughlin sequence $\nu = 1/(2n+1)$, such an exponent is *always negative*, except for the metallic case $n = 1$. This means that both $\overline{\langle J_C(t)\rangle}$ and $\mathcal{S}_C$ will show a divergent behavior whenever q approaches an integer value, as the l-th contribution to both signals will diverge as $1/\varepsilon^{1-2\nu}$ for $\varepsilon \to 0$. We will discuss this feature in more detail and show how finite temperature effects regularize the divergence in a moment.

3.4.4 Current and noise due to a dc bias

Let us now focus on the purely dc case, namely $\alpha = 0$ with $q \neq 0$. Here the photoassisted coefficients reduce to $p_l(\alpha = 0) = \delta_{l,0}$ and current and noise

read[2]

$$\langle J_C \rangle = e^* |\lambda|^2 \left[\hat{P}_{2\nu}(e^* V_{\rm dc}) - \hat{P}_{2\nu}(-e^* V_{\rm dc}) \right] = \\ = \frac{2e^* |\lambda|^2}{\Gamma(2\nu)\omega_{\rm c}} \left(\frac{2\pi\theta}{\omega_{\rm c}} \right)^{2\nu-1} \left| \Gamma\left(\nu - i \frac{e^* V_{\rm dc}}{2\pi\theta} \right) \right|^2 \sinh\left(\frac{e^* V_{\rm dc}}{2\theta} \right), \tag{3.118}$$

$$\mathcal{S}_C = 2(e^*)^2 |\lambda|^2 \left[\hat{P}_{2\nu}(e^* V_{\rm dc}) + \hat{P}_{2\nu}(-e^* V_{\rm dc}) \right] = \\ = \frac{4(e^*)^2 |\lambda|^2}{\Gamma(2\nu)\omega_{\rm c}} \left(\frac{2\pi\theta}{\omega_{\rm c}} \right)^{2\nu-1} \left| \Gamma\left(\nu - i \frac{e^* V_{\rm dc}}{2\pi\theta} \right) \right|^2 \cosh\left(\frac{e^* V_{\rm dc}}{2\theta} \right), \tag{3.119}$$

since $q\omega = e^* V_{\rm dc}$. We report their behavior in Fig. 3.6 both at zero and finite temperature θ. As anticipated before, the fractional power law gives rise to a diverging behavior of the tunneling rate near $V_{\rm dc} = 0$, both in the current and the noise (red curves in Fig. 3.6). The current is an odd function of the bias, with $\text{sign}\,\langle J_C \rangle = \text{sign}\, V_{\rm dc}$, while $\mathcal{S}_C$ is an even function of $V_{\rm dc}$ and satisfies always $\mathcal{S}_C > 0$. At finite temperature θ the divergent behavior around $V_{\rm dc} = 0$ gets regularized, as shown by the dashed black curves in Fig. 3.6. Finite temperature effects are substantially negligible in the limit $e^* V_{\rm dc} \gg \theta$, where the two curves overlap perfectly.

It is now worth exploiting the duality property between electronic fields $\Psi^{(\rm el)}_{R/L}$ and quasiparticle fields $\Psi^{(\rm qp)}_{R/L}$, and commenting on the power-law behavior induced by tunneling of electrons. As discussed before, one just needs to replace the parameter ν with $1/\nu$ in the tunneling exponents. One thus discovers that backscattering current induced by electron tunneling is governed by the power law $J_C^{(\rm el)} \sim V_{\rm dc}^{2/\nu-1}$. Since $\nu = 1/(2n+1)$ for the Laughlin sequence, the current due to electron tunneling goes rapidly to zero as the dc bias decreases, and is *always negligible with respect to the quasiparticle contribution* at low energy. This is a particular manifestation of a much more profound principle which can be fully understood in the renormalization group approach: tunneling of electrons is an *irrelevant* perturbation at low energies, while tunneling of quasiparticles is *relevant* [144]. For this reason, we will only focus on quasiparticle tunneling in the rest of this thesis.

Using the detailed balance relation it is not difficult to show that noise and current are linked to each other by

$$\mathcal{S}_C = 2(e^*)^2 |\lambda|^2 \coth\left(\frac{e^* V_{\rm dc}}{2\theta} \right) (1 - e^{-e^* V_{\rm dc}/\theta}) \hat{P}_{2\nu}(e^* V_{\rm dc}) = \\ = 2e^* \coth\left(\frac{e^* V_{\rm dc}}{2\theta} \right) \langle J_C \rangle . \tag{3.120}$$

[2] In this regime there's no need for the notation $\overline{X(t)}$ indicating the average over one period of the signal $X(t)$, as the current is constant in t. We will denote the current in the dc regime simply with $\langle J_C \rangle$.

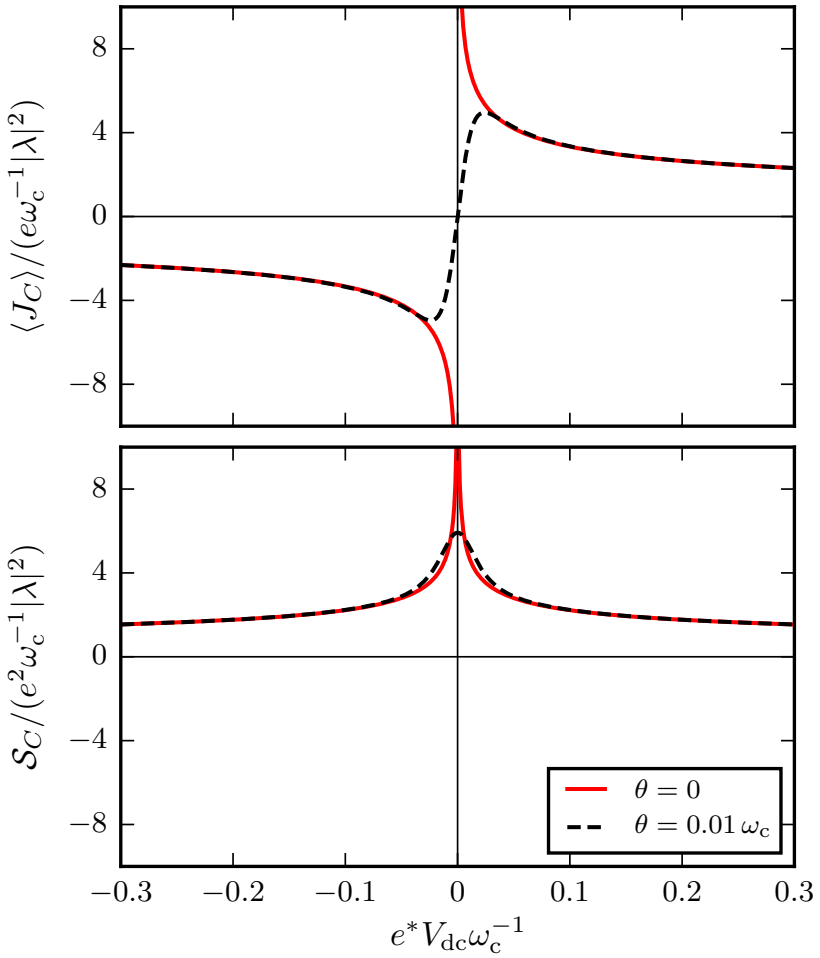

Figure 3.6: Backscattering current $\langle J_C\rangle$ and zero-frequency noise $\mathcal{S}_C$ at $\nu = 1/3$ for a pure dc bias ($V_{ac} = 0$) as a function of the dimensionless parameter $e^*V_{dc}\omega_c^{-1}$. The two curves show the cases of zero temperature and finite temperature $\theta = 0.01\omega_c$.

This result is extremely similar to the finite temperature shot noise in a tunnel junction shown in Chapter 1, Eq. (1.58), the only difference being the presence of the fractional charge e^* instead of e. In particular, in the limit $\theta \to 0$ we get (assuming $V_{\rm dc} > 0$)

$$\mathcal{S}_C = 2e^* \langle J_C \rangle \,, \tag{3.121}$$

reproducing the Schottky result for a system with fractionally charged carriers. We have already shown in Sec. 2.3.2 that experiments by Saminadayar *et al.*, De-Picciotto *et al.* and Reznikov *et al.* have measured the values $e^* = e/3$ and $e^* = e/5$ by determining the ratio between noise and backscattering current reflected off the QPC [50–52]. Equation (3.121) represents the theoretical background of the results anticipated in Sec. 2.3.2.

3.5 Excess noise and minimal excitations

Building upon the above results, in this section we tackle the problem of minimal excitation states in the FQH regime.

We claim that minimal excitations give rise to the minimum possible shot noise compatible with the Schottky result Eq. (3.121). We thus propose the following definition for the excess noise at zero temperature:

$$\Delta\mathcal{S}_C = \mathcal{S}_C - 2e^* \overline{\langle J_C(t) \rangle}. \tag{3.122}$$

It is basically the difference between the full noise $\mathcal{S}_C$ and a Poissonian reference value given by the averaged time-dependent current over one period. We give two physically sound reasons for this definition to be the most suitable one at fractional filling factor. First, in the limit $\nu = 1$ it is exactly coincident with the one given in the context of the Floquet scattering matrix formalism. Indeed, in Chapter 2 we defined the excess noise as $\Delta\mathcal{S}_C = \mathcal{S}_C - \mathcal{S}_C|_{\alpha=0}$, where the second term is the shot noise in the presence of a simple dc bias with amplitude $eV_{\rm dc} = q\omega > 0$. Our definition Eq. (3.122) is perfectly consistent with the previous one, since for integer filling factor and $\theta = 0$ one has

$$\mathcal{S}_C\big|_{\alpha=0} = 2\frac{|\Lambda|^2}{v^2}\frac{e^2}{2\pi}eV_{\rm dc} = 2e\overline{\langle J_C(t) \rangle}. \tag{3.123}$$

This can be readily checked by setting $\nu = 1$ and $p_l = \delta_{l,0}$ in Eqs. (3.116) and (3.117). Thus, the reference noise subtracted from $\mathcal{S}_C$ at $\nu = 1$ can be viewed either as the shot noise without any ac component of the drive ($\mathcal{S}_C|_{\alpha=0}$) or as an averaged current, and we argue that the proper definition of $\Delta\mathcal{S}_C$ at fractional filling factor involves the latter interpretation. A second important point relies on the particle-hole interpretation of the excess noise, and is developed in the next subsection.

3.5.1 Particle-hole excitations due to voltage pulses

A key feature of $\Delta\mathcal{S}_C$ is that it gives access to the number of holes excited by the voltage pulses. To see that, one can simply evaluate the number of electrons excited above the Fermi level and holes below it in presence of the voltage drive. We roughly follow the idea sketched in Ref. [9] for the case of a non-interacting one-dimensional wire. Let us count the number of particles excited above the Fermi level (N_e) or holes created below it (N_h) with respect to the unperturbed Fermi sea in the right-moving edge. We set $\theta = 0$, $E_{\rm F} = 0$ and write

$$N_e(t) = \sum_{k=-\infty}^{+\infty} n_{\rm F}(-vk) \left\langle c_k^\dagger(t) c_k(t) \right\rangle , \tag{3.124}$$

$$N_h(t) = \sum_{k=-\infty}^{+\infty} n_{\rm F}(vk) \left\langle c_k(t) c_k^\dagger(t) \right\rangle , \tag{3.125}$$

with $n_{\rm F}(k) = 1 - n_{\rm F}(-k) = \Theta(-k)$ the Fermi distribution at zero temperature. Here, operators $c_k^\dagger$ and c_k create and annihilate an electron with momentum k respectively. They can be written as

$$c_k(t) = \frac{1}{\sqrt{L}} \int_{-\infty}^{+\infty} e^{-ikx} \Psi(x,t) dx. \tag{3.126}$$

We recall that the Fermi distribution is related to the Fourier transform of the Green function $P_g(t)$. One has $\hat{P}_g(E) = \mathcal{D}_g(E) n_{\rm F}(-E)$, with $\mathcal{D}_g(E)$ the effective DOS of the Luttinger liquid given in Eq. (3.101). For integer filling $\nu = 1$ (i.e. for a 1D Fermi liquid) one has $\hat{P}_{g=1}(E) = 2\pi\omega_{\rm c}^{-1} n_{\rm F}(-E)$. We thus

write N_h as

$$\begin{aligned}
N_h(t) &= \sum_{k=-\infty}^{+\infty} \frac{v}{2\pi a}\hat{P}_{\nu=1}(-vk)\frac{1}{L}\int dx \int dx' e^{-ik(x-x')}\left\langle \Psi_R(x,t)\Psi_R^\dagger(x',t)\right\rangle = \\
&= \sum_{k=-\infty}^{+\infty} \frac{v}{2\pi a}\frac{1}{L}\int d\tau e^{-ivk\tau}e^{\mathcal{G}(\tau)}\int dx \int dx' e^{-ik(x-x')}\times \\
&\quad \times \exp\left[ie\int_{t-(x+d)/v}^{t-(x'+d)/v} dt' V(t')\right]\frac{1}{2\pi a}e^{\mathcal{G}\left(\frac{x'-x}{v}\right)} = \\
&= \frac{v}{(2\pi a)^2}\int d\tau \int dx \int dx'\, \delta(x'-x-v\tau)\times \\
&\quad \times \exp\left[ie\int_{t-(x+d)/v}^{t-(x'+d)/v} dt' V(t')\right] e^{\mathcal{G}(\tau)}e^{\mathcal{G}\left(\frac{x'-x}{v}\right)} = \\
&= \frac{v^2}{(2\pi a)^2}\int d\tau' \int d\tau \exp\left[ie\int_{\tau'}^{\tau'-\tau} dt' V(t')\right] e^{2\mathcal{G}(\tau)} = \\
&= \frac{v^2}{(2\pi a)^2}\int d\tau' \int d\tau \exp\left[-ie\int_{\tau'-\tau}^{\tau'} dt' V(t')\right] e^{2\mathcal{G}(\tau)}.
\end{aligned} \tag{3.127}$$

Let us compare the last expression with Eqs. (3.97) and (3.108). We find that the excess noise as an integral in the time domain reads

$$\Delta\mathcal{S}_C = 4(e^*)^2\left|\lambda\right|^2\int_0^T \frac{dt}{T}\int_{-\infty}^{+\infty} d\tau\, \exp\left[-ie^*\int_{t-\tau}^{t} V(t'')dt''\right] e^{2\nu\mathcal{G}(\tau)} \tag{3.128}$$

at temperature $\theta = 0$, and is thus proportional to N_h at $\nu = 1$. In practice, $\Delta\mathcal{S}_C$ represents a direct measure of the number of holes excited by the time dependent drive, as suggested by Levitov and coworkers [9]. Minimal excitation states are generated by a drive which excites a single electron, while no particle-hole pairs are created ($N_h = 0$). Generalizing to a chiral Luttinger liquid describing a FQH edge state, these excitations should correspond to a vanishingly small value of the quantity

$$\mathcal{N} = \frac{v^2}{(2\pi a)^2}\int d\tau' \int d\tau \exp\left[-ie^*\int_{\tau'-\tau}^{\tau'} dt' V(t')\right] e^{2\nu\mathcal{G}(\tau)}. \tag{3.129}$$

The excess noise $\Delta\mathcal{S}_C$ is thus identified as the most suitable quantity to study minimal excitations. At $\theta = 0$, one recovers in $\mathcal{N}$ precisely the excess noise, up to a prefactor which depends on the tunneling amplitude [see Eq. (3.128)] [9]. This legitimizes our definition of excess noise and shows that clean pulses in the FQH must satisfy the condition $\Delta\mathcal{S}_C = 0$.

3.5.2 Minimal excitation states

As shown above, we have defined the excess noise $\Delta\mathcal{S}_C = \mathcal{S}_C - 2e^*\overline{\langle J_C(t)\rangle}$ as the best candidate to highlight the occurrence of a minimal excitation state in a Laughlin FQH system. In practice, $\Delta\mathcal{S}_C$ gives us information about how much noise is produced in excess to the ordinary Poissonian noise $\mathcal{S}_C|_{\alpha=0} = 2e^*\overline{\langle J_C\rangle}$. From Eqs. (3.116) and (3.117) one immediately gets, at $\theta = 0$,

$$\Delta\mathcal{S}_C = \frac{(e^*)^2}{\omega}|\lambda|^2\frac{8\pi}{\Gamma(2\nu)}\left(\frac{\omega}{\omega_c}\right)^{2\nu}\sum_{l<-q}|p_l|^2|q+l|^{2\nu-1}. \tag{3.130}$$

At finite temperature the definition of excess noise needs to be slightly modified. Indeed, we have already shown that the noise reads

$$\mathcal{S}_C\big|_{\alpha=0} = 2e^*\overline{\langle J_C\rangle}\coth\left(\frac{q\omega}{2\theta}\right) \tag{3.131}$$

for the case of dc bias at temperature $\theta > 0$. We thus propose the following definition for the finite temperature excess noise:

$$\Delta\mathcal{S}_C = \mathcal{S}_C - 2e^*\overline{\langle J_C\rangle}\coth\left(\frac{q\omega}{2\theta}\right). \tag{3.132}$$

One should note that Eq. (3.132) corresponds to $\Delta\mathcal{S}_C = \mathcal{S}_C - 2e^*\overline{\langle J_C\rangle}$ in the zero temperature limit $\theta \to 0$, since $\coth(1/x) \approx \mathrm{sign}(x)$ as x approaches zero.

We now consider three different signals for the train of voltage pulses and discuss the excess noise they generate. We focus on the same three waveforms of Sec. 2.2.3, namely

$$V_{\sin}(t) = V_{\mathrm{dc}}[1-\cos(\omega t)], \tag{3.133a}$$

$$V_{\mathrm{sqr}}(t) = 2V_{\mathrm{dc}}\sum_{k=-\infty}^{+\infty}\Theta\left(t-kT\right)\Theta\left(\frac{T}{2}-t+kT\right), \tag{3.133b}$$

$$V_{\mathrm{Lor}}(t) = \frac{V_{\mathrm{dc}}}{\pi}\sum_{k=-\infty}^{+\infty}\frac{\eta}{\eta^2+(t/T-k)^2}. \tag{3.133c}$$

Let us notice that we have imposed a constraint on the dc and ac amplitudes of the voltage signals ($q = e^*V_{\mathrm{dc}}/\omega$ and $\alpha = e^*V_{\mathrm{ac}}/\omega$ respectively). Indeed, q and α are no longer independent from each other, but are locked by the request $V(t) \geq 0$. We also impose that the minimum value inside each single pulse is $V_{\mathrm{min}} = 0$, to ensure that there is no overall dc offset. To fulfill these requests, we set $q = \alpha$.

It is now sufficient to insert the suitable coefficients $p_l(\alpha = q)$, which are calculated in Appendix A. Fig. 3.7 shows the excess noise for the three signals considered both at zero temperature (red curves) and $\theta = 0.1\,\omega$ (dashed black curves). We consider here the first and most accessible FQH plateau of the Laughlin sequence, i.e. $\nu = 1/3$. Let us first focus on the case $\theta = 0$ and

comment on the common behavior of the curves. The Figure tells us that there is a local minimum in the noise whenever q is an integer, that is whenever each pulse carries an integer number of electron charges.[3] This is exactly the quantization condition already discussed in Chapter 2 (see Fig. 2.4), where we have shown that optimal pulses in an ordinary Fermi liquid must carry an integer number of electrons q. However, we notice an interesting feature at $\nu = 1/3$. While curves drop to a local minimum for $q = n$, $n \in \mathbb{N}$, they show a diverging behavior for $q = n - \varepsilon$, where ε is a small positive quantity. This linked to the orthogonality catastrophe argument discussed by Levitov [7]: non-optimal pulses generate a quantum state that is orthogonal to the unperturbed ground state, and this manifests as a huge number of particle-hole pairs contributing to the transport. In particular, the diverging curves follow the power-law $\varepsilon^{2\nu-1}$ discussed previously, which is replicated infinite times by the photoassisted mechanism.

Let us now closely inspect the values of the minima. One easily sees that cosine and square voltages still generate a finite excess noise $\Delta\mathcal{S}_C > 0$, even in correspondence of integer values of q. On the contrary, the Lorentzian signal at $\theta = 0$ *vanishes exactly* for $q = 1, 2, 3 \ldots$. We thus claim that *integer Lorentzian voltage pulses generate minimal excitation states in the Laughlin FQH regime*. In other words, the leviton is extremely robust against electron-electron interactions, since its noiseless status is confirmed even in a strongly interacting environment such as the $\nu = 1/3$ FQH state. This very important conclusion is the principal result of Ref. [24].

Interestingly enough, there is absolutely no feature in correspondence of fractional values of q, as clean pulses are associated with an integer number q of electrons. Apart from the power-law divergent behavior, $\Delta\mathcal{S}_C$ is qualitatively similar to the case of a normal metal: each signal shows interesting features *only* at integer q (namely, a local minimum), with Lorentzian pulses completely suppressing the excess noise for such values of q.

An interesting question remains open: is this the only possibility to achieve zero excess noise? Indeed, we have only shown that integer Lorentzian pulses generate clean excitations while the cosine and square signal do not, but other waveforms may in principle give $\Delta\mathcal{S}_C = 0$, even at different values of q. To answer this question, let us rewrite the excess noise at $\theta = 0$ in the following way

$$\Delta\mathcal{S}_C = \frac{(e^*)^2}{\omega} |\lambda|^2 \frac{8\pi}{\Gamma(2\nu)} \left(\frac{\omega}{\omega_c}\right)^{2\nu} \sum_{l<-q} |p_l(q)|^2 |q+l|^{2\nu-1}. \tag{3.134}$$

Each contribution in the sum is positive, due to the absolute value on both the coefficients p_l and on the factor $q+l$. It is now clear that $\Delta\mathcal{S}_C$ may vanish only if each contribution vanishes individually, that is, if all the coefficients p_l are zero for $l < -q$. We have already shown in Chapter 2 that only integer Lorentzian

[3] Remember that the total charge associated with each pulse is $Q = \int_0^T dt\, \nu \frac{e^2}{2\pi} V(t) = eq$.

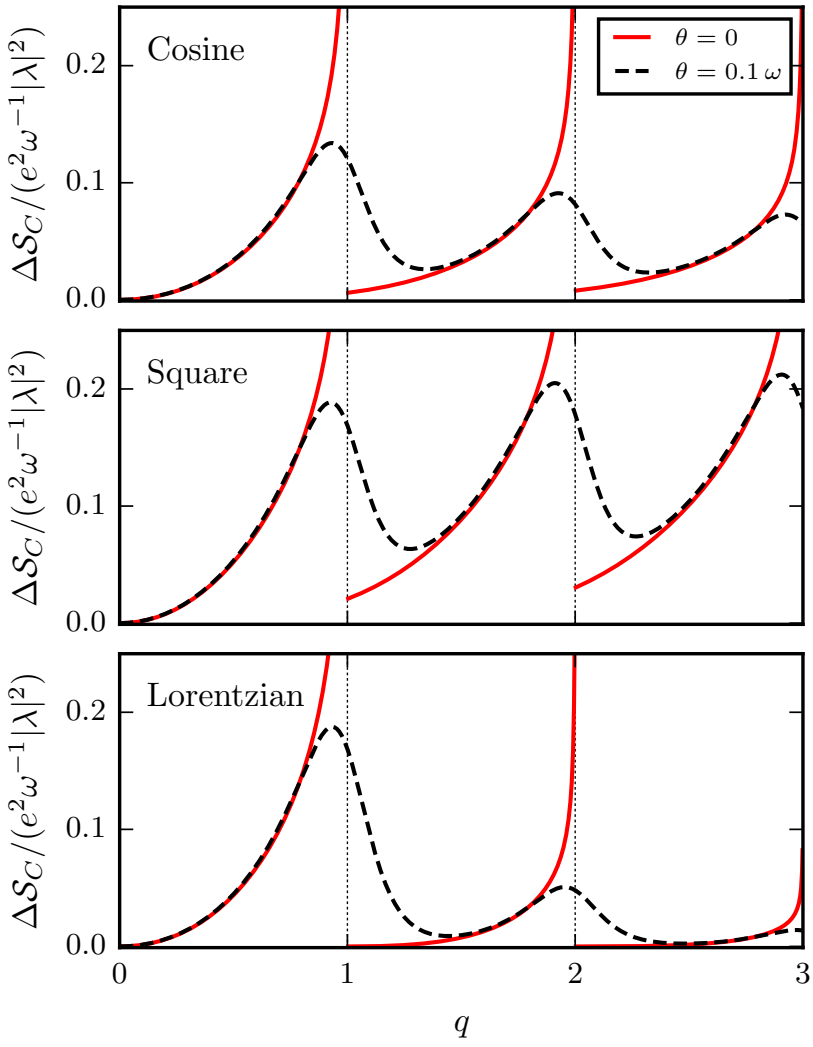

Figure 3.7: Excess noise $\Delta\mathcal{S}_C$ in units of $e^2\omega^{-1}\,|\lambda|^2$ at filling factor $\nu = \frac{1}{3}$ as a function of q. We compare the sinusoidal, square and Lorentzian signals in Eqs. (3.133) at $\theta = 0$ and $\theta/\omega = 0.1$. The dimensionless width of Lorentzian pulses is $\eta = 0.1$.

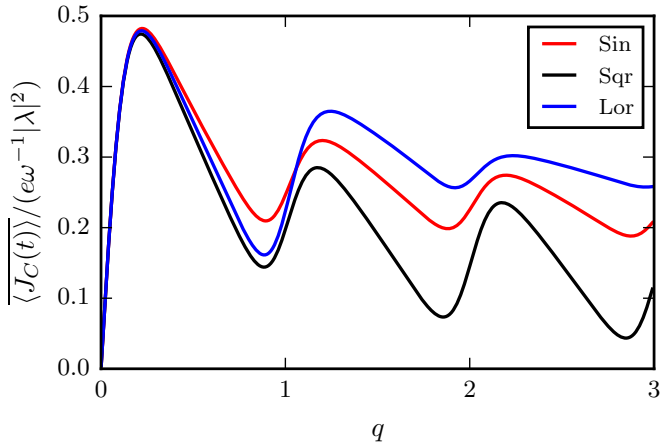

Figure 3.8: Backscattering current $\overline{\langle J_C(t)\rangle}$ averaged over one period in units of $e\omega^{-1}\,|\lambda|^2$ at filling factor $\nu = \frac{1}{3}$. We compare the sinusoidal, square and Lorentzian signals in Eqs. (3.133) as a function of the dc amplitude q. The temperature is $\theta/\omega = 0.1$ and the dimensionless width of Lorentzian pulses is $\eta = 0.1$.

pulses satisfy this property. Thus, they are the *only minimal excitation states* allowed at $\nu = 1/(2m+1)$, $m \in \mathbb{N}$.

This calculation seems to rule out the possibility of exciting a single anyon with well-shaped voltage pulses, since the minimal excitation state (i.e. leviton) carries a full electron charge e. However, it has been proposed that the QPC may break a leviton into a single quasiparticle reflected into the lower edge, with the two remaining quasiparticles transmitted through the QPC [151]. This protocol may in principle be able to generate a clean single-quasiparticle state, which can be probed by measuring the excess noise with the help of a second QPC. Other possibilities may involve fractional filling factors of the Jain sequence, where several edge modes contribute simultaneously to transport, or the exotic even-denominator FQH states [116].

Let us now briefly comment on the case $\theta > 0$. Black dashed curves in Fig. 3.7 are obtained at $\theta/\omega = 0.1$, and show that the diverging behavior disappears at finite temperature and is replaced by smooth, continuous curves. We notice that the excess noise is now always greater than zero, a fact that was already observed in the Fermi liquid case (see again Fig. 2.4). Strictly speaking, a theoretical analysis of minimal excitation states only makes sense at $\theta = 0$, as additional excitations generated by thermal agitation will always come into play at finite temperature. It's interesting to notice that, even at $\theta > 0$, Lorentzian pulses still generate an extremely small excess noise around $q \approx 1.4, 2.4\ldots$.

Finally, in addition to the excess noise, the time-averaged backscattering current $\overline{\langle J_C(t)\rangle}$ also bears peculiar features. In contrast to the Ohmic behavior observed in the Fermi liquid case, $\overline{\langle J_C(t)\rangle}$ shows large dips for integer values

of q (see Fig. 3.8). These dips are present for all types of periodic drives, and cannot be used to detect minimal excitations. However, the spacing between these dips provides an alternative diagnosis (from dc shot noise [50, 51]) to access the fractional charge e^* of Laughlin quasiparticles, as q is known from the frequency and amplitude of V_{dc} [152].

3.6 Photoassisted spectroscopy

To study minimal excitation states in the FQH regime we have restricted ourselves to very specific voltage pulses with $q = \alpha$. In this section we relax this constraint and consider the more general situation of independent dc and ac amplitudes $q = e^*V_{\mathrm{dc}}/\omega$ and $\alpha = e^*V_{\mathrm{ac}}/\omega$. We will specifically consider the sinusoidal wave $V_{\sin}(t) = V_{\mathrm{dc}} - V_{\mathrm{ac}}\cos(\omega t)$ and the Lorentzian drive

$$V_{\mathrm{Lor}} = V_{\mathrm{dc}} + V_{\mathrm{ac}}\left[\frac{1}{\pi}\sum_{k=-\infty}^{+\infty}\frac{\eta}{\eta^2+(t/T+k)^2} - 1\right]. \tag{3.135}$$

The starting point is the photoassisted expression for the shot noise:

$$\mathcal{S}_C = 2(e^*)^2|\lambda|^2\sum_{l=-\infty}^{+\infty}|p_l(\alpha)|^2\left\{\hat{P}_{2\nu}\left[(q+l)\,\omega\right] + \hat{P}_{2\nu}\left[-(q+l)\,\omega\right]\right\}. \tag{3.136}$$

As already discussed in the context of photoassisted transport, it can be viewed as a superposition of several dc contributions, whose effective bias is shifted by an amount $l\omega$ with respect to the dc value $q\omega$ and weighted by a probability $|p_l(\alpha)|^2$, which is nothing but the probability for a quasiparticle to absorb or emit l energy quanta [112]. We note that the ac and dc amplitudes are well separated in Eq. (3.136). Indeed, the former emerges as the argument α of the coefficients p_l, while the latter appears in the functions $\hat{P}_{2\nu}(E)$ via the parameter q.

While the expression for the shot noise generally consists of an infinite superposition of dc contributions, each one weighted by the corresponding photoassisted probability, we show in the following that the FQH physics allows to extract each single contribution to the PASN in a surprisingly simple fashion. Following the results published in Ref. [26], we provide a recipe to reconstruct the typical absorption and emission probabilities of the photoassisted formalism by independently tuning the ac and dc components of the voltage drive. We also discuss the experimental feasibility of this study, identifying a set of reasonable experimental parameters under which our protocol should be applicable.

3.6.1 Results

To begin, let us first discuss a set of reasonable values for θ, ω and η. Experiments testing levitons in two-dimensional electron gases are usually performed

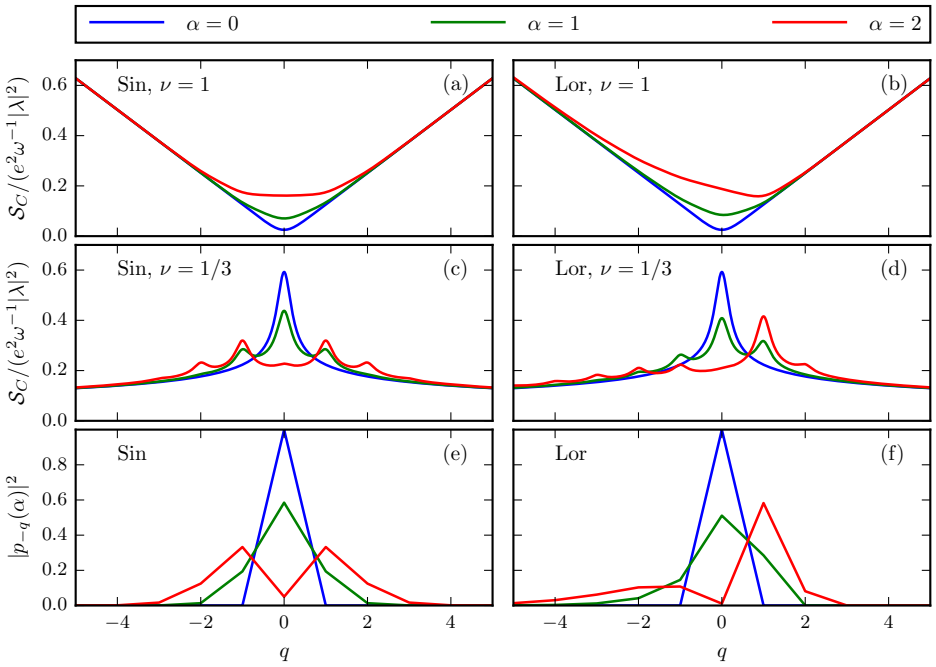

Figure 3.9: (a)-(d) PASN as a function of the dc amplitude q for $\nu = 1$ and $\nu = 1/3$ and different values of the ac amplitude α. (e)-(f) Coefficients $|p_{-q}(\alpha)|^2$ for different values of α as a function of q. In (e) and (f) the continuous lines are guides for the eyes, with the coefficients $|p_{-q}(\alpha)|^2$ only defined for integer values of q.

at $\theta = 10 - 100$ mK [10, 15, 18], which also happens to be a range of temperature where well defined FQH states can be spotted [153]. The Lorentzian voltage drive usually operates at a frequency $f = \frac{\omega}{2\pi} = 5 - 6$ GHz, with dimensionless width of each pulse $\eta = 0.1 - 0.2$ [10, 15, 18]. Higher frequencies are also used for the sinusoidal wave [10], and photoassisted transport in graphene nanoribbons illuminated with THz radiation was recently reported [154]. We initially set $\eta = 0.1$ and $\theta = 0.1\,\omega$, but lower values of the ratio θ/ω can be reached in principle and will be discussed later.

Figure 3.9 shows the behavior of $\mathcal{S}_C$ as a function of q for fixed values of α. In panels (a) and (b) we report the case of sinusoidal and Lorentzian voltage pulses at integer filling factor $\nu = 1$. The blue curve represents the pure dc case where no ac component is present in the voltage drive ($\alpha = 0$). In this case $\mathcal{S}_C$ grows linearly with q as expected, since $\mathcal{S}_C \propto q \coth\left(\frac{q\omega}{2\theta}\right) \approx |q|$ in the integer quantum Hall regime at sufficiently low temperature. Conversely, when a finite ac component is present ($\alpha = 1, 2$) the behavior at low q is clearly non-linear and some excess noise due to the presence of the oscillating drive can be identified. Switching to the FQH regime [panels (c) and (d)], the linear (or almost linear) profile of the integer case is replaced by a strongly non-linear behavior, even for a dc voltage drive. This is a typical signature of the chiral Luttinger liquid theory. In particular the $\alpha = 0$ curve, which is

proportional to $\hat{P}_{2\nu}(q\omega) + \hat{P}_{2\nu}(-q\omega)$, shows a sharp peak around $q = 0$ (this is exactly the black dashed curve already shown in Fig. 3.6 up to a constant factor). Such a structure is visible for $\alpha = 1$ and $\alpha = 2$ as well, with additional peaks arising for integer values of q. The different peaks in Fig. 3.9 (c) and (d) reproduce the features of the $\alpha = 0$ curve at shifted values $q + l$, since the photoassisted transport can be interpreted as an infinite superposition of shifted dc cases weighted by the probabilities $|p_l(\alpha)|^2$, as we mentioned before. Indeed, due to the sharply peaked structure of the tunneling rates in the FQH regime, the dominant contribution to the noise around integer q is given by the photoassisted amplitudes with $l = -q$. In such a case the PASN is well approximated by

$$\mathcal{S}_C \approx 4(e^*)^2|\lambda|^2\hat{P}_{2\nu}(0)\,|p_{-q}(\alpha)|^2\,, \tag{3.137}$$

allowing to reconstruct the probabilities $|p_l(\alpha)|^2$ from the relative height of the different peaks. Thus, by fixing the ac component of the voltage drive and tuning the dc component, we can explore all the coefficients $|p_l(\alpha)|^2$ for $l = 0, \pm 1, \pm 2 \ldots$. This is similar to the spectroscopic protocol developed by Dubois *et al.* in Refs. [10, 112] for the free fermion case, although the fractional regime treated in the present work makes it much more effective and easy to visualize, due to the peculiar structure of the tunneling rate $\hat{P}_{2\nu}(E)$ at fractional filling (see also a similar analysis in the framework of finite frequency noise spectroscopy discussed in Refs. [155, 156]). For instance, Fig. 3.9 (d) suggests that all $p_{-q}(\alpha)$ with $q > \alpha$ vanish for a Lorentzian drive with integer α, since we cannot see any further peak at $q > \alpha$. This is the striking property that allows the Lorentzian voltage pulse to generate a single electron above the Fermi level, with no disturbance below it [7, 9]. Conversely, no cancellation arises in the sinusoidal case, where Fourier coefficients manifestly satisfy $|p_q(\alpha)|^2 = |p_{-q}(\alpha)|^2$ [see Fig. 3.9 (c)]. To check the validity of our spectroscopic protocol we also show the coefficients $|p_{-q}(\alpha)|^2$ for $\alpha = 0, 1, 2$ in Fig. 3.9 (e) and (f). One can easily see that the relative heights of all the peaks in Fig. 3.9 (c) and (d) are very well reproduced by the coefficients $|p_{-q}(\alpha)|^2$. As an example, the absence (almost total) of peaks at $q = 0$ for both the sinusoidal and the Lorentzian drive with $\alpha = 2$ is linked to the fact that $|p_0(2)|^2 \ll 1$ for both signals. Moreover, the value of $|p_{-1}(2)|^2$ explains the high asymmetric peak at $q = 1$ for the Lorentzian drive with $\alpha = 2$.

We now turn to the opposite case, in which the dc component is fixed and we allow the parameter α to vary continuously. As shown in Fig. 3.10 (a) and (b), at $\nu = 1$ we get a linear behavior at high values of $|\alpha|$ both for the sinusoidal and the Lorentzian drive. In the vicinity of $\alpha = 0$, the curves deviate from the linear regime and the noise is more or less proportional to q. We note once again the sharp asymmetry for $q \neq 0$ of the Lorentzian voltage drive, as opposed to the symmetric profile of the sinusoidal wave. For fractional filling factor $\nu = 1/3$ [panels (c) and (d)] the curves are evidently non-linear and oscillate in a non-monotonous fashion as a function of α. However, the behavior at $\nu = 1/3$ is much more interesting since we can link the value of $\mathcal{S}_C$

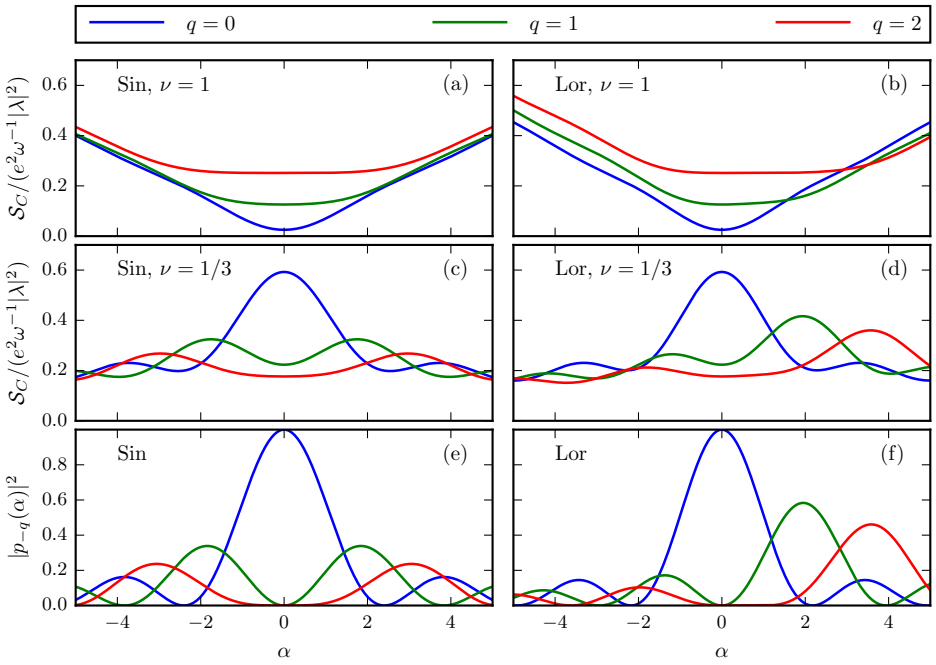

Figure 3.10: (a)-(d) PASN for $q = 0, 1, 2$ as a function of α at $\nu = 1$ and $\nu = 1/3$. (e)-(f) Coefficients $|p_{-q}(\alpha)|^2$ for $q = 0, 1, 2$ as a function of α.

to the probability $|p_{-q}(\alpha)|^2$, following Eq. (3.137). In contrast with the case of fixed ac component, in this case we can explore the dependence of the q-th Fourier coefficients upon its argument α. Comparing with Fig. 3.10 (e) and (f), where we report the coefficients $|p_{-q}(\alpha)|^2$ as a function of α, we observe that the approximation works well from a qualitative point of view, although an additional contribution due to finite temperature effects is present in all curves at $\nu = 1/3$, thus preventing us from getting a good quantitative match.

In order to improve the spectroscopic protocol from a quantitative point of view, let us remark that the peculiar peak of the function $\hat{P}_{2\nu}(E) + \hat{P}_{2\nu}(-E)$ around $E = 0$ becomes more and more pronounced as the ratio θ/ω decreases. Indeed, we have already commented on the diverging power-law behavior of the Luttinger liquid theory in the limit $\theta \to 0$, which is shown in Fig. 3.6. Thus, the approximation Eq. (3.137) becomes more efficient at lower temperatures (or higher frequencies), since the relative weight of the term $l = -q$ in the PASN with respect to all other terms $l' \neq -q$ is given by $2\hat{P}_{2\nu}(0)/[\hat{P}_{2\nu}(l'\omega + q\omega) + \hat{P}_{2\nu}(-l'\omega - q\omega)]$. The recent exploration of PASN in the THz regime [154] suggests that our results could be tested in the near future in EQO experiments at fractional filling factor [151].

Chapter 4

Minimal excitations for heat transport

In this Chapter, which is based on Ref. [25], we investigate minimal excitation states for heat transport in a HBT setup. Excitations are studied through heat and mixed noise generated by the random partitioning at the QPC. It is shown that levitons represent the cleanest states even for heat transport properties, since excess heat and mixed shot noise both vanish *only* when Lorentzian voltage pulses carrying integer electric charge are applied to the conductor. This happens in the integer QH regime and for Laughlin fractional states as well, with no signature associated to fractional excitations. In addition, we demonstrate the robustness of such excitations to the overlap of Lorentzian wavepackets. Even though mixed and heat noise have nonlinear dependence on the voltage bias, and despite the non-integer power-law behavior arising from the FQH physics, an arbitrary superposition of levitons always generates minimal excitation states.

4.1 Heat transport in the quantum Hall regime

Despite several challenging and fascinating problems concerning charge transport properties, electric charge is far from being the only interesting degree of freedom we should look at in the framework of EQO. Energy, for instance, can be coherently transmitted over very long distances along the edge of QH systems, as was experimentally proved by Granger *et al.* [157]. This observation is of particular interest, as typical dimensions of chips and transistors are rapidly getting smaller and smaller due to the great technological advance during the last decades. Indeed, the problem of heat conduction and manipulation at the nanoscale has become more actual than ever [42], as demonstrated by great recent progress in the field of quantum thermodynamics. Topics like

quantum fluctuation-dissipation theorems [158–162], energy exchanges in open quantum systems [163, 164], energy dynamics and pumping at the quantum level [165–169], coherent caloritronics [170, 171], and thermoelectric phenomena [172–174] have been extensively investigated, in an attempt to extend the known concepts of thermodynamics to the quantum realm. In this context, a particular emphasis has been focused on the role of QH edge states both from the theoretical [29, 175–179] and experimental point of view [128, 129, 157, 180–183].

A natural question immediately arises when one considers energy dynamics in EQO, namely what kind of voltage drive gives rise to minimal excitation states for heat transport in mesoscopic conductors. This is the fundamental question we try to answer in this Chapter. To this end, we study heat conduction along the topologically-protected chiral edge states of the QH effect. We analyze heat current fluctuations as well as mixed charge-heat correlations [184, 185] when periodic voltage pulses are sent to the conductor and partitioned off a QPC [10]. Starting from the dc regime of the voltage drive, where simple relations between noises and currents can be derived in the spirit of the Schottky's formula [32, 43], and from the analogy with the charge current and noise, we introduce the *excess signals* for heat and mixed fluctuations, which basically measure the difference between the zero-frequency noises in an ac-driven system and their respective reference signals in the dc configuration. The vanishing of excess heat and mixed noise is thus used to flag the occurrence of a minimal excitation state for heat transport in the QH regime. With this powerful tool we demonstrate that minimal noise states for heat transport can be achieved only when *levitons* are injected into the QH edge states. We study this problem both in the integer regime and in the FQH regime. Our results are robust against interactions, since integer levitons still represent minimal excitation states despite the highly non-linear physics occurring at the QPC due to the peculiar collective excitations of the FQH state.

Having recognized levitons as the fundamental building block for heat transport, we then turn to the second central issue of this Chapter, which deals with the robustness of multiple overlapping Lorentzian pulses as minimal excitation states. Indeed, Levitov and collaborators demonstrated that N levitons traveling through a quantum conductor with transmission $\mathcal{T} < 1$ represent N independent attempts to pass the barrier, with the total noise not affected by the overlap between their wavepackets. This is no more guaranteed when we look for quantities which have a non-linear dependence on the voltage bias. Two types of nonlinearities are considered here. The first one comes from the mixed and heat shot noise, whose behaviors are $\sim V^2(t)$ and $\sim V^3(t)$ respectively in Fermi liquid systems. The second one is a natural consequence of FQH physics, which give rise to power laws with non-integer exponents. We show that, while currents and noises are sensitive to the actual number of particles sent to the QPC, excess signals always vanish for arbitrary superposition of integer levitons. One then concludes that levitons show a

remarkable stability even with regard to heat transport properties, combined with the equally surprising robustness in the strongly-correlated FQH liquid. This provides further evidence of the uniqueness of the leviton state in the QH regime.

4.2 Model

We adopt the same model used in Chapter 3 and shown schematically in Fig. 3.4. For completeness, and for a better readability of the present Chapter, we summarize the main points of the model here below:

- ✓ We consider a QH system with filling factor $\nu = 1/(2n+1)$, $n \in \mathbb{N}$. The special case $n = 0$ corresponds to the integer QH regime at $\nu = 1$, where the single chiral state on each edge is well described by a one-dimensional Fermi liquid theory. Conversely, values $n > 0$ describe a fractional system in the Laughlin sequence [20], with still one chiral mode per edge.

- ✓ The total Hamiltonian is $H = H_0 + H_V + H_T$, consisting of edge states, source and tunneling terms respectively. The free Hamiltonian H_0 modeling right-moving and left-moving states on opposite edges is given by Eq. (3.57). The source term H_V is given by Eq. (3.61) for the case $\mathcal{V}_R(x,t) = \Theta(-x-d)V(t)$ and $\mathcal{V}_L(x,t) = 0$, accounting for the capacitive coupling with a time-dependent voltage gate. Finally, quasiparticle tunneling occurs at $x = 0$ due the the presence of a QPC, and is modeled through the tunneling Hamiltonian H_T given in Eq. (3.79).[1]

- ✓ One can relate the bosonic description to creation and annihilation of quasiparticles through bosonization identities Eqs. (3.60). The periodic voltage bias $V(t) = V_{\rm dc} + V_{\rm ac}(t)$ generates a phase shift of quasiparticle fields [see Eqs. (3.76)], which will be conveniently handled through the Fourier series $e^{-ie^*\int_0^t dt'\, V(t')} = e^{-iq\omega t}\sum_{l=-\infty}^{+\infty} p_l e^{-il\omega t}$, with $q = e^*V_{\rm dc}/\omega$. Details of the calculation of the photoassisted coefficients p_l are given in Appendix A.

4.3 Heat current operator in the chiral Luttinger liquid

To calculate heat transport properties, one first needs a sound definition of heat current [186, 187]. To this end, let us consider a thermodynamical system described by the internal energy E and the particle number N (here we focus

[1] Here we suppress the redundant label $^{(\rm qp)}$ from the quasiparticle field, since we will not consider tunneling of electrons.

on a single species of particle). The entropy $S(E,N)$ changes at the rate

$$\frac{dS}{dt} = \frac{1}{\theta}\frac{dE}{dt} - \frac{\mu}{\theta}\frac{dN}{dt}, \tag{4.1}$$

with θ the temperature and μ the chemical potential. This suggest the following definition for the entropy current in terms of energy (J_E) and particle (J_N) currents respectively:

$$J_S = \frac{1}{\theta}J_E - \frac{\mu}{\theta}J_N. \tag{4.2}$$

At the same time we have $dQ = \theta dS$ from basic thermodynamical principles, where dQ is the infinitesimal heat exchanged in the process. One then finds the heat current J_Q:

$$J_Q = J_E - \mu J_N. \tag{4.3}$$

The heat current is thus viewed as an excess energy flux with respect to the value set by the local chemical potential. For a quantum system with Hamiltonian $\mathcal{H}$ and particle number $\mathcal{N}$, it is thus customary to define the heat current operator as

$$J_Q = \dot{\mathcal{H}} - \mu\dot{\mathcal{N}}. \tag{4.4}$$

However, when dealing with the chiral Luttinger liquid model of FQH edge states, the above considerations must be revisited carefully. Indeed, the chemical potential contribution is automatically subtracted in the chiral Luttinger liquid Hamiltonian. This is shown in more detail in Appendix B, where we demonstrate explicitly how the bosonic Hamiltonian is equivalent to a fermionic model where energy and particle number are counted with respect to the many-particle Fermi sea. Thus, the operator for the heat current reflected into the lower, left-moving edge of the setup shown in Fig. 3.4 is just

$$J_Q = \dot{H}_L = -i[H_L, H_T]. \tag{4.5}$$

We now use the Baker-Campbell-formula Eq. (C.6) to calculate the commutator in Eq. (4.5):

$$\begin{aligned}
J_Q &= -i\frac{v}{4\pi}\int dx \left[[\partial_x\Phi_L(x)]^2, \frac{\Lambda}{2\pi a}e^{i\sqrt{\nu}\Phi_R(0)}e^{-i\sqrt{\nu}\Phi_L(0)} + \text{h.c.}\right] = \\
&= -i\frac{v}{4\pi}\frac{\Lambda}{2\pi a}\int dx \Big\{\partial_x\Phi_L(x)e^{i\sqrt{\nu}\Phi_R(0)}e^{-i\sqrt{\nu}\Phi_L(0)}\partial_x\left[\Phi_L(x), (-i\sqrt{\nu})\Phi_L(0)\right] + \\
&\quad + e^{i\sqrt{\nu}\Phi_R(0)}e^{-i\sqrt{\nu}\Phi_L(0)}\partial_x\left[\Phi_L(x), (-i\sqrt{\nu})\Phi_L(0)\right]\partial_x\Phi_L(x)\Big\} + \text{h.c.} = \\
&= -\frac{v}{2}\frac{\Lambda}{2\pi a}\int dx \Big\{(-i\sqrt{\nu})\partial_x\Phi_L(x)e^{i\sqrt{\nu}\Phi_R(0)}e^{-i\sqrt{\nu}\Phi_L(0)} + \\
&\quad + e^{i\sqrt{\nu}\Phi_R(0)}e^{-i\sqrt{\nu}\Phi_L(0)}(-i\sqrt{\nu})\partial_x\Phi_L(x)\Big\}\delta(x) + \text{h.c.} = \\
&= -v\frac{\Lambda}{2\pi a}(-i\sqrt{\nu})\partial_x\Phi_L(0)e^{i\sqrt{\nu}\Phi_R(0)}e^{-i\sqrt{\nu}\Phi_L(0)} + \text{h.c.} = \\
&= -v\frac{\Lambda}{2\pi a}e^{i\sqrt{\nu}\Phi_R(0)}\partial_x e^{-i\sqrt{\nu}\Phi_L(0)} + \text{h.c.}.
\end{aligned} \tag{4.6}$$

Here the notation $\partial_x f(0)$ stands for $[\partial_x f(x)]_{x=0}$. It's easy to check that J_Q in terms of quasiparticle operators $\Psi^{(\mathrm{qp})}_{R/L}$ reads

$$\begin{aligned} J_Q &= -v\frac{\Lambda}{2\pi a}e^{i\sqrt{\nu}\Phi_R(0)}\partial_x\left[e^{ik_\mathrm{F}x}e^{-ik_\mathrm{F}x}e^{-i\sqrt{\nu}\Phi_L(x)}\right]_{x=0} + \mathrm{h.c.} = \\ &= -v\sum_{\varepsilon=+,-}\left[\Lambda\Psi_R^{(\mathrm{qp})\dagger}(0)\partial_x\Psi_L^{(\mathrm{qp})}(0)\right]^\varepsilon - ivk_\mathrm{F}\sum_{\varepsilon=+,-}\varepsilon\left[\Psi_R^{(\mathrm{qp})\dagger}(0)\Psi_L^{(\mathrm{qp})}(0)\right]^\varepsilon = \\ &= J_E - \frac{\mu}{e^*}J_C, \end{aligned} \tag{4.7}$$

with $\mu = vk_\mathrm{F}$ the chemical potential and $J_C = e^*J_N$ the charge current operator given by Eq. (3.83). Here, in analogy with Eq. (4.3), we have defined

$$J_E = -v\sum_{\varepsilon=+,-}\left[\Lambda\Psi_R^{(\mathrm{qp})\dagger}(0)\partial_x\Psi_L^{(\mathrm{qp})}(0)\right]^\varepsilon. \tag{4.8}$$

Now it's evident that, as stated before, the term μJ_N is already implicitly subtracted in the definition of $J_Q = \dot{H}_L$.

4.4 Averaged backscattered heat current

We apply the Keldysh non-equilibrium contour formalism (see Appendix D) to calculate the current $\langle J_Q(t)\rangle$ backscattered off the barrier and detected in terminal 2. In this framework one has

$$\langle J_Q(t)\rangle = \frac{1}{2}\sum_{\eta_0}\left\langle T_\mathrm{K}J_E(t^{\eta_0})e^{-i\int_{c_\mathrm{K}}dt' H_T(t')}\right\rangle - \frac{\mu}{e^*}\langle J_C(t)\rangle, \tag{4.9}$$

with T_K the time-ordering operator along the back-and-forth Keldysh contour c_K, whose two branches are labeled by $\eta_0 = \{+,-\}$. The transparency of the QPC can be finely tuned with the help of gate voltages. In the low reflectivity regime, tunneling can be treated as a perturbative correction to the perfectly

transmitting setup. Then at first order in the perturbation we have

$$
\begin{aligned}
&\langle J_Q(t)\rangle = \\
&= -\frac{i}{2}\sum_{\eta_0,\eta_1}\eta_1\int_{-\infty}^{+\infty}dt'\left\langle T_{\rm K}J_E(t^{\eta_0})H_T(t'^{\eta_1})\right\rangle - \frac{\mu}{e^*}\langle J_C(t)\rangle = \\
&= \frac{i}{2}\sum_{\eta_0,\eta_1}\eta_1\int_{-\infty}^{+\infty}dt'\sum_{\varepsilon,\varepsilon'}e^{i\varepsilon e^*\int_0^t V(t'')dt''}e^{i\varepsilon' e^*\int_0^{t'}V(t'')dt''}\times \\
&\quad\times\left\langle T_{\rm K}\left[\Lambda\psi_R^\dagger(0,t^{\eta_0})\partial_t\psi_L(0,t^{\eta_0})\right]^{\varepsilon}\left[\Lambda\psi_R^\dagger(0,t'^{\eta_1})\psi_L(0,t'^{\eta_1})\right]^{\varepsilon'}\right\rangle - \frac{\mu}{e^*}\langle J_C(t)\rangle = \\
&= \frac{i}{2}|\Lambda|^2\sum_{\eta_0,\eta_1}\eta_1\int_{-\infty}^{+\infty}dt'\times \\
&\quad\times\left\{e^{ie^*\int_{t'}^t V(t'')dt''}\left\langle T_{\rm K}\psi_R^\dagger(0,t^{\eta_0})\psi_R(0,t'^{\eta_1})\right\rangle\partial_t\left\langle T_{\rm K}\psi_L(0,t^{\eta_0})\psi_L^\dagger(0,t'^{\eta_1})\right\rangle\right. \\
&\quad\left.+e^{-ie^*\int_{t'}^t V(t'')dt''}\left\langle T_{\rm K}\psi_R(0,t^{\eta_0})\psi_R^\dagger(0,t'^{\eta_1})\right\rangle\partial_t\left\langle T_{\rm K}\psi_L^\dagger(0,t^{\eta_0})\psi_L(0,t'^{\eta_1})\right\rangle\right\}+ \\
&\quad-\frac{\mu}{e^*}\langle J_C(t)\rangle\,. \qquad (4.10)
\end{aligned}
$$

The derivatives ∂_t give rise to two terms:

$$\partial_t\left\langle T_{\rm K}\psi_L(0,t^{\eta_0})\psi_L^\dagger(0,t'^{\eta_1})\right\rangle = \frac{1}{2\pi a}e^{-ik_{\rm F}v(t-t')}\left(-i\mu+\partial_t\right)e^{\nu\mathcal{G}^{\eta_0\eta_1}(t-t')}, \qquad (4.11)$$

$$\partial_t\left\langle T_{\rm K}\psi_L^\dagger(0,t^{\eta_0})\psi_L(0,t'^{\eta_1})\right\rangle = \frac{1}{2\pi a}e^{ik_{\rm F}v(t-t')}\left(i\mu+\partial_t\right)e^{\nu\mathcal{G}^{\eta_0\eta_1}(t-t')}. \qquad (4.12)$$

It's straightforward to check that terms proportional to $\mu = vk_{\rm F}$ are canceled by the last term of Eq. (4.10), and the only remaining contribution is

$$
\begin{aligned}
\langle J_Q(t)\rangle = i|\lambda|^2\sum_{\eta_0,\eta_1}\int_{-\infty}^{+\infty}d\tau\eta_1\cos\left[e^*\int_{t-\tau}^t dt''V(t'')\right]\times \\
\times\exp\left[\nu\mathcal{G}^{\eta_0\eta_1}(\tau)\right]\partial_\tau\exp\left[\nu\mathcal{G}^{\eta_0\eta_1}(\tau)\right], \qquad (4.13)
\end{aligned}
$$

with $\lambda = \Lambda/(2\pi a)$ the reduced tunneling constant. In the last equation we explicitly showed the matrix structure of Keldysh Green's functions due to the two-fold time contour. Using Eq. (3.91) we thus get

$$\langle J_Q(t)\rangle = i|\lambda|^2\int_0^{+\infty}d\tau\cos\left[e^*\int_{t-\tau}^t dt''V(t'')\right]\left[\partial_\tau e^{2\nu\mathcal{G}(\tau)}-\partial_\tau e^{2\nu\mathcal{G}(-\tau)}\right]. \qquad (4.14)$$

The dc component of charge and heat currents in presence of the periodic drive is then obtained by averaging over one period T. At this stage, it is useful to introduce the Fourier transform $\hat{P}_g(E) = \int d\tau e^{iE\tau}e^{g\mathcal{G}(\tau)}$ of the bosonic Green's function, which was given in Eq. (3.100) of the previous Chapter. For generic filling factor of the Laughlin sequence we get

$$\overline{\langle J_Q(t)\rangle} = |\lambda|^2\frac{\omega}{2}\sum_l|p_l|^2(q+l)\left\{\hat{P}_{2\nu}\left[(q+l)\omega\right]-\hat{P}_{2\nu}\left[-(q+l)\omega\right]\right\}, \qquad (4.15)$$

where the notation $\overline{\langle \ldots \rangle}$ stands for $\int_0^T \frac{dt}{T} \langle \ldots \rangle$. We have found a result similar to the averaged charge current, Eq. (3.102). The l-th contribution to the averaged heat current is indeed the difference between two opposite tunneling rates, weighted by the corresponding energy $(q+l)\omega$ transferred between edges.

4.5 Zero-frequency heat and mixed noise

We now turn to the calculation of heat and mixed fluctuations. Our focus will be on the zero-frequency component of the power spectra

$$\mathcal{S}_Q = 2 \int_0^T \frac{dt}{T} \int_{-\infty}^{+\infty} dt' \, \langle \Delta J_Q(t) \Delta J_Q(t') \rangle \,, \tag{4.16}$$

$$\mathcal{S}_X = 2 \int_0^T \frac{dt}{T} \int_{-\infty}^{+\infty} dt' \, \langle \Delta J_C(t) \Delta J_Q(t') \rangle \,, \tag{4.17}$$

with operators $\Delta J_i(t) = J_i(t) - \langle J_i(t) \rangle$, $i = \{C, Q\}$, describing charge and heat current fluctuations. First of all, we note that all terms $\langle J_i(t) \rangle \langle J_j(t) \rangle$, with $i, j = \{C, Q\}$, are $O(|\lambda|^4)$, and the lowest order terms in the perturbative expansion are thus given by

$$\left\langle T_{\mathrm{K}} \Delta J_i(t^+) \Delta J_j(t'^-) e^{-i \int_{c_{\mathrm{K}}} d\tau H_T(\tau)} \right\rangle = \left\langle J_i(t^+) J_j(t'^-) \right\rangle + O(|\lambda|^4). \tag{4.18}$$

As in the previous Chapter, we have placed operators $\Delta J_i(t)$ and $\Delta J_j(t')$ on different portions of the Keldysh contour (the former on the forward branch, the latter on the backward branch). Calculations are lengthy but straightforward, and rely uniquely on the function $\exp\left[\nu \mathcal{G}^{+-}(t,t')\right] = \exp\left[\nu \mathcal{G}(t'-t)\right]$ and its appropriate derivatives. To lowest order in the tunneling we obtain

$$\mathcal{S}_X = 4e^*|\lambda|^2 \int_0^T \frac{dt}{T} \int_{-\infty}^{+\infty} dt' \sin\left[e^* \int_{t'}^{t} dt'' V(t'') \right] e^{\nu \mathcal{G}(t'-t)} \partial_{t'} e^{\nu \mathcal{G}(t'-t)}, \tag{4.19}$$

$$\mathcal{S}_Q = 4|\lambda|^2 \int_0^T \frac{dt}{T} \int_{-\infty}^{+\infty} dt' \cos\left[e^* \int_{t'}^{t} dt'' V(t'') \right] e^{\nu \mathcal{G}(t'-t)} \partial_t \partial_{t'} e^{\nu \mathcal{G}(t'-t)}. \tag{4.20}$$

Once again, it's convenient to use the Fourier transform $\hat{P}_g(E)$ of the function $e^{g\mathcal{G}(\tau)}$ and the series representation for $e^{-i\varphi(t)} = e^{-ie^* \int_0^t dt' \, V_{\mathrm{ac}}(t')}$. We finally get a physically reasonable result in terms of the tunneling rates, which reads

$$\mathcal{S}_X = e^* \omega |\lambda|^2 \sum_l |p_l|^2 (q+l) \left\{ \hat{P}_{2\nu}\left[(q+l)\omega\right] + \hat{P}_{2\nu}\left[-(q+l)\omega\right] \right\}, \tag{4.21}$$

$$\mathcal{S}_Q = \frac{|\lambda|^2}{\pi} \sum_l |p_l|^2 \int_{-\infty}^{+\infty} dE E^2 \hat{P}_\nu(E) \times$$
$$\times \left\{ \hat{P}_\nu\left[(q+l)\omega - E\right] + \hat{P}_\nu\left[-(q+l)\omega - E\right] \right\}, \tag{4.22}$$

for the zero-frequency component of the noises. To perform the integral in the equation for $\mathcal{S}_Q$, we make use of the identity

$$\int_{-\infty}^{+\infty} \frac{dY}{2\pi} Y^2 \hat{P}_{g_1}(Y)\hat{P}_{g_2}(X-Y) = \frac{\hat{P}_{g_1+g_2}(X)}{1+g_1+g_2}\left[g_1 g_2 \pi^2\theta^2 + \frac{g_1(1+g_1)}{g_1+g_2}X^2\right] \tag{4.23}$$

demonstrated in Appendix F [see Eq. (F.24)]. The latter leads to

$$\begin{aligned}\mathcal{S}_Q = |\lambda|^2 \sum_l |p_l|^2 \left[\frac{2\pi^2\nu^2}{1+2\nu}\theta^2 + \frac{1+\nu}{1+2\nu}(q+l)^2\omega^2\right] \\ \times \left\{\hat{P}_{2\nu}\left[(q+l)\omega\right] + \hat{P}_{2\nu}\left[-(q+l)\omega\right]\right\}.\end{aligned} \tag{4.24}$$

While the result for $\mathcal{S}_X$ is reasonably simple (each contribution is the sum of opposite tunneling rates times the energy exchanged), the one for $\mathcal{S}_Q$ has not a straightforward interpretation, as it is made of a thermal contribution plus a second term involving the squared energy $(q+l)^2\omega^2$. One should note that for $\nu = 1$ and finite temperature we have

$$\mathcal{S}_X = \frac{e|\Lambda|^2\omega^2}{2\pi v^2}\sum_{l=-\infty}^{+\infty} |p_l|^2 (q+l)^2 \coth\left[\frac{(q+l)\omega}{2\theta}\right], \tag{4.25}$$

$$\mathcal{S}_Q = \frac{|\Lambda|^2\omega^3}{3\pi v^2}\sum_{l=-\infty}^{+\infty} |p_l|^2 \left[\left(\frac{\pi\theta}{\omega}\right)^2 + (q+l)^2\right](q+l)\coth\left[\frac{(q+l)\omega}{2\theta}\right], \tag{4.26}$$

consistently with previous results in the literature [160, 162, 188, 189].

4.5.1 Zero temperature

At $\theta = 0$ we resort to the asymptotic expansion Eq. (3.113) to perform the zero-temperature limit of Eqs. (4.15), (4.21) and (4.24). We thus find the following results:

$$\overline{\langle J_Q(t)\rangle} = |\lambda|^2 \frac{\pi}{\Gamma(2\nu)}\left(\frac{\omega}{\omega_c}\right)^{2\nu}\sum_l |p_l|^2 |q+l|^{2\nu}, \tag{4.27}$$

$$\mathcal{S}_X = e^*|\lambda|^2 \frac{2\pi}{\Gamma(2\nu)}\left(\frac{\omega}{\omega_c}\right)^{2\nu}\sum_l |p_l|^2 |q+l|^{2\nu}\,\mathrm{sign}(q+l), \tag{4.28}$$

$$\mathcal{S}_Q = \omega|\lambda|^2 \frac{2\pi(1+\nu)}{\Gamma(2\nu)(1+2\nu)}\left(\frac{\omega}{\omega_c}\right)^{2\nu}\sum_l |p_l|^2 |q+l|^{2\nu+1}. \tag{4.29}$$

Equations (4.27), (4.28) and (4.29) show the familiar power-law behavior of the Luttinger liquid [23, 190]. We have already seen a similar power-law in the charge current $\overline{\langle J_C(t)\rangle}$ and noise $\mathcal{S}_C$, although in a slightly different form.

While all contributions to $\overline{\langle J_C(t)\rangle}$ and $\mathcal{S}_C$ are proportional to $|q+l|^{2\nu-1}$ [see Eqs. (3.116) and (3.117)], here we have found the behavior $|q+l|^{2\nu}$ for $\overline{\langle J_Q(t)\rangle}$ and $\mathcal{S}_X$, and $|q+l|^{2\nu+1}$ for $\mathcal{S}_Q$. This hierarchy in the power-law exponents implies interesting consequences that we will explore in the next Section.

4.6 Excess signals and noiseless drive

4.6.1 From Schottky formula to the ac regime

We start the discussion considering a dc-biased conductor, i.e. $V(t) = V_{\rm dc}$ with $V_{\rm ac}(t) = 0$. Such a situation entails that photoassisted coefficients reduce to $p_l = \delta_{l,0}$. As we have seen in the previous Chapter, charge current and noise at temperature $\theta = 0$ are linked by [50, 51, 191]

$$\mathcal{S}_C = 2e^* \langle J_C \rangle . \tag{4.30}$$

Interestingly, similar expressions can be derived relating mixed and heat noise to the heat current for a dc bias. From Eq. (4.27) and assuming $V_{\rm dc} > 0$, one gets the following formula for the heat current

$$\langle J_Q \rangle = |\lambda|^2 \frac{\pi}{\Gamma(2\nu)} \left(\frac{e^* V_{\rm dc}}{\omega_c} \right)^{2\nu} . \tag{4.31}$$

Similarly, mixed and heat noise are obtained from Eqs. (4.28) and (4.29) with the condition $p_l = \delta_{l,0}$. They read

$$\mathcal{S}_X = e^* |\lambda|^2 \frac{2\pi}{\Gamma(2\nu)} \left(\frac{e^* V_{\rm dc}}{\omega_c} \right)^{2\nu} , \tag{4.32}$$

$$\mathcal{S}_Q = e^* V_{\rm dc} |\lambda|^2 \frac{2\pi\,(1+\nu)}{\Gamma(2\nu)\,(1+2\nu)} \left(\frac{e^* V_{\rm dc}}{\omega_c} \right)^{2\nu} . \tag{4.33}$$

Comparing the last three results, we immediately notice a proportionality between $\mathcal{S}_X$, $\mathcal{S}_Q$ and $\langle J_Q \rangle$, namely

$$\mathcal{S}_X = 2e^* \langle J_Q \rangle , \tag{4.34}$$

$$\mathcal{S}_Q = 2e^* \frac{1+\nu}{1+2\nu} V_{\rm dc} \langle J_Q \rangle . \tag{4.35}$$

Equations (4.34) and (4.35) are generalizations of Schottky's formula to the heat and mixed noise. They show that the uncorrelated backscattering of Laughlin quasiparticles at the QPC leaves Poissonian signature in heat transport properties also, in addition to the well-known Poissonian behavior of the charge shot noise described by Eq. (4.30). This holds both in a chiral Fermi liquid (i.e. at $\nu = 1$, when tunneling involves integer electrons only) and in the FQH regime, with proportionality constants governed by the filling factor

ν. Similar relations for transport across a quantum dot were recently reported [184, 192].

We now address the central quantities of interest for the present Chapter. Equation (4.34), representing a proportionality between the mixed charge-heat correlator $\mathcal{S}_X$ and the heat current for a dc voltage drive governed by the charge e^*, leads us to introduce the *excess mixed noise* given by

$$\Delta\mathcal{S}_X = \mathcal{S}_X - 2e^*\overline{\langle J_Q(t)\rangle}. \tag{4.36}$$

As for the excess charge noise $\Delta\mathcal{S}_C = \mathcal{S}_C - 2e^*\overline{\langle J_C(t)\rangle}$ (see Sec. 3.5), this quantity measures the difference between the noise in presence of a generic periodic voltage drive and the dc reference value. Using Eqs. (4.27) and (4.28) the excess mixed noise reads

$$\Delta\mathcal{S}_X = -e^*|\lambda|^2\frac{4\pi}{\Gamma(2\nu)}\left(\frac{\omega}{\omega_c}\right)^{2\nu}\sum_{l<-q}|p_l|^2|q+l|^{2\nu}. \tag{4.37}$$

The vanishing of $\Delta\mathcal{S}_X$ should highlight an energetically clean pulse, for which the mixed noise reaches the minimal value $\mathcal{S}_X = 2e^*\overline{\langle J_Q(t)\rangle}$ expected from the Schottky-like formula Eq. (4.34). With a very similar procedure it is possible to extract the excess component of the zero-frequency heat noise due to the time dependent drive. Equation (4.35) states that $\mathcal{S}_Q$ is proportional to the heat current multiplied by the voltage bias in the dc limit. In view of this consideration we define the *excess heat noise*

$$\Delta\mathcal{S}_Q = \mathcal{S}_Q - 2e^*\frac{1+\nu}{1+2\nu}\overline{V(t)\,\langle J_Q(t)\rangle}. \tag{4.38}$$

The time-averaged value of $V(t)\,\langle J_Q(t)\rangle$ can be calculated from Eq. (4.14) using the relation $e^*V(t)e^{-i\varphi(t)} = (\omega q + i\partial_t)e^{-i\varphi(t)}$, with $\varphi(t) = e^*\int_0^t dt'\,V_{\rm ac}(t')$. Then from the above definition we get

$$\Delta\mathcal{S}_Q = \omega|\lambda|^2\frac{4\pi(1+\nu)}{\Gamma(2\nu)(1+2\nu)}\left(\frac{\omega}{\omega_c}\right)^{2\nu}\sum_{l<-q}|p_l|^2|q+l|^{2\nu+1}. \tag{4.39}$$

4.6.2 Physical content of the excess signals

Let us now look for the physics described by Eqs. (4.37) and (4.39). We consider the energy associated with hole-like excitations for an integer QH state with $\nu = 1$. At temperature $\theta = 0$ it reads

$$E_h = -\sum_{k=-\infty}^{+\infty} n_{\rm F}(vk)vk\left\langle c_k(t)c_k^\dagger(t)\right\rangle, \tag{4.40}$$

with $n_{\rm F} = \Theta(-k)$ the Fermi distribution. This quantity can be written as

$$\begin{aligned} E_h &= \frac{i}{2}\frac{v^2}{(2\pi a)^2}\int d\tau' \int d\tau\, e^{-ie\int_{\tau'-\tau}^{\tau'} dt' V(t')}\partial_\tau e^{2\mathcal{G}(\tau)} = \\ &= \frac{1}{2}\frac{v^2}{(2\pi a)^2}\int d\tau' \int d\tau \left\{ \sin\left[e\int_{\tau'-\tau}^{\tau'} dt' V(t')\right] + \right. \\ &\quad \left. + i\cos\left[e\int_{\tau'-\tau}^{\tau'} dt' V(t')\right]\right\}\partial_\tau e^{2\mathcal{G}(\tau)}. \end{aligned} \tag{4.41}$$

Then, comparing this result with Eqs. (4.19) and (4.14), we find that $\Delta\mathcal{S}_X$ measures the energy associated with the unwanted holes generated through the periodic voltage drive at $\nu = 1$, namely

$$E_h \propto -\mathcal{S}_X + 2e\overline{\langle J_Q(t)\rangle} = -\Delta\mathcal{S}_X. \tag{4.42}$$

This accounts for the negative value of $\Delta\mathcal{S}_X$ arising from Eq. (4.37). It is worth noticing that Eq. (4.41) holds in an unperturbed system without tunneling between opposite edges. The noise induced by the presence of the QPC can thus be viewed as a probe for excitations generated by ac pulses. A similar relation, involving the sum of the squared energy for each value of k, holds for $\Delta\mathcal{S}_Q$:

$$\sum_{k=-\infty}^{+\infty} n_{\rm F}(vk)(vk)^2 \left\langle c_k(t)c_k^\dagger(t)\right\rangle \propto \Delta\mathcal{S}_Q. \tag{4.43}$$

Generalizing to FQH state of the Laughlin sequence, we conclude that clean energy states must arise for vanishing values of the excess mixed and heat noises $\Delta\mathcal{S}_X$ and $\Delta\mathcal{S}_Q$.

In Fig. 4.1 we show the behavior of the excess mixed noise as a function of the charge q injected during one period T. Notice that we normalize $\Delta\mathcal{S}_X$ by a negative quantity, in order to deal with a positive function. Two types of bias are considered: a sinusoidal drive and a train of Lorentzian pulses given respectively by

$$V_{\rm sin}(t) = V_{\rm dc}[1-\cos(\omega t)], \tag{4.44}$$

$$V_{\rm Lor}(t) = \frac{V_{\rm dc}}{\pi}\sum_k \frac{\eta}{\eta^2 + (t/T-k)^2}, \tag{4.45}$$

with $\eta = W/T$ the ratio between the half width W at half maximum of the Lorentzian peak and the period T. The former is representative of all kinds of non-optimal voltage drive, while the latter is known to give rise to minimal charge noise both at integer [9] and fractional [24] fillings. We will set $\eta = 0.1$, a value lying in the range investigated by experiments [10]. At $\nu = 1$, both curves display local minima whenever q assumes integer values. However, while

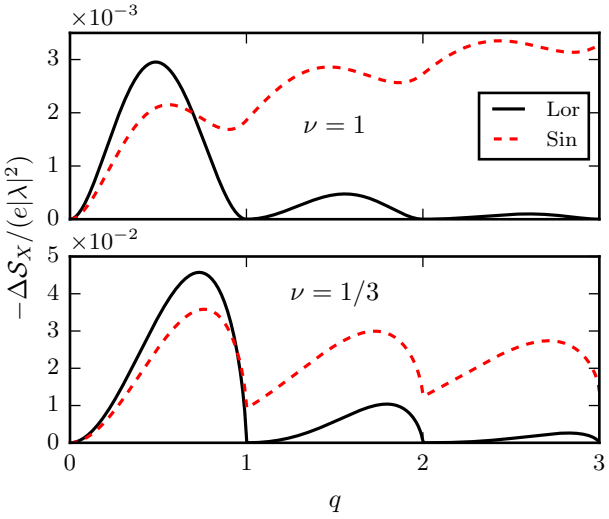

Figure 4.1: Excess mixed noise $-\Delta\mathcal{S}_X$ as a function of the charge per period q at zero temperature. The high energy cutoff is set to $\omega_c = 10\,\omega$. Behavior for Lorentzian pulses (full black line) and sinusoidal voltage drive (dashed red line) is reported.

the sinusoidal drive always generates an additional noise with respect to the reference Schottky value $2e^*\overline{\langle J_Q(t)\rangle}$, the Lorentzian signal drops to zero for $q \in \mathbb{N}$, indicating that the mixed noise $\mathcal{S}_X$ due to levitons exactly matches the Poissonian value set by Eq. (4.34). Since the excess mixed noise is linked to the unwanted energy introduced into the system as a result of hole injection [see Eq. (4.42)], Fig. 4.1 shows that there is no hole-like excitation carrying energy in our system. The bottom panel of Fig. 4.1 shows the same situation in a $\nu = 1/3$ FQH bar. The hierarchy of the $\nu = 1$ configuration is confirmed, with Lorentzian pulses generating minimal mixed noise for $q \in \mathbb{N}$ and sinusoidal voltage displaying non-optimal characteristics with non-zero $\Delta\mathcal{S}_X$. As for the charge excess noise, no signature for fractional values of q arises, signaling once again the robustness of levitons in interacting fractional systems. This is markedly different from driven-quantum-dot systems, where a strategy to inject a periodic train of fractionally charged quasiparticles in the FQH regime has been recently discussed [193].

The same analysis can be carried out for the excess heat noise $\Delta\mathcal{S}_Q$. Equation (4.39) suggests that the excess heat noise vanishes for the very same conditions that determine the vanishing of $\Delta\mathcal{S}_C$ and $\Delta\mathcal{S}_X$, given that we get a similar structure with only a different power law behavior. This expectation is confirmed in Fig. 4.2, where we report the behavior of $\Delta\mathcal{S}_Q$ for both $\nu = 1$ and $\nu = 1/3$. Lorentzian pulses carrying integer charge per period represent minimal-heat-noise states, independently of the filling factor.

We conclude this Section with a brief mathematical remark on the vanishing of the excess signals. Equations (3.130), (4.37) and (4.39) all share a similar

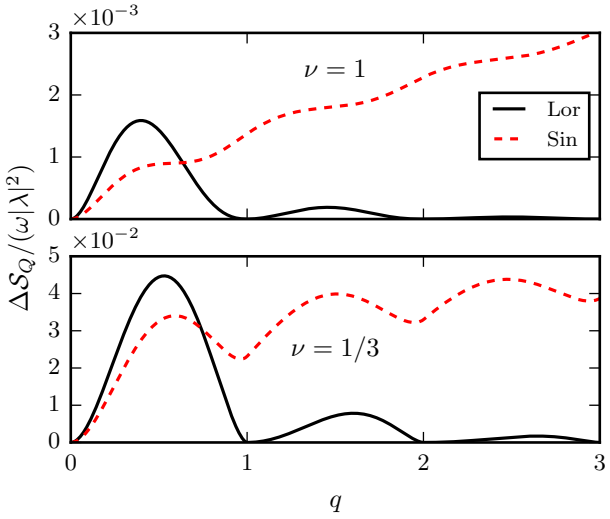

Figure 4.2: Excess heat noise $\Delta\mathcal{S}_Q$ as a function of the charge per period q. Full black and dashed red lines represent Lorentzian and sinusoidal drives respectively. The temperature is $\theta = 0$ and the cutoff is $\omega_c = 10\,\omega$.

structure in terms of the Fourier coefficients p_l, the only difference being the power law exponents $2\nu - 1$, 2ν and $2\nu + 1$ respectively. Then, we can explain the common features of $\Delta\mathcal{S}_C$, $\Delta\mathcal{S}_X$ and $\Delta\mathcal{S}_Q$ by looking at the Fourier coefficients of the Lorentzian voltage drive. In such case, the analytical behavior of $e^{-i\varphi(t)}$ as a function of the complex variable $z = e^{i\omega t}$ guarantees that $p_{l<-q} = 0$ when q is an integer, as shown in Appendix A. This immediately leads to the simultaneous vanishing of the three excess signals at integer charge q. Let us also remark that the Lorentzian pulse is the only drive showing this striking feature, as Eqs. (3.130), (4.37) and (4.39) all correspond to sums of positive terms and can thus *only* vanish if $|p_l|^2$ is zero for all l below $-q$. The only way this is possible is with quantized Lorentzian pulses.

4.7 Multiple Lorentzian pulses

In the previous section we demonstrated that quantized Lorentzian pulses with integer charge q represent minimal excitation states for the heat transport in the FQH regime, but this statement may potentially fail when different Lorentzian pulses have a substantial overlap. Indeed, nonlinear quantities such as J_Q, $\mathcal{S}_X$ and $\mathcal{S}_Q$ may behave very differently from charge current and noise, which are linear functions of the bias $V(t)$ in a Fermi liquid. For instance, at $\nu = 1$ one already sees a fundamental difference between average charge and heat currents in their response to the external drive, as J_C is independent of V_{ac} [see Eq. (3.116)], while J_Q goes like $\overline{V^2(t)} = V_{dc}^2 + \overline{V_{ac}^2(t)}$ [see Eq. (4.27) and the sum rule demonstrated in Appendix A, Sec. A.4]. Then, one might wonder whether the independence of overlapping levitons survives when we

look at such nonlinearity. In this regard, Battista *et al.* [188] pointed out that N levitons emitted in the same pulse in Fermi liquid systems are not truly independent excitations, since heat current and noise associated with such a drive are proportional to N^2 times the single-particle heat current and N^3 times the single-particle heat noise respectively. Nevertheless, well-separated levitons always give rise to really independent excitations, with J_Q and $\mathcal{S}_Q$ both equal to N times their corresponding single-particle signal, due to the vanishing of their overlap [188]. Moreover, an additional source of nonlinearity is provided by electron-electron interactions giving rise to the FQH phase, whose power-law behavior is governed by fractional exponents, thus strongly deviating from the linear regime.

In the following we study how nonlinearities due to heat transport properties and interactions affect the excess signals we introduced in Sec. 4.6. For this purpose, we consider a periodic signal made of a cluster of N pulses described by

$$V_N(t) = \sum_{j=0}^{N-1} \widetilde{V}\left(t - j\frac{\alpha}{N}T\right), \tag{4.46}$$

where $\widetilde{V}(t)$ is periodic of period T. We still consider the parameter q as the total charge injected during one complete period T of the drive $V_N(t)$, which means that each pulse in the cluster carries a fraction q/N of the total charge. Inside a single cluster, the N signals in Eq. (4.46) are equally spaced with a fixed time delay $\Delta t = \alpha T/N$ between successive pulses. Note that $\alpha = 0$ corresponds to several superimposed pulses, giving $V_N(t)|_{\alpha=0} = N\widetilde{V}(t)$. Also, for $\alpha = 1$ we just get a new periodic signal with period T/N. We thus restrict the parameter α to the interval $0 \leq \alpha < 1$. An example of such a voltage drive for the case of Lorentzian pulses is provided in Fig. 4.3.

Fourier coefficients for a periodic multi-pulse cluster can be factorized in a convenient way (see Appendix A). Here we take as an example the simple case $N = 2$, whose coefficients are given by

$$p_l^{(2)}(q) = \sum_{m=-\infty}^{+\infty} e^{i\pi\alpha m} p_{l-m}\left(\frac{q}{2}\right) p_m\left(\frac{q}{2}\right), \tag{4.47}$$

Each pulse carries one half of the total charge q, a fact that is clearly reflected in the structure of Eq. (4.47).

Let us first focus on an integer QH effect with $\nu = 1$. It is easy to see that, at least in the dc regime, $\mathcal{S}_X$ and $\mathcal{S}_Q$ scale as V^2 and V^3 respectively. It is then natural to wonder if a cluster of Lorentzian pulses still gives rise to minimal values of $\mathcal{S}_X$ and $\mathcal{S}_Q$ when the interplay of nonlinearities, ac effects and overlapping comes into play. We thus look for the excess mixed and heat noises for the case of $N = 2$ Lorentzian pulses per period, in order to shed light on this problem. The top and bottom panels of Fig. 4.4 show the excess mixed and heat noises respectively in presence of two pulses per period at $\nu = 1$. For

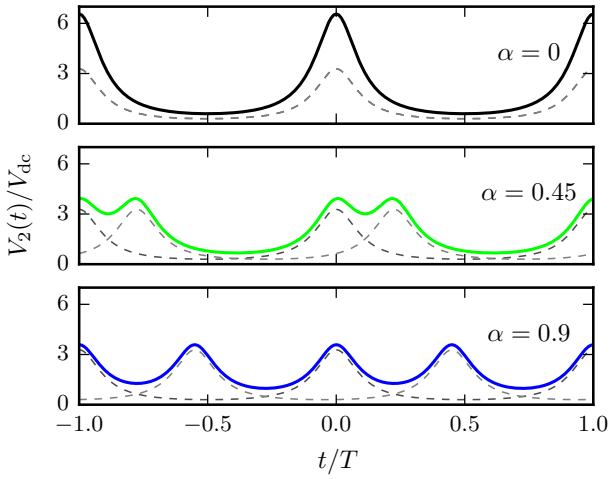

Figure 4.3: Time-periodic voltage drive given by Eq. (4.46) in the case of $N = 2$ Lorentzian-shaped pulses per period at total charge $q = 1$ (i.e. $1/2$ for each pulse). The top panel represents two completely overlapping pulses ($\alpha = 0$), for which we simply have $V_2(t) = 2\widetilde{V}(t)$. The central and bottom panels correspond to non-trivial cases $\alpha = 0.45$ and $\alpha = 0.9$ with finite overlap between pulses. In all cases the behavior of individual Lorentzian pulses $\widetilde{V}(t)$ and $\widetilde{V}\left(t - \frac{\alpha}{N}T\right)$ are depicted with dashed, thin lines.

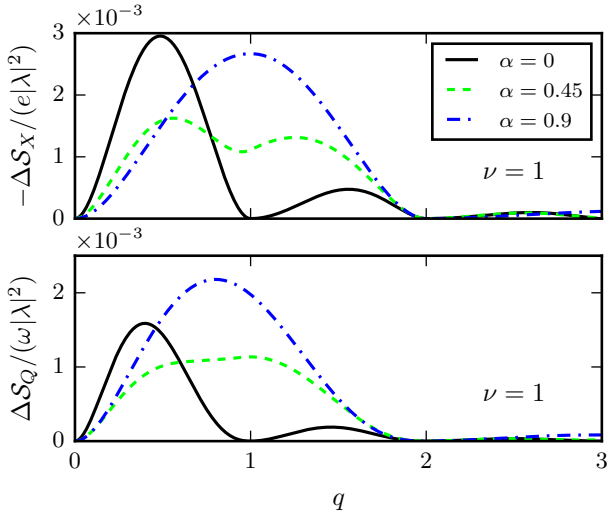

Figure 4.4: Excess signals $-\Delta\mathcal{S}_X$ (top panel) and $\Delta\mathcal{S}_Q$ (bottom panel) as a function of q for a cluster of two identical Lorentzian pulses separated by a time delay $\alpha T/2$. All curves refer to the case of $\nu = 1$ and zero temperature. The cutoff is set to $\omega_{\rm c} = 10\,\omega$.

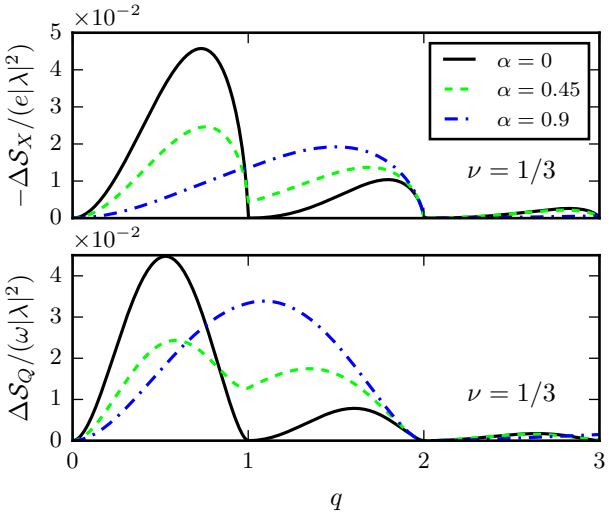

Figure 4.5: Excess signals $-\Delta\mathcal{S}_X$ and $\Delta\mathcal{S}_Q$ as a function of q for two identical Lorentzian pulses with time delay $\alpha T/2$ at fractional filling $\nu = 1/3$ and zero temperature. The cutoff is set to $\omega_c = 10\,\omega$.

$\alpha = 0$ we get a perfect superposition between pulses, and we are left with a single Lorentzian carrying the total charge q. This case displays zeros whenever the total charge reaches an integer value. Higher values of α represent non-trivial behavior corresponding to different, time-resolved Lorentzian pulses. A Lorentzian voltage source injecting $q = 1/2$ electrons per period is not an optimal drive (and so is, a fortiori, an arbitrary superposition of such pulses). As a result, signals for $\alpha = 0.45$ and $\alpha = 0.9$ turn out to be greater than zero at $q = 1$. However $\Delta\mathcal{S}_X$ and $\Delta\mathcal{S}_Q$ still vanish at $q = 2$, where they correspond to a pair of integer levitons, showing the typical behavior of minimal excitation states with no excess noise. This demonstrates that integer levitons, *although overlapping*, always generate the Poissonian value for heat and mixed noises expected from their respective Schottky formulas. It is worth noticing that the blue curves in Fig. 4.4 (nearly approaching the limit $\alpha \to 1$) almost totally forget the local minimum in $q = 1$ and get close to a simple rescaling of the single-pulse excess noises $\Delta\mathcal{S}_X\left(\frac{q}{2}\right)$ and $\Delta\mathcal{S}_Q\left(\frac{q}{2}\right)$. This is because $\alpha \to 1$ is a trivial configuration corresponding to one pulse per period with $T' = \frac{T}{2}$, as was mentioned before.

It is even more remarkable, however, to still observe a similar qualitative behavior in the FQH regime, where one may expect this phenomenon to break down as a result of the strong nonlinearities due to the chiral Luttinger liquid physics. Figure 4.5 shows that both signals drop to zero for $q = 2$, representing a robust evidence for a minimal excitation state even in a strongly-interacting fractional liquid. We stress that such a strong stability of heat transport properties is an interesting and unexpected result both at integer and fractional filling factor. Indeed, the bare signals $\overline{\langle J_Q \rangle}$, $\mathcal{S}_X$ and $\mathcal{S}_Q$ are affected by the

parameters governing the overlap between pulses, namely

$$\overline{\langle J_Q \rangle}^{(N)} \neq N \overline{\langle J_Q \rangle}^{(1)}, \tag{4.48a}$$

$$\mathcal{S}_X{}^{(N)} \neq N \mathcal{S}_X{}^{(1)}, \tag{4.48b}$$

$$\mathcal{S}_Q{}^{(N)} \neq N \mathcal{S}_Q{}^{(1)}, \tag{4.48c}$$

even at $q = N$, in accordance with Ref. [188]. Nonetheless, such differences are washed out when the dc Schottky-like signals are subtracted from $\mathcal{S}_X$ and $\mathcal{S}_Q$ in Eqs. (4.36) and (4.38), giving

$$\Delta\mathcal{S}_X{}^{(N)} = \Delta\mathcal{S}_X{}^{(1)} = 0, \tag{4.49}$$

$$\Delta\mathcal{S}_Q{}^{(N)} = \Delta\mathcal{S}_Q{}^{(1)} = 0. \tag{4.50}$$

While multiple levitons are not independent [in the sense of Eqs. (4.48)], they do represent minimal excitation states even in presence of a finite overlap between Lorentzian pulses. This is a remarkable property which seems to distinguish the Lorentzian drive from every other type of voltage bias.

Let us note that the robustness with respect to the overlap of Lorentzian pulses is an interesting result for the charge transport at fractional filling as well. Indeed $\overline{\langle J_C \rangle}$ and $\mathcal{S}_C$ do not show a trivial rescaling at $\nu \neq 1$. Nevertheless, we have checked that the excess charge noise $\Delta\mathcal{S}_C$ is insensitive to different overlap between levitons, as it vanishes when exactly one electron is transported under each pulse, i.e. when $q = N$. Note that a very similar behavior was described for the excess charge noise in Ref. [194], where multiple pulses were generated as a result of fractionalization due to inter-channel interactions in the integer QH regime at $\nu = 2$.

To provide a further proof for our results, we analyze a two-pulse configuration with an asymmetrical charge distribution, namely a case in which the first pulse carries $1/3$ of the total charge q while the second pulse takes care of the remainder. It is straightforward to verify that the phase $e^{-i\varphi(t)}$ associated with such a drive is represented by a Fourier series with coefficients

$$p_l^{(2)}(q) = \sum_{m=-\infty}^{+\infty} e^{i\pi\alpha m} p_{l-m}\left(\frac{q}{3}\right) p_m\left(\frac{2q}{3}\right), \tag{4.51}$$

where the asymmetry in the charge distribution is manifest, as opposed to the symmetric case in Eq. (4.47). In view of previous considerations, we expect this signal to be an optimal voltage drive when both pulses carry an integer amount of charge. This condition is obviously fulfilled when $q = 3$, so that the total charge can be divided into one and two electrons associated with the first and second pulse respectively. Figure 4.6 confirms our prediction, showing the first universal vanishing point shared by all three curves at $q = 3$ instead of $q = 2$.

In passing, it is worth remarking that the choice of multiple Lorentzian pulses with identical shape was only carried out for the sake of simplicity. A

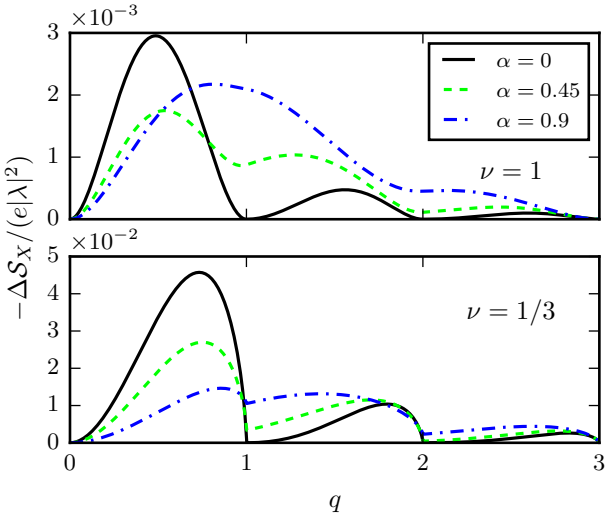

Figure 4.6: Excess mixed noise $-\Delta\mathcal{S}_X$ as a function of q for a cluster of two Lorentzian pulses. Here q is partitioned asymmetrically, with the two pulses carrying respectively $1/3$ and $2/3$ of the total charge per period. One should compare this figure with Figs. 4.4 and 4.5, where $-\Delta\mathcal{S}_X$ for identical pulses is plotted. The time delay between pulses is $\alpha T/2$, with different values of α according to the legend. The cutoff is set to $\omega_c = 10\,\omega$ and the temperature is $\theta = 0$.

generalization to more complicated clusters with different width η gives rise to a very similar qualitative behavior (not shown).

Chapter 5

Hong-Ou-Mandel interferometry

In this final Chapter we analyze collisions of multi-electronic excitations in a quantum Hall interferometer, in the spirit of the quantum-optical HOM experiment. We find that the Pauli dip, namely the suppression of shot noise in the output arms of the interferometer due to indistinguishability effects, occurs both for integer and fractional filling factors in the Laughlin sequence. However, additional sub-dips appear in the fractional quantum Hall regime, denoting the emergence of an unexpected substructure in the backscattered current. We also observe that minimal excitation states of integer and fractional quantum conductors, i.e. levitons, are clearly detectable through HOM spectroscopy. Results presented here are partly based on Refs. [24, 27].

5.1 Shot noise in a two-sources interferometer

In the celebrated HOM experiment (see Sec. 1.4.1), indistinguishable photons impinge on the opposite sides of a beam splitter and are detected at the output arms of an interferometer [53]. By looking at coincidence counts between detectors (or, alternatively, at fluctuations in the number of detected particles) it is possible to extract information about the statistical properties of the colliding particles (thanks to the so-called *photon bunching*) and the temporal extension of their wavefunction. A solid state counterpart of the HOM experiment has been realized in the context of EQO, using both driven quantum dots and voltage pulses as sources for indistinguishable electrons [10, 12]. In this case, the outcome of the experiment is heavily influenced by the Pauli exclusion principle, preventing two identical fermions to emerge on the same arm of the interferometer (this effect is known as *fermion anti-bunching*). Here we aim to extend HOM physics to the FQH regime, and present a theoretical

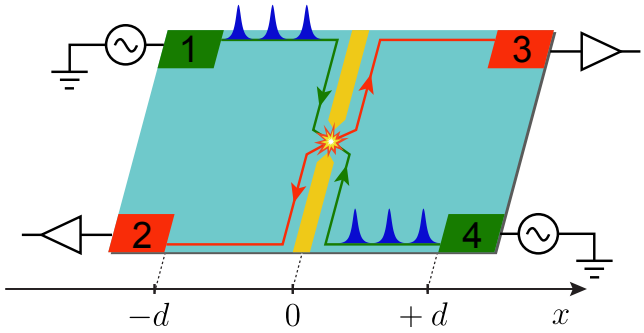

Figure 5.1: Four-terminal setup for HOM interferometry in the QH regime. Contact 1 and 4 are used as input terminals, while contact 2 and 3 are the output terminals where the current and the noise are measured.

analysis of current fluctuations in a QH interferometer at integer and fractional filling factor.

We basically rely on a modified version of the setup already considered in Chapters 3 and 4, shown in Fig. 5.1. In a 2DEG driven into the FQH regime, two oppositely propagating edge states are put in contact at the coordinate $x = 0$ thanks to a QPC, inducing tunneling of Laughlin quasiparticles between opposite edges. This is accounted for by the tunneling Hamiltonian (3.79). Differently from the previous Chapters, we now imagine that both incoming channels are subjected to periodic voltage pulses, as suggested by Fig. 5.1. This configuration will be denoted HOM setup.

Analytical results for HOM interferometry at fractional filling factor are readily obtained from previous work with few additional effort. The central quantity of interest is still the operator for the charge tunneling current, which is given by Eq. (3.83):

$$J_C = ie^* \sum_{\varepsilon=+,-} \varepsilon \left[\Lambda \Psi_R^{(\mathrm{qp})\dagger}(0)\Psi_L^{(\mathrm{qp})}(0)\right]^{\varepsilon}. \tag{5.1}$$

The main difference with respect to the previous Chapters is that time evolution of J_C is now governed by both voltage sources $V_R(t)$ and $V_L(t)$. In view of Eqs. (3.76) we have

$$J_C(t) = ie^* \sum_{\varepsilon=+,-} \varepsilon e^{i\varepsilon e^* \int_0^t \Delta V(t')dt'} \left[\Lambda \psi_R^\dagger(0,t)\psi_L(0,t)\right]^{\varepsilon}, \tag{5.2}$$

where the quantity $\Delta V(t) = V_R(t) - V_L(t)$ has been introduced. A comparison of the above result with Eq. (3.84) leads now to the following important conclusion: the model for the two-sources interferometer maps into a single-source HBT setup, where the voltage drive is applied on the upper-left contact and takes the form $V_R'(t) = \Delta V(t) = V_R(t) - V_L(t)$. Thus, current and noise in the HOM setup are given by the corresponding signals in the HBT configuration upon the substitution of $V(t)$ with $\Delta V(t)$. The desired result for

current-current fluctuations follows directly from Eq. (3.111): it's just a matter of finding the suitable photoassisted coefficient for the new voltage drive $\Delta V(t)$. It should be remarked that only voltage-pulse sources satisfy this property. When dealing with HOM experiments with a pair of mesoscopic capacitors [12], both sources must be treated independently and any mapping into a single-source setup is impossible.

Using $\Delta V(t)$ as the new effective voltage drive, the zero-frequency shot noise reads[1]

$$\mathcal{S}^{\mathrm{HOM}} = 2(e^*)^2|\lambda|^2 \sum_{l=-\infty}^{+\infty} |\tilde{p}_l(\alpha_R,\alpha_L)|^2 \left\{ \hat{P}_{2\nu}\left[(l+\Delta q)\omega\right] + \hat{P}_{2\nu}\left[-(l+\Delta q)\omega\right] \right\}, \tag{5.3}$$

with $\Delta q = q_R - q_L$ and $q_{R/L} = e^* V_{R/L,\mathrm{dc}}/\omega$. The new coefficients $|\tilde{p}_l(\alpha_R,\alpha_L)|^2$ are given by

$$\tilde{p}_l = \int_0^T \frac{dt}{T} e^{il\omega t} e^{-ie^* \int_0^t d\tau \Delta V_{\mathrm{ac}}(\tau)}, \tag{5.4}$$

with $\Delta V_{\mathrm{ac}}(t) = \Delta V(t) - (\omega/e^*)\Delta q$, and depend on the ac amplitudes α_L and α_L of both voltage sources. Let us notice that (5.3) is the auto-correlation spectrum of current fluctuations measured in terminal 2 (see Fig. 5.1). For charge conservation, this is identical to the cross-correlation spectrum between current fluctuations at outputs 2 and 3 with an opposite sign [32].

An interesting remark should be emphasized before getting into the details of the results. Despite an evident analogy, the substitution $V(t) \to \Delta V(t)$ *does not arise from a gauge transformation*. Indeed there is no gauge transformation that is able to map the equation of motion for the HOM configuration into an effective HBT setup with $V_R'(t) = \Delta V(t)$ and $V_L'(t) = 0$. However, the current operator in Eq. (5.2) looks like the effective HBT contribution due to the peculiarity of point-like tunneling. This is linked to the fact that, in the Landauer-Büttiker picture of quantum transport, the transmission function for point-like tunneling between opposite edge states is energy independent. Any similarity between the HOM setup and an effective HBT would vanish for more complicated tunneling geometries such as multiple QPC or extended contacts, where the transmission function acquires a dependence upon energy [29, 30, 195, 196].

5.1.1 Hong-Ou-Mandel ratio

Strictly speaking, a solid-state HOM geometry is reproduced when identical excitations collide at the QPC [10, 112]. Contacts 1 and 4 are thus driven with identical periodic voltage signals, the only difference being a tunable time delay t_D between them. However, we will consider a broader class of HOM collisions

[1] The label C identifying the charge shot noise is now unnecessary. From now on we will refer to charge fluctuations only, and mixed and heat signals won't be considered anymore.

where the left and right contact are driven with an identical shape in time but different amplitudes, namely

$$\begin{cases} V_R(t) = q_R V_1(t), \\ V_L(t) = q_L V_1(t + t_D). \end{cases} \tag{5.5}$$

Here, the signal $V_1(t)$ is normalized in such a way to carry exactly one electron per period. We also set $q_{R/L} = \alpha_{R/L}$ in order to have $V_{R/L}(t) \geq 0$ with no additional dc offset. Photoassisted coefficients $\tilde{p}_l$ are thus given by

$$\begin{aligned} \tilde{p}_l(q_R, q_L) &= \int_0^T \frac{dt}{T} e^{il\omega t} e^{-ie^* q_R \int_0^t d\tau V_1(\tau)} e^{ie^* q_L \int_0^t d\tau V_1(\tau + t_D)} = \\ &= \int_0^T \frac{dt}{T} e^{il\omega t} e^{-ie^* q_R \int_0^t d\tau V_1(\tau)} e^{ie^* q_L \int_0^{t+t_D} d\tau V_1(\tau)} e^{-ie^* q_L \int_0^{t_D} d\tau V_1(\tau)} = \\ &= e^{-ie^* q_L \int_0^{t_D} d\tau V_1(\tau)} \int_0^T \frac{dt}{T} e^{il\omega t} \sum_{m,n} p_m(q_R) e^{-im\omega t} p_n^*(q_L) e^{in\omega(t+t_D)} = \\ &= e^{-ie^* q_L \int_0^{t_D} d\tau V_1(\tau)} \sum_n p_{l+n}(q_R) p_n^*(q_L) e^{in\omega t_D}. \end{aligned} \tag{5.6}$$

Since Eq. (5.3) involves the squared modulus of $\tilde{p}_l$, we can safely neglect the constant phase factor in front of the sum in the above result. Equation (5.6) bears similarities with the photoassisted coefficients for clusters of multiple pulses, Eq. (4.47), discussed in the previous Chapter. Indeed, the effective drive $\Delta V(t) = V_R(t) - V_L(t)$ is nothing but a cluster of two pulses with opposite sign [hence the complex conjugation of the second coefficient $p_n^*(q_L)$].

When one of the input terminals is driven with a periodic signal $V_{R/L}(t)$ while the other one is grounded, we refer to HBT interferometry [11, 105, 106]. In this case, one of the two amplitudes is set to zero and one recovers the result

$$\mathcal{S}_{R/L}^{\mathrm{HBT}} = 2(e^*)^2 |\lambda|^2 \sum_{l=-\infty}^{+\infty} \left| p_l(q_{R/L}) \right|^2 \left\{ \hat{P}_{2\nu} \left[\left(q_{R/L} + l \right) \omega \right] + \hat{P}_{2\nu} \left[- \left(q_{R/L} + l \right) \omega \right] \right\}, \tag{5.7}$$

depending on which of the sources is switched on. The signal $\mathcal{S}_{R/L}^{\mathrm{HBT}}$ is manifestly independent on the delay t_D.

It is customary to normalize the HOM noise to the value expected for the random partitioning of a single source, namely the HBT signal [10, 12]. For this purpose we define the ratio

$$\mathcal{R}(t_D) = \frac{\mathcal{S}^{\mathrm{HOM}} - \mathcal{S}^{(0)}}{\mathcal{S}_R^{\mathrm{HBT}} + \mathcal{S}_L^{\mathrm{HBT}} - 2\mathcal{S}^{(0)}}. \tag{5.8}$$

Notice that we have subtracted the equilibrium noise $\mathcal{S}^{(0)} = 4(e^*)^2 |\lambda|^2 \hat{P}_{2\nu}(0)$ (obtained with $q_R = q_L = 0$) from both the numerator and the denominator in Eq. (5.8).

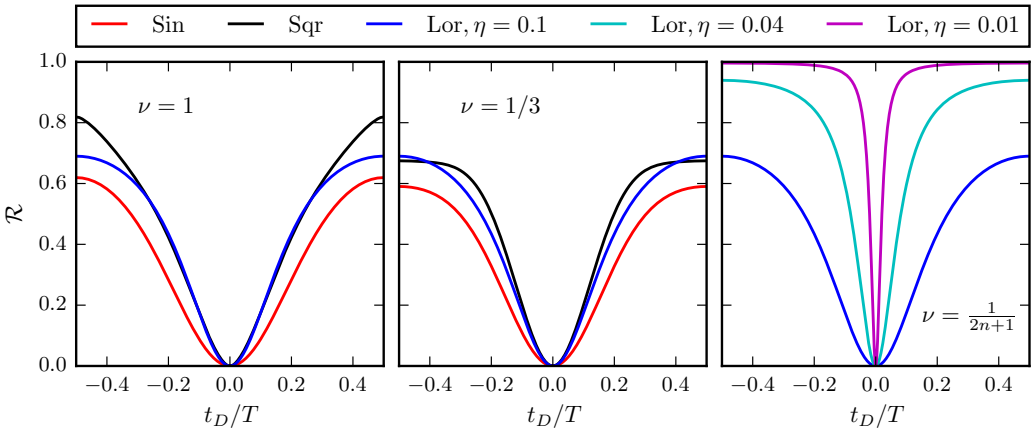

Figure 5.2: HOM ratio $\mathcal{R}$ for collisions of identical excitations as a function of the delay t_D. Sinusoidal, square and Lorentzian pulses with $q = 1$ are considered. The temperature is $\theta = 0.01\,\omega$.

5.2 Results

Let us begin the analysis of the HOM ratio from the simple case $q_R = q_L = 1$. We consider three different waveforms, namely the sinusoidal, square and Lorentzian signals given in Eqs. (3.133) of Chapter 3.

As can be seen from Fig. 5.2 (left panel), at $\nu = 1$ all three curves generate a vanishing HOM ratio at $t_D = 0$, i.e. when identical pulses collide simultaneously at the QPC. This is consistent with the anti-bunching effect expected for identical fermionic particles colliding at the QPC, which forces identical fermions to leave the interferometer on opposite output arms, thus causing a drop (the so-called Pauli dip) in the fluctuations [10, 12]. Such a suppression of current fluctuations has been confirmed in experiments conducted by D.C. Glattli's group in Saclay, both with Lorentzian and sinusoidal voltage pulses [10, 18].

Quite surprisingly, one still observes a complete dip in the ratio $\mathcal{R}$ at $\nu = 1/3$, despite the presence of anyonic quasiparticles in the system. This is shown in the middle panel of Fig. 5.2, where we have reported the ratio $\mathcal{R}$ for the very same signals as in the left panel. All three curves evidently lead to a complete suppression of the noise at $t_D = 0$.

Once again, we ascribe this particular behavior to the geometry of our interferometer, which consists of a single QPC connecting the upper and lower edge. Indeed, we have already shown that the HOM setup is equivalent, under these particular conditions, to a simpler single-source HBT configuration driven with the effective voltage $\Delta V(t) = V_R(t) - V_L(t)$. For a two-source interferometer with identical amplitudes one has $V_L(t) = V_R(t + t_D)$, which leads to the vanishing of ΔV at $t_D = 0$. An HOM with null delay is effectively equivalent to an unbiased setup, and thus fluctuations in the tunneling current get suppressed. From a more physical point of view, we argue that any effect

of the fractional statistics is invisible in this single-QPC geometry, since the point-like tunneling does not allow for closed-loop trajectories of one Laughlin quasiparticles around another.

A very remarkable feature emerges however from the comparison between the cases $\nu = 1$ and $\nu = 1/3$ in Fig. 5.2, namely that the Lorentzian signal appears to be *exactly the same*. This is indeed the case, as we show here below by calculating separately both the numerator and the denominator of Eq. (5.8) for quantized Lorentzian pulses with $q_R = q_L = 1$. To begin, let us define the useful function

$$s(x) = 2(e^*)^2|\lambda|^2 \left[\hat{P}_{2\nu}(x\omega) + \hat{P}_{2\nu}(-x\omega)\right]. \tag{5.9}$$

With this compact notation, the following simple expressions for $\mathcal{S}^{\mathrm{HOM}}$, $\mathcal{S}^{\mathrm{HBT}}_{R/L}$ and $\mathcal{S}^{(0)}$ are obtained at $q_R = q_L = 1$:

$$\mathcal{S}^{\mathrm{HOM}} = \sum_{l=-\infty}^{+\infty} |\tilde{p}_l|^2 s(l), \tag{5.10}$$

$$\mathcal{S}^{\mathrm{HBT}}_R = \mathcal{S}^{\mathrm{HBT}}_L = \sum_{l=-\infty}^{+\infty} |p_l|^2 s(l+1), \tag{5.11}$$

$$\mathcal{S}^{(0)} = s(0). \tag{5.12}$$

Photoassisted coefficients for the Lorentzian waveform at $q = 1$ are calculated analytically in Appendix A. Their square modulus reads

$$|p_l|^2 = \begin{cases} (1-e^{-4\pi\eta})^2 e^{-4\pi l\eta}, & l \geq 0, \\ e^{-4\pi\eta}, & l = -1, \\ 0, & l \leq -2, \end{cases} \tag{5.13}$$

for the case of a single voltage drive (HBT signal) and

$$|\tilde{p}_l|^2 = \begin{cases} 4e^{-4\pi|l|\eta} R(\eta,\zeta), & l \neq 0, \\ 1 + 4[1-\coth(2\pi\eta)]R(\eta,\zeta), & l = 0, \end{cases} \tag{5.14}$$

for the HOM configuration. Here we have introduced the dimensionless delay $\zeta = t_D/T$ and the function $R(\eta,\zeta)$ given by

$$R(\eta,\zeta) = \frac{\sinh^2(2\pi\eta)\sin^2(\pi\zeta)}{\sinh^2(2\pi\eta) + \sin^2(\pi\zeta)}. \tag{5.15}$$

Let us now evaluate the numerator and the denominator of $\mathcal{R}$ separately. The

former reads

$$\begin{aligned}\mathcal{S}^{\mathrm{HOM}} - \mathcal{S}^{(0)} &= \sum_{l=-\infty}^{+\infty} |\tilde{p}_l|^2 s(l) - s(0) = \\ &= 2\sum_{l=1}^{+\infty} |\tilde{p}_l|^2 s(l) + (|\tilde{p}_0|^2 - 1)s(0) = \\ &= 4R(\eta,\zeta)\left\{2\sum_{l=1}^{+\infty} e^{-4\pi l\eta} s(l) + [1-\coth(2\pi\eta)]s(0)\right\}, \end{aligned} \tag{5.16}$$

where we have used the fact that $s(x)$ is an even function of x and $|\tilde{p}_l|^2 = |\tilde{p}_{-l}|^2$ for the Lorentzian drive. Similarly, the denominator is given by

$$\begin{aligned}\mathcal{S}_R^{\mathrm{HBT}} + \mathcal{S}_L^{\mathrm{HBT}} - 2\mathcal{S}^{(0)} &= 2\sum_{l=-\infty}^{+\infty} |p_l|^2 s(l+1) - 2s(0) = \\ &= 2(1-e^{-4\pi\eta})^2 \sum_{l=0}^{+\infty} e^{-4\pi l\eta} s(l+1) + 2(e^{-4\pi\eta}-1)s(0) = \\ &= 4\sinh^2(2\pi\eta)\left\{2\sum_{l=1}^{+\infty} e^{-4\pi l\eta} s(l) + [1-\coth(2\pi\eta)]s(0)\right\}. \end{aligned} \tag{5.17}$$

To get the last equality we have used the identity

$$\sinh^2(x)\,[1-\coth(x)] = -\sinh(x)e^{-x} = \frac{1}{2}\left(e^{-2x}-1\right). \tag{5.18}$$

It is clear from Eqs. (5.16) and (5.17) that the sum involving the function $s(l)$ factorizes in the same way for the numerator and the denominator of $\mathcal{R}$. Remarkably, all the dependence on both the filling factor and the temperature is encoded in $s(l)$, and we thus obtain the following universal expression for the HOM ratio of leviton-leviton collisions:

$$\mathcal{R}(t_D) = \frac{\sin^2(\pi\zeta)}{\sinh^2(2\pi\eta) + \sin^2(\pi\zeta)}. \tag{5.19}$$

This striking factorization is intimately related to the particular values of the photoassisted coefficients in Eqs. (5.13) and (5.14), and holds only for the single-leviton excitation. In the right panel of Fig. 5.2 we show the behavior of the single-leviton HOM ratio (5.19) for different values of the dimensionless width η. The dip in the noise becomes more and more narrow as the pulses become sharper, allowing to extract the temporal extension of the levitonic wavepacket from a shot noise measurement.

The fact that the HOM ratio $\mathcal{R}$ does not depend on the temperature for leviton-leviton collisions has been confirmed experimentally by the Saclay

group in a Fermi liquid system [18]. We here predict that the same behavior should be observed in any FQH state of the Laughlin sequence, as both the temperature and the filling factor factorize away in Eq. (5.19). We believe that such a remarkable behavior is linked to the fact that the Lorentzian pulse with $q = 1$ generates a minimal excitation state in the conductor.

5.2.1 Multiple leviton collisions

We now extend the analysis to generic values of the amplitude $q = q_R = q_L$. The interest is two-fold. On one side, it's natural to ask whether the Levitov quantization condition for minimal noise [Eq. (2.23), which requires integer values of the dc amplitude q] has any effect on the HOM ratio, and what happens to $\mathcal{R}$ if one works instead with non-integer pulses. On the other hand, interesting collisions of minimal multi-electron packets can be investigated by setting $q = 2, 3, 4 \ldots$. From now on we focus only on Lorentzian voltage pulses.

We first look at the HOM ratio $\mathcal{R}(t_D)$ in the case of integer filling factor ($\nu = 1$) and identical drives ($q_R = q_L = q$). Here exact results based on the scattering matrix formalism are available in the literature, both on the theoretical and the experimental side [10, 18, 112]. The behavior of $\mathcal{R}(t_D)$ in the integer regime is reported in panels a and b of Fig. 5.3. As discussed previously, the noise is totally suppressed when colliding packets arrive simultaneously at the QPC ($t_D = 0$) due to the anti-bunching effect. We point out that a complete suppression of the noise is observed also for non integer values of q, i.e. when colliding packets are formed by several particle-hole pairs instead of a single electron-like excitation: the HOM ratio at $\nu = 1$ always consists of a single, smooth dip for any value of q. We also note that brighter regions in Fig. 5.3a occur more or less in correspondence of integer values of q, but the qualitative behavior of $\mathcal{R}(t_D)$ as a function of the time delay (a single, well-defined dip for $t_D = 0$) is almost unaffected by variations of q.

Things look quite differently in the fractional regime, where new features linked to the strongly-correlated FQH phase come into play. In Fig. 5.3c we report the behavior of the HOM ratio for filling factor $\nu = 1/3$. One still observes a completely destructive interference between the two signals at $t_D = 0$ for any value of q (as demonstrated by the total central dip), despite the presence of anyonic quasiparticles in the system. This shows that electron-electron interactions in single-edge-mode Laughlin states do not induce decoherence effects, in contrast with the role played by interactions in the $\nu = 2$ integer quantum Hall effect, where two co-propagating edge states exist [197, 198]. At the same time, we note that the simple structure consisting of one single dip at $t_D = 0$ is replaced by a much richer phenomenology that distinguish between the non-interacting and the strongly correlated phase. Indeed Fig. 5.3c evidently shows the existence of sub-dips for values $q > 1$, whose spacing is more or less of the order of the width η. This is even more evident in Fig. 5.3d, where we have isolated the behavior of $\mathcal{R}(t_D)$ at fixed integer values of

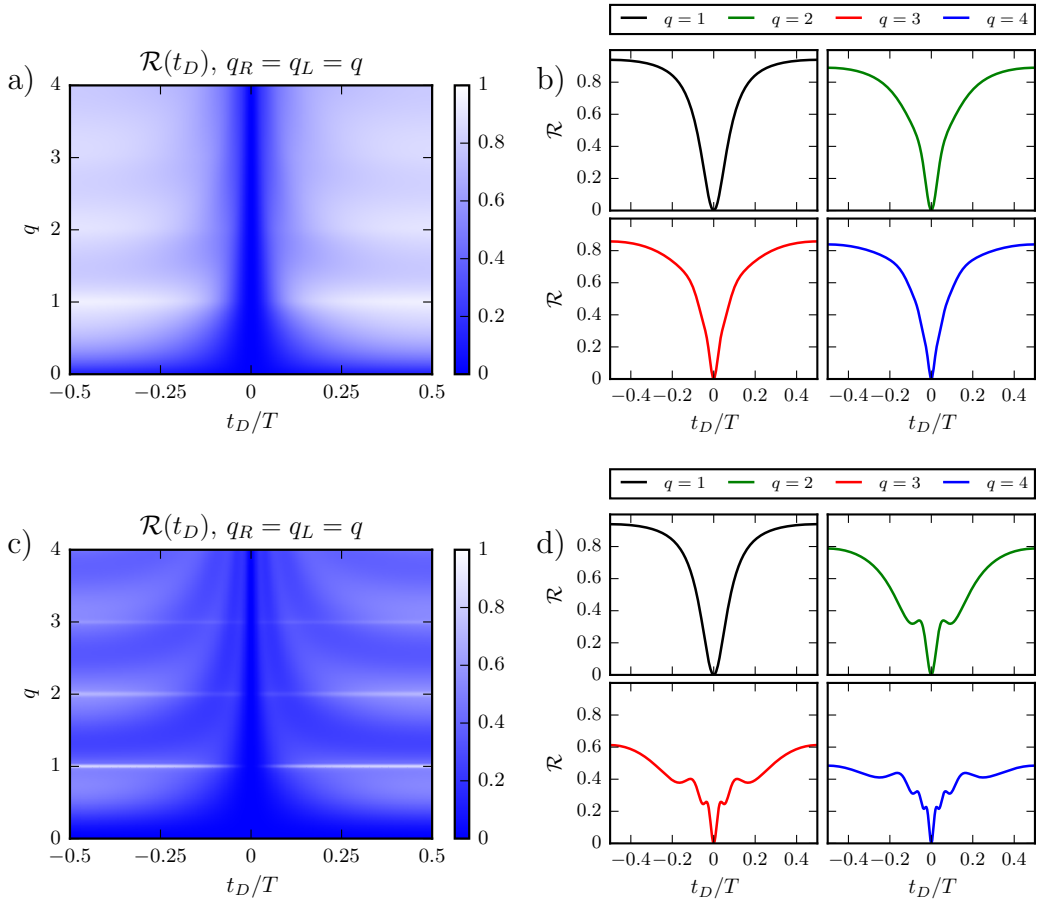

Figure 5.3: HOM ratio $\mathcal{R}$ for collisions of identical excitations as a function of the delay t_D and the amplitude q. Top panels (a and b) refer to the case of integer filling factor, while bottom panels (c and d) correspond to fractional filling $\nu = 1/3$. Curves in b and d are extracted respectively from a and c at $q = 1, 2, 3, 4$. The temperature is $\theta = 0.01\,\omega$ and the dimensionless width of the pulses is $\eta = 0.04$.

q. Here, one clearly notes the presence of oscillations in the current-current correlators for $q > 1$, with $2q-2$ new dips aside of the principal one at $t_D = 0$. Such an unexpected behavior suggests that the backscattered packet splits into several sub-peaks when one works with more than one electron at a time. It's interesting to notice that the spacing between maxima/minima of $\mathcal{R}(t_D)$ tends to widen while approaching the ends of the period.

These features unambiguously identify the effects of the strongly correlated FQH phase on leviton excitations, in striking contrast with the uncorrelated Fermi liquid phase. A similar pattern was predicted in Ref. [198] and experimentally observed in Ref. [16], where the internal peak/valley structure is generated by a fractionalization effect in a $\nu = 2$ QH interferometer. Here we argue that the new side dips must be related to the existence of an unexpected composite structure in the multi-leviton state at fractional filling factors, as no fractionalization occurs in our single-edge-mode setup. It is revealed by the appearance of local maxima and minima in the current-current correlators.

It is worth noting that the same behavior of the ratio can be observed for all filling factors in the Laughlin sequence. Indeed, as we have already discussed in Sec. 3.6, the function $s(x)$ defined in Eq. (5.9) is extremely peaked around $x = 0$ in the fractional regime, with a maximum more and more pronounced as the temperature is lowered. Then, a very efficient approximation for the noise is obtained by retaining only the leading contribution in the infinite sum, namely the one involving $s(0)$. We get

$$\mathcal{S}^{\mathrm{HOM}} \approx |\tilde{p}_0|^2 s(0), \tag{5.20}$$

$$\mathcal{S}_R^{\mathrm{HBT}} = \mathcal{S}_L^{\mathrm{HBT}} \approx |p_{-q}|^2 s(0), \tag{5.21}$$

$$\mathcal{S}^{(0)} = s(0). \tag{5.22}$$

This only makes sense, of course, for integer values of q. Under this approximation, the HOM ratio becomes

$$\mathcal{R}(t_D) = \frac{1}{2}\frac{1-|\tilde{p}_0|^2}{1-|p_{-q}|^2}. \tag{5.23}$$

Equation (5.23) is manifestly independent on the filling factor since $s(0)$ factorizes out, as for the case of HOM collisions of single-leviton excitations. However, while the universal expression (5.19) is obtained exactly by summing up all terms of the infinite series, here we have obtained the universal formula (5.23) only at sufficiently low temperature ($\theta/\omega \ll 1$), where one single term gives a dominant contribution over all the others. The interesting fact is that this is indeed the typical regime where EQO experiments are performed, with $\theta/\omega \approx 0.1$ [10, 15, 18].

Finally, the uniqueness of integer Lorentzian pulses is even more evident in the fractional regime when looking at the behavior for long delays between colliding packets (i.e. $t_D/T \approx \pm 0.5$). We observe that generic values of q lead to a rather low HOM noise compared with the HBT contribution, which means

that excitations consisting of several particle-hole pairs are colliding at the beam splitter. However, integer Lorentzian pulses generate bright horizontal lines in Fig. 5.3c, meaning that the HOM ratio approaches unity. We find that this is another striking signature of minimal excitation states in the FQH regime [24, 25].

5.2.2 Asymmetric collisions

We now examine what happens when wavepackets carrying different charges are injected in terminals 1 and 4 and sent to the collider. For simplicity we inject integer Lorentzian pulses with $q_R = 1$ (i.e. levitons) on the upper right-moving edge, while the opposite contact is driven with a generic Lorentzian drive with tunable amplitude q_L and delay t_D. Starting from the $\nu = 1$ case, we observe that the total suppression of HOM noise is achieved only for $q_L = q_R = 1$, as expected. Different values of q_L generate a partial dip in the noise, as one can infer by looking at Fig. 5.4a. For instance, by fixing the value of q_L we obtain the four curves shown in Fig. 5.4b, which clearly demonstrate that the anti-bunching effect is not perfect when different excitations are sent to the QPC.

When looking at the same situation in the FQH regime, we expect to find some signature of the composite structure observed for symmetric collisions. This is indeed the case for Figs. 5.4c and 5.4d, where multiple sub-dips appear in the HOM ratio $\mathcal{R}$. They are extremely well visible in the case of integer q_L, while they are almost totally washed out when considering non-integer pulses. This suggest that an integer Lorentzian drive, which generates clean states in the conductor, is the best possible candidate to observe the breaking up of multi-electronic packets. However, from the phenomenology reported in Figs. 5.3c and 5.3d we expect to see an increasing number of sub-dips for higher values of q_L [roughly, we expect N minima with $N = \mathrm{int}(q_L)$]. Conversely, Figs. 5.4c and 5.4d only show two sub-dips even for $q_L = 3$. This may suggest that a much thinner probe is required to resolve exactly each peak and valley of the composite structure (ideally, a delta-like function instead of the $q_R = 1$ Lorentzian). It's easy to check that the HOM ratio for the case of asymmetric collisions is described by a generalized version of the approximation Eq. (5.23), given by

$$\mathcal{R}(t_D) = \frac{1 - |\tilde{p}_{-q_R+q_L}(q_R, q_L)|^2}{2 - |p_{-q_R}(q_R)|^2 - |p_{-q_L}(q_L)|^2}. \tag{5.24}$$

This is valid in the low temperature limit for integer values of q_R and q_L. Curves in Fig. 5.4d describe thus a universal behavior in the filling factor ν (provided that $\nu \neq 1$).

Once again, the robustness of integer Lorentzian pulses is glaring, even from a merely visual point of view (see the horizontal sharp lines in Fig. 5.4c).

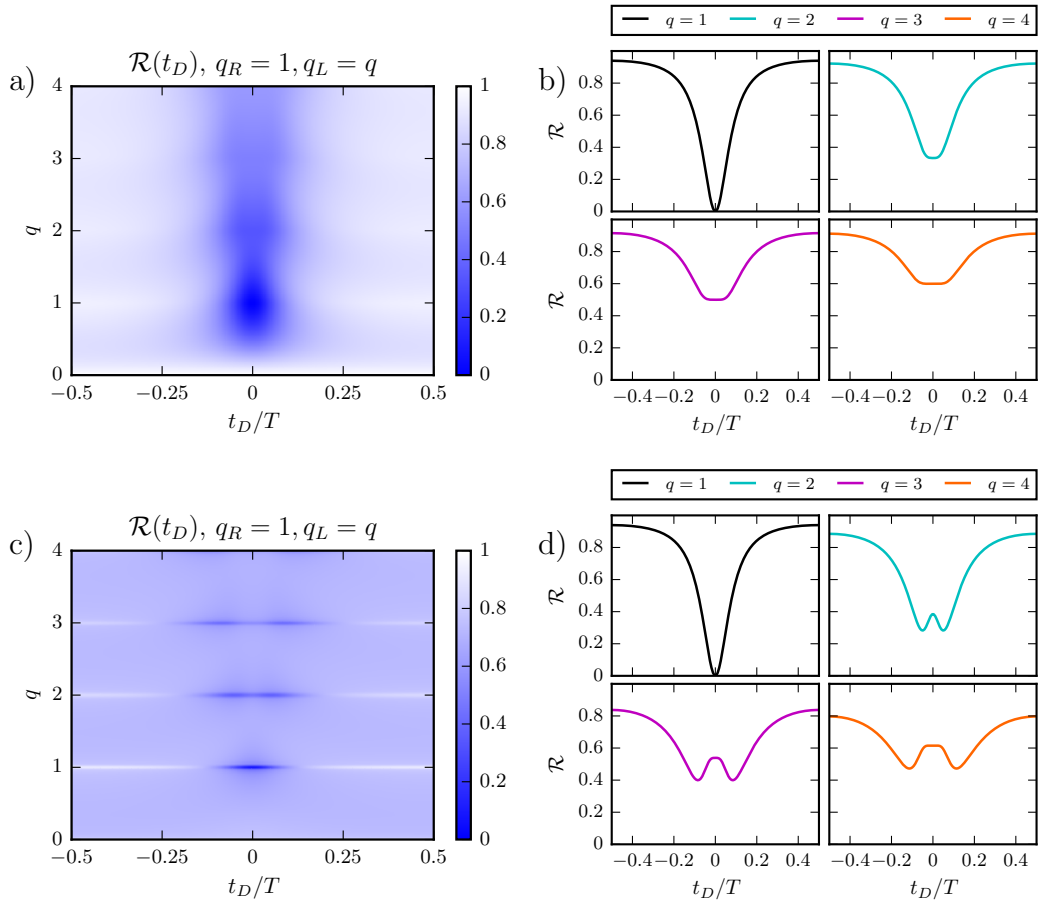

Figure 5.4: Collisions of single-electron ($q_R = 1$) and generic ($q_L = q$) pulses as a function of the delay t_D and the charge q injected in the left-moving edge. Top panels (a and b) refer to the case of integer filling factor, while bottom panels (c and d) correspond to fractional filling $\nu = 1/3$. Curves in b and d are extracted respectively from a and c at $q = 1, 2, 3, 4$. The temperature is $\theta = 0.01\,\omega$ and the dimensionless width of the pulses is $\eta = 0.04$.

Conclusions and perspectives

In this thesis we have tackled the problem of EQO in the Laughlin FQH regime. A thorough analysis of the physics of levitons (and, more in general, of photoassisted transport due to an arbitrary periodic voltage drive) at fractional filling factor has been presented.

We have theoretically studied a class of quantum-optical experiment belonging to the following protocol, which closely resembles actual experimental setups in the field of EQO. First of all, periodic trains of electronic excitations are generated in the QH liquid by means of periodic voltage pulses. Incoming beams then travel along the QH edge states and are partitioned off a QPC, which serves as an effective beam splitter in the context of EQO. This is modeled through tunneling of fractional Laughlin quasiparticles between opposite edge states occurring at the QPC. Both charge and heat are backscattered as a result of reflection at the QPC, and can be theoretically evaluated in the appropriate output contact. To this end, we have adopted a chiral Luttinger liquid model, which is the most suitable tool to inspect the strongly correlated FQH state generated by electron-electron interactions. Most importantly, charge-charge, heat-heat and mixed charge-heat correlations bring information about the original excitations generated through voltage pulses. They bear signatures similar to Poissonian dc transport when conditions for minimal excitation states are satisfied.

When only a single source is operating we refer to HBT interferometry, in full analogy with the optical HBT experiment. Conversely, two active sources allow for the study of HOM interferometry, where identical excitations collide on opposite sides of the beam splitter. The considered setup is shown in panel a) of Fig. C.1, which is a final summary of the main results of this thesis. The latter are collected here below, in the same order as they appear in the text:

- ✓ Despite strong electron-electron correlations, minimal excitation states do emerge in Laughlin FQH states in response to properly shaped pulses. These occur when applying a periodic Lorentzian drive with quantized flux, and can be detected as they produce Poissonian noise at the out-

put of a HBT setup in the weak backscattering regime. Although FQH quasiparticles carry a fractional charge, the charge of these noiseless excitations generated through Lorentzian voltage pulses corresponds to an integer number of electrons, and no signature emerges when the area underneath each pulse matches a fractional value of the electron charge. This shows that levitons, the time-resolved minimal excitation states of a Fermi sea, are stable against electron-electron interaction in the Laughlin FQH regime and emerge also on top of a strongly correlated ground state [**Chapter 3**].

✓ Independently of the waveform of the voltage drive, the photoassisted expression for the noise can be approximated in a remarkably simple way, due to the typical non-linear behavior of Green's functions at fractional filling factor. This allows for a full spectroscopy of the photoassisted probabilities by varying both the dc and the ac amplitudes of the voltage pulses. Such a spectroscopic technique is within reach of current experimental technologies [**Chapter 3**].

✓ Mixed and heat noises measured in one of the output arms of an HBT interferometer all reach their minimal value (set by the respective Poissonian dc relations) only when levitons impinge on the beam splitter. These results extend the notion of leviton as a minimal excitation state in quantum conductors to the heat transport domain. This is valid both in the integer QH effect and in the Laughlin fractional regime, despite the exotic physics due to the presence of fractionally charged quasiparticles induced by strong electron-electron interactions [**Chapter 4**].

✓ Superpositions of multiple levitons demonstrate their robustness with respect to arbitrary overlap. This happens regardless of the nonlinear dependence on the voltage bias typical of heat-transport-related quantities, and despite the characteristic nonlinear power laws of the chiral Luttinger liquid theory. Such properties designate levitons as universal minimal excitation states for mesoscopic quantum transport of both charge and heat [**Chapter 4**].

✓ Despite the presence of anyonic quasiparticles, synchronized HOM collisions in a QH system always generate a complete Pauli dip in the noise, both at integer and fractional filling. However, the scenario for fractional filling factor is enriched by the presence of several sub-dips in the HOM ratio, which reveal an unexpected composite structure of the reflected packet [**Chapter 5**].

Possible extensions of this work could address more involved interferometry of minimal excitations as well as their generalization to non-Abelian states. On one side, it would be extremely interesting to investigate whether related setups can serve as optimal sources for fractionally charged single-anyons. In

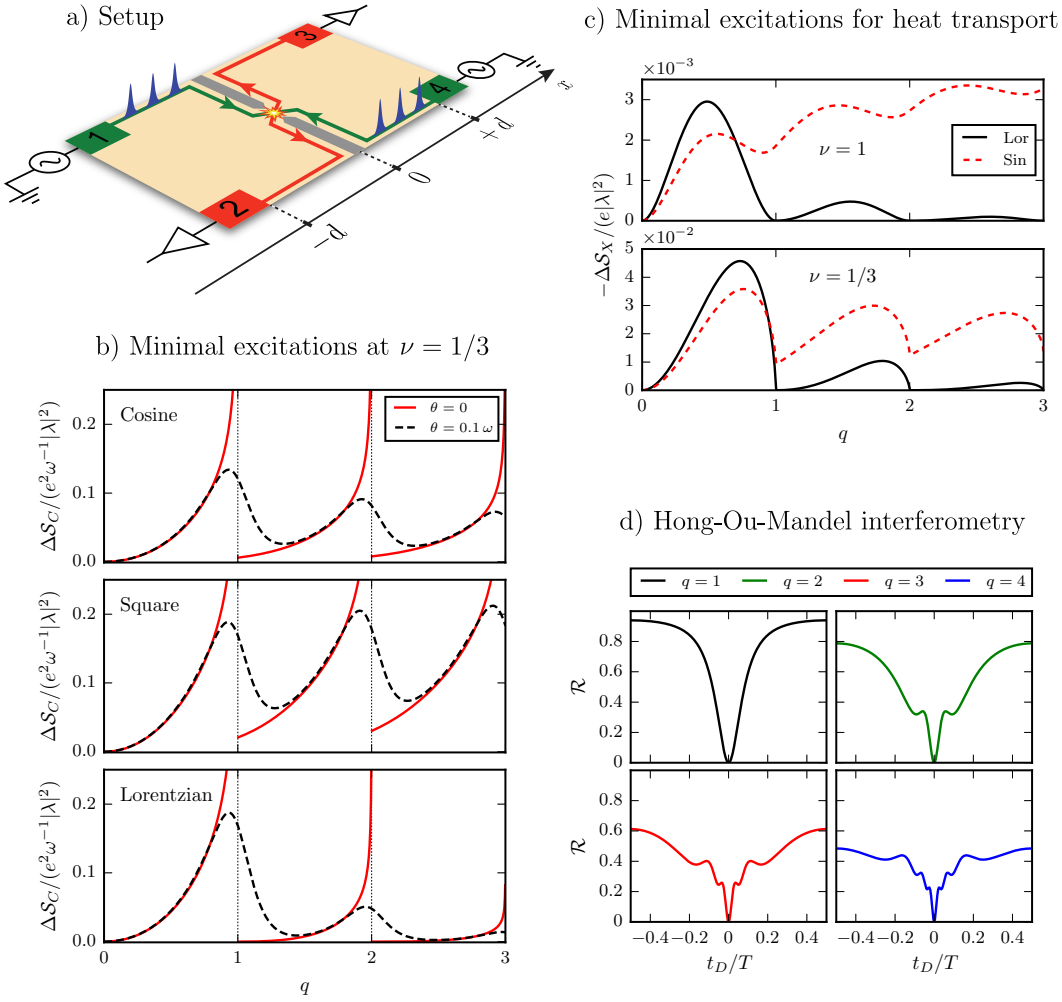

Figure C.1: Recap of the main results obtained in this thesis investigating the setup shown in a). b) Minimal excitations in the FQH regime arise in response to quantized Lorentzian voltage pulses with dc amplitude $q = e^*V_{\rm dc}/\omega = 1, 2, 3\ldots$, as demonstrated by the vanishing of the excess noise $\Delta\mathcal{S}_C$ [Fig. 3.7]. c) Similarly, quantized Lorentzian pulses give rise to minimal excitations for heat transport (here the mixed charge-heat excess noise $\Delta\mathcal{S}_X$ is zero) [Fig. 4.1]. d) HOM interferometry in the FQH regime reveals an intriguing oscillatory pattern in current-current fluctuations [Fig. 5.3].

this sense, it has been proposed that the QPC may be used to break the leviton into a coherent quasiparticle reflected off the barrier and a pair of Laughlin quasiparticles transmitted. The outcome of such a setup should then be used as the input of a HBT interferometer, in order to investigate the cleanliness of such a state [151]. On the other hand, multiple-QPC setups such as Fabry-Pérot interferometers could be investigated in an attempt to reveal signatures of the fractional statistics through HOM interferometry.

Moreover, the exotic physics of the quantum Hall effect allows for the existence of peculiar neutral edge modes for some values of the filling factor. While they can't contribute to charge transport, they do carry a finite amount of energy, which often flows in opposite direction with respect to the charged modes. Thermal currents along neutral edge modes were indeed spotted in Refs. [128, 129] using quantum dots as local thermometers. A finite heat current was measured upstream with respect to the "heater" point, a fact that can only be explained in presence of counter-propagating neutral modes. An application of EQO paradigms to FQH states supporting neutral modes let us envisage an exciting setup were single-particle charge and energy are separated on-demand into different output terminals, exploiting the composite edge structure of two-dimensional systems in the QH regime.

Very preliminary experimental results about PASN in the FQH regime are starting to be available [199]. This is of particular importance in a field like mesoscopic physics, where theory and experiments have always fed each other on the pursuit of new exciting discoveries. We believe that this is only the first step towards a full experimental EQO at fractional filling factor.

Appendices

Appendix A

Photoassisted coefficients

A.1 Single source

When subjected to a spatially homogeneous time-dependent voltage pulse $V(t)$, a particle with charge e^* acquires the phase factor[1]

$$\exp\left[-ie^*\int_0^t dt'\,V(t')\right]. \tag{A.1}$$

This happens for electrons in metals, for which we simply set $e^* = e$ in the above equation, and for Laughlin quasiparticles in FQH edge states, where we write $e^* = \nu e$ with ν the filling factor. A particularly interesting case in the one of periodic signals, where the phase factor can be written as a Fourier series. However, one should note that the integral of a periodic quantity is not, in principle, a periodic signal as well, since

$$\int_0^{t+T} dt'\,V(t') = \int_0^t dt'\,V(t') + \int_t^{t+T} dt'\,V(t') = \int_0^t dt'\,V(t') + TV_{\mathrm{dc}}. \tag{A.2}$$

To get a periodic integral, one has to subtract the dc amplitude V_{dc} of the periodic voltage. It is thus convenient to separate the dc and ac amplitude of the signal, $V(t) = V_{\mathrm{dc}} + V_{\mathrm{ac}}(t)$. When considering a QH system with conductance $G = \nu e^2/h$, the former is linked to the charge carried by each single pulse (in units of e):

$$q = \frac{1}{e}\int_0^T dt\,GV(t) = \frac{e^*}{\omega}V_{\mathrm{dc}}. \tag{A.3}$$

[1] Here we set $\hbar = 1$.

The phase factor in Eq. (A.1) becomes

$$\exp\left[-ie^*\int_0^t dt'\,V(t')\right] = e^{-iq\omega t}e^{-i\varphi(t)}, \tag{A.4}$$

with $\varphi(t) = e^*\int_0^t dt' V_{\rm ac}(t')$. The second phase factor in the right-hand side of Eq. (A.4) can now be expressed as a Fourier series:

$$e^{-i\varphi(t)} = \sum_{l=-\infty}^{+\infty} p_l e^{-il\omega t}. \tag{A.5}$$

As discussed in Section 1.7, the coefficients p_l are linked to the probability amplitude for photon absorption from the ac field ($l > 0$) or emission ($l < 0$). They are given by

$$p_l = \int_{-\frac{T}{2}}^{+\frac{T}{2}} \frac{dt}{T} e^{il\omega t}e^{-i\varphi(t)}. \tag{A.6}$$

A.1.1 Cosine wave

For a sinusoidal drive of the form $V_{\rm sin}(t) = V_{\rm dc} - V_{\rm ac}\cos(\omega t)$ one has

$$\begin{aligned} p_l &= \int_{-\frac{T}{2}}^{+\frac{T}{2}} \frac{dt}{T} e^{il\omega t}e^{ie^*V_{\rm ac}\int_0^t dt'\cos(\omega t')} = \int_{-\frac{T}{2}}^{+\frac{T}{2}} \frac{dt}{T} e^{il\omega t}e^{i\alpha\sin(\omega t)} = \\ &= \frac{1}{2\pi}\int_{-\pi}^{+\pi} d\tau\,\{\cos[\alpha\sin(\tau) + l\tau] + i\sin[\alpha\sin(\tau) + l\tau]\} = \\ &= \frac{1}{\pi}\int_0^{\pi} d\tau\cos[\alpha\sin(\tau) + l\tau] = J_{-l}(\alpha), \end{aligned} \tag{A.7}$$

where in the last step we recognized an integral representation of the Bessel function of the first kind [80]. Note that we have introduced the dimensionless ac amplitude $\alpha = e^*V_{\rm ac}/\omega$. Probabilities $P_l = |p_l|^2$ to emit or absorb a photon from the external electromagnetic field are symmetric with respect to the inversion $l \to -l$. This is linked to the fact that $V(t)$ has a symmetric variation around its dc value.

A.1.2 Square wave

We consider a square wave made of a periodic signal oscillating between $+V_{\rm ac}$ and $-V_{\rm ac}$ plus an additional dc contribution. It reads

$$V_{\rm sqr}(t) = V_{\rm dc} + V_{\rm ac}\left[2\sum_{k=-\infty}^{+\infty}\Theta(t - kT)\,\Theta\left(\frac{T}{2} - t + kT\right) - 1\right]. \tag{A.8}$$

Using the dimensionless parameter $\alpha = e^* V_{\rm ac}/\omega$, the photoassisted coefficients read

$$\begin{aligned} p_l &= \int_{-\frac{T}{2}}^{+\frac{T}{2}} \frac{dt}{T} e^{il\omega t} e^{-i\alpha\omega|t|} = \int_{-\frac{T}{2}}^{0} \frac{dt}{T} e^{i(l+\alpha)\omega t} + \int_{0}^{\frac{T}{2}} \frac{dt}{T} e^{i(l-\alpha)\omega t} = \\ &= \frac{1}{2\pi i}\left[\frac{1-e^{-i\pi(l+\alpha)}}{l+\alpha} + \frac{e^{i\pi(l-\alpha)}-1}{l-\alpha}\right] = \\ &= \frac{i}{\pi}\frac{\alpha}{l^2-\alpha^2}\left[1-(-1)^l e^{-i\pi\alpha}\right]. \end{aligned} \tag{A.9}$$

The probability to absorb or emit l photon is thus

$$P_l = |p_l|^2 = \left(\frac{\alpha}{l+\alpha}\frac{\sin\left[\frac{\pi}{2}(l-\alpha)\right]}{\frac{\pi}{2}(l-\alpha)}\right)^2. \tag{A.10}$$

For integer values of α we get $P_l = \frac{4}{\pi^2}\frac{\alpha^2}{(l^2-\alpha^2)^2}$ when $l-\alpha$ is odd, $P_l = 0$ when $l-\alpha$ is even and $P_l = \frac{1}{4}$ for $\alpha = l$, as in Ref. [112]. Since $V_{\rm sqr}(t)$ is symmetric with respect to its dc value, we have again $P_l = P_{-l}$.

A.1.3 Lorentzian wave

The function

$$V_{\rm Lor}(t) = V_{\rm dc} + V_{\rm ac}\left[\frac{1}{\pi}\sum_{k=-\infty}^{+\infty}\frac{\eta}{\eta^2+(t/T-k)^2} - 1\right] \tag{A.11}$$

describes a periodic train of Lorentzian pulses with period $T = 2\pi/\omega$ with the addition of a constant dc signal $V_{\rm dc}$. Note that we have isolated a pure ac contribution in the square brackets. Indeed, integrating the latter over one period we get

$$\int_0^T \frac{dt}{T}\left[\frac{1}{\pi}\sum_{k=-\infty}^{+\infty}\frac{\eta}{\eta^2+(t/T-k)^2} - 1\right] = \frac{1}{\pi}\int_{-\infty}^{+\infty} d\tau \frac{1}{1+\tau^2} - 1 = 0. \tag{A.12}$$

The parameter η is the ratio between the half width at half maximum of a single Lorentzian pulse and T. To evaluate the coefficients p_l, we first rewrite $\varphi(t) = e^* \int_0^t dt' V_{\rm ac}(t')$ as follows

$$\begin{aligned} \varphi(t) &= e^* V_{\rm ac}\int_0^t dt'\left[\frac{1}{\pi}\sum_{k=-\infty}^{+\infty}\frac{\eta}{\eta^2+(t/T-k)^2} - 1\right] = \\ &= 2\alpha\sum_{k=-\infty}^{+\infty}\int_{-k/\eta}^{+t/(\eta T)-k/\eta} d\tau\frac{1}{1+\tau^2} - \alpha\omega t = \\ &= 2\alpha\sum_{k=-\infty}^{+\infty}\left[\arctan\left(\frac{t}{\eta T}-k\frac{1}{\eta}\right) - \arctan\left(-k\frac{1}{\eta}\right)\right] - \alpha\omega t. \end{aligned} \tag{A.13}$$

The second term in the square brackets sum up to zero and the remaining term can be rearranged as

$$\begin{aligned}\varphi(t)+\alpha\omega t &= 2\alpha\sum_{k=-\infty}^{+\infty}\arctan\left(\frac{t}{\eta T}-k\frac{1}{\eta}\right)= \\ &= i\alpha\sum_{k=-\infty}^{+\infty}\ln\left(\frac{i+\frac{t}{\eta T}-k\frac{1}{\eta}}{i-\frac{t}{\eta T}+k\frac{1}{\eta}}\right)= \\ &= i\alpha\left[\sum_{k=-\infty}^{+\infty}\ln(k-i\eta-u)-\sum_{k=-\infty}^{\infty}\ln(k-i\eta+u)\right]= \\ &= i\alpha\ln\left[\frac{\sin(i\pi\eta+\pi u)}{\sin(i\pi\eta-\pi u)}\right], \end{aligned} \tag{A.14}$$

where we have used the dimensionless time $u = t/T$ and the useful identities [80, 200, 201]

$$\arctan(z) = \frac{i}{2}\ln\left(\frac{i+z}{i-z}\right), \tag{A.15}$$

$$\sum_{k=-\infty}^{+\infty}\ln(k+\gamma) = \ln[\sin(\pi\gamma)] + \sum_{k=-\infty}^{+\infty}\ln(k+1/2). \tag{A.16}$$

Now the coefficients p_l can be recast as a complex integral with the substitution $z = e^{i\omega u}$, namely

$$\begin{aligned} p_l &= \int_{-\frac{T}{2}}^{+\frac{T}{2}}\frac{1}{T}e^{il\omega t}e^{-i\varphi(t)}= \\ &= \int_{-\frac{T}{2}}^{+\frac{T}{2}}\frac{1}{T}e^{i(l+\alpha)\omega t}\left[\frac{\sin(i\pi\eta+\pi u)}{\sin(i\pi\eta-\pi u)}\right]^{\alpha}= \\ &= \frac{1}{2\pi i}\oint_{|z|=1}\frac{dz}{z}z^{l+\alpha}\left(\frac{1-\gamma z}{z-\gamma}\right)^{\alpha}, \end{aligned} \tag{A.17}$$

with $\gamma = e^{-2\pi\eta}$. Note that l is always an integer number, while α can assume in general non integer values. Since $|z| = 1$ and $\gamma < 1$, we can make use of the generalized binomial series

$$\begin{aligned}(1-\xi)^{\beta} &= 1-\beta\xi+\cdots+(-1)^n\frac{\beta(\beta-1)\cdots(\beta-n+1)}{n!}\xi^n+\cdots= \\ &= \sum_{n=0}^{+\infty}(-1)^n\frac{\Gamma(\beta+1)}{\Gamma(\beta-n+1)}\frac{\xi^n}{n!}, \end{aligned} \tag{A.18}$$

that is convergent in the disc $|\xi| < 1$ [110]. Expanding both the numerator and the denominator in Eq. (A.17) we obtain

$$p_l = \frac{1}{2\pi i}\oint_{|z|=1}dz\sum_{n,m=0}^{+\infty}(-1)^{n+m}\frac{\Gamma(1+\alpha)}{\Gamma(1-n+\alpha)}\frac{\Gamma(1-\alpha)}{\Gamma(1-m-\alpha)}\frac{z^{l+n-m-1}\gamma^{n+m}}{n!m!}. \tag{A.19}$$

We now extend one of the two sums to include negative values of the integer m, using the fact that $\Gamma(m+1) = m!$ for $m \geq 0$ and $1/\Gamma(m+1) = 0$ for $m \leq -1$ [80]:

$$p_l = \frac{1}{2\pi i} \oint_{|z|=1} dz \sum_{n=0}^{+\infty} \sum_{m=-\infty}^{+\infty} (-1)^{n+m} \frac{\Gamma(1+\alpha)}{\Gamma(1-n+\alpha)} \frac{\Gamma(1-\alpha)}{\Gamma(1-m-\alpha)} \frac{z^{l+n-m-1}\gamma^{n+m}}{n!\Gamma(m+1)}. \tag{A.20}$$

Cauchy's theorem tells us that the only non-vanishing contribution to this integral comes from $l+n-m=0$, so we are left with

$$\begin{aligned} p_l &= \sum_{n=0}^{+\infty} \sum_{m=-\infty}^{+\infty} \delta_{m,l+n} (-1)^{n+m} \frac{\Gamma(1+\alpha)\Gamma(1-\alpha)}{\Gamma(1-n+\alpha)\Gamma(1-m-\alpha)} \frac{\gamma^{n+m}}{n!\Gamma(m+1)} = \\ &= \sum_{n=0}^{+\infty} (-1)^l \frac{\Gamma(1+\alpha)\Gamma(1-\alpha)}{\Gamma(1-n+\alpha)\Gamma(1-n-l-\alpha)} \frac{\gamma^{2n+l}}{n!\Gamma(n+l+1)} = \\ &= \sum_{n=0}^{+\infty} (-1)^l \frac{\Gamma(1+\alpha)\Gamma(1-\alpha)}{\Gamma(l+n+\alpha)\Gamma(1-n-l-\alpha)} \frac{\Gamma(l+n+\alpha)}{\Gamma(1-n+\alpha)} \frac{\gamma^{2n+l}}{n!\Gamma(n+l+1)}. \end{aligned} \tag{A.21}$$

Exploiting the property $\Gamma(\xi)\Gamma(1-\xi) = \pi/\sin(\pi\xi)$ valid for $\xi \neq 0, \pm 1, \ldots$ [80] we have

$$\frac{\Gamma(1+\alpha)\Gamma(1-\alpha)}{\Gamma(l+n+\alpha)\Gamma(1-n-l-\alpha)} = (-1)^{l+n}\alpha, \tag{A.22}$$

and finally

$$p_l = \alpha\gamma^l \sum_{n=0}^{+\infty} (-1)^n \frac{\Gamma(l+n+\alpha)}{\Gamma(1-n+\alpha)} \frac{\gamma^{2n}}{n!\Gamma(n+l+1)} \tag{A.23}$$

for non-integer values of α. Equation (A.23) can be used for integer values of α as well, since $\lim_{\alpha \to i} p_l$ with $i \in \mathbb{N}$ is well defined.

A.1.4 Leviton

In the following we focus on the simple case $\alpha = 1$, with a single electron excitation carried by each voltage pulse. Equation (A.17) reduces to

$$p_l = \frac{1}{2\pi i} \oint_{|z|=1} dz\, z^l \frac{1-z\gamma}{z-\gamma}. \tag{A.24}$$

One should then distinguish between three different cases.
A: $l \geq 0$. Here the integrand function

$$f_l(z) = z^l \frac{1-z\gamma}{z-\gamma} \tag{A.25}$$

has a pole of order 1 in $z=\gamma$. Fourier coefficients are readily evaluated with the help of Cauchy theorem: we just look for the residue inside the unit circle

$$p_l = \mathrm{Res}\left[f_l(z),\gamma\right] = z^l(1-z\gamma)\big|_{z=\gamma} = \gamma^l(1-\gamma^2). \tag{A.26}$$

B: $l \leq -2$. In this case $f_l(z)$ has two poles at $z=\gamma$ and $z=0$ respectively, but is analytic everywhere outside the unit circle, even at infinity. This guarantees that $p_l = 0$ for $l \leq -2$, since the unit circle (swept counterclockwise) encloses an area without residues. Alternatively, one can still sweep clockwise the unit circle and check that $\mathrm{Res}\left[f_l(z),\gamma\right] + \mathrm{Res}\left[f_l(z),0\right] = 0$.
C: $l=-1$. For $l=-1$ one should note that z^{-1} has a residue at infinity [111], so that the previous statement doesn't hold anymore. One has

$$p_{-1} = \mathrm{Res}\left[f_{-1}(z),\gamma\right] + \mathrm{Res}\left[f_{-1}(z),0\right] = \frac{1}{\gamma}(1-\gamma^2) - \frac{1}{\gamma} = -\gamma. \tag{A.27}$$

Collecting the three results together we have

$$p_l(\alpha=1) = \begin{cases} \gamma^l(1-\gamma^2) & \text{if } l \geq 0, \\ -\gamma & \text{if } l=-1, \\ 0 & \text{if } l \leq -2. \end{cases} \tag{A.28}$$

A.2 Two sources: Hong-Ou-Mandel setup

Two identical single-electron sources with a tunable delay are necessary to describe a HOM experiment. They are implemented by two trains of voltage pulses $V_R(t) = V(t)$ and $V_L(t) = V(t+t_D)$. The periodic phase factor involves in this case the combination $\Delta V(t) = V_R(t) - V_L(t)$, namely

$$e^{-ie^*\int_0^t dt'[V(t')-V(t'+t_D)]} = e^{-i\varphi(t)}e^{i\varphi(t+t_D)}e^{-i\varphi(t_D)} = \sum_{l=-\infty}^{+\infty} \tilde{p}_l e^{-il\omega t}, \tag{A.29}$$

where the new coefficients $\tilde{p}_l$ read

$$\tilde{p}_l = \int_0^T \frac{dt}{T} e^{il\omega t}e^{-i\varphi(t)}e^{i\varphi(t+t_D)}e^{-i\varphi(t_D)} = e^{-i\varphi(t_D)} \sum_{m=-\infty}^{+\infty} p_{l+m}p_m^* e^{im\omega t_D}. \tag{A.30}$$

Lorentzian wave

For a periodic train of Lorentzian voltage pulses we can get rid of the sum to find a simpler expression for the coefficients $\tilde{p}_l$. Using Eq. (A.14) it is possible to write

$$\begin{aligned}\tilde{p}_l &= e^{-i\varphi(t_D)}e^{-i\alpha\omega t_D}\int_0^T \frac{dt}{T} e^{i2\pi lu}\left[\frac{\sin\left(i\pi\eta+\pi u\right)}{\sin\left(i\pi\eta-\pi u\right)}\right]^\alpha \left[\frac{\sin\left(i\pi\eta-\pi u-\pi t_D/T\right)}{\sin\left(i\pi\eta+\pi u+\pi t_D/T\right)}\right]^\alpha = \\ &= e^{-i\varphi(t_D)}\phi^\alpha \frac{1}{2\pi i}\oint_{|z|=1}\frac{dz}{z} z^l \left(\frac{1-z\gamma}{z-\gamma}\right)^\alpha \left(\frac{\gamma\phi - z}{\gamma z - \phi}\right)^\alpha,\end{aligned} \tag{A.31}$$

with the new parameter $\phi = e^{-i2\pi t_D/T}$ in addition to $\gamma = e^{-2\pi\eta}$. For an integer Lorentzian with $\alpha = 1$, we simply have to calculate the residues of the integrand function. Again, we shall distinguish between three cases.
A: $l \geq 1$. The function

$$\tilde{f}_l(z) = z^{l-1}\frac{(1-z\gamma)\left(\phi - \frac{z}{\gamma}\right)}{(z-\gamma)\left(z - \frac{\phi}{\gamma}\right)} \tag{A.32}$$

has a pole at $z = \gamma$ and another one at $z = \phi/\gamma$. Since $|\phi| = 1$ and $\gamma < 1$, the latter lies outside the unit circle and the only contribution to $\tilde{p}_l$ comes from the residue at $z = \gamma$:

$$\tilde{p}_l = e^{-i\varphi(t_D)}\phi\,\mathrm{Res}\left[\tilde{f}_l(z), \gamma\right] = e^{-i\varphi(t_D)}\phi\gamma^l\frac{(1-\gamma^2)(1-\phi)}{\phi-\gamma^2}. \tag{A.33}$$

B: $l \leq -1$. Under this condition, we can either look for the residues at $z = 0$ and $z = \gamma$ inside the circle or evaluate the residue at $z = \phi/\gamma$ outside the circle, with a change of sign (note that there's no residue at infinity for $l \leq -1$). The latter gives

$$\tilde{p}_l = -e^{-i\varphi(t_D)}\phi\,\mathrm{Res}\left[\tilde{f}_l(z), \frac{\phi}{\gamma}\right] = e^{-i\varphi(t_D)}\phi\gamma^{-l}\phi^l\frac{(1-\gamma^2)(1-\phi)}{\phi-\gamma^2}. \tag{A.34}$$

C: $l = 0$. The function $\tilde{f}_0(z)$ has residues at infinity and at $z = \phi/\gamma$ outside the unit circle, or residues at $z = 0$ and $z = \gamma$ inside. Thus

$$\begin{aligned}\tilde{p}_l &= e^{-i\varphi(t_D)}\phi\,\mathrm{Res}\left[\tilde{f}_0(z), 0\right] + e^{-i\varphi(t_D)}\phi\,\mathrm{Res}\left[\tilde{f}_0(z), \gamma\right] = \\ &= e^{-i\varphi(t_D)}\phi\left[1 + \frac{(1-\gamma^2)(1-\phi)}{\phi-\gamma^2}\right].\end{aligned} \tag{A.35}$$

A.3 Multiple pulses

Finally, let us briefly focus on the case of multiple pulses discussed in Chapter 4. The phase accumulated for the periodic signal $V_N(t) = \sum_{j=0}^{N-1}\widetilde{V}\left(t - j\frac{\alpha}{N}T\right)$ is given by

$$\begin{aligned}\varphi_N(t) &= e^*\int_0^t dt'\left[\sum_{j=0}^{N-1}\widetilde{V}\left(t' - j\frac{\alpha}{N}T\right) - \widetilde{V}_{\mathrm{dc}}\right] \\ &= \sum_{j=0}^{N-1}\left[\widetilde{\varphi}\left(t - j\frac{\alpha}{N}T\right) - \widetilde{\varphi}\left(-j\frac{\alpha}{N}T\right)\right],\end{aligned} \tag{A.36}$$

where $\widetilde{\varphi}(t) = e^*\int_0^t dt'\left[\widetilde{V}(t') - \widetilde{V}_{\mathrm{dc}}\right]$. Each phase factor $e^{-i\widetilde{\varphi}(t)}$ can be written as

$$e^{-i\widetilde{\varphi}(t)} = \sum_l p_l\left(\frac{q}{N}\right)e^{-il\omega t}, \tag{A.37}$$

since each pulse $\widetilde{V}$ involves only a fraction of the total charge q. The corresponding Fourier coefficients for $e^{-i\varphi_N(t)}$ read

$$
\begin{aligned}
p_l^{(N)}(q) &= \exp\left[i\sum_{j=0}^{N-1}\widetilde{\varphi}\left(-j\frac{\alpha}{N}T\right)\right]\int_0^T\frac{dt}{T}e^{il\omega t}\prod_{j=0}^{N-1}e^{-i\widetilde{\varphi}\left(t-j\frac{\alpha}{N}T\right)} = \\
&= \exp\left[i\sum_{j=0}^{N-1}\widetilde{\varphi}\left(-j\frac{\alpha}{N}T\right)\right]\int_0^T\frac{dt}{T}\exp(il\omega t)\sum_{m_0=-\infty}^{+\infty}\sum_{m_1=-\infty}^{+\infty}\cdots\sum_{m_{N-1}=-\infty}^{+\infty}\times \\
&\quad\times\exp(-im_0\omega t)p_{m_0}\left(\frac{q}{N}\right)\exp\left\{-im_1\omega\left[t-\frac{\alpha}{N}T\right]\right\}p_{m_1}\left(\frac{q}{N}\right)\cdots\times \\
&\quad\times\exp\left\{-im_{N-1}\omega\left[t-(N-1)\frac{\alpha}{N}T\right]\right\}p_{m_{N-1}}\left(\frac{q}{N}\right) = \\
&= \exp\left[i\sum_{j=0}^{N-1}\widetilde{\varphi}\left(-j\frac{\alpha}{N}T\right)\right]\sum_{m_1=-\infty}^{+\infty}\cdots\sum_{m_{N-1}=-\infty}^{+\infty}\times \\
&\quad\times\exp\left\{i\frac{2\pi}{N}\alpha\left[m_1+\cdots+(N-1)m_{N-1}\right]\right\}\times \\
&\quad\times p_{l-m_1-\ldots-m_{N-1}}\left(\frac{q}{N}\right)p_{m_1}\left(\frac{q}{N}\right)\cdots p_{m_{N-1}}\left(\frac{q}{N}\right).
\end{aligned}
\tag{A.38}
$$

As an example, coefficients for $N = 2$ are given by

$$
p_l^{(2)}(q) = e^{i\widetilde{\varphi}\left(-\frac{\alpha T}{2}\right)}\sum_{m=-\infty}^{+\infty}e^{i\pi\alpha m}p_{l-m}\left(\frac{q}{2}\right)p_m\left(\frac{q}{2}\right). \tag{A.39}
$$

Note that the time-independent phase $e^{i\widetilde{\varphi}\left(-\frac{\alpha T}{2}\right)}$ has been omitted in the main text, as it is washed out as soon as we compute the squared modulus of $p_l^{(2)}$.

A.4 Useful sum rule for the photoassisted coefficients

In this section we prove a useful sum rule for the coefficients p_l, namely

$$
\sum_{l=-\infty}^{+\infty}l^s|p_l|^2 = \left(\frac{e^*}{\omega}\right)^s\int_0^T\frac{dt}{T}V_{\mathrm{ac}}^s(t), \tag{A.40}
$$

which is valid for any integer number s. As a first step, we exploit the definition of the coefficients p_l and write the factor l^s as a derivative

$$\begin{aligned}\sum_{l=-\infty}^{+\infty} l^s|p_l|^2 &= \sum_{l=-\infty}^{+\infty} l^s \int_0^T \frac{dt}{T} e^{il\omega t} e^{-i\varphi(t)} \int_0^T \frac{dt'}{T} e^{-il\omega t'} e^{i\varphi(t')} = \\ &= \int_0^T \frac{dt}{T} \int_0^T \frac{dt'}{T} \sum_{l=-\infty}^{+\infty} l^s e^{il\omega(t-t')} e^{-i\varphi(t)} e^{i\varphi(t')} = \\ &= \int_0^T \frac{dt}{T} \int_0^T \frac{dt'}{T} \sum_{l=-\infty}^{+\infty} \left(\frac{i}{\omega}\right)^s \partial_{t'}^s e^{il\omega(t-t')} e^{-i\varphi(t)} e^{i\varphi(t')} = \\ &= \int_0^T \frac{dt}{T} \int_0^T dt' \left(-\frac{i}{\omega}\right)^s \delta(t-t') e^{-i\varphi(t)} \partial_{t'}^s e^{i\varphi(t')} = \\ &= \int_0^T \frac{dt}{T} \left(-\frac{i}{\omega}\right)^s e^{-i\varphi(t)} \partial_t^s e^{i\varphi(t)}. \end{aligned} \tag{A.41}$$

We now look for a generic expression of the s-th derivative of the phase factor. By considering the cases $s = \{1, 2, 3\}$, which read

$$\partial_t e^{i\varphi(t)} = ie^* V_{\rm ac}(t) e^{i\varphi(t)} \tag{A.42}$$

$$\partial_t^2 e^{i\varphi(t)} = ie^* \partial_t V_{\rm ac}(t) e^{i\varphi(t)} + (ie^*)^2 V_{\rm ac}^2(t) e^{i\varphi(t)} \tag{A.43}$$

$$\partial_t^3 e^{i\varphi(t)} = ie^* \partial_t^2 V_{\rm ac}(t) e^{i\varphi(t)} + \frac{3}{2}(ie^*)^2 \partial_t V_{\rm ac}(t) e^{i\varphi(t)} + (ie^*)^3 V_{\rm ac}^3(t) e^{i\varphi(t)}, \tag{A.44}$$

we realize that the s-th derivative must be given by

$$\partial_t^s e^{i\varphi(t)} = D[V_{\rm ac}(t)] e^{i\varphi(t)} + (ie^*)^s V_{\rm ac}^s(t) e^{i\varphi(t)}, \tag{A.45}$$

where $D[V_{\rm ac}(t)]$ contains only first- and higher-order derivatives of $V_{\rm ac}(t)$. It is clear that, multiplying by $e^{-i\varphi(t)}$ and averaging over one period, we are only left with the second term of Eq. (A.45), namely

$$\int_0^T \frac{dt}{T} e^{-i\varphi(t)} \partial_t^s e^{i\varphi(t)} = (ie^*)^s \int_0^T \frac{dt}{T} V_{\rm ac}^s(t), \tag{A.46}$$

and we can finally write

$$\sum_{l=-\infty}^{+\infty} l^s |p_l|^2 = \left(\frac{e^*}{\omega}\right)^s \int_0^T \frac{dt}{T} V_{\rm ac}^s(t). \tag{A.47}$$

From Eq. (A.47) we immediately get the two simple relations $\sum_l |p_l|^2 = 1$ and $\sum_l l|p_l|^2 = 0$ used in the main text. It is worth noticing that we can also add

the dc component $q = e^* V_{\rm dc}/\omega$ to get the full sum rule

$$\begin{aligned}
\sum_{l=-\infty}^{+\infty} |p_l|^2 (q+l)^s &= \sum_{l=-\infty}^{+\infty} |p_l|^2 \sum_{k=0}^{s} \binom{s}{k} q^{s-k} l^k = \\
&= \sum_{k=0}^{s} \binom{s}{k} \left(\frac{e^* V_{\rm dc}}{\omega}\right)^{s-k} \left(\frac{e^*}{\omega}\right)^k \int_0^T \frac{dt}{T} V_{\rm ac}^k(t) = \\
&= \left(\frac{e^*}{\omega}\right)^s \int_0^T \frac{dt}{T} \left[\sum_{k=0}^{s} \binom{s}{k} V_{\rm dc}^{s-k} V_{\rm ac}^k(t)\right] = \\
&= \left(\frac{e^*}{\omega}\right)^s \int_0^T \frac{dt}{T} \left[V_{\rm dc} + V_{\rm ac}(t)\right]^s = \\
&= \left(\frac{e^*}{\omega}\right)^s \int_0^T \frac{dt}{T} V^s(t). \qquad \text{(A.48)}
\end{aligned}$$

Appendix B

Bosonic commutators and point splitting

In this Appendix we evaluate the bosonic commutation relations introduced in Eqs. (3.47) and (3.48) and used throughout this thesis. We also show the equivalence between the bosonic formalism and a theory of free fermions in one dimension for the case of integer filling factor $\nu = 1$.

B.1 Bosonic commutators

We first recall the full expression for the bosonic field introduced in the main text. For simplicity, we will work only with the field Φ_R and drop all the labels R referring to its right-moving character. We have

$$\Phi(x) = \varphi(x) + \varphi^\dagger(x) = i\sqrt{\frac{2\pi}{L}} \sum_{k>0} \frac{e^{-ak/2}}{\sqrt{k}} \left(e^{+ikx} b_k - e^{-ikx} b_k^\dagger \right), \tag{B.1}$$

where bosonic creation and annihilation operators satisfy $[b_k, b_q^\dagger] = \delta_{k,q}$. Here we have split the Hermitian operator Φ into two conjugate contributions $\varphi(x)$ and $\varphi^\dagger(x)$. The former is given by

$$\varphi(x) = i\sqrt{\frac{2\pi}{L}} \sum_{k>0} \frac{e^{-ak/2}}{\sqrt{k}} e^{ikx} b_k. \tag{B.2}$$

Commutators for the new bosonic field $\varphi(x)$ are readily obtained. One finds

$$\begin{aligned}\left[\varphi(x),\varphi^\dagger(y)\right] &= \frac{2\pi}{L}\sum_{k,q>0}\frac{e^{-a(k+q)/2}}{\sqrt{kq}}e^{ikx}e^{-iqy}\left[b_k,b_q^\dagger\right] = \\ &= \frac{2\pi}{L}\sum_{k>0}\frac{e^{-ak}}{k}e^{ik(x-y)} = \sum_{n>0}\frac{1}{n}\left[e^{i\frac{2\pi}{L}(x-y+ia)}\right]^n = \\ &= -\ln\left[1-e^{i\frac{2\pi}{L}(x-y+ia)}\right], \end{aligned} \tag{B.3}$$

where we have used the series $\sum_{n=1}^{\infty}\frac{x^n}{n} = -\ln(1-x)$. Expanding the last result for $L\to\infty$ we obtain

$$\begin{aligned}\left[\varphi(x),\varphi^\dagger(y)\right] &= -\ln\left[1-1-i\frac{2\pi}{L}(x-y+ia)+\dots\right] = \\ &\approx -\ln\left[-i\frac{2\pi}{L}(x-y+ia)\right]. \end{aligned} \tag{B.4}$$

From Eq. (B.3) we also obtain the commutator for Φ. It reads

$$\left[\Phi(x),\Phi(y)\right] = \left[\varphi(x),\varphi^\dagger(y)\right] + \left[\varphi^\dagger(x),\varphi(y)\right] = -\ln\left[\frac{1-e^{i\frac{2\pi}{L}(x-y+ia)}}{1-e^{i\frac{2\pi}{L}(y-x+ia)}}\right]. \tag{B.5}$$

We focus again on the limit $L\to\infty$ and get

$$\begin{aligned}\left[\Phi(x),\Phi(y)\right] &= -\ln\left[\frac{1-1-i\frac{2\pi}{L}(x-y+ia)+\dots}{1-1-i\frac{2\pi}{L}(y-x+ia)+\dots}\right] = \\ &\approx -\ln\left(\frac{i+\frac{x-y}{a}}{i-\frac{x-y}{a}}\right) = \\ &= -\frac{2}{i}\arctan\left(\frac{x-y}{a}\right). \end{aligned} \tag{B.6}$$

In the last passage we used the identity $\arctan z = \frac{i}{2}\ln\left(\frac{i+z}{i-z}\right)$ [80]. Now we can safely take the limit $a\to 0$ (remember that a is nothing but a short-distance regularization cutoff) to finally obtain

$$\left[\Phi(x),\Phi(y)\right] = i\pi\,\mathrm{sign}(x-y). \tag{B.7}$$

This proves the relation (3.47) for the case of right-moving excitations. Since the bosonic density is linked to Φ by a spatial derivative, $\rho = -(\sqrt{\nu}/2\pi)\partial_x\Phi$, we immediately get the commutator (3.48) as well:

$$\left[\rho(x),\Phi(y)\right] = -\frac{\sqrt{\nu}}{2\pi}i\pi\partial_x\,\mathrm{sign}(x-y) = -i\sqrt{\nu}\delta(x-y). \tag{B.8}$$

One should notice that the above results depend on the assumption of infinite length L. A special care in retaining the terms $\sim 1/L$ is required when dealing with finite size systems, as shown for instance in Refs. [138, 140].

B.2 Bosonization at integer filling factor using point splitting

We now show that the bosonic description of low-energy excitations is fully equivalent to a one-dimensional fermionic model of noninteracting electrons with linear spectrum. In such a case, the Hamiltonian is [135, 138, 140]

$$H_{R/L} = \int dx : \Psi^{\dagger}_{R/L}(x)(\mp iv\partial_x - vk_{\mathrm{F}})\Psi_{R/L}(x) : . \tag{B.9}$$

with the fermionic fields $\Psi_{R/L}$ given by

$$\Psi_{R/L}(x) = \frac{1}{\sqrt{L}} \sum_{k=-\infty}^{+\infty} e^{\pm ikx} c_{R/L,k}. \tag{B.10}$$

Note that the second contribution in Eq. (B.9) is proportional to vk_{F}, and plays the role of a chemical potential to fix the ground state charge and energy, as pointed out by Haldane in his original work [135]. The notation $: X_1 X_2 \ldots :$ in Eq. (B.9) stands for normal ordering of the product of operators $X_1 X_2 \ldots$. It means that all operators that destroy the ground state (i.e. all operators X_i such that $X_i \left|0\right\rangle = 0$) are moved to the right of all other operators [135, 138, 140]. For the case of a fermionic system, the ground state is the filled Fermi sea with Fermi momentum k_{F}. Thus, both $c_{k>k_{\mathrm{F}}}$ and $c^{\dagger}_{k<k_{\mathrm{F}}}$ destroy the ground state, and must be anti-commuted to the right of the remaining operators. For bosons, the ground state is nothing but the bosonic vacuum, and only annihilation operators b_k are involved in the normal ordering process.

Fermionic fields in Eq. (B.9) obey the following anti-commutation relations:

$$\left\{\Psi_{R/L}(x), \Psi^{\dagger}_{R/L}(y)\right\} = \delta(x-y). \tag{B.11}$$

Charge and energy density operators in terms of fermionic fields read

$$\rho_{R/L}(x) =: \Psi^{\dagger}_{R/L}(x)\Psi_{R/L}(x) :, \tag{B.12}$$

$$\mathcal{H}_{R/L}(x) = \mp iv : \Psi^{\dagger}_{R/L}(x)\partial_x \Psi_{R/L}(x) : -vk_{\mathrm{F}}\rho_{R/L}(x). \tag{B.13}$$

The tool that maps the fermionic model into the bosonic approach is nothing but the bosonization identity for integer electrons, which for the case $\nu = 1$ reads

$$\Psi_{R/L}(x) = \frac{F_{R/L}}{\sqrt{2\pi a}} e^{\pm ik_{\mathrm{F}}x} e^{-i\Phi_{R/L}(x)}. \tag{B.14}$$

We will show that bosonization of Eqs. (B.9), (B.12) and (B.13) will lead us to

$$\rho_{R/L}(x) = \mp \frac{1}{2\pi}\partial_x \Phi_R(x), \tag{B.15}$$

$$\mathcal{H}_{R/L}(x) = \frac{v}{4\pi} : [\partial_x \Phi_R(x)]^2 : . \tag{B.16}$$

B.2.1 Particle density

Let us first consider the density operator ρ_R. We focus again on the case of right-moving excitations, and drop the label R for brevity. Following the notation of Ref. [138] we also drop for the moment the factor $e^{ik_F x}$ in the definition of $\Psi_R(x)$, Eq. (B.14), which will be reinstated at the end of the calculation. We thus consider the field

$$\widetilde{\Psi}(x) = \frac{F}{\sqrt{L}} e^{-i\varphi^\dagger(x)} e^{-i\varphi(x)} = \frac{F}{\sqrt{2\pi a}} e^{-i\Phi(x)}. \tag{B.17}$$

Note that the operator in the middle of Eq. (B.17) is normal ordered, while the right-hand side of the equation is not, hence the presence of the diverging factor $(2\pi a)^{-1/2}$ [138, 140].

With this result under our belt, we can now work out the bosonized expression for the density $\widetilde{\rho}(x) =: \widetilde{\Psi}^\dagger(x)\widetilde{\Psi}(x) :$. We use the point splitting technique to regularize such a diverging quantity, using $\delta = ia$ as the splitting parameter and taking the limit $a \to 0$ at the end of the calculation [138, 140]. Using Eq. (C.8) from Appendix C we have

$$\begin{aligned}\widetilde{\Psi}^\dagger(x+ia)\widetilde{\Psi}(x) &= \frac{1}{L} e^{i\varphi^\dagger(x+ia)} e^{i\varphi(x+ia)} F^\dagger F e^{-i\varphi^\dagger(x)} e^{-i\varphi(x)} = \\ &= \frac{1}{L} e^{i\varphi^\dagger(x+ia)} e^{-i\varphi^\dagger(x)} e^{i\varphi(x+ia)} e^{-i\varphi(x)} e^{\left[\varphi(x+ia),\varphi^\dagger(x)\right]}.\end{aligned} \tag{B.18}$$

We can safely discard the regularization parameter in the commutator, since it was already regularized in Eq. (B.3). Thus, we get

$$\exp\left\{\left[\varphi(x),\varphi^\dagger(x)\right]\right\} = \exp\left(-\ln\frac{2\pi a}{L}\right) = \frac{L}{2\pi a}. \tag{B.19}$$

Equation (B.18) now reads

$$\widetilde{\Psi}^\dagger(x+ia)\widetilde{\Psi}(x) = \frac{1}{2\pi a} e^{i\left[\varphi^\dagger(x+ia)-\varphi^\dagger(x)\right]} e^{i[\varphi(x+ia)-\varphi(x)]}. \tag{B.20}$$

We now expand the exponentials in powers of a:

$$\begin{aligned}\widetilde{\Psi}^\dagger(x+ia)\widetilde{\Psi}(x) &= \frac{1}{2\pi a}\left[1 + i\partial_x\varphi^\dagger(x)ia + O(a^2)\right]\left[1 + i\partial_x\varphi(x)ia + O(a^2)\right] = \\ &= \frac{1}{2\pi a} - \frac{1}{2\pi}\left[\partial_x\varphi^\dagger(x) + \partial_x\varphi(x)\right] + O(a) = \\ &= \frac{1}{2\pi a} - \frac{1}{2\pi}\partial_x\Phi(x) + O(a).\end{aligned} \tag{B.21}$$

Finally, normal ordering the last expression and taking the limit $a \to 0$ we get the final result

$$\widetilde{\rho}(x) = \lim_{a\to 0} :\widetilde{\Psi}^\dagger(x+ia)\widetilde{\Psi}(x): = \tag{B.22}$$

$$= \lim_{a\to 0}\left[\widetilde{\Psi}^\dagger(x+ia)\widetilde{\Psi}(x) - \left\langle\widetilde{\Psi}^\dagger(x+ia)\widetilde{\Psi}(x)\right\rangle_0\right] = \tag{B.23}$$

$$= -\frac{1}{2\pi}\partial_x\Phi(x). \tag{B.24}$$

where the notation $\langle \ldots \rangle_0$ stands for a quantum average over the ground state. Notice that the normal ordering allowed us to get rid of the diverging contribution $(2\pi a)^{-1}$.

B.2.2 Hamiltonian density

We proceed similarly for the energy density $\mathcal{H}(x)$. However, this calculation presents some tricky passages that need to be performed carefully. Consider the first term in Eq. (B.13) for the case of right-moving fermions, which we will denote as $\mathcal{H}_0$. We have

$$\mathcal{H}_0(x) = -iv : \Psi^\dagger(x)\partial_x\Psi(x) : . \tag{B.25}$$

Now, let us drop the exponential factor $e^{ik_F x}$ and work with the field $\widetilde{\Psi} = e^{-ik_F x}\Psi$. We resort to the point splitting and write

$$\begin{aligned}
&\widetilde{\Psi}^\dagger(x+ia)\partial_x\widetilde{\Psi}(x) = \\
&= \frac{1}{L}e^{i\varphi^\dagger(x+ia)}e^{i\varphi(x+ia)}F^\dagger F\partial_x\left[e^{-i\varphi^\dagger(x)}e^{-i\varphi(x)}\right] = \\
&= \frac{1}{L}e^{i\varphi^\dagger(x+ia)}e^{i\varphi(x+ia)}e^{-i\varphi^\dagger(x)}\left[-i\partial_x\varphi^\dagger(x)e^{-i\varphi(x)} - ie^{-i\varphi(x)}\partial_x\varphi(x)\right] = \\
&= \frac{1}{L}e^{i\varphi^\dagger(x+ia)}e^{i\varphi(x+ia)}e^{-i\varphi^\dagger(x)}e^{-i\varphi(x)}\left\{-i\partial_x\varphi^\dagger(x) - i\partial_x\varphi(x) - \left[\partial_x\varphi^\dagger(x),\varphi(x)\right]\right\}.
\end{aligned} \tag{B.26}$$

It is worth noticing that we had to move the exponential $e^{-i\varphi(x)}$ to the left of $\partial_x\varphi^\dagger(x)$, thus generating an additional commutator. The latter is given by

$$\begin{aligned}
\left[\partial_x\varphi^\dagger(x),\varphi(x)\right] &= -\partial_y\left[\varphi(x),\varphi^\dagger(y)\right]_{x=y} \approx \partial_y \ln\left[-i\frac{2\pi}{L}(x-y+ia)\right]_{x=y} = \\
&= \left[\frac{i\frac{2\pi}{L}}{-i\frac{2\pi}{L}(x-y+ia)}\right]_{x=y} = \frac{i}{a}.
\end{aligned} \tag{B.27}$$

Then we obtain

$$\begin{aligned}
&\widetilde{\Psi}^\dagger(x+ia)\partial_x\widetilde{\Psi}(x) = \\
&= \frac{1}{L}e^{i\left[\varphi^\dagger(x+ia)-\varphi^\dagger(x)\right]}e^{i[\varphi(x+ia)-\varphi(x)]}e^{\left[\varphi(x+ia),\varphi^\dagger(x)\right]}\left[-i\partial_x\varphi^\dagger(x) - i\partial_x\varphi(x) - \frac{i}{a}\right].
\end{aligned} \tag{B.28}$$

At this stage, one should notice that the exponential of the commutator $\left[\varphi(x),\varphi^\dagger(x)\right]$ is proportional to $1/a$ [see Eq. (B.19)], and we also have a term $\sim 1/a$ into the square brackets. It follows immediately that we need to expand the exponential of φ and $\varphi^\dagger$ up to the order a^2 to get the correct result. We

have

$$
\begin{aligned}
&e^{i\left[\varphi^\dagger(x+ia)-\varphi^\dagger(x)\right]} = \\
&= 1 + a\left\{\partial_a e^{i\left[\varphi^\dagger(x+ia)-\varphi^\dagger(x)\right]}\right\}_{a=0} + \frac{a^2}{2}\left\{\partial_a^2 e^{i\left[\varphi^\dagger(x+ia)-\varphi^\dagger(x)\right]}\right\}_{a=0} + O(a^3) = \\
&= 1 - a\partial_x\varphi^\dagger(x) + \frac{a^2}{2}\partial_a\left\{-\partial_x\varphi^\dagger(x+ia)e^{i\left[\varphi^\dagger(x+ia)-\varphi^\dagger(x)\right]}\right\}_{a=0} + O(a^3) \\
&= 1 - a\partial_x\varphi^\dagger(x) + \frac{a^2}{2}\left\{-i\partial_x^2\varphi^\dagger(x) + \left[\partial_x\varphi^\dagger(x)\right]^2\right\} + O(a^3),
\end{aligned}
\tag{B.29}
$$

and we obtain similarly an expansion for $\exp\{i\left[\varphi(x+ia)-\varphi(x)\right]\}$. Inserting both results into Eq. (B.28) we get

$$
\begin{aligned}
&\widetilde{\Psi}^\dagger(x+ia)\partial_x\widetilde{\Psi}(x) = \\
&= -\frac{i}{2\pi a}\left[\partial_x\Phi(x) + \frac{1}{a}\right]\left\{1 - a\partial_x\varphi^\dagger(x) - i\frac{a^2}{2}\partial_x^2\varphi^\dagger(x) + \frac{a^2}{2}\left[\partial_x\varphi^\dagger(x)\right]^2\right\}\times \\
&\quad\times\left\{1 - a\partial_x\varphi(x) - i\frac{a^2}{2}\partial_x^2\varphi(x) + \frac{a^2}{2}\left[\partial_x\varphi(x)\right]^2 + O(a^3)\right\} = \\
&= -\frac{i}{2\pi a}\left[\partial_x\Phi(x) + \frac{1}{a}\right]\left\{1 - a\partial_x\varphi(x) - i\frac{a^2}{2}\partial_x^2\varphi(x) + \frac{a^2}{2}\left[\partial_x\varphi(x)\right]^2 - a\partial_x\varphi^\dagger(x) + \right. \\
&\quad\left. + a^2\partial_x\varphi^\dagger(x)\partial_x\varphi(x) - i\frac{a^2}{2}\partial_x^2\varphi^\dagger(x) + \frac{a^2}{2}\left[\partial_x\varphi^\dagger(x)\right]^2 + O(a^3)\right\} = \\
&= -\frac{i}{2\pi a}\left[\partial_x\Phi(x) + \frac{1}{a}\right]\left\{1 - a\partial_x\Phi(x) - i\frac{a^2}{2}\partial_x^2\Phi(x) + \frac{a^2}{2} : \left[\partial_x\Phi(x)\right]^2 : + O(a^3)\right\}.
\end{aligned}
\tag{B.30}
$$

In the last passage we recognized that

$$
\frac{a^2}{2}\left\{\left[\partial_x\varphi^\dagger(x)\right]^2 + \partial_x\varphi^\dagger(x)\partial_x\varphi(x) + \left[\partial_x\varphi^\dagger(x)\right]^2\right\} = \frac{a^2}{2} : \left[\partial_x\Phi(x)\right]^2 : \tag{B.31}
$$

is a normal ordered expression, since the field $\varphi^\dagger$ is always on the left of φ (which means that operators $b_k^\dagger$ are on the left of all b_k). We are left with

$$
\begin{aligned}
&\widetilde{\Psi}^\dagger(x+ia)\partial_x\widetilde{\Psi}(x) = \\
&= -i\left\{\frac{1}{2\pi a^2} - \frac{1}{2\pi}\left[\partial_x\Phi(x)\right]^2 - i\frac{1}{4\pi}\partial_x^2\Phi(x) + \frac{1}{4\pi} : \left[\partial_x\Phi(x)\right]^2 : + O(a)\right\}.
\end{aligned}
\tag{B.32}
$$

We can drop the term $\sim \partial_x^2\Phi(x)$, which is a total derivative and vanishes as we integrate over x. Indeed, we should remember that the only meaningful physical quantity (the total Hamiltonian) is proportional to $\int dx\widetilde{\Psi}^\dagger\partial_x\widetilde{\Psi}$. Finally, we normal order the entire expression and take the limit $a \to 0$. This yields

$$
\begin{aligned}
: \widetilde{\Psi}^\dagger(x)\partial_x\widetilde{\Psi}(x) : &= \lim_{a\to 0}\left[\widetilde{\Psi}^\dagger(x+ia)\partial_x\widetilde{\Psi}(x) - \left\langle\widetilde{\Psi}^\dagger(x+ia)\partial_x\widetilde{\Psi}(x)\right\rangle_0\right] = \\
&= i\frac{1}{4\pi} : \left[\partial_x\Phi(x)\right]^2 : .
\end{aligned}
\tag{B.33}
$$

We only have to multiply by $-iv$ to get $\widetilde{\mathcal{H}}_0$:

$$\widetilde{\mathcal{H}}_0(x) = -iv : \widetilde{\Psi}^\dagger(x)\partial_x\widetilde{\Psi}(x) := \frac{v}{4\pi} : [\partial_x\Phi(x)]^2 : . \tag{B.34}$$

Introducing the Fermi momentum

As a final step, we restore the oscillating exponential factor $e^{ik_\mathrm{F}x}$ dropped at the beginning of the calculation. This is similar to the comparison between Haldane notation [135] and Von Delft notation discussed in Ref. [138], Sec. 10.A.4. Considering a right-moving field, we have $\Psi(x) = e^{ik_\mathrm{F}x}\widetilde{\Psi}(x)$. The particle density in our formalism is left unchanged since

$$\rho(x) =: \Psi^\dagger(x)\Psi(x) :=: \widetilde{\Psi}^\dagger(x)\widetilde{\Psi}(x) := -\frac{1}{2\pi}\partial_x\Phi(x). \tag{B.35}$$

Differently, the energy density acquires an additional term due to the derivative acting on the exponential $e^{ik_\mathrm{F}x}$:

$$\begin{aligned}\mathcal{H}_0(x) &= -iv : \Psi^\dagger(x)\partial_x\Psi(x) := -iv : \widetilde{\Psi}^\dagger(x)\partial_x\widetilde{\Psi}(x) : +vk_\mathrm{F} : \widetilde{\Psi}^\dagger(x)\widetilde{\Psi}(x) := \\ &= \frac{v}{4\pi} : [\partial_x\Phi(x)]^2 : +vk_\mathrm{F}\rho(x).\end{aligned} \tag{B.36}$$

We finally get the result anticipated in Eq. (B.16), since

$$\mathcal{H}(x) = \mathcal{H}_0(x) - vk_\mathrm{F}\rho(x) = \frac{v}{4\pi} : [\partial_x\Phi(x)]^2 : \tag{B.37}$$

Appendix C

Baker-Campbell-Hausdorff theorem

In this Appendix we demonstrate the Baker-Campbell-Hausdorff theorem and some useful formulas used in the main text [138].

C.1 Theorem

Given two operators A and B, the following identity holds:

$$\boxed{e^{-B}Ae^{B} = A + [A,B] + \frac{1}{2!}\left[[A,B],B\right] + \cdots = \sum_{n=0}^{+\infty}\frac{1}{n!}\left[A,B\right]_n .} \tag{C.1}$$

Here, we have defined the symbol $[A,B]_n$ by induction as $[A,B]_n = \left[[A,B]_{n-1},B\right]$, with $[A,B]_0 = A$.

To demonstrate Eq. (C.1) we introduce the operator $O(s) = e^{-sB}Ae^{sB}$, which depends on the parameter s. We note that its derivatives are

$$\frac{dO}{ds} = -Be^{-sB}Ae^{sB} + e^{-sB}Ae^{sB}B = e^{-sB}[A,B]e^{sB}, \tag{C.2}$$

$$\frac{d^2O}{ds^2} = -Be^{-sB}[A,B]e^{sB} + e^{-sB}[A,B]e^{sB}B = e^{-sB}\left[[A,B],B\right]e^{sB}, \tag{C.3}$$

$$\cdots$$

$$\frac{d^nO}{ds^n} = -Be^{-sB}[A,B]_{n-1}e^{sB} + e^{-sB}[A,B]_{n-1}e^{sB}B = e^{-sB}\left[A,B\right]_n e^{sB}. \tag{C.4}$$

The Taylor expansion for $O(s)$ around $s = 0$ in then

$$O(s) = e^{-sB}Ae^{sB} = \sum_{n=0}^{+\infty}\frac{1}{n!}\left[A,B\right]_n s^n. \tag{C.5}$$

Calculating $O(s=1)$ we get the Baker-Campbell-Hausdorff theorem (C.1).

C.2 Useful identities

The following equalities holds for $C=[A,B]$ and $[A,C]=[B,C]=0$.
A

$$\boxed{[A,e^B]=Ce^B.} \tag{C.6}$$

Let us consider the theorem (C.1) with $C=[A,B]$ and $[A,C]=[B,C]=0$. We have $[A,B]_1=C$ and $[A,B]_n=0$ for every $n>1$. Then we are left with

$$e^{-B}Ae^B=A+C. \tag{C.7}$$

Multiplying each side by e^B from left we get the commutation relation (C.6).
B

$$\boxed{e^Ae^B=e^Be^Ae^C.} \tag{C.8}$$

Let us consider the identity

$$e^{-B}e^Ae^B=\sum_{n=0}^{+\infty}\frac{1}{n!}\left[e^A,B\right]_n, \tag{C.9}$$

which is given by theorem (C.1) with the substitution $A\to e^A$. When $C=[A,B]$ and $[A,C]=[B,C]=0$ we have

$$\left[e^A,B\right]_0=e^A, \tag{C.10}$$
$$\left[e^A,B\right]_1=Ce^A, \tag{C.11}$$
$$\dots$$
$$\left[e^A,B\right]_n=C^ne^A, \tag{C.12}$$

thanks to Eq. (C.6). This gives rise to an exponential power series for C:

$$e^{-B}e^Ae^B=e^A\sum_{n=0}^{+\infty}\frac{1}{n!}C^n=e^Ae^C. \tag{C.13}$$

We get Eq. (C.8) multiplying by e^B from left.
C

$$\boxed{e^Ae^B=e^{A+B+C/2}=e^{A+B}e^{C/2}.} \tag{C.14}$$

We demonstrate this result by resorting to the parametric operator $T(s)=e^{sA}e^{sB}$. Its evident that $T(s=0)=1$, and its derivative is

$$\frac{dT}{ds}=Ae^{sA}e^{sB}+e^{sA}e^{sB}B=T(A+sC+B), \tag{C.15}$$

where we have commuted the operator A to the right of $e^{sA}e^{sB}$ exploiting Eq. (C.6). The differential equation

$$\begin{cases} \frac{d}{ds}T(s) = T(s)(A + sC + B), \\ T(0) = 1, \end{cases} \tag{C.16}$$

is solved by $T(s) = e^{A+B+C/2}$, giving $e^A e^B = e^{A+B+C/2}$ for $s = 1$. This tells us that for X, Y satisfying $[X, Y] = 0$ we have

$$e^X e^Y = e^{X+Y}. \tag{C.17}$$

Since $[A + B, C] = 0$, we use the latest result to move C out of the sum and write it as a second exponential, obtaining Eq. (C.14).

Appendix D

Keldysh contour formalism

In this Appendix we introduce the Schwinger-Keldysh contour formalism to deal with out-of-equilibrium systems [146, 202]. As a first step, we recap the essential features of time evolution pictures in quantum mechanics. We then introduce the equilibrium Green's function formalism, discuss its failure in the context of nonequilibrium many-body theory and show how troubles are circumvented with the Schwinger-Keldysh technique.

D.1 Time evolution pictures

D.1.1 Schrödinger picture

In the Schrödinger picture state vectors evolve with time, while observables do not. We introduce the time evolution operator which is defined by

$$|\phi(t)\rangle = U(t,t_0)\,|\phi(t_0)\rangle\,. \tag{D.1}$$

From the well known Schrödinger equation $i\hbar\partial_t\,|\phi(t)\rangle = \mathcal{H}(t)\,|\phi(t)\rangle$, with $\mathcal{H}(t)$ the total Hamiltonian, one has

$$i\hbar\partial_t U(t,t_0)\,|\phi(t_0)\rangle = \mathcal{H}(t)U(t,t_0)\,|\phi(t_0)\rangle\,. \tag{D.2}$$

Thus the time evolution operator satisfies

$$\partial_t U(t,t_0) = -\frac{i}{\hbar}\mathcal{H}(t)U(t,t_0), \tag{D.3}$$

from which we obtain

$$U(t,t_0) = 1 - \frac{i}{\hbar}\int_{t_0}^{t} dt_1 \mathcal{H}(t_1)U(t_1,t_0). \tag{D.4}$$

This is an integral equation that can be solved by iteration:

$$U(t,t_0) = 1 - \frac{i}{\hbar}\int_{t_0}^{t} dt_1 \mathcal{H}(t_1) + \left(\frac{i}{\hbar}\right)^2 \int_{t_0}^{t} dt_1 \mathcal{H}(t_1) \int_{t_0}^{t_1} dt_2 \mathcal{H}(t_2) + \dots$$
$$\cdots + \left(-\frac{i}{\hbar}\right)^n \int_{t_0}^{t} dt_1 \mathcal{H}(t_1) \cdots \int_{t_0}^{t_{n-1}} dt_n \mathcal{H}(t_n) + \cdots . \tag{D.5}$$

To properly handle this infinite sum, we note that the second term can be rewritten as [203]

$$\begin{aligned}
&\left(\frac{i}{\hbar}\right)^2 \int_{t_0}^{t} dt_1 \mathcal{H}(t_1) \int_{t_0}^{t_1} dt_2 \mathcal{H}(t_2) = \\
&= \frac{1}{2}\left(\frac{i}{\hbar}\right)^2 \left[\int_{t_0}^{t} dt_1 \mathcal{H}(t_1) \int_{t_0}^{t_1} dt_2 \mathcal{H}(t_2) + \int_{t_0}^{t} dt_2 \mathcal{H}(t_2) \int_{t_0}^{t_2} dt_1 \mathcal{H}(t_1)\right] = \\
&= \frac{1}{2}\left(\frac{i}{\hbar}\right)^2 \left[\int_{t_0}^{t} dt_1 \mathcal{H}(t_1) \int_{t_0}^{t} dt_2 \mathcal{H}(t_2)\Theta(t_1 - t_2) + \right. \\
&\quad \left. + \int_{t_0}^{t} dt_2 \mathcal{H}(t_2) \int_{t_0}^{t} dt_1 \mathcal{H}(t_1)\Theta(t_2 - t_1)\right] = \\
&= \frac{1}{2}\left(\frac{i}{\hbar}\right)^2 \int_{t_0}^{t} dt_1 \int_{t_0}^{t} dt_2 \left[\mathcal{H}(t_1)\mathcal{H}(t_2)\Theta(t_1 - t_2) + \mathcal{H}(t_2)\mathcal{H}(t_1)\Theta(t_2 - t_1)\right] = \\
&= \frac{1}{2}\left(\frac{i}{\hbar}\right)^2 \int_{t_0}^{t} dt_1 \int_{t_0}^{t} dt_2 \mathcal{T}\left[\mathcal{H}(t_1)\mathcal{H}(t_2)\right] = \\
&= \mathcal{T}\left\{\frac{1}{2}\left[\frac{i}{\hbar}\int_{t_0}^{t} dt_1 \mathcal{H}(t_1)\right]^2\right\},
\end{aligned} \tag{D.6}$$

where $\mathcal{T}$ (known as *time-ordering operator*) automatically orders a product of time dependent operators in the time-descending sequence. In general one has

$$\mathcal{T}\left[O(t_1)\cdots O(t_n)\right] = \sum_{p\in S_p} O(t_{p_1})\cdots O(t_{p_n})\Theta(t_{p_1} - t_{p_2})\cdots\Theta(t_{p_{n-1}} - t_{p_n}), \tag{D.7}$$

so that the n-th order term in the sum (D.5) can be recast as

$$\mathcal{T}\left\{\frac{1}{n!}\left[\left(-\frac{i}{\hbar}\right)^n \int_{t_0}^{t} dt_1 \mathcal{H}(t_1)\right]^n\right\}. \tag{D.8}$$

We can finally collect all the terms in Eq. (D.5) into the simple expression

$$U(t,t_0) = \mathcal{T}\left[e^{-\frac{i}{\hbar}\int_{t_0}^{t}\mathcal{H}(t')dt'}\right]. \tag{D.9}$$

For a time-independent Hamiltonian, the time evolution operator is just $U(t,t_0) = e^{-\frac{i}{\hbar}\mathcal{H}(t-t_0)}$. It's also worth noting that the time-ordering operator $\mathcal{T}$ in unnecessary in such cases where the time dependent Hamiltonian commutes with

itself at different times. Indeed, if $[\mathcal{H}(t_1), \mathcal{H}(t_2)] = 0$ for arbitrary t_1, t_2, we can swap $\mathcal{H}(t_2)$ and $\mathcal{H}(t_1)$ in the third-to-last passage of the previous calculation and we get

$$\frac{1}{2}\left(\frac{i}{\hbar}\right)^2 \int_{t_0}^{t} dt_1 \int_{t_0}^{t} dt_2 \left[\mathcal{H}(t_1)\mathcal{H}(t_2)\Theta(t_1 - t_2) + \mathcal{H}(t_1)\mathcal{H}(t_2)\Theta(t_2 - t_1)\right] = \\ = \frac{1}{2}\left(\frac{i}{\hbar}\right)^2 \int_{t_0}^{t} dt_1 \int_{t_0}^{t} dt_2 \mathcal{H}(t_1)\mathcal{H}(t_2) = \frac{1}{2}\left[\frac{i}{\hbar}\int_{t_0}^{t} dt_1 \mathcal{H}(t_1)\right]^2, \quad \text{(D.10)}$$

irrespectively of the time-ordering. One must resort to the $\mathcal{T}$ operator only when $[\mathcal{H}(t), \mathcal{H}(t')] \neq 0$. We note that the following useful properties hold:

- $U^\dagger(t, t_0) = U^{-1}(t, t_0) = U(t_0, t) \to U(t, t_0)U^\dagger(t, t_0) = 1$, with 1 the identity operator. Note that $U^\dagger(t, t_0)$ is given by

$$U^\dagger(t, t_0) = \widetilde{\mathcal{T}}\left[e^{\frac{i}{\hbar}\int_{t_0}^{t} \mathcal{H}(t')dt'}\right], \quad \text{(D.11)}$$

  where the anti-time-ordering operator $\widetilde{\mathcal{T}}$ acts in the opposite way with respect to $\mathcal{T}$.

- $U(t, t')U(t', t'') = U(t, t'')$.

We can also obtain an equation of motion for the density operator $\rho(t) = \sum_n p_n |\phi_n(t)\rangle \langle\phi_n(t)|$. Making use of the Schrödinger equation one has

$$\partial_t \rho(t) = \sum_n p_n \left[(\partial_t |\phi_n(t)\rangle) \langle\phi_n(t)| + |\phi_n(t)\rangle (\partial_t \langle\phi_n(t)|)\right] = \quad \text{(D.12)}$$

$$= \sum_n p_n \left[-\frac{i}{\hbar}\mathcal{H}(t) |\phi_n(t)\rangle \langle\phi_n(t)| + |\phi_n(t)\rangle \langle\phi_n(t)| \frac{i}{\hbar}\mathcal{H}(t)\right] = \quad \text{(D.13)}$$

$$= \frac{i}{\hbar}\left[\rho(t), \mathcal{H}(t)\right]. \quad \text{(D.14)}$$

This differential equation is solved by

$$\rho(t) = U(t, t_0)\rho(t_0)U^\dagger(t, t_0). \quad \text{(D.15)}$$

D.1.2 Heisenberg picture

In quantum mechanics, we'd usually like to know the expectation value of some observable O at time t, that is

$$\langle\phi(t)|O|\phi(t)\rangle = \left\langle\phi(t_0)|U^\dagger(t, t_0)OU(t, t_0)|\phi(t_0)\right\rangle = \langle\phi(t_0)|O(t)|\phi(t_0)\rangle. \quad \text{(D.16)}$$

It's evident from the last step that we can formulate the same problem in a picture where state vectors are fixed at the initial time t_0 and observables

acquire time dependence through $O(t) = U^\dagger(t,t_0)OU(t,t_0)$. This is known as the Heisenberg picture. One can verify that observables obey the equation

$$i\partial_t O(t) = \frac{1}{\hbar}[O(t), \mathcal{H}(t)] + (\partial_t O)(t), \tag{D.17}$$

where the notation $O(t)$ denotes the observables in the Heisenberg picture. For operators that do not depend explicitly on time, the equation of motion is simply $i\partial_t O(t) = \frac{1}{\hbar}[O(t), \mathcal{H}(t)]$.

In passing, it's worth noticing that the equation of motion for an operator in the Heisenberg picture is structurally equivalent to the evolution of the density operator in Schrödinger picture, apart for an opposite sign: this leads to the fact that ρ does not depend on time in Heisenberg representation.

D.1.3 Interaction picture

There is a third way of working out the problem of time evolution in quantum mechanics, known as Interaction picture. It is particularly useful as a tool to construct perturbative expansions. Suppose that we have an Hamiltonian of the form

$$\mathcal{H} = H + V(t), \tag{D.18}$$

where H is a time independent operator whose eigenstate and eigenvectors are known, while $V(t)$ includes the 'difficult' (i.e. non-diagonalizable), time dependent part of the Hamiltonian, that we will treat as a perturbation. In the interaction picture, we separate the well known time evolution due to H from the highly non-trivial one linked to $V(t)$. As a consequence, both state vectors and observables acquire time dependence. We start again from the expectation value of O at time t and rewrite it in the following manner:

$$\begin{aligned}
&\langle\phi(t_0)|\, U^\dagger(t,t_0)OU(t,t_0)\,|\phi(t_0)\rangle = \\
&\quad = \langle\phi(t_0)|\, U^\dagger(t,t_0)e^{-\frac{i}{\hbar}H(t-t_0)}e^{\frac{i}{\hbar}H(t-t_0)}Oe^{-\frac{i}{\hbar}H(t-t_0)}e^{\frac{i}{\hbar}H(t-t_0)}U(t,t_0)\,|\phi(t_0)\rangle = \\
&\quad = \left\langle \hat{\phi}(t)\right| \hat{O}(t) \left|\hat{\phi}(t)\right\rangle .
\end{aligned} \tag{D.19}$$

Here, we defined state vectors and observables in the interaction representation as[1]

$$\left|\hat{\phi}(t)\right\rangle = e^{\frac{i}{\hbar}H(t-t_0)}\,|\phi(t)\rangle = e^{\frac{i}{\hbar}H(t-t_0)}U(t,t_0)\,|\phi(t_0)\rangle = \hat{U}(t,t_0)\,|\phi(t_0)\rangle\,, \tag{D.20}$$

$$\hat{O}(t) = e^{\frac{i}{\hbar}H(t-t_0)}Oe^{-\frac{i}{\hbar}H(t-t_0)}, \tag{D.21}$$

with $\hat{U}(t,t_0) = e^{\frac{i}{\hbar}H(t-t_0)}U(t,t_0)$ the time evolution operator in the interaction representation. One immediately sees that observables are defined similarly to Heisenberg operators, but they evolve according to the unperturbed part of

[1] To avoid confusion, in this Appendix we denote every quantity in the interaction picture with a caret ($|\hat{\phi}\rangle$, $\hat{U}(t,t_0)$, ecc...).

the Hamiltonian only (that is, sH). In contrast, state vectors are sensitive to the perturbation $V(t)$ through the operator $\hat{U}(t,t_0)$. The equation of motion for $\hat{O}$ is $i\partial_t\hat{O} = \frac{1}{\hbar}[\hat{O},H]$, while $|\hat{\phi}\rangle$ evolves in accordance with [203]

$$\begin{aligned}
\partial_t \left|\hat{\phi}(t)\right\rangle &= \partial_t \left[e^{\frac{i}{\hbar}H(t-t_0)}\left|\phi(t)\right\rangle\right] = \\
&= \frac{i}{\hbar}e^{\frac{i}{\hbar}H(t-t_0)}H\left|\phi(t)\right\rangle + e^{\frac{i}{\hbar}H(t-t_0)}\partial_t\left|\phi(t)\right\rangle = \\
&= \frac{i}{\hbar}e^{\frac{i}{\hbar}H(t-t_0)}[H-\mathcal{H}(t)]\left|\phi(t)\right\rangle = \\
&= -\frac{i}{\hbar}e^{\frac{i}{\hbar}H(t-t_0)}V(t)e^{-\frac{i}{\hbar}H(t-t_0)}e^{\frac{i}{\hbar}H(t-t_0)}\left|\phi(t)\right\rangle = \\
&= -\frac{i}{\hbar}\hat{V}(t)\left|\hat{\phi}(t)\right\rangle . \qquad \text{(D.22)}
\end{aligned}$$

This means that time dependence of the state vector is determined solely by the perturbative sector of the Hamiltonian. We now derive an expression for the time evolution operator $\hat{U}$ suitable for perturbative calculations. From Eq. (D.22) we have

$$\partial_t\left|\hat{\phi}(t)\right\rangle = \partial_t\hat{U}(t,t_0)\left|\phi(t_0)\right\rangle = -\frac{i}{\hbar}\hat{V}(t)\hat{U}(t,t_0)\left|\phi(t_0)\right\rangle . \qquad \text{(D.23)}$$

We thus get the time derivative of $\hat{U}$, namely

$$\partial_t\hat{U}(t,t_0) = -\frac{i}{\hbar}\hat{V}(t)\hat{U}(t,t_0), \qquad \text{(D.24)}$$

that is very similar to Eq. (D.3). In analogy with Eq. (D.5) we get

$$\hat{U}(t,t_0) = \mathcal{T}\left[e^{-\frac{i}{\hbar}\int_{t_0}^{t}\hat{V}(t')dt'}\right] . \qquad \text{(D.25)}$$

Here, the crucial feature of the interaction picture is manifest: the time evolution operator contains only powers of the perturbation term $\hat{V}(t)$. This turns out to be very useful in constructing a perturbative expansion for the Green's functions. For the density operator we have

$$\begin{aligned}
\partial_t\hat{\rho}(t) &= \sum_n p_n\left[\left(\partial_t\left|\hat{\phi}_n(t)\right\rangle\right)\left\langle\hat{\phi}_n(t)\right| + \left|\hat{\phi}_n(t)\right\rangle\left(\partial_t\left\langle\hat{\phi}_n(t)\right|\right)\right] = \\
&= \sum_n p_n\left[-\frac{i}{\hbar}\hat{V}(t)\left|\hat{\phi}_n(t)\right\rangle\left\langle\hat{\phi}_n(t)\right| + \left|\hat{\phi}_n(t)\right\rangle\left\langle\hat{\phi}_n(t)\right|\frac{i}{\hbar}\hat{V}(t)\right] = \\
&= \frac{i}{\hbar}\left[\hat{\rho}(t),\hat{V}(t)\right] , \qquad \text{(D.26)}
\end{aligned}$$

and thus, recalling that the three pictures must be equivalent at the initial time t_0,

$$\hat{\rho}(t) = \hat{U}(t,t_0)\rho(t_0)\hat{U}^\dagger(t,t_0). \qquad \text{(D.27)}$$

Finally, we establish a bridge between operators in Heisenberg and interaction pictures:

$$\begin{aligned}\hat{O}(t) &= e^{\frac{i}{\hbar}H(t-t_0)}Oe^{-\frac{i}{\hbar}H(t-t_0)} = \\ &= e^{\frac{i}{\hbar}H(t-t_0)}U(t,t_0)U^\dagger(t,t_0)OU(t,t_0)U^\dagger(t,t_0)e^{-\frac{i}{\hbar}H(t-t_0)} = \\ &= \hat{U}(t,t_0)O(t)\hat{U}^\dagger(t,t_0),\end{aligned} \tag{D.28}$$

hence

$$O(t) = \hat{U}^\dagger(t,t_0)\hat{O}(t)\hat{U}(t,t_0). \tag{D.29}$$

It is worth noting that Eq. (D.29) generates the following perturbative expansion for the operator $O(t)$ in the Heisenberg picture

$$\begin{aligned}O(t) &= \widetilde{\mathcal{T}}\left[e^{\frac{i}{\hbar}\int_{t_0}^t \hat{V}(t')dt'}\right]\hat{O}(t)\mathcal{T}\left[e^{-\frac{i}{\hbar}\int_{t_0}^t \hat{V}(t')dt'}\right] = \\ &= \left\{\widetilde{\mathcal{T}}\left[1+\frac{i}{\hbar}\int_{t_0}^t dt'\hat{V}(t')+\frac{1}{2}\left(\frac{i}{\hbar}\right)^2\int_{t_0}^t\int_{t_0}^t dt'dt''\hat{V}(t')\hat{V}(t'')+\dots\right]\hat{O}(t)\times\right. \\ &\quad\left.\times\mathcal{T}\left[1-\frac{i}{\hbar}\int_{t_0}^t dt'\hat{V}(t')+\frac{1}{2}\left(-\frac{i}{\hbar}\right)^2\int_{t_0}^t\int_{t_0}^t dt'dt''\hat{V}(t')\hat{V}(t'')+\dots\right]\right\} = \\ &= \hat{O}(t)-\frac{i}{\hbar}\int_{t_0}^t dt'\left[\hat{O}(t),\hat{V}(t')\right]+ \\ &\quad+\left(-\frac{i}{\hbar}\right)^2\int_{t_0}^t\int_{t_0}^t dt'dt''\,\Theta(t'-t'')\left[\left[\hat{O}(t),\hat{V}(t')\right],\hat{V}(t'')\right]+\dots.\end{aligned} \tag{D.30}$$

One recovers the Kubo formula for linear response theory at first order in the perturbation [94]:

$$\begin{aligned}\langle O(t)\rangle &= \mathrm{Tr}\left[O(t)\rho(t_0)\right] = \\ &= \mathrm{Tr}\left[\hat{O}(t)\rho(t_0)\right]-\frac{i}{\hbar}\int_{t_0}^t dt'\,\mathrm{Tr}\left\{\left[\hat{O}(t),\hat{V}(t')\right]\rho(t_0)\right\}+o(V^2) = \\ &= \langle O(t)\rangle_0-\frac{i}{\hbar}\int_{t_0}^t dt'\left\langle\left[\hat{O}(t),\hat{V}(t')\right]\right\rangle_0+o(V^2),\end{aligned} \tag{D.31}$$

where the symbol $\langle\dots\rangle_0$ stands for expectation values with respect to $\rho(t_0)$, i.e. over an unperturbed ensemble.

D.2 Equilibrium Green's functions

The problem of equilibrium Green's function is generally stated as follows. We want to evaluate

$$G(x,t;x',t') = -i\left\langle\mathcal{T}[\psi(x,t)\psi^\dagger(x',t')]\right\rangle = -i\,\mathrm{Tr}\left\{\rho\mathcal{T}[\psi(x,t)\psi^\dagger(x',t')]\right\}, \tag{D.32}$$

where $\psi(x,t)$ and $\psi^\dagger(x',t')$ are fermionic operators in Heisenberg picture.[2] The $\mathcal{T}$ operator generates the following expression for G:

$$G(x,t;x',t') = -i\left\langle \psi(x,t)\psi^\dagger(x',t')\right\rangle \Theta(t-t') + i\left\langle \psi^\dagger(x',t')\psi(x,t)\right\rangle \Theta(t'-t). \tag{D.33}$$

We now write the field operators in the interaction picture using Eq. (D.29):

$$\begin{aligned}
&G(x,t;x',t') = \\
&\quad = -i\left\langle \hat{U}^\dagger(t,t_0)\hat{\psi}(x,t)\hat{U}(t,t_0)\hat{U}^\dagger(t',t_0)\hat{\psi}^\dagger(x',t')\hat{U}(t',t_0)\right\rangle \Theta(t-t') + \\
&\qquad + i\left\langle \hat{U}^\dagger(t',t_0)\hat{\psi}^\dagger(x',t')\hat{U}(t',t_0)\hat{U}^\dagger(t,t_0)\hat{\psi}(x,t)\hat{U}(t,t_0)\right\rangle \Theta(t'-t) = \\
&\quad = -i\left\langle \hat{U}^\dagger(t,t_0)\hat{\psi}(x,t)\hat{U}(t,t')\hat{\psi}^\dagger(x',t')\hat{U}(t',t_0)\right\rangle \Theta(t-t') + \\
&\qquad + i\left\langle \hat{U}^\dagger(t',t_0)\hat{\psi}^\dagger(x',t')\hat{U}(t',t)\hat{\psi}(x,t)\hat{U}(t,t_0)\right\rangle \Theta(t'-t).
\end{aligned} \tag{D.34}$$

In equilibrium perturbation theory, one usually considers the reference initial instant in the far past, $t_0 \to -\infty$. We assume that the system was initially unperturbed, and the term $V(t)$ was adiabatically switched on starting from the far past. Thus, inserting $U^\dagger(+\infty,t)U(+\infty,t) = I$ we can rewrite G as

$$\begin{aligned}
&G(x,t;x',t') = \\
&\quad = -i\left\langle \hat{U}^\dagger(t,-\infty)U^\dagger(+\infty,t)U(+\infty,t)\hat{\psi}(x,t)\hat{U}(t,t')\hat{\psi}^\dagger(x',t')\hat{U}(t',-\infty)\right\rangle \times \\
&\qquad \times \Theta(t-t') + \\
&\qquad + i\left\langle \hat{U}^\dagger(t',-\infty)U^\dagger(+\infty,t')U(+\infty,t')\hat{\psi}^\dagger(x',t')\hat{U}(t',t)\hat{\psi}(x,t)\hat{U}(t,-\infty)\right\rangle \times \\
&\qquad \times \Theta(t'-t) = \\
&\quad = -i\left\langle \hat{U}(-\infty,+\infty)\mathcal{T}[\hat{\psi}(x,t)\hat{\psi}^\dagger(x',t')\hat{U}(+\infty,-\infty)]\right\rangle,
\end{aligned} \tag{D.35}$$

where we used the fact that each term in $U(+\infty,-\infty)$ acts in the proper order under the $\mathcal{T}$ operator. Here the physical structure of the term

$$\mathcal{T}[\hat{\psi}(x,t)\hat{\psi}^\dagger(x',t')\hat{U}(+\infty,-\infty)] \tag{D.36}$$

is evident. Let us assume, for example, $t > t'$. We start the time evolution from $t_0 = -\infty$ and propagate up to the time t' where we find the field $\hat{\psi}^\dagger(x',t')$. The operator $U(t,t')$ then brings us to time t, corresponding to the field $\hat{\psi}(x,t)$. Finally we travel all the way up to $+\infty$ through the action of $U(+\infty,t)$.

Let us now assume an equilibrium configuration at zero temperature. We are thus evaluating the expectation value with respect to the ground state $|GS\rangle$ of H at $t_0 = -\infty$ (remember that the perturbation is absent at $t_0 = -\infty$, and

[2] Here we are considering the case of fermionic operators, but the present formalism applies to the bosonic case as well.

we know the eigenstates of H). We have

$$G(x,t;x',t') = \\ = -i \langle GS(-\infty)| \hat{U}(-\infty,+\infty)\mathcal{T}[\hat{\psi}(x,t)\hat{\psi}^\dagger(x',t')\hat{U}(+\infty,-\infty)] |GS(-\infty)\rangle . \tag{D.37}$$

Now the crucial assumption comes. We assume that the perturbation is adiabatically switched *on and off*, that is, the Hamiltonian is of the form $\mathcal{H} = H + e^{-\varepsilon|t|}V(t)$ with $\varepsilon \to 0$. Under this condition, the adiabatic theorem ensures that the system will stay in the ground state even at $t \to +\infty$, acquiring at most a phase factor $e^{i\gamma}$ [96]. We can write

$$U(+\infty,-\infty)\,|GS(-\infty)\rangle = |GS(+\infty)\rangle = e^{i\gamma}\,|GS(-\infty)\rangle\,, \tag{D.38}$$

with $e^{i\gamma} = \langle GS(-\infty)|GS(+\infty)\rangle = \langle GS(-\infty)|U(+\infty,-\infty)|GS(-\infty)\rangle$. Finally, denoting $|GS(-\infty)\rangle$ with $|G_0\rangle$ for simplicity, we obtain

$$G(x,t;x',t') = -i\frac{\langle G_0|\,\mathcal{T}[\hat{\psi}(x,t)\hat{\psi}^\dagger(x',t')\hat{U}(+\infty,-\infty)]\,|G_0\rangle}{\langle G_0|U(+\infty,-\infty)|G_0\rangle}, \tag{D.39}$$

that is a nice expression suitable for a perturbative expansion. We can now apply Wick's theorem to work out the Feynman diagrams allowed by the perturbation $V(t)$.

This procedure seems very reasonable in high energy physics, where one deals with unperturbed free particle states both at $t_0 = -\infty$ and $t \to +\infty$. Perturbation acts only for intermediate times, when particles collide with each other. However this picture immediately fails if we try to apply similar methods to out-of-equilibrium configurations, as we can see from a fundamental example. In the context of condensed matter physics, for instance, the simplest non-equilibrium setup we may run into is the following: two tunnel-coupled systems driven out of equilibrium with an external voltage (which is exactly the kind of system we are inspecting in this thesis). Here the adiabatic switching on seems to be reasonable, but the perturbation is *never switched off*. Usually we are interested in a steady state solution for out-of-equilibrium systems, and this means that we are looking for a solution where the perturbation is still acting at $t \to +\infty$. It is clear that Eq. (D.38) does not hold anymore in this regime. Moreover, the Gell-Mann and Low theorem holds only for the ground state, while in condensed matter we often deals with a finite temperature, and states other than the ground state may be involved in calculations. How can we bypass these limitation? A clever solution was firstly pointed out by J. Schwinger and L.V. Keldysh and will be developed in the next section [204, 205].

D.3 Non-equilibrium Green's functions: closed time contour

Let us have a deeper look at Eq. (D.35). What does its intrinsic structure suggest? We start from $t_0 = -\infty$ and evolve all the way up to $t \to +\infty$, counting every field operator featuring in the Green's function of interest. Then, operator $U(-\infty, +\infty)$ brings us back to $t_0 = -\infty$. Schwinger thus proposed to introduce a new time-ordering operator T_{K} whose action is defined along the time contour c_{K} extending from $-\infty$ to $+\infty$ and then back to $-\infty$ (see Fig. D.1). The operator T_{K} orders time variables along the contour c_{K}, so that times along the backward portion of c_{K} are always greater (in the contour sense) than times on the forward segment, independently of their real values. We can now include $U(-\infty, +\infty)$ under the new time-ordering operator and write the Green's function in Eq. (D.35) as

$$G(x,t;x',t') = -i \left\langle T_{\mathrm{K}}[\hat{\psi}(x,t)\hat{\psi}^{\dagger}(x',t')S(-\infty,-\infty)] \right\rangle , \tag{D.40}$$

with $S(-\infty,-\infty) = T_{\mathrm{K}} \exp\left[-i \int_{c_{\mathrm{K}}} d\tau \hat{V}(\tau)\right]$. We have recovered a good starting point for a perturbative expansion even in the finite temperature case, since now we can evaluate expectation values on statistical ensembles as

$$G(x,t;x',t') = -i \,\mathrm{Tr}\left\{ \rho(-\infty) T_{\mathrm{K}} \left[\hat{\psi}(x,t)\hat{\psi}^{\dagger}(x',t')S(-\infty,-\infty) \right] \right\}, \tag{D.41}$$

with $\rho(-\infty) = Z^{-1} e^{-\beta H}$ the equilibrium density matrix in the far past (remember that the *adiabatic switching on* assumption still holds, and states in the far past are at equilibrium!). One just needs to avoid any reference to the asymptotic future, rewinding the time contour back to the past.

As shown in Fig. D.1, it is customary to split the time contour in two branches, namely C_+ and C_-, accounting for the forward and backward evolution respectively. One can then label each time variable with an index $\eta = \{+,-\}$ and write

$$\begin{aligned} G^{\eta,\eta'}(x,t;x',t') &= G(x,t^{\eta};x',t'^{\eta'}) = \\ &= -i \sum_{\eta} \left\langle T_{\mathrm{K}}[\hat{\psi}(x,t^{\eta})\hat{\psi}^{\dagger}(x',t'^{\eta'}) e^{-i\eta'' \int_{-\infty}^{+\infty} d\tau \hat{V}(\tau^{\eta''})}] \right\rangle . \end{aligned} \tag{D.42}$$

It is clear that the Green's function (D.42) has now the structure of a 2×2 matrix. However, each entry of the matrix is related to the following real-time Green's functions:

$$G^{>}(x,t;x',t') = -i \left\langle \psi(x,t)\psi^{\dagger}(x',t') \right\rangle , \tag{D.43a}$$

$$G^{<}(x,t;x',t') = i \left\langle \psi^{\dagger}(x',t')\psi(x,t) \right\rangle , \tag{D.43b}$$

$$G^{T}(x,t;x',t') = \Theta(t-t')G^{>}(x,t;x',t') + \Theta(t'-t)G^{<}(x,t;x',t'), \tag{D.43c}$$

$$G^{\tilde{T}}(x,t;x',t') = \Theta(t'-t)G^{>}(x,t;x',t') + \Theta(t-t')G^{<}(x,t;x',t'). \tag{D.43d}$$

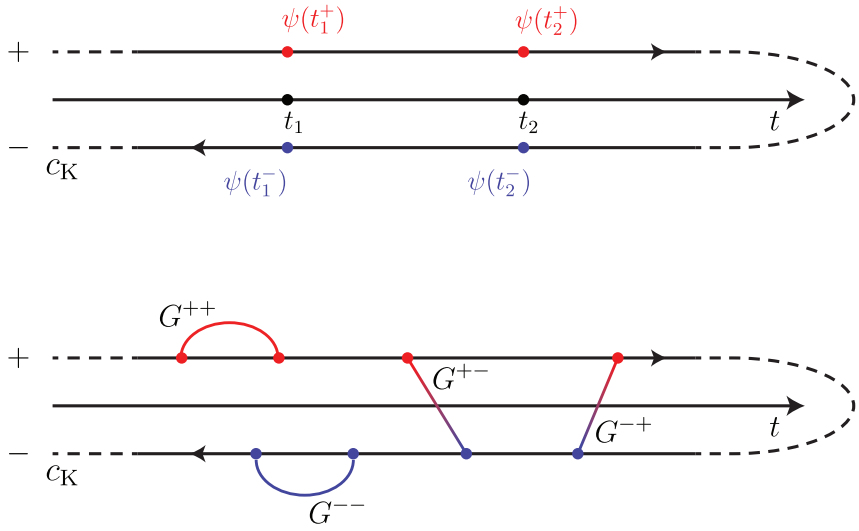

Figure D.1: Schwinger-Keldysh contour and time-ordering. Time variables are labeled with $\eta = \{+, -\}$ according to the branch of the contour they lie on (forward or backward). Accordingly, Green's functions acquire a 2×2 matrix structure in the space of contour labels.

Indeed, when both time variables lie on C_+ (that is, $\eta = \eta' = +$) we recover the usual time-ordered Green's function G^T, while $\eta = \eta' = -$ gives rise to the anti-time-ordered function $G^{\tilde{T}}$, since time on C_- flows from $+\infty$ to $-\infty$. Mixed terms $(\eta, \eta') = (+, -)$ and $(-, +)$ correspond, respectively, to the lesser and greater Green's function $G^<$ and $G^>$, since T_{K} automatically orders times on C_- ahead of times on C_+. In a compact matrix form we can write

$$\begin{aligned} G(x,t;x',t') &= \begin{pmatrix} G^{++}(x,t;x',t') & G^{+-}(x,t;x',t') \\ G^{-+}(x,t;x',t') & G^{--}(x,t;x',t') \end{pmatrix} = \\ &= \begin{pmatrix} G^{T}(x,t;x',t') & G^{<}(x,t;x',t') \\ G^{>}(x,t;x',t') & G^{\tilde{T}}(x,t;x',t') \end{pmatrix}. \end{aligned} \tag{D.44}$$

As a final remark, we note that the majority of the Schwinger-Keldysh contour is somewhat unnecessary. If we know that the system at the finite time t_0 is described by the equilibrium density matrix $\rho(t_0)$, we can simply write

$$G(x,t;x',t') = -i \left\langle T_{\mathrm{K}}[\hat{\psi}(x,t)\hat{\psi}^\dagger(x',t')S(t_0,t_0)] \right\rangle, \tag{D.45}$$

where the contour extends from t_0 to $\max\{t,t'\}$ and then back to t_0, as in Fig. D.2. This is exact, since the evolution from $\max\{t,t'\}$ to $+\infty$ and from $+\infty$ to $\max\{t,t'\}$ does not give any significant contribution (there are no additional fields from $\max\{t,t'\}$ on).

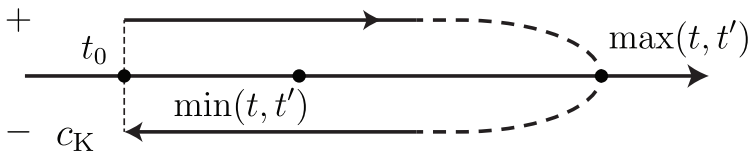

Figure D.2: Closed Schwinger-Keldysh contour.

Appendix E

Bosonic correlation function

The present Appendix deals with the calculation of the bosonic correlation function

$$\mathcal{G}_{R/L}(x,t) = \langle \phi_{R/L}(x,t)\phi_{R/L}(0,0) - \phi^2_{R/L}(0,0)\rangle, \tag{E.1}$$

where field operators $\phi_{R/L}(x,t)$ are obtained from the chiral time evolution of $\Phi_{R/L}(x)$ given in Eq. (3.56) of the main text and read

$$\phi_{R/L}(x,t) = i\sqrt{\frac{2\pi}{L}}\sum_{k>0}\frac{e^{-ak/2}}{\sqrt{k}}\left[e^{-ik(vt\mp x)}b_{R/L,k} - e^{ik(vt\mp x)}b^\dagger_{R/L,k}\right]. \tag{E.2}$$

The upper sign refers to the right-moving edge, while the lower sign is for the left-moving mode. The free Hamiltonian for bosonic chiral fields has a linear spectrum with velocity v,

$$H = \frac{v}{4\pi}\int dx\Big[(\partial_x\phi_R)^2 + (\partial_x\phi_L)^2\Big] = \sum_{k>0} vk b^\dagger_{R,k}b_{R,k} + \sum_{k>0} vk b^\dagger_{L,k}b_{L,k}, \tag{E.3}$$

and bosonic occupation numbers are thus distributed according to the Bose-Einstein distribution function

$$\langle b^\dagger_{R/L,k}b_{R/L,k'}\rangle = \frac{\delta_{k,k'}}{e^{\beta vk}-1}, \tag{E.4}$$

with $\beta = 1/\theta$ the inverse temperature (and $k_B = 1$). Note that we have neglected terms $\sim 1/L$ in Eq. (E.3), since we are assuming an infinite edge.

It's easy to check that the following equalities hold:

$$\langle\phi_{R/L}(0,0)\phi_{R/L}(0,0)\rangle = \frac{2\pi}{L}\sum_{q>0}\frac{e^{-aq}}{q}\left(\frac{2}{e^{\beta vq}-1}+1\right), \tag{E.5}$$

$$\langle\phi_{R/L}(x,t)\phi_{R/L}(0,0)\rangle = \frac{2\pi}{L}\sum_{q>0}\frac{e^{-aq}}{q}\left[e^{-iq(vt\mp x)}\left(\frac{1}{e^{\beta vq}-1}+1\right)+\frac{e^{iq(vt\mp x)}}{e^{\beta vq}-1}\right]. \tag{E.6}$$

In the limit of infinite edge, $L\to\infty$, we transform the sum into an integral through the substitution $\sum_{q>0}\to\int_0^\infty \frac{L}{2\pi}dq$ and get

$$\mathcal{G}_{R/L}(x,t) = \int_0^\infty dq\frac{e^{-aq}}{q}\frac{1}{e^{\beta vq}-1}\left[e^{\beta vq}e^{-iq(vt\mp x)}+e^{iq(vt\mp x)}-(e^{\beta vq}+1)\right]. \tag{E.7}$$

We notice that space and time coordinates appear only through the chiral combination $vt\mp x$. Thus, we can write both the right and left moving correlation functions in terms of a new function $\mathcal{G}(z)$ of one single variable. We have $\mathcal{G}_{R/L}(x,t)=\mathcal{G}\left(t\mp\frac{x}{v}\right)$, with $\mathcal{G}(z)$ given by

$$\mathcal{G}(z) = \int_0^\infty \frac{d\omega}{\omega}e^{-\omega/\omega_c}\left[\frac{1}{\tanh\beta\omega/2}(\cos\omega z-1)-i\sin\omega z\right], \tag{E.8}$$

where we introduced the high energy cutoff $\omega_c=\frac{v}{a}$. It's useful to isolate two terms in $\mathcal{G}$ representing the zero temperature and finite temperature contributions, denoted with $\mathcal{G}^{(0)}$ and $\mathcal{G}^{(\beta)}$ respectively. They are given by

$$\mathcal{G}^{(0)}(z) = \int_0^\infty \frac{d\omega}{\omega}e^{-\omega/\omega_c}(e^{-i\omega z}-1), \tag{E.9}$$

$$\mathcal{G}^{(\beta)}(z) = \int_0^\infty \frac{d\omega}{\omega}e^{-\omega/\omega_c}\left(\frac{1}{\tanh\beta\omega/2}-1\right)(\cos\omega z-1). \tag{E.10}$$

We observe that $\mathcal{G}^{(\beta)}$ is indeed a finite temperature contribution, since it vanishes for $\theta\to 0$:

$$\lim_{\theta\to 0}\left(\frac{1}{\tanh\beta\omega/2}-1\right) = \lim_{\beta\to+\infty}\left(\frac{e^{\beta\omega/2}+e^{-\beta\omega/2}}{e^{\beta\omega/2}-e^{-\beta\omega/2}}-1\right)=0. \tag{E.11}$$

Consider now the zero-temperature contribution $\mathcal{G}^{(0)}$. Writing the exponential as a power series we obtain

$$\mathcal{G}^{(0)}(z) = \int_0^\infty d\omega\, e^{-\omega/\omega_c}\sum_{n=1}^\infty\frac{(-iz)^n\omega^{n-1}}{n!} = \sum_{n=1}^\infty\frac{(-i\omega_c z)^n}{n} = -\ln(1+i\omega_c z), \tag{E.12}$$

where we resorted to the integral representation of the Gamma function,

$$\Gamma(x) = \int_0^\infty u^{x-1}e^{-u}du, \tag{E.13}$$

and to the Taylor series for the logarithm,

$$\ln(1-x) = -\sum_{n=1}^{\infty} \frac{x^n}{n}. \tag{E.14}$$

The finite temperature contribution necessitates of some additional algebra. As a first step, we re-elaborate $\mathcal{G}^{(\beta)}$ as follows:

$$\begin{aligned}\mathcal{G}^{(\beta)}(z) = \int_0^{\infty} du \frac{u^{-1}}{1-e^{-u}} \Bigg\{ \exp\left[-u\left(1+\frac{1}{\beta\omega_c} - \frac{iz}{\beta}\right)\right] + \\ + \exp\left[-u\left(1+\frac{1}{\beta\omega_c} + \frac{iz}{\beta}\right)\right] - 2\exp\left[-u\left(1+\frac{1}{\beta\omega_c}\right)\right]\Bigg\}.\end{aligned} \tag{E.15}$$

The latter expression corresponds to the limit

$$\begin{aligned}\mathcal{G}^{(\beta)}(z) = \lim_{s\to 0}\Gamma(s)\Bigg[\zeta\left(s, 1+\frac{1}{\beta\omega_c} - \frac{iz}{\beta}\right) + \\ +\zeta\left(s, 1+\frac{1}{\beta\omega_c} + \frac{iz}{\beta}\right) - 2\zeta\left(s, 1+\frac{1}{\beta\omega_c}\right)\Bigg],\end{aligned} \tag{E.16}$$

where we recognized the integral representation of the Hurwitz Zeta function, given by [80]

$$\zeta(s,q) = \frac{1}{\Gamma(s)}\int_0^{\infty} \frac{u^{s-1}e^{-uq}}{1-e^{-u}} du. \tag{E.17}$$

We then expand the functions $\Gamma(s)$ and $\zeta(s,q)$ around $s=0$. The leading terms are

$$\Gamma(s) \approx \frac{1}{s}, \tag{E.18}$$

$$\zeta(s,q) \approx \frac{1}{2} - q + \left(\ln\Gamma(q) - \frac{\ln 2\pi}{2}\right). \tag{E.19}$$

Substituting into Eq. (E.16) we obtain

$$\mathcal{G}^{(\beta)}(z) = \ln\left[\Gamma\left(1+\frac{1}{\beta\omega_c} - \frac{iz}{\beta}\right)\Gamma\left(1+\frac{1}{\beta\omega_c} + \frac{iz}{\beta}\right)\right] - \ln\left[\Gamma\left(1+\frac{1}{\beta\omega_c}\right)\right]^2. \tag{E.20}$$

From the integral representation of the Gamma function, Eq. (E.13), it's immediate to verify that the following property holds true:

$$\Gamma(x)\Gamma(x^*) = \Gamma(x)\Gamma^*(x) = |\Gamma(x)|^2. \tag{E.21}$$

Thus, we can write the finite temperature contribution $\mathcal{G}^{(\beta)}$ in the compact expression

$$\mathcal{G}^{(\beta)}(z) = \ln\frac{\left|\Gamma\left(1+\frac{1}{\beta\omega_c} - \frac{iz}{\beta}\right)\right|^2}{\Gamma^2\left(1+\frac{1}{\beta\omega_c}\right)}. \tag{E.22}$$

Recasting together the two contributions in Eqs. (E.12) and (E.22), we obtain the full expression for $\mathcal{G}$. It reads

$$\mathcal{G}(z) = \ln \frac{\left|\Gamma\left(1+\frac{1}{\beta\omega_c}-\frac{iz}{\beta}\right)\right|^2}{\Gamma^2\left(1+\frac{1}{\beta\omega_c}\right)(1+i\omega_c z)}. \tag{E.23}$$

Since ω_c is the high-energy cutoff (and thus the largest energy scale involved in any calculation), we will always work in the limit $\beta\omega_c \gg 1$. In this regime we can use the identity

$$|\Gamma(1+iy)|^2 = \frac{\pi y}{\sinh(\pi y)}, \quad y \in \mathbb{R}, \tag{E.24}$$

so that the bosonic correlation function at finite temperature finally takes the form

$$\mathcal{G}(z) = \ln\left[\frac{\pi\theta z}{\sinh(\pi\theta z)}\frac{1}{1+i\omega_c z}\right]. \tag{E.25}$$

In terms of the original right and left moving modes we have

$$\mathcal{G}_{R/L}(x,t) = \mathcal{G}\left(t \mp \frac{x}{v}\right) = \ln\left\{\frac{\pi\theta\left(t\mp\frac{x}{v}\right)}{\sinh\left[\pi\theta\left(t\mp\frac{x}{v}\right)\right]}\frac{1}{1+i\omega_c\left(t\mp\frac{x}{v}\right)}\right\}. \tag{E.26}$$

It's evident from the above equation that correlation functions at $x = 0$ are equal, namely $\mathcal{G}_R(0,t) = \mathcal{G}_L(0,t) = \mathcal{G}(t)$.

Appendix $\mathcal{F}$

Fourier transform of the Green's function

Here we calculate the Fourier transform $\hat{P}_g(E)$ of the function $P_g(t) = e^{g\mathcal{G}(t)}$, and show some useful properties of $\hat{P}_g(E)$. The Fourier transform is defined as

$$\hat{P}_g(E) = \int_{-\infty}^{+\infty} dt\, e^{iEt} P_g(t), \tag{F.1}$$

with inverse transform given by

$$P_g(t) = \frac{1}{2\pi} \int_{-\infty}^{+\infty} dE\, e^{-iEt} \hat{P}_g(E). \tag{F.2}$$

The function $P_g(t)$, which is essentially the Green's function for electron and quasiparticle fields (depending on the value of the parameter g), is given by

$$P_g(t) = \left(\frac{\left|\Gamma\left(1 + \frac{1}{\beta\omega_c} - \frac{it}{\beta}\right)\right|^2}{\Gamma^2\left(1 + \frac{1}{\beta\omega_c}\right)(1 + i\omega_c t)} \right)^g. \tag{F.3}$$

First, it is convenient to rewrite the argument of $P_g(t)$ as

$$\frac{\left|\Gamma\left(1 + \frac{1}{\beta\omega_c} - \frac{it}{\beta}\right)\right|^2}{\Gamma^2\left(1 + \frac{1}{\beta\omega_c}\right)(1 + i\omega_c t)} = \frac{\Gamma\left(\frac{1}{\beta\omega_c} + \frac{it}{\beta}\right)\Gamma\left(1 + \frac{1}{\beta\omega_c} - \frac{it}{\beta}\right)}{\beta\omega_c \Gamma^2\left(1 + \frac{1}{\beta\omega_c}\right)}, \tag{F.4}$$

thanks to the recurrence relation $\Gamma(1 + z) = z\Gamma(z)$ of the Gamma function [80]. We then make the change of variable $t' = t - i\beta/2$ in the definition of $\hat{P}_g(E)$, Eq. (F.1). Let us notice that this would generate an imaginary part in the limits of the integral, which now reads $\int_{-\infty - i\beta/2}^{+\infty - i\beta/2} dt' \ldots$. This is however

identical to a simple integration along the real axis, as one can readily verify by choosing a suitable contour in the complex plane and exploiting the Cauchy theorem [109–111]. We obtain

$$\hat{P}_g(E) = \int_{-\infty}^{+\infty} dt' \, e^{iEt'} e^{E\beta/2} \left[\frac{\Gamma\left(\frac{1}{2} + \frac{1}{\beta\omega_c} + \frac{it'}{\beta}\right) \Gamma\left(\frac{1}{2} + \frac{1}{\beta\omega_c} - \frac{it'}{\beta}\right)}{\beta\omega_c \Gamma^2\left(1 + \frac{1}{\beta\omega_c}\right)} \right]^g , \quad \text{(F.5)}$$

which in the limit $\beta\omega_c \gg 1$ becomes

$$\hat{P}_g(E) = \int_{-\infty}^{+\infty} dt \, e^{iEt} e^{E\beta/2} \left[\frac{\Gamma\left(\frac{1}{2} + \frac{it}{\beta}\right) \Gamma\left(\frac{1}{2} - \frac{it}{\beta}\right)}{\beta\omega_c} \right]^g . \quad \text{(F.6)}$$

We now note that the Gamma function satisfies the property [80]

$$\Gamma\left(\frac{1}{2} + iy\right) \Gamma\left(\frac{1}{2} - iy\right) = \frac{\pi}{\cosh \pi y}, \quad \text{(F.7)}$$

which allows to rewrite $\hat{P}_g(E)$ as

$$\hat{P}_g(E) = \int_{-\infty}^{+\infty} dt \, e^{\beta E/2} (\cos Et + i \sin Et) \left[\frac{\pi}{\beta\omega_c \cosh(\pi t/\beta)} \right]^g . \quad \text{(F.8)}$$

Both $\cos(Et)$ and $\cosh(\pi t/\beta)$ are even functions of the variable t, while $\sin(Et)$ is odd. Thus, we are only left with

$$\hat{P}_g(E) = 2e^{\beta E/2} \int_0^{+\infty} dt \cos Et \left[\frac{\pi}{\beta\omega_c \cosh(\pi t/\beta)} \right]^g . \quad \text{(F.9)}$$

We can perform the integral in Eq. (F.9) exploiting two changes of variable, in such a way to connect Eq. (F.9) to the Euler Beta function $\mathcal{B}(z, w)$. An integral representation of $\mathcal{B}(z, w)$ is given by [80]

$$\mathcal{B}(z, w) = \int_0^1 dt \, t^{z-1} (1 - t)^{w-1}. \quad \text{(F.10)}$$

First, we introduce the new variable $z = e^{-\pi t/\beta}$, by which Eq. (F.9) becomes

$$\hat{P}_g(E) = \frac{2}{\omega_c} e^{\beta E/2} \left(\frac{2\pi}{\beta\omega_c} \right)^{g-1} \int_0^1 dz \, z^{g-1} \frac{z^{-iE\beta/\pi} + z^{iE\beta/\pi}}{(1 + z^2)^g}. \quad \text{(F.11)}$$

Then, we perform the second substitution $s = \frac{z^2}{z^2+1}$ (i.e. $1 - s = \frac{1}{z^2+1}$) which leads to

$$\hat{P}_g(E) = \left(\frac{2\pi}{\beta\omega_c} \right)^{g-1} \frac{e^{\beta E/2}}{\omega_c} \int_0^{1/2} ds \times \\ \times \left[s^{\frac{g}{2}-1+i\frac{E\beta}{2\pi}} (1 - s)^{\frac{g}{2}-1-i\frac{E\beta}{2\pi}} + s^{\frac{g}{2}-1-i\frac{E\beta}{2\pi}} (1 - s)^{\frac{g}{2}-1+i\frac{E\beta}{2\pi}} \right]. \quad \text{(F.12)}$$

The last equation is very similar to the integral representation of the Euler Beta function, Eq. (F.10). We only need to substitute the variable s in the second term of Eq. (F.12) with $s' = 1 - s$. We finally get

$$\begin{aligned}\hat{P}_g(E) &= \left(\frac{2\pi}{\beta\omega_c}\right)^{g-1} \frac{e^{\beta E/2}}{\omega_c} \int_0^1 ds\, s^{\frac{g}{2}+i\frac{E\beta}{2\pi}-1}(1-s)^{\frac{g}{2}-i\frac{E\beta}{2\pi}-1} = \\ &= \left(\frac{2\pi}{\beta\omega_c}\right)^{g-1} \frac{e^{\beta E/2}}{\omega_c} \mathcal{B}\left(\frac{g}{2}+\frac{iE\beta}{2\pi}, \frac{g}{2}-\frac{iE\beta}{2\pi}\right). \end{aligned} \tag{F.13}$$

We notice that the order of the arguments z and w in the Beta function $\mathcal{B}(z,w)$ is irrelevant, as $\mathcal{B}(z,w) = \mathcal{B}(w,z)$. One can easily check this starting from Eq. (F.10) and introducing again the variable $s' = 1 - s$. Moreover, $\mathcal{B}(z,w)$ has a simple representation in terms of the Gamma function, namely

$$\mathcal{B}(z,w) = \frac{\Gamma(z)\Gamma(w)}{\Gamma(z+w)}. \tag{F.14}$$

Then, $\hat{P}_g(E)$ can be written in the simpler form

$$\hat{P}_g(E) = \left(\frac{2\pi}{\beta\omega_c}\right)^{g-1} \frac{e^{\beta E/2}}{\Gamma(g)\omega_c} \left|\Gamma\left(\frac{g}{2}+\frac{iE\beta}{2\pi}\right)\right|^2. \tag{F.15}$$

The detailed balance relation is now manifest, since one immediately finds $\hat{P}_g(-E) = e^{-\beta E}\hat{P}_g(E)$ from Eq. (F.15). However, one should notice that we resorted to the limit $\beta\omega_c \gg 1$ at the beginning of the calculation. For completeness we will also give a general proof of the detailed balance relation in Sec. F.2, regardless of the value of $\beta\omega_c$. We also quote the zero temperature limit of Eq. (F.15), which is readily obtained from the asymptotic expansion $|\Gamma(x+iy)| \sim \sqrt{2\pi}|y|^{x-1/2}e^{-\pi|y|/2}$, valid for $y \to \pm\infty$ [80]. For $\theta \to 0$ (that is, $\beta \to \infty$) the function $\hat{P}_g(E)$ reads

$$\hat{P}_g(E) = \frac{2\pi}{\Gamma(g)\omega_c^g} E^{g-1}\Theta(E). \tag{F.16}$$

Finally, it's useful to notice that $\hat{P}_g(E)$ is linked to the Fermi distribution multiplied by an effective tunneling density of states. Indeed, introducing $n_F(E) = 1/(e^{\beta E}+1)$, we have $\hat{P}_g(E) = \mathcal{D}_g(E)n_F(-E)$ with

$$\mathcal{D}_g(E) = \frac{(2\pi)^g}{\Gamma(g)\omega_c}\left(\frac{\theta}{\omega_c}\right)^{g-1} \frac{\left|\Gamma\left(\frac{g}{2}-i\frac{E}{2\pi\theta}\right)\right|^2}{\left|\Gamma\left(\frac{1}{2}-i\frac{E}{2\pi\theta}\right)\right|^2}. \tag{F.17}$$

F.1 Useful properties

Here we demonstrate some useful properties of $\hat{P}_g(E)$ used in the main text.

Prop. 1

$$\boxed{\int \frac{dE}{2\pi}\hat{P}_{g_1}(E)\hat{P}_{g_2}(\omega - E) = \hat{P}_{g_1+g_2}(\omega).} \tag{F.18}$$

This is basically the energy-space counterpart of $P_{g_1}(t)P_{g_2}(t) = P_{g_1+g_2}(t)$, that follows directly from the definition of $P_g(t) = e^{g\mathcal{G}(t)}$. The proof is given here below:

$$\begin{aligned}\int \frac{dE}{2\pi}\hat{P}_{g_1}(E)\hat{P}_{g_2}(\omega - E) &= \int \frac{dE}{2\pi}\int dt \int dt' e^{iEt}e^{i(\omega-E)t'}P_{g_1}(t)P_{g_2}(t') = \\ &= \int dt\, e^{i\omega t}P_{g_1}(t)P_{g_2}(t) = \\ &= \int dt\, e^{i\omega t}P_{g_1+g_2}(t) = \\ &= \hat{P}_{g_1+g_2}(\omega). \end{aligned} \tag{F.19}$$

Prop. 2

$$\boxed{\int \frac{dE}{2\pi}E\hat{P}_{g_1}(E)\hat{P}_{g_2}(\omega - E) = \frac{g_1}{g_1+g_2}\omega\hat{P}_{g_1+g_2}(\omega).} \tag{F.20}$$

This second property comes from $[\partial_t P_{g_1}(t)]P_{g_2}(t) = \frac{g_1}{g_1+g_2}\partial_t P_{g_1+g_2}(t)$. Indeed, since the Fourier transform of $\partial_t P_g(t)$ is $-iE\hat{P}_g(E)$, we have

$$\begin{aligned}\int \frac{dE}{2\pi}E\hat{P}_{g_1}(E)\hat{P}_{g_2}(\omega - E) &= i\int \frac{dE}{2\pi}\int dt \int dt' e^{iEt}e^{i(\omega-E)t'}\left[\partial_t P_{g_1}(t)\right]P_{g_2}(t') = \\ &= i\int dt\, e^{i\omega t}[\partial_t P_{g_1}(t)]P_{g_2}(t) = \\ &= i\int dt\, e^{i\omega t}\frac{g_1}{g_1+g_2}\partial_t P_{g_1+g_2}(t) = \\ &= \frac{g_1}{g_1+g_2}\omega\hat{P}_{g_1+g_2}(\omega). \end{aligned} \tag{F.21}$$

Prop. 3 and Prop. 4.

$$\boxed{\int \frac{dE}{2\pi}\hat{P}_{g_1}\left(E+\frac{\omega}{2}\right)\hat{P}_{g_2}\left(\frac{\omega}{2}-E\right) = \hat{P}_{g_1+g_2}(\omega)} \tag{F.22}$$

$$\boxed{\int \frac{dE}{2\pi}E\hat{P}_{g_1}\left(E+\frac{\omega}{2}\right)\hat{P}_{g_2}\left(\frac{\omega}{2}-E\right) = \frac{\omega}{2}\frac{g_1-g_2}{g_1+g_2}\hat{P}_{g_1+g_2}(\omega).} \tag{F.23}$$

They both follow from the substitution $E' = E - \omega/2$ in Prop. 1 and Prop. 2.

Prop. 5

$$\boxed{\int_{-\infty}^{+\infty}\frac{dE}{2\pi}E^2\hat{P}_{g_1}(E)\hat{P}_{g_2}(\omega - E) = \frac{\hat{P}_{g_1+g_2}(X)}{1+g_1+g_2}\left[g_1g_2\pi^2\theta^2 + \frac{g_1(1+g_1)}{g_1+g_2}\omega^2\right].} \tag{F.24}$$

This can be proved using the Barnes' Beta Integral [80]

$$\int_{-\infty}^{+\infty}\frac{dt}{2\pi}\Gamma(a+it)\Gamma(b+it)\Gamma(c-it)\Gamma(d-it)=\frac{\Gamma(a+c)\Gamma(a+d)\Gamma(b+c)\Gamma(b+d)}{\Gamma(a+b+c+d)}. \tag{F.25}$$

In particular, we massage Eq. (F.24) a little bit in such a way to match the four Gamma functions in the Barnes' Beta Integral. This can be done by writing E^2 as

$$\begin{aligned}E^2&=(2\pi\theta)^2\left[\left(\frac{g_1}{2}\right)^2-\left(i\frac{E}{2\pi\theta}\right)^2-\left(\frac{g_1}{2}\right)^2\right]=\\&=(2\pi\theta)^2\left[\left(\frac{g_1}{2}+i\frac{E}{2\pi\theta}\right)\left(\frac{g_1}{2}-i\frac{E}{2\pi\theta}\right)-\frac{g_1^2}{4}\right].\end{aligned} \tag{F.26}$$

We also exploit the recurrence formula $\Gamma(1+z)=z\Gamma(z)$ and Prop. 1 to obtain

$$\begin{aligned}&\int_{-\infty}^{+\infty}\frac{dE}{2\pi}E^2\hat{P}_{g_1}(E)\hat{P}_{g_2}(\omega-E)=\\&=\left(\frac{2\pi\theta}{\omega_c}\right)^{g_1+g_2}\frac{e^{\omega/2\theta}}{\Gamma(g_1)\Gamma(g_2)}\int\frac{dE}{2\pi}\left|\Gamma\left(1+\frac{g_1}{2}+i\frac{E}{2\pi\theta}\right)\right|^2\left|\Gamma\left(\frac{g_2}{2}+i\frac{\omega-E}{2\pi\theta}\right)\right|^2+\\&\quad-\frac{g_1^2}{4}(2\pi\theta)^2\hat{P}_{g_1+g_2}(\omega).\end{aligned} \tag{F.27}$$

Using Eq. (F.25) with $a=c=1+\frac{g_1}{2}$ and $b=d^*=\frac{g_2}{2}-i\frac{\omega}{2\pi\theta}$ we now get

$$\begin{aligned}&\int_{-\infty}^{+\infty}\frac{dE}{2\pi}E^2\hat{P}_{g_1}(E)\hat{P}_{g_2}(\omega-E)=\\&=\hat{P}_{g_1+g_2}(\omega)(2\pi\theta)^2\left\{\frac{(1+g_1)g_1}{(1+g_1+g_2)(g_1+g_2)}\left[\left(\frac{g_1+g_2}{2}\right)^2+\left(\frac{\omega}{2\pi\theta}\right)^2\right]-\frac{g_1^2}{4}\right\}=\\&=\frac{\hat{P}_{g_1+g_2}(\omega)}{1+g_1+g_2}\left[\omega^2\frac{(1+g_1)g_1}{g_1+g_2}+\pi^2\theta^2g_1g_2\right].\end{aligned} \tag{F.28}$$

F.2 Detailed balance from general considerations

Here we demonstrate the detailed balance relation relying on symmetry properties of correlation function in the imaginary time domain. Firstly, we recall that $\hat{P}_g(E)$ is defined as

$$\hat{P}_g(E)=\int_{-\infty}^{+\infty}dt\,e^{iEt}e^{g\mathcal{G}(t)}, \tag{F.29}$$

where g is a real parameter and $\mathcal{G}$ is the bosonic correlation function $\mathcal{G}(t)=\langle\phi(0,t)\phi(0,0)-\phi^2(0,0)\rangle$ (we have dropped the label R/L since it's unimportant for $x=0$). The latter satisfies the property

$$\mathcal{G}(-t)=\mathcal{G}(t-i\beta), \tag{F.30}$$

which is readily demonstrated. Indeed, invariance under time translations implies that

$$\mathcal{G}(-t) = \langle \phi(0,-t)\phi(0,0) - \phi^2(0,0)\rangle = \langle \phi(0,0)\phi(0,t) - \phi^2(0,0)\rangle. \tag{F.31}$$

Taking into account the term explicitly dependent on t and performing the thermal average we have

$$\begin{aligned}\langle \phi(0,0)\phi(0,t)\rangle &= \frac{1}{Z}\mathrm{Tr}[e^{-\beta H}\phi(0,0)\phi(0,t)] = \\ &= \frac{1}{Z}\mathrm{Tr}[e^{iHi\beta}\phi(0,0)e^{-iHi\beta}e^{iHi\beta}\phi(0,t)].\end{aligned} \tag{F.32}$$

The operator $e^{iHi\beta}\phi(0,0)e^{-iHi\beta}$ is equivalent to the time evolution of $\phi(0,0)$ at the imaginary time $\tilde{t} = i\beta$. Recalling the cyclic property of the trace we get

$$\begin{aligned}\langle \phi(0,-t)\phi(0,0)\rangle &= \frac{1}{Z}\mathrm{Tr}[e^{-\beta H}\phi(0,t)\phi(0,i\beta)] = \\ &= \langle \phi(0,t)\phi(0,i\beta)\rangle = \langle \phi(0,t-i\beta)\phi(0,0)\rangle,\end{aligned} \tag{F.33}$$

thus proving the validity of Eq. (F.30). Let us now consider the function $\hat{P}_g(-E)$. Thanks to Eq. (F.30) we have

$$\hat{P}_g(-E) = \int_{-\infty}^{+\infty} dt\, e^{-iEt}e^{g\mathcal{G}(t)} = \int_{-\infty}^{+\infty} dt\, e^{iEt}e^{g\mathcal{G}(t-i\beta)}. \tag{F.34}$$

We now make the change of variable $t' = t - i\beta$, which transforms the last equation into

$$\hat{P}_g(-E) = \int_{-\infty-i\beta}^{+\infty-i\beta} dt\, e^{iEt}e^{-\beta E}e^{g\mathcal{G}(t)}. \tag{F.35}$$

As discussed previously, shifting the integration limits into the complex plane has no effect on the final result. The function $\hat{P}_g(-E)$ thus becomes

$$\hat{P}_g(-E) = e^{-\beta E}\int_{-\infty}^{+\infty} dt\, e^{iEt}e^{g\mathcal{G}(t)} = e^{-\beta E}\hat{P}_g(E). \tag{F.36}$$

Equation (F.36) is the detailed balance relation.

Acronyms

2DEG Two-Dimensional Electron Gas.

DOS Density Of States.

EQO Electron Quantum Optics.

FQH Fractional Quantum Hall.

HBT Hanbury Brown-Twiss.

HOM Hong-Ou-Mandel.

PASN Photoassisted Shot Noise.

QH Quantum Hall.

QPC Quantum Point Contact.

Bibliography

[1] S. Haroche, and J. M. Raimond, *Exploring the Quantum. Atoms, Cavities and Photons* (Oxford University Press, Oxford, 2006).

[2] E. Bocquillon, et al., "Electron quantum optics in ballistic chiral conductors", Ann. Phys. (Berlin) **526**, 1 (2014).

[3] K. von Klitzing, G. Dorda, and M. Pepper, "New Method for High-Accuracy Determination of the Fine-Structure Constant Based on Quantized Hall Resistance", Phys. Rev. Lett. **45**, 494 (1980).

[4] B. I. Halperin, "Quantized Hall conductance, current-carrying edge states, and the existence of extended states in a two-dimensional disordered potential", Phys. Rev. B **25**, 2185 (1982).

[5] M. Büttiker, "Capacitance, admittance, and rectification properties of small conductors", J. Phys.: Condens. Matter **5**, 9361 (1993).

[6] G. Fève, et al., "An On-Demand Coherent Single-Electron Source", Science **316**, 1169 (2007).

[7] L. S. Levitov, H. Lee, and G. B. Lesovik, "Electron counting statistics and coherent states of electric current", J. Math. Phys. **37**, 4845 (1996).

[8] D. A. Ivanov, H. W. Lee, and L. S. Levitov, "Coherent states of alternating current", Phys. Rev. B **56**, 6839 (1997).

[9] J. Keeling, I. Klich, and L. S. Levitov, "Minimal Excitation States of Electrons in One-Dimensional Wires", Phys. Rev. Lett. **97**, 116403 (2006).

[10] J. Dubois, et al., "Minimal-excitation states for electron quantum optics using levitons", Nature (London) **502**, 659 (2013).

[11] E. Bocquillon, et al., "Electron Quantum Optics: Partitioning Electrons One by One", Phys. Rev. Lett. **108**, 196803 (2012).

[12] E. Bocquillon, et al., "Coherence and Indistinguishability of Single Electrons Emitted by Independent Sources", Science **339**, 1054 (2013).

[13] R. J. Glauber, "The Quantum Theory of Optical Coherence", Phys. Rev. **130**, 2529 (1963).

[14] C. Grenier, et al., "Single-electron quantum tomography in quantum Hall edge channels", New J. Phys. **13**, 093007 (2011).

[15] T. Jullien, P. Roulleau, B. Roche, A. Cavanna, Y. Jin, and D. C. Glattli, "Quantum tomography of an electron", Nature (London) **514**, 603 (2014).

[16] V. Freulon, A. Marguerite, J.-M. Berroir, B. Plaçais, A. Cavanna, Y. Jin, and G. Fève, "Hong-Ou-Mandel experiment for temporal investigation of single-electron fractionalization", Nat. Commun. **6**, 6854 (2015).

[17] A. Marguerite, et al., "Decoherence and relaxation of a single electron in a one-dimensional conductor", Phys. Rev. B **94**, 115311 (2016).

[18] D. C. Glattli, and P. Roulleau, "Hanbury-Brown Twiss noise correlation with time controlled quasi-particles in ballistic quantum conductors", Phys. E **76**, 216 (2016).

[19] D. C. Tsui, H. L. Stormer, and A. C. Gossard, "Two-Dimensional Magnetotransport in the Extreme Quantum Limit", Phys. Rev. Lett. **48**, 1559 (1982).

[20] R. B. Laughlin, "Anomalous Quantum Hall Effect: An Incompressible Quantum Fluid with Fractionally Charged Excitations", Phys. Rev. Lett. **50**, 1395 (1983).

[21] A. Stern, "Anyons and the quantum Hall effect—A pedagogical review", Ann. Phys. **323**, 204 (2008).

[22] X. Wen, "Topological orders and edge excitations in fractional quantum Hall states", Adv. Phys. **44**, 405 (1995).

[23] T. Giamarchi, *Quantum physics in one dimension* (Oxford University Press, Oxford, 2003).

[24] J. Rech, D. Ferraro, T. Jonckheere, L. Vannucci, M. Sassetti, and T. Martin, "Minimal Excitations in the Fractional Quantum Hall Regime", Phys. Rev. Lett. **118**, 076801 (2017).

[25] L. Vannucci, F. Ronetti, J. Rech, D. Ferraro, T. Jonckheere, T. Martin, and M. Sassetti, "Minimal excitation states for heat transport in driven quantum Hall systems", Phys. Rev. B **95**, 245415 (2017).

[26] L. Vannucci, F. Ronetti, D. Ferraro, J. Rech, T. Jonckheere, T. Martin, and M. Sassetti, "Photoassisted shot noise spectroscopy at fractional filling factor", arXiv:1709.05112, [J. Phys. Conf. Ser., in press].

[27] F. Ronetti, L. Vannucci, D. Ferraro, T. Jonckheere, J. Rech, T. Martin, and M. Sassetti, "Crystallization of Levitons in the fractional quantum Hall regime", arXiv:1712.07094.

[28] G. Dolcetto, L. Vannucci, A. Braggio, R. Raimondi, and M. Sassetti, "Current enhancement through a time-dependent constriction in fractional topological insulators", Phys. Rev. B **90**, 165401 (2014).

[29] L. Vannucci, F. Ronetti, G. Dolcetto, M. Carrega, and M. Sassetti, "Interference-induced thermoelectric switching and heat rectification in quantum Hall junctions", Phys. Rev. B **92**, 075446 (2015).

[30] F. Ronetti, L. Vannucci, G. Dolcetto, M. Carrega, and M. Sassetti, "Spin-thermoelectric transport induced by interactions and spin-flip processes in two-dimensional topological insulators", Phys. Rev. B **93**, 165414 (2016).

[31] R. Landauer, "Condensed-matter physics: The noise is the signal", Nature (London) **392**, 658 (1998).

[32] Y. M. Blanter, and M. Büttiker, "Shot noise in mesoscopic conductors", Phys. Rep. **336**, 1 (2000).

[33] N. M. Ashcroft, and N. D. Mermin, *Solid State Physics* (Saunders College, Philadelphia, 1976).

[34] C. Kittel, *Elementary Statistical Physics* (Wiley, New York, 1958).

[35] D. Arovas, *Lecture Notes on Nonequilibrium Statistical Physics*, University of California, San Diego, Nov. 2015, Lecture notes available at `https://courses.physics.ucsd.edu/2013/Fall/physics210b/LECTURES/STOCHASTIC.pdf`.

[36] R. Zwanzig, *Nonequilibrium statistical mechanics* (Oxford University Press, Oxford, 2001).

[37] J. B. Johnson, "Thermal Agitation of Electricity in Conductors", Phys. Rev. **32**, 97 (1928).

[38] H. Nyquist, "Thermal Agitation of Electric Charge in Conductors", Phys. Rev. **32**, 110 (1928).

[39] H. B. Callen, and T. A. Welton, "Irreversibility and Generalized Noise", Phys. Rev. **83**, 34 (1951).

[40] R. A. Kamper, and J. E. Zimmerman, "Noise Thermometry with the Josephson Effect", J. Appl. Phys. **42**, 132 (1971).

[41] R. A. Webb, R. P. Giffard, and J. C. Wheatley, "Noise thermometry at ultralow temperatures", J. Low Temp. Phys. **13**, 383 (1973).

[42] F. Giazotto, T. T. Heikkilä, A. Luukanen, A. M. Savin, and J. P. Pekola, "Opportunities for mesoscopics in thermometry and refrigeration: Physics and applications", Rev. Mod. Phys. **78**, 217 (2006).

[43] W. Schottky, "Über spontane Stromschwankungen in verschiedenen Elektrizitätsleitern", Ann. Phys. **362**, 541 (1918).

[44] T. Ihn, *Semiconductor Nanostructures. Quantum States and Electronic Transport* (Oxford University Press, Oxford, 2010).

[45] C. Schönenberger, S. Oberholzer, E. V. Sukhorukov, and H. Grabert, "Shot Noise in Schottky's Vacuum Tube", arXiv:cond-mat/0112504.

[46] A. F. Andreev, "Thermal conductivity of the intermediate state of superconductors", Sov. Phys. JETP **19**, 1228 (1964), [Russian original: Zh. Eksp. Teor. Fiz. **46**, 1823 (1964)].

[47] X. Jehl, M. Sanquer, R. Calemczuk, and D. Mailly, "Detection of doubled shot noise in short normal-metal/superconductor junctions", Nature **405**, 50 (2000).

[48] A. A. Kozhevnikov, R. J. Schoelkopf, and D. E. Prober, "Observation of Photon-Assisted Noise in a Diffusive Normal Metal-Superconductor Junction", Phys. Rev. Lett. **84**, 3398 (2000).

[49] F. Lefloch, C. Hoffmann, M. Sanquer, and D. Quirion, "Doubled Full Shot Noise in Quantum Coherent Superconductor-Semiconductor Junctions", Phys. Rev. Lett. **90**, 067002 (2003).

[50] L. Saminadayar, D. C. Glattli, Y. Jin, and B. Etienne, "Observation of the $e/3$ Fractionally Charged Laughlin Quasiparticle", Phys. Rev. Lett. **79**, 2526 (1997).

[51] R. de-Picciotto, M. Reznikov, M. Heiblum, V. Umansky, G. Bunin, and D. Mahalu, "Direct observation of a fractional charge", Nature (London) **389**, 162 (1997).

[52] M. Reznikov, R. D. Picciotto, T. G. Griffiths, M. Heiblum, and V. Umansky, "Observation of quasiparticles with one-fifth of an electron's charge", Nature **399**, 238 (1999).

[53] C. K. Hong, Z. Y. Ou, and L. Mandel, "Measurement of subpicosecond time intervals between two photons by interference", Phys. Rev. Lett. **59**, 2044 (1987).

[54] M. Büttiker, "Scattering theory of current and intensity noise correlations in conductors and wave guides", Phys. Rev. B **46**, 12485 (1992).

[55] T. Martin, "Noise in mesoscopic physics", in *Nanophysics: Coherence and Transport. Les Houches Session LXXXI*, edited by H. Bouchiat, Y. Gefen, S. Guéron, G. Montambaux, and J. Dalibard, (Elsevier, Amsterdam, 2005), p. 283.

[56] Y. V. Nazarov, and Y. M. Blanter, *Quantum transport. introduction to nanoscience* (Cambridge University Press, Cambridge, 2009).

[57] G. B. Lesovik, and I. A. Sadovskyy, "Scattering matrix approach to the description of quantum electron transport", Phys.-Usp. **54**, 1007 (2011).

[58] M. J. M. de Jong, and C. W. J. Beenakker, "Shot noise in mesoscopic systems", in *Mesoscopic electron transport*, edited by L. L. Sohn, L. P. Kouwenhoven, and G. Schön, NATO ASI Series E (Kluwer Academic Publishers, Dordrecht, 1997), p. 225.

[59] L. D. Landau, and E. M. Lifshitz, *Quantum Mechanics - Non-relativistic Theory*, 3rd ed. (Pergamon Press, Oxford, 1977).

[60] J. J. Sakurai, and J. Napolitano, *Modern quantum mechanics*, 2nd ed. (Addison-Wesley, Boston, 2010).

[61] R. Landauer, "Spatial Variation of Currents and Fields Due to Localized Scatterers in Metallic Conduction", IBM J. Res. Dev. **1**, 223 (1957).

[62] R. Landauer, "Electrical resistance of disordered one-dimensional lattices", Philos. Mag. **21**, 863 (1970).

[63] M. Büttiker, "Four-Terminal Phase-Coherent Conductance", Phys. Rev. Lett. **57**, 1761 (1986).

[64] M. Büttiker, "Symmetry of electrical conduction", IBM J. Res. Dev. **32**, 317 (1988).

[65] G. B. Lesovik, "Excess quantum noise in 2D ballistic point contacts", JETP Lett. **49**, 592 (1989).

[66] U. Fano, "Ionization Yield of Radiations. II. The Fluctuations of the Number of Ions", Phys. Rev. **72**, 26 (1947).

[67] H. Birk, M. J. M. de Jong, and C. Schönenberger, "Shot-Noise Suppression in the Single-Electron Tunneling Regime", Phys. Rev. Lett. **75**, 1610 (1995).

[68] B. J. van Wees, H. van Houten, C. W. J. Beenakker, J. G. Williamson, L. P. Kouwenhoven, D. van der Marel, and C. T. Foxon, "Quantized conductance of point contacts in a two-dimensional electron gas", Phys. Rev. Lett. **60**, 848 (1988).

[69] D. A. Wharam, et al., "One-dimensional transport and the quantisation of the ballistic resistance", J. Phys. C: Solid State Phys. **21**, L209 (1988).

[70] M. Reznikov, M. Heiblum, H. Shtrikman, and D. Mahalu, "Temporal Correlation of Electrons: Suppression of Shot Noise in a Ballistic Quantum Point Contact", Phys. Rev. Lett. **75**, 3340 (1995).

[71] A. Kumar, L. Saminadayar, D. C. Glattli, Y. Jin, and B. Etienne, "Experimental Test of the Quantum Shot Noise Reduction Theory", Phys. Rev. Lett. **76**, 2778 (1996).

[72] C. W. J. Beenakker, and M. Büttiker, "Suppression of shot noise in metallic diffusive conductors", Phys. Rev. B **46**, 1889 (1992).

[73] C. W. J. Beenakker, "Random-matrix theory of quantum transport", Rev. Mod. Phys. **69**, 731 (1997).

[74] M. Henny, S. Oberholzer, C. Strunk, and C. Schönenberger, "1/3-shot-noise suppression in diffusive nanowires", Phys. Rev. B **59**, 2871 (1999).

[75] H. E. van den Brom, and J. M. van Ruitenbeek, "Quantum Suppression of Shot Noise in Atom-Size Metallic Contacts", Phys. Rev. Lett. **82**, 1526 (1999).

[76] J. Bardeen, "Tunnelling from a many-particle point of view", Phys. Rev. Lett. **6**, 57 (1961).

[77] M. H. Cohen, L. M. Falicov, and J. C. Phillips, "Superconductive tunneling", Phys. Rev. Lett. **8**, 316 (1962).

[78] A. H. Dayem, and R. J. Martin, "Quantum Interaction of Microwave Radiation with Tunneling Between Superconductors", Phys. Rev. Lett. **8**, 246 (1962).

[79] P. K. Tien, and J. P. Gordon, "Multiphoton process observed in the interaction of microwave fields with the tunneling between superconductor films", Phys. Rev. **129**, 647 (1963).

[80] F. W. J. Olver, D. W. Lozier, R. F. Boisvert, and C. W. Clark, *NIST Handbook of mathematical functions* (Cambridge University Press, Cambridge, 2010).

[81] L. P. Kouwenhoven, et al., "Photon-assisted tunneling through a quantum dot", Phys. Rev. B **50**, 2019 (1994).

[82] L. P. Kouwenhoven, S. Jauhar, J. Orenstein, P. L. McEuen, Y. Nagamune, J. Motohisa, and H. Sakaki, "Observation of Photon-Assisted Tunneling through a Quantum Dot", Phys. Rev. Lett. **73**, 3443 (1994).

[83] R. J. Schoelkopf, A. A. Kozhevnikov, D. E. Prober, and M. J. Rooks, "Observation of "Photon-Assisted" Shot Noise in a Phase-Coherent Conductor", Phys. Rev. Lett. **80**, 2437 (1998).

[84] G. B. Lesovik, and L. S. Levitov, "Noise in an ac biased junction: Nonstationary Aharonov-Bohm effect", Phys. Rev. Lett. **72**, 538 (1994).

[85] M. H. Pedersen, and M. Büttiker, "Scattering theory of photon-assisted electron transport", Phys. Rev. B **58**, 12993 (1998).

[86] M. Moskalets, and M. Büttiker, "Floquet scattering theory of quantum pumps", Phys. Rev. B **66**, 205320 (2002).

[87] V. S. Rychkov, M. L. Polianski, and M. Büttiker, "Photon-assisted electron-hole shot noise in multiterminal conductors", Phys. Rev. B **72**, 155326 (2005).

[88] L.-H. Reydellet, P. Roche, D. C. Glattli, B. Etienne, and Y. Jin, "Quantum Partition Noise of Photon-Created Electron-Hole Pairs", Phys. Rev. Lett. **90**, 176803 (2003).

[89] G. Platero, and R. Aguado, "Photon-assisted transport in semiconductor nanostructures", Phys. Rep. **395**, 1 (2004).

[90] D. Tong, *The Quantum Hall Effect*, Centre for Mathematical Sciences, Cambridge, Jan. 2016, Lecture notes available at http://www.damtp.cam.ac.uk/user/tong/qhe.html.

[91] K. von Klitzing, "Quantum Hall Effect: Discovery and Application", Annu. Rev. Condens. Matter Phys. **8**, 13 (2017).

[92] K. von Klitzing, "Metrology in 2019", Nat. Phys. **13**, 198 (2017).

[93] D. J. Thouless, M. Kohmoto, M. P. Nightingale, and M. den Nijs, "Quantized Hall Conductance in a Two-Dimensional Periodic Potential", Phys. Rev. Lett. **49**, 405 (1982).

[94] R. Kubo, "The fluctuation-dissipation theorem", Rep. Prog. Phys. **29**, 255 (1966).

[95] M. Kohmoto, "Topological Invariant and the Quantization of the Hall Conductance", Ann. Phys. (N.Y.) **160**, 343 (1985).

[96] M. Born, and V. Fock, "Beweis des Adiabatensatzes", Z. Phys. **51**, 165 (1928), English translation: Y. N. Demkov, "Proof of the Adiabatic Theorem", in *V.A. Fock - Selected Works: Quantum Mechanics and Quantum Field Theory*, edited by L. Faddeev, L. Khalfin, and I. Komarov, (Chapman & Hall/CRC, Boca Raton, 2004), p. 69.

[97] M. Berry, "Quantal phase factors accompanying adiabatic changes", Proc. R. Soc. Lond. A **392**, 45 (1984).

[98] B. Simon, "Holonomy, the Quantum Adiabatic Theorem, and Berry's Phase", Phys. Rev. Lett. **51**, 2167 (1983).

[99] R. Resta, *Geometry and Topology in Electronic Structure Theory*, Università di Trieste, Mar. 2016, Lecture notes available at http://www-dft.ts.infn.it/~resta/gtse/draft.pdf.

[100] M. Nakahara, *Geometry, topology, and physics*, 2nd ed. (Institute of Physics Publishing, Bristol, 2003).

[101] V. L. Ginzburg, and L. D. Landau, "On the Theory of superconductivity", in *Collected Papers of L.D. Landau*, edited by D. ter Haar, (Pergamon Press, Oxford, 1965), p. 546, [Russian original: Zh. Eksp. Teor. Fiz. **20**, 1064 (1950)].

[102] R. B. Laughlin, "Quantized Hall conductivity in two dimensions", Phys. Rev. B **23**, 5632 (1981).

[103] P. W. Anderson, "Absence of Diffusion in Certain Random Lattices", Phys. Rev. **109**, 1492 (1958).

[104] M. Büttiker, H. Thomas, and A. Prêtre, "Mesoscopic capacitors", Phys. Lett. A **180**, 364 (1993).

[105] R. Hanbury Brown, and R. Q. Twiss, "Correlation between photons in two coherent beams of light", Nature **177**, 27 (1956).

[106] R. Hanbury Brown, and R. Q. Twiss, "A test of a new type of stellar interferometer on Sirius", Nature **178**, 1046 (1956).

[107] E. Purcell, "The Question of Correlation between Photons in Coherent Light Rays", Nature **178**, 1449 (1956).

[108] P. W. Anderson, "Infrared Catastrophe in Fermi Gases with Local Scattering Potentials", Phys. Rev. Lett. **18**, 1049 (1967).

[109] G. B. Arfken, and H. J. Weber, *Mathematical methods for physicists*, 5th ed. (Academic Press, San Diego, 2001).

[110] T. Needham, *Visual complex analysis* (Clarendon Press, Oxford, 1997).

[111] N. Zanghí, *Appunti di metodi matematici della fisica*, Università di Genova, Lecture notes available at `https://www.ge.infn.it/~zanghi/metodi/ZUL.pdf`.

[112] J. Dubois, T. Jullien, C. Grenier, P. Degiovanni, P. Roulleau, and D. C. Glattli, "Integer and fractional charge Lorentzian voltage pulses analyzed in the framework of photon-assisted shot noise", Phys. Rev. B **88**, 085301 (2013).

[113] J. Eisenstein, and H. Stormer, "The Fractional Quantum Hall Effect", Science **248**, 1510 (1990).

[114] J. K. Jain, "Composite-fermion approach for the fractional quantum Hall effect", Phys. Rev. Lett. **63**, 199 (1989).

[115] R. Willett, J. P. Eisenstein, H. L. Störmer, D. C. Tsui, A. C. Gossard, and J. H. English, "Observation of an even-denominator quantum number in the fractional quantum Hall effect", Phys. Rev. Lett. **59**, 1776 (1987).

[116] R. Willett, "The quantum Hall effect at 5/2 filling factor", Rep. Prog. Phys. **76**, 076501 (2013).

[117] C. Nayak, S. H. Simon, A. Stern, M. Freedman, and S. Das Sarma, "Non-abelian anyons and topological quantum computation", Rev. Mod. Phys. **80**, 1083 (2008).

[118] V. Goldman, and B. Su, "Resonant tunneling in the quantum Hall regime: measurement of fractional charge", Science **267**, 1010 (1995).

[119] J. Franklin, et al., "The Aharonov-Bohm effect in the fractional quantum Hall regime", Surf. Sci. **360**, 17 (1996).

[120] J. Leinaas, and J. Myrheim, "On the Theory of Identical Particles", Nuovo Cim. B **37**, 1 (1977).

[121] F. Wilczek, "Quantum Mechanics of Fractional-Spin Particles", Phys. Rev. Lett. **49**, 957 (1982).

[122] M. O. Goerbig, "Quantum Hall Effects", arXiv:0909.1998.

[123] B. I. Halperin, "Statistics of Quasiparticles and the Hierarchy of Fractional Quantized Hall States", Phys. Rev. Lett. **52**, 1583 (1984).

[124] D. Arovas, J. R. Schrieffer, and F. Wilczek, "Fractional Statistics and the Quantum Hall Effect", Phys. Rev. Lett. **53**, 722 (1984).

[125] J. Fröhlich, and A. Zee, "Large scale physics of the quantum hall fluid", Nucl. Phys. B **364**, 517 (1991).

[126] A. Zee, "Quantum Hall fluids", in *Field Theory, Topology and Condensed Matter Physics*, edited by H. B. Geyer, (Springer, Berlin, Heidelberg, 1995), pp. 99–153.

[127] E. Witten, "Three lectures on topological phases of matter", Riv. Nuovo Cimento **39**, 313 (2016).

[128] V. Venkatachalam, S. Hart, L. Pfeiffer, K. West, and A. Yacoby, "Local thermometry of neutral modes on the quantum Hall edge", Nat. Phys. **8**, 676 (2012).

[129] I. Gurman, R. Sabo, M. Heiblum, V. Umansky, and D. Mahalu, "Extracting net current from an upstream neutral mode in the fractional quantum Hall regime", Nat. Commun. **3**, 1289 (2012).

[130] A. Lopez, and E. Fradkin, "Universal structure of the edge states of the fractional quantum Hall states", Phys. Rev. B **59**, 15323 (1999).

[131] V. Kac, *Infinite dimensional Lie algebras* (Cambridge University Press, Cambridge, 1990).

[132] S.-I. Tomonaga, "Remarks on Bloch's Method of Sound Waves applied to Many-Fermion Problems", Prog. Theor. Phys. **5**, 544 (1950).

[133] J. M. Luttinger, "An Exactly Soluble Model of a Many-Fermion System", J. Math. Phys. **4**, 1154 (1963).

[134] D. C. Mattis, and E. H. Lieb, "Exact Solution of a Many-Fermion System and Its Associated Boson Field", J. Math. Phys. **6**, 304 (1965).

[135] F. D. M. Haldane, "'Luttinger liquid theory' of one-dimensional quantum fluids. I. Properties of the Luttinger model and their extension to the general 1D interacting spinless Fermi gas", J. Phys. C: Solid State Phys. **14**, 2585 (1981).

[136] M. R. Geller, and D. Loss, "Coulomb blockade in the fractional quantum Hall effect regime", Phys. Rev. B **62**, R16298 (2000).

[137] X. Wen, "Chiral Luttinger liquid and the edge excitations in the fractional quantum Hall states", Phys. Rev. B **41**, 12838 (1990).

[138] J. von Delft, and H. Schoeller, "Bosonization for beginners - refermionization for experts", Ann. Phys. (Leipzig) **7**, 225 (1998).

[139] P. Di Francesco, P. Mathieu, and D. Sénéchal, *Conformal Field Theory*, Graduate Texts in Contemporary Physics (Springer-Verlag, New York, 1997).

[140] E. Miranda, "Introduction to bosonization", Braz. J. Phys. **33**, 3 (2003).

[141] C. de C. Chamon, D. E. Freed, and X. G. Wen, "Nonequilibrium quantum noise in chiral Luttinger liquids", Phys. Rev. B **53**, 4033 (1996).

[142] L. C. Evans, *Partial differential equations*, 2nd ed., Graduate studies in mathematics (American Mathematical Society, Providence, 2010).

[143] N. Goldenfeld, *Lectures on phase transitions and the renormalization group* (Perseus Books, Reading, 1992).

[144] C. L. Kane, and M. P. A. Fisher, "Transmission through barriers and resonant tunneling in an interacting one-dimensional electron gas", Phys. Rev. B **46**, 15233 (1992).

[145] R. Guyon, P. Devillard, T. Martin, and I. Safi, "Klein factors in multiple fractional quantum Hall edge tunneling", Phys. Rev. B **65**, 153304 (2002).

[146] J. Rammer, *Quantum field theory of non-equilibrium states* (Cambridge University Press, Cambridge, 2007).

[147] C. Chamon, D. E. Freed, S. A. Kivelson, S. L. Sondhi, and X. G. Wen, "Two point-contact interferometer for quantum Hall systems", Phys. Rev. B **55**, 2331 (1997).

[148] R. Shankar, "Solvable model of a metal-insulator transition", J. Mod. Phys. B **04**, 2371 (1990).

[149] J. Voit, "One-dimensional Fermi liquids", Rep. Prog. Phys. **58**, 977 (1995).

[150] M. Sassetti, and U. Weiss, "Transport of 1D Interacting Electrons Through Barriers and Effective Tunnelling Density of States", Europhys. Lett. **27**, 311 (1994).

[151] D. C. Glattli, and P. Roulleau, "Levitons for electron quantum optics", Phys. Status Solidi B **254**, 1600650 (2017).

[152] A. Crépieux, P. Devillard, and T. Martin, "Photoassisted current and shot noise in the fractional quantum Hall effect", Phys. Rev. B **69**, 205302 (2004).

[153] D. C. Tsui, "Nobel Lecture: Interplay of disorder and interaction in two-dimensional electron gas in intense magnetic fields", Rev. Mod. Phys. **71**, 891 (1999).

[154] F. D. Parmentier, L. N. Serkovic-Loli, P. Roulleau, and D. C. Glattli, "Photon-Assisted Shot Noise in Graphene in the Terahertz Range", Phys. Rev. Lett. **116**, 227401 (2016).

[155] M. Carrega, D. Ferraro, A. Braggio, N. Magnoli, and M. Sassetti, "Spectral noise for edge states at the filling factor $\nu = 5/2$", New J. Phys. **14**, 023017 (2012).

[156] D. Ferraro, M. Carrega, A. Braggio, and M. Sassetti, "Multiple quasiparticle Hall spectroscopy investigated with a resonant detector", New J. Phys. **16**, 043018 (2014).

[157] G. Granger, J. P. Eisenstein, and J. L. Reno, "Observation of Chiral Heat Transport in the Quantum Hall Regime", Phys. Rev. Lett. **102**, 086803 (2009).

[158] M. Campisi, P. Talkner, and P. Hänggi, "Fluctuation Theorem for Arbitrary Open Quantum Systems", Phys. Rev. Lett. **102**, 210401 (2009).

[159] M. Campisi, P. Hänggi, and P. Talkner, "Colloquium. Quantum fluctuation relations: Foundations and applications", Rev. Mod. Phys. **83**, 771 (2011).

[160] D. V. Averin, and J. P. Pekola, "Violation of the Fluctuation-Dissipation Theorem in Time-Dependent Mesoscopic Heat Transport", Phys. Rev. Lett. **104**, 220601 (2010).

[161] R. S. Whitney, "Non-Markovian quantum thermodynamics: second law and fluctuation theorems", arXiv:1611.00670.

[162] M. Moskalets, "Floquet Scattering Matrix Theory of Heat Fluctuations in Dynamical Quantum Conductors", Phys. Rev. Lett. **112**, 206801 (2014).

[163] M. Carrega, P. Solinas, A. Braggio, M. Sassetti, and U. Weiss, "Functional integral approach to time-dependent heat exchange in open quantum systems: general method and applications", New J. Phys. **17**, 045030 (2015).

[164] M. Carrega, P. Solinas, M. Sassetti, and U. Weiss, "Energy Exchange in Driven Open Quantum Systems at Strong Coupling", Phys. Rev. Lett. **116**, 240403 (2016).

[165] M. F. Ludovico, J. S. Lim, M. Moskalets, L. Arrachea, and D. Sánchez, "Dynamical energy transfer in ac-driven quantum systems", Phys. Rev. B **89**, 161306 (2014).

[166] M. F. Ludovico, M. Moskalets, D. Sánchez, and L. Arrachea, "Dynamics of energy transport and entropy production in ac-driven quantum electron systems", Phys. Rev. B **94**, 035436 (2016).

[167] A. Calzona, M. Acciai, M. Carrega, F. Cavaliere, and M. Sassetti, "Time-resolved energy dynamics after single electron injection into an interacting helical liquid", Phys. Rev. B **94**, 035404 (2016).

[168] A. Calzona, F. M. Gambetta, M. Carrega, F. Cavaliere, and M. Sassetti, "Non-equilibrium effects on charge and energy partitioning after an interaction quench", Phys. Rev. B **95**, 085101 (2017).

[169] F. Ronetti, M. Carrega, D. Ferraro, J. Rech, T. Jonckheere, T. Martin, and M. Sassetti, "Polarized heat current generated by quantum pumping in two-dimensional topological insulators", Phys. Rev. B **95**, 115412 (2017).

[170] F. Giazotto, and M. J. Martínez-Pérez, "The Josephson heat interferometer", Nature (London) **492**, 401 (2012).

[171] A. Fornieri, G. Timossi, P. Virtanen, P. Solinas, and F. Giazotto, "0-π phase-controllable thermal Josephson junction", Nat. Nanotechnol. **12**, 425 (2017).

[172] G. Benenti, G. Casati, K. Saito, and R. S. Whitney, "Fundamental aspects of steady-state conversion of heat to work at the nanoscale", Phys. Rep. **694**, 1 (2017).

[173] D. Sánchez, and R. López, "Nonlinear phenomena in quantum thermoelectrics and heat", C. R. Phys. **17**, 1060 (2016).

[174] R. S. Whitney, "Most Efficient Quantum Thermoelectric at Finite Power Output", Phys. Rev. Lett. **112**, 130601 (2014).

[175] E. Grosfeld, and S. Das, "Probing the Neutral Edge Modes in Transport across a Point Contact via Thermal Effects in the Read-Rezayi Non-Abelian Quantum Hall States", Phys. Rev. Lett. **102**, 106403 (2009).

[176] L. Arrachea, and E. Fradkin, "Chiral heat transport in driven quantum Hall and quantum spin Hall edge states", Phys. Rev. B **84**, 235436 (2011).

[177] H. Aita, L. Arrachea, C. Naón, and E. Fradkin, "Heat transport through quantum Hall edge states: Tunneling versus capacitive coupling to reservoirs", Phys. Rev. B **88**, 085122 (2013).

[178] R. Sánchez, B. Sothmann, and A. N. Jordan, "Chiral Thermoelectrics with Quantum Hall Edge States", Phys. Rev. Lett. **114**, 146801 (2015).

[179] P. Samuelsson, S. Kheradsoud, and B. Sothmann, "Optimal Quantum Interference Thermoelectric Heat Engine with Edge States", Phys. Rev. Lett. **118**, 256801 (2017).

[180] C. Altimiras, H. Le Sueur, U. Gennser, A. Cavanna, D. Mailly, and F. Pierre, "Non-equilibrium edge-channel spectroscopy in the integer quantum Hall regime", Nat. Phys. **6**, 34 (2010).

[181] C. Altimiras, H. le Sueur, U. Gennser, A. Anthore, A. Cavanna, D. Mailly, and F. Pierre, "Chargeless Heat Transport in the Fractional Quantum Hall Regime", Phys. Rev. Lett. **109**, 026803 (2012).

[182] M. Banerjee, M. Heiblum, A. Rosenblatt, Y. Oreg, D. E. Feldman, A. Stern, and V. Umansky, "Observed Quantization of Anyonic Heat Flow", Nature **545**, 75 (2017).

[183] A. Rosenblatt, et al., "Transmission of heat modes across a potential barrier", Nat. Commun. **8**, 2251 (2017).

[184] A. Crépieux, and F. Michelini, "Mixed, charge and heat noises in thermoelectric nanosystems", J. Phys.: Condens. Matter **27**, 015302 (2014).

[185] A. Crépieux, and F. Michelini, "Heat-charge mixed noise and thermoelectric efficiency fluctuations", J. Stat. Mech. **2016**, 054015 (2016).

[186] H. B. Callen, *Thermodynamics and an Introduction to Thermostatistics*, 2nd ed. (Wiley, New York, 1985).

[187] N. Zanghí, *Appunti di meccanica statistica*, Università di Genova, Lecture notes available at `https://www.ge.infn.it/~zanghi/FS/FS1.html`.

[188] F. Battista, F. Haupt, and J. Splettstoesser, "Energy and power fluctuations in ac-driven coherent conductors", Phys. Rev. B **90**, 085418 (2014).

[189] F. Battista, F. Haupt, and J. Splettstoesser, "Correlations between charge and energy current in ac-driven coherent conductors", J. Phys.: Conf. Ser. **568**, 052008 (2014).

[190] M. P. A. Fisher, and L. I. Glazman, "Transport in a one-dimensional Luttinger liquid", in *Mesoscopic electron transport*, edited by L. L. Sohn, L. P. Kouwenhoven, and G. Schön, NATO ASI Series E (Kluwer Academic Publishers, Dordrecht, 1997), pp. 331–373.

[191] C. L. Kane, and M. P. A. Fisher, "Nonequilibrium noise and fractional charge in the quantum Hall effect", Phys. Rev. Lett. **72**, 724 (1994).

[192] P. Eyméoud, and A. Crépieux, "Mixed electrical-heat noise spectrum in a quantum dot", Phys. Rev. B **94**, 205416 (2016).

[193] D. Ferraro, J. Rech, T. Jonckheere, and T. Martin, "Single quasiparticle and electron emitter in the fractional quantum Hall regime", Phys. Rev. B **91**, 205409 (2015).

[194] C. Grenier, J. Dubois, T. Jullien, P. Roulleau, D. C. Glattli, and P. Degiovanni, "Fractionalization of minimal excitations in integer quantum Hall edge channels", Phys. Rev. B **88**, 085302 (2013).

[195] D. Chevallier, J. Rech, T. Jonckheere, C. Wahl, and T. Martin, "Poissonian tunneling through an extended impurity in the quantum Hall effect", Phys. Rev. B **82**, 155318 (2010).

[196] G. Dolcetto, S. Barbarino, D. Ferraro, N. Magnoli, and M. Sassetti, "Tunneling between helical edge states through extended contacts", Phys. Rev. B **85**, 195138 (2012).

[197] D. Ferraro, B. Roussel, C. Cabart, E. Thibierge, G. Fève, C. Grenier, and P. Degiovanni, "Real-Time Decoherence of Landau and Levitov Quasiparticles in Quantum Hall Edge Channels", Phys. Rev. Lett. **113**, 166403 (2014).

[198] C. Wahl, J. Rech, T. Jonckheere, and T. Martin, "Interactions and Charge Fractionalization in an Electronic Hong-Ou-Mandel Interferometer", Phys. Rev. Lett. **112**, 046802 (2014).

[199] D. C. Glattli, Talk given at the 28th International Conference on Low Temperature Physics, August 9-16, 2017 (Gothenburg, Sweden).

[200] M. Moskalets, G. Haack, and M. Büttiker, "Single-electron source: Adiabatic versus nonadiabatic emission", Phys. Rev. B **87**, 125429 (2013).

[201] I. S. Gradshteyn, and I. M. Ryzhik, *Table of integrals, series, and products*, 7th ed. (Academic Press, San Diego, 2007).

[202] A. Kamenev, and A. Levchenko, "Keldysh technique and non-linear σ-model: basic principles and applications", Adv. Phys. **58**, 197 (2009).

[203] H. Bruus, and K. Flensberg, *Many-Body Quantum Theory in Condensed Matter Physics: An Introduction* (Oxford University Press, Oxford, 2004).

[204] J. Schwinger, "Brownian Motion of a Quantum Oscillator", J. Math. Phys. **2**, 407 (1961).

[205] L. V. Keldysh, "Diagram technique for nonequilibrium processes", Sov. Phys. JETP **20**, 1018 (1965), [Russian original: Zh. Eksp. Teor. Fiz. **47**, 1515 (1964)].